

Combinatorial Screening of Functional Polymers for Organic Electronics *via* Inkjet Printing

Dissertation

zur Erlangung des akademischen Grades
doctor rerum naturalium (Dr. rer. nat.)



seit 1558

vorgelegt dem Rat der Chemisch-Geowissenschaftlichen Fakultät
der Friedrich-Schiller-Universität Jena

von Diplom-Chemikerin Anke Teichler
geboren am 02. Oktober 1984 in Wolfen

Gefördert durch das Dutch Polymer Institute (DPI), Technologiebereich HTE, Projekt 620.

Supported by the Dutch Polymer Institute (DPI), technology area HTE, project 620.

Gutachter:

1. Prof. Dr. Ulrich S. Schubert (Friedrich-Schiller-Universität Jena)
2. Prof. Dr. Reinhard R. Baumann (Technische Universität Chemnitz)

Tag der öffentlichen Verteidigung: 30.08.2013

Table of contents

Table of contents	1
Documentation of authorship	3
1 Introduction.....	7
2 Combinatorial screening <i>via</i> inkjet printing	11
3 Fluid characteristics of π -conjugated polymer inks	15
4 Influence of process conditions to the quality of inkjet printed films	21
5 Thin-film optimization by selective modification of the solvent system	27
6 Screening of π -conjugated polymers for organic photovoltaics	33
7 Inkjet printing towards organic light emitting diodes.....	41
8 Inkjet printing of organic electrodes for radical batteries.....	49
9 Summary	53
10 Zusammenfassung.....	57
References	61
Publication list.....	65
Curriculum vitae.....	71
Acknowledgement/Danksagung.....	73
Declaration of authorship/Selbstständigkeitserklärung.....	77
List of abbreviations	79
Publications	81

Documentation of authorship

This section contains a list of the individual authors' contributions to the publications reprinted in this thesis.

- 1) A. Teichler, J. Perelaer, U. S. Schubert, "Inkjet printing of organic electronics – Comparison of deposition techniques and classification of state-of-the-art developments", *J. Mater. Chem. C* **2013**, *1*, 1910-1925.

A. Teichler: preparation of the manuscript
J. Perelaer: correction of the manuscript, supervision
U. S. Schubert: correction of the manuscript, supervision

- 2) A. Teichler, J. Perelaer, U. S. Schubert, "Screening of film formation qualities of various solvent systems for π -conjugated polymers *via* combinatorial inkjet printing", *Macromol. Chem. Phys.* **2013**, *214*, 547-555.

A. Teichler: conceptual development, performance of experiments, preparation of the manuscript
J. Perelaer: correction of the manuscript, supervision
U. S. Schubert: correction of the manuscript, supervision

- 3) A. Teichler, J. Perelaer, F. Kretschmer, M. D. Hager, U. S. Schubert, "Systematic investigation of a novel low-bandgap terpolymer library *via* inkjet printing: Influence of ink properties and processing conditions", *Macromol. Chem. Phys.* **2013**, *214*, 664-672.

A. Teichler: inkjet printing, film characterization, ink characterization, preparation of the manuscript, conceptual development
J. Perelaer: correction of the manuscript
F. Kretschmer: synthesis, optical characterization of solutions, correction of the manuscript
M. D. Hager: correction of the manuscript, supervision of F. Kretschmer
U. S. Schubert: correction of the manuscript, supervision

- 4) A. Teichler, Z. Shu, A. Wild, C. Bader, J. Nowotny, G. Kirchner, S. Harkema, J. Perelaer, U. S. Schubert, "Inkjet printing of chemically tailored light-emitting polymers", *Eur. Polym. J.* **2013**, *49*, 2186-2195.

A. Teichler: ink characterization, supervision of Z. Shu, preparation of the manuscript, conceptual development
Z. Shu: inkjet printing, interferometry, OLED characterization, correction of the manuscript
A. Wild: synthesis, preparation of the manuscript (synthesis part)
C. Bader: synthesis
J. Nowotny: optical characterization of films
G. Kirchner: preparation of OLED devices
S. Harkema: preparation of OLED devices
J. Perelaer: correction of the manuscript, supervision
U. S. Schubert: correction of the manuscript, supervision

- 5) A. Teichler, S. Hölzer, J. Nowotny, J. Perelaer, S. Hoepfner, F. Kretschmer, C. Bader, M. D. Hager, U. S. Schubert, "Combinatorial screening of inkjet printed ternary blends for organic electronics – Absorption behavior and morphology", *ACS Comb. Sci.* **2013**, *15*, 410-418.

A. Teichler: inkjet printing, optical characterization, interferometry, conceptual development, preparation of the manuscript
S. Hölzer: AFM measurements, correction of the manuscript
J. Nowotny: optical characterization of films
J. Perelaer: correction of the manuscript
S. Hoepfner: correction of the manuscript
F. Kretschmer: synthesis
C. Bader: synthesis
M. D. Hager: correction of the manuscript, supervision of F. Kretschmer
U. S. Schubert: correction of the manuscript, supervision

- 6) A. Wild, A. Teichler, C.-L. Ho, X.-Z. Wang, H. Zhan, F. Schlütter, A. Winter, M. D. Hager, W.-Y. Wong, U. S. Schubert, "Formation of dynamic metallo-polymers by inkjet printing: Towards white-emitting materials", *J. Mater. Chem. C* **2013**, *1*, 1812-1822.

A. Teichler: inkjet printing, interferometry, correction of the manuscript
A. Wild: synthesis, optical characterization, conceptual development, preparation of the manuscript
X.-Z. Wang, H. Zhan: synthesis
C.-L. Ho: supervision of X.-Z. Wang and H. Zhan
F. Schlütter: synthesis, correction of the manuscript
A. Winter: correction of the manuscript, supervision of A. Wild
M. D. Hager: correction of the manuscript, supervision of A. Wild
W.-Y. Wong: correction of the manuscript, supervision of X.-Z. Wang and H. Zhan
U. S. Schubert: correction of the manuscript, supervision

- 7) A. Wild, A. Teichler, C. v. d. Ehe, A. Winter, M. D. Hager, B. Yao, B. Zhang, Z. Xie, W.-Y. Wong, U. S. Schubert, "Zn^{II} bisterpyridine metallopolymers: Improved processability by the introduction of polymeric side chains", *Macromol. Chem. Phys.* **2013**, *214*, 1072-1080.

A. Teichler: inkjet printing, interferometry, correction of the manuscript
A. Wild: synthesis, characterization, conceptual development, preparation of the manuscript
C. v. d. Ehe: synthesis, correction of the manuscript
A. Winter: correction of the manuscript, supervision of A. Wild
M. D. Hager: correction of the manuscript, supervision of A. Wild
B. Yao, B. Zhang: device preparation
Z. Xie: supervision of B. Yao and B. Zhang
W.-Y. Wong: correction of the manuscript, supervision of B. Yao, B. Zhang and Z. Xie
U. S. Schubert: correction of the manuscript, supervision

- 8) T. Janoschka, A. Teichler, A. Krieg, M. D. Hager, U. S. Schubert, "Polymerization of free secondary amine bearing monomers by RAFT polymerization and other controlled radical techniques", *J. Polym. Sci., Part A: Polym. Chem.* **2012**, *50*, 1395-1407.

A. Teichler: inkjet printing, interferometry, correction of the manuscript
T. Janoschka: synthesis, preparation of the manuscript
A. Krieg: synthesis, correction of the manuscript
M. D. Hager: correction of the manuscript, supervision of T. Janoschka
U. S. Schubert: correction of the manuscript, supervision

- 9) T. Janoschka, A. Teichler, B. Häupler, T. Jähnert, M. D. Hager, U. S. Schubert, "Reactive inkjet printing of organic radical batteries", *Adv. Energy Mater.* **2013**, *3*, 1025-1028.

A. Teichler: inkjet printing, interferometry, correction of the manuscript, conceptual development
T. Janoschka: synthesis, measurements, preparation of the manuscript, conceptual development
B. Häupler: CV measurements, correction of the manuscript
T. Jähnert: correction of the manuscript
M. D. Hager: correction of the manuscript, supervision of T. Janoschka, B. Häupler, T. Jähnert
U. S. Schubert: correction of the manuscript, supervision

Jena, den ____ 2013

1 Introduction

Organic electronics based on polymer films are attractive alternatives for inorganic devices due to their easy and cheap processing *via* solution deposition methods and the possibility to use flexible substrates.^[1] As a result, the low cost production on larger areas by the roll-to-roll-processing (R2R) on foil substrates is enabled. Organic electronic devices reveal a layered structure, whereby the active layer is sandwiched between the electrodes. The active layer is typically a light emitting material in organic light emitting diodes (OLEDs)^[2] or a light harvesting polymer/fullerene blend in organic photovoltaics (OPVs).^[3] Favorable techniques for the preparation of organic electronics are characterized by low processing costs as well as low materials consumption. The sizes of the final devices, the processing speeds as well as the possibility to use flexible substrates represent important factors as well.^[4] Whereas lab scale methods are sufficient for fundamental studies, R2R processes are required for the up-scaling of organic electronics production. Solution deposition techniques like spin-coating,^[5,6] inkjet printing,^[7,8] and doctor blading^[9,10] were used for the fabrication of lab devices, whereas screen printing^[11,12] and knife-over-edge coating^[11] are R2R processes. However, all patterning techniques require a continuous development in order to produce efficient devices in a reproducible manner.

For a reproducible preparation of efficient devices, solution properties, like the solvent and the concentration, which affect the rheological properties of the coating solution, need to be controlled.^[13] However, the used coating process itself influences the final film characteristics as well.^[14] In particular, the processing time has a significant effect on the obtained morphology. The drying time is determined by the boiling point of the used solvent and the applied processing technique.^[14,15] Whereas spin-coating is seen as being a fast drying method, doctor blading and inkjet printing are techniques where the film drying proceeds at a longer time scale. Therefore, by choosing one of the latter preparation techniques one has to take into account that the best working conditions that show a good film forming performance in the spin-coating process cannot be adapted easily. In fact, the control over the obtained morphology represents a complicated interaction between various parameters and can certainly not be predicted.

Inkjet printing represents a solution deposition technique that is characterized by its non-contact, material-efficient and reproducible processing.^[16,17] Basic drying principles of inkjet printed features are understood and fundamental correlations between processing properties and film characteristics can be drawn.^[18] It is, however, a long way to gain a full

understanding of the complete drying process, since the process conditions as well as the ink properties correlate in a complex relation with the final device properties.^[19] For inkjet printing, all solute parameters have a significant influence on the preparation of the printed patterns, which makes the ink development crucial. Important factors include the contact angle, ink viscosity and surface tension as well as the nozzle diameter. Via inkjet printing features with a thickness of several tens of nanometers up to multiple tens of micrometers can be produced in a reproducible manner.^[16] By using multiple print heads, a high speed production of thin films can be performed. Therefore, inkjet printing can be used as a R2R coating technique.^[20] However, for the application of inkjet printing in a commercial available device, there are many challenges to overcome, which is the reason why inkjet printing is up to now mainly used in scientific research environment.

For a detailed understanding of the preparation techniques as well as to evaluate whether inkjet printing has the potential for producing efficient devices, the drying processes and resulting film morphologies need to be well understood.

This thesis provides an overview of methodical investigations of ink characteristics, printing conditions and final film properties. The combinatorial screening of different functional polymers enables the elucidation of structure-property-relationships (Figure 1.1).

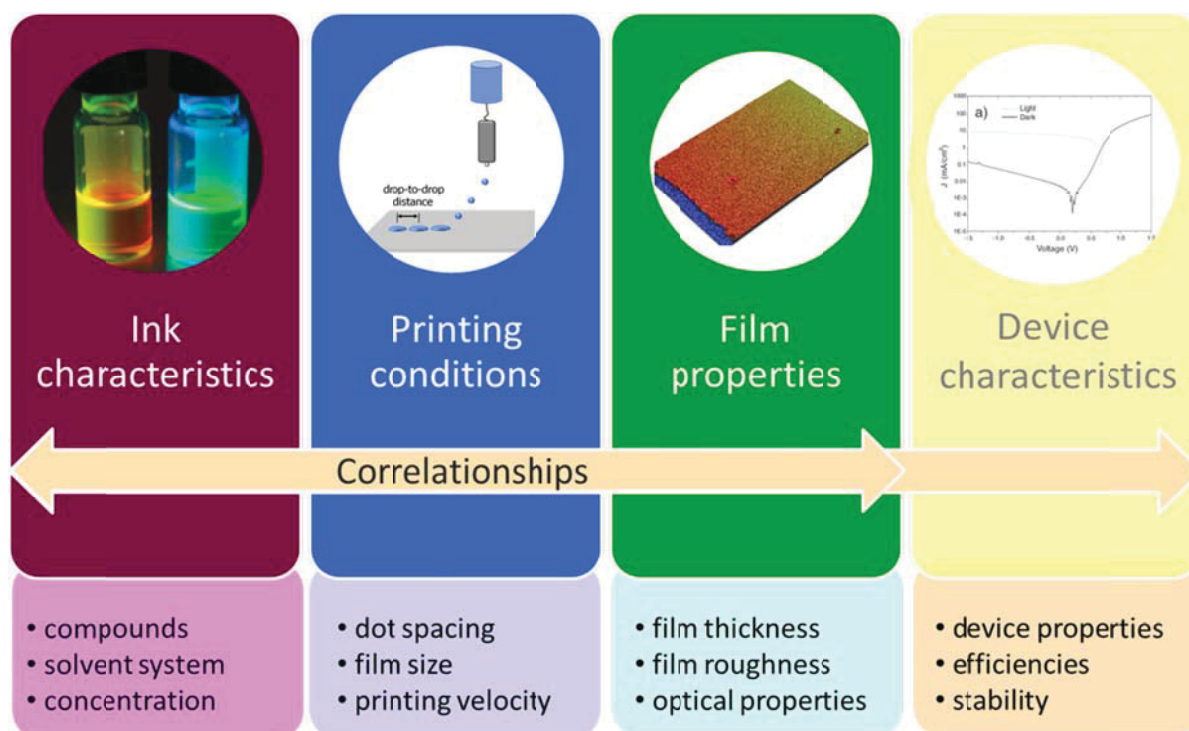


Figure 1.1 Schematic representation of the evaluation of correlations between ink characteristics, printing conditions, film properties and device characteristics.

Following the introduction, Chapter 2 discusses the advantages and drawbacks of the inkjet printing process in comparison to other solution-based film formation techniques. In particular, the possibility to integrate inkjet printing into a combinatorial screening workflow evolves inkjet printing to a distinguished tool for a fast screening of new materials for organic electronics applications.

In Chapter 3, fluid characteristics like surface tension and viscosity of π -conjugated polymer inks are investigated, since these parameters reveal a crucial effect to the applicability of materials in the inkjet printing process. The influence of processing conditions, such as the dot spacing, concentration, printing velocity and film size, on the quality of inkjet printed films is discussed in Chapter 4. A complex interaction between these parameters reveals important correlations between processing conditions and final film properties. As most important factor, the boiling point of the applied solvent system shows a significant effect towards the thin-film optimization. Chapter 5 discusses a systematic investigation of the drying behavior of inkjet printed films by the use of a variety of low and high boiling main and *co*-solvents. Furthermore, an overview of most important parameters, which affect the thin-film formation, is provided.

Finally, the optical and morphological properties of optimized inkjet printed films of functional polymers are investigated with regard to their respective application in organic electronic devices. A π -conjugated polymer library is screened for its potential use in organic photovoltaics (Chapter 6), whereas inkjet printed films of red, green and blue emitting π -conjugated and metallo-polymers are employed in organic light emitting diodes (Chapter 7). Finally, radical polymers were investigated with regard to the development of organic batteries (Chapter 8).

2 Combinatorial screening *via* inkjet printing

Parts of this chapter have been published: 1) A. Teichler, J. Perelaer, U. S. Schubert, *J. Mater. Chem. C* **2013**, *1*, 1910-1925.

Inkjet printing has been used as an on-demand, digital patterning as well as film forming technique in several printed electronics applications, including organic thin film transistors (OTFTs),^[21,22] organic light emitting diodes (OLEDs)^[23,24] and organic photovoltaics (OPVs).^[7,25] For the development of organic electronics, raw materials like indium-tin-oxide (ITO) should be replaced by organic materials, such as π -conjugated polymers, in order to realize a more cost-effective production.^[26] An important characteristic of polymers is their solubility in various organic solvents, which enables the use of simple processing conditions, *i.e.* at atmospheric pressure conditions.^[4] A variety of coating techniques, *e.g.* spin-coating^[27] and doctor blading,^[28] or printing processes, like screen printing^[11,12] and inkjet printing,^[25,29] have been applied in the field of organic electronics.

With regard to device preparation, research is mainly focused on spin-coating. The main reason is that spin-coating is characterized by an easy material handling and fast processing. However, this technique shows a high materials loss during processing^[8] and is not able to pattern a substrate selectively.^[4] Inkjet printing, in contrast, is able to pattern in an automated as well as digital manner and shows many advantages, including a non-contact, highly reproducible and combinatorial processing, wherein different materials or ink compositions can be screened while consuming only little amounts of materials.^[7,30] Besides many benefits, inkjet printing also has disadvantages, for example, its complex drying behavior, which makes a prediction of final film properties difficult. To form a complete picture of the advantages and drawbacks of the inkjet printing method as well as to elucidate potential developments of this process, an overview of properties and challenges is depicted in Figure 2.1.

An attractive issue when using inkjet printing is its little demand on materials and low waste production during processing.^[31] Since inkjet printing is an additive technique, there are no limitations for the used substrates; flexible substrates can be applied besides rigid, planar surfaces.^[32] Furthermore, inkjet printing can be used in a combinatorial workflow to characterize thin-film properties.^[7,33] This approach significantly accelerates materials research.

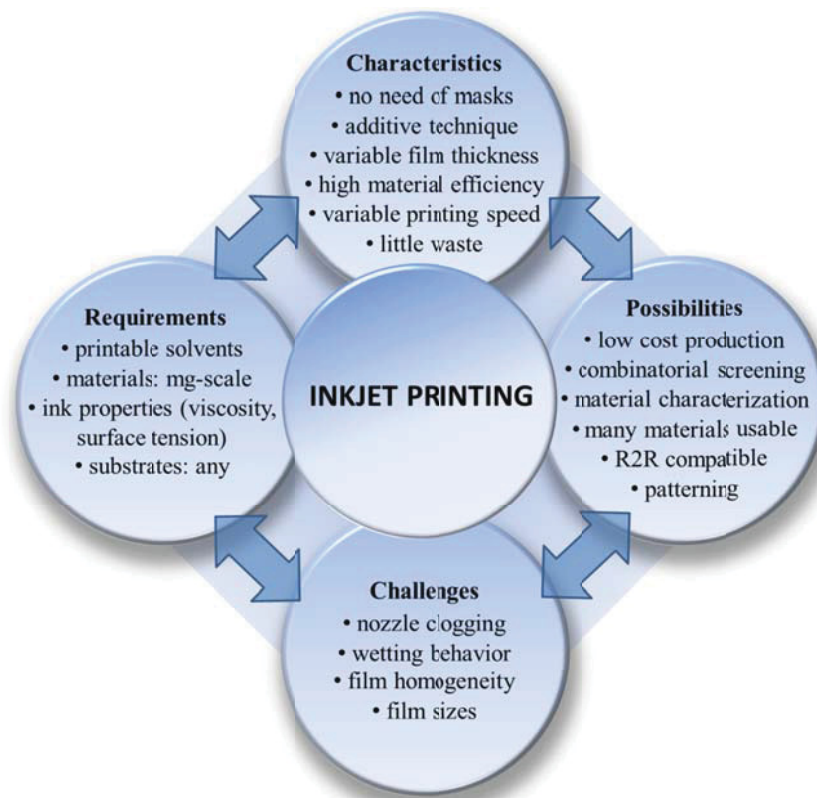


Figure 2.1 Schematic representation of characteristics, requirements, possibilities and challenges of the inkjet printing process.

However, the solute properties, *i.e.* solvent, viscosity and surface tension, are critical parameters for the applicability of a material in the inkjet printing process.^[16] Depending on the chosen inkjet printer system, there is a specific range of useable surface tensions and viscosities. Besides the ink's rather small working window, a second challenge of the inkjet printing process is the ink's wetting behavior on the substrate. For a thin film preparation, a good wetting behavior and, hence, a low contact angle of the ink on the substrate is preferred. Despite that film size and thickness can be easily varied by changing the number of deposited droplets, the drying control of different film sizes is very complicated. Applying solute and printing parameters, which were found to be the optimized values for small films, does not automatically result in a good film formation for increased film sizes.

One of the main challenges in the inkjet printing process is to gain control over the resulting film homogeneity during drying. The drying kinetics as well as the fluid flow within a drying droplet are at this moment not fully understood. Processes taking place in a drying droplet/film are very complex, as the coffee-drop effect and the Marangoni flow are considered to be both important factors.^[34,35] The coffee-drop effect^[18] describes the accumulation of solute material at the rim of a drying droplet and is a result of an inhomogeneous evaporation of the solvent and of a pinned contact line.^[36] A frequently used

solution to the coffee-drop effect is to print from a solvent mixture, in which the main solvent has a lower boiling point than the *co*-solvent.^[37] Typically, the minor component of the solvent mixture is added in a few tens of volume percentages.^[36] During the drying of the printed feature, *i.e.* droplet, line or film, the low-boiling solvent evaporates first at the contact line, which induces an outward flow of the solvent carrying solute towards the edge. The addition of a high-boiling solvent strongly reduces the evaporation of the solvent at the edges, since the amount of high-boiling solvent is here locally higher than that of the low-boiling solvent. At the same time, a surface tension gradient is induced in the printed feature that leads to an inward flow of material – the Marangoni flow.^[38] A resulting circulation of the material results in a homogeneous material distribution upon drying. Figure 2.2 shows the improvement of film formation by increasing the content of the high boiling solvent *ortho*-dichlorobenzene (*o*-DCB) from 1 vol.% to 10 vol.% in the solvent system toluene/*o*-DCB for inkjet printed poly(phenylene-ethynylene)-*alt*-(polyphenylene-vinylene) (PPE-PPV) films.^[39]

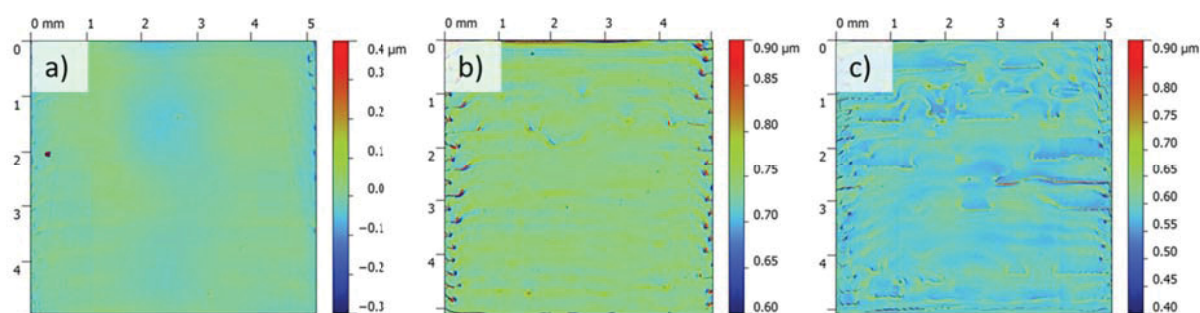


Figure 2.2 Optical profiler images of PPE-PPV films inkjet printed from the solvent system toluene/*o*-DCB in the ratios 90/10 (a), 95/5 (b), and 99/1 (c) ($c = 4 \text{ mg/mL}$).

For a lab scale technique that provides fundamental understanding, a combinatorial screening of materials and parameters is crucial to assure reproducibility as well as reliability. Not only process-depending parameters like the dot spacing need to be optimized but also the solvent/solute parameters like the used solvent(s) and concentration.^[40] Several studies report the optimization of single parameters: concentration,^[41] solvent system,^[7] blend ratio,^[42] dot spacing,^[39] and substrate temperature,^[43] but in most cases, a combinatorial screening was not performed, which leave possible synergies between the parameters undiscovered. Consequently, the results are difficult to compare. Therefore, a large number of crucial parameters needs to be evaluated in a systematical screening in order to identify optimal conditions for the used film preparation technique.

A screening workflow was developed that included the ink preparation with a pipetting robot, the thin-film library preparation by using inkjet printing and the

characterization of the compound libraries by using high-throughput analytical tools, including UV/Vis plate readers (Figure 2.3).^[7] Hereby, a complete combinatorial screening of solute properties and their impact on the thin-film properties of the inkjet printed films was introduced. Subsequently, structure-property relationships were evaluated, which lead to optimized processing conditions for the used polymer/fullerene combinations.

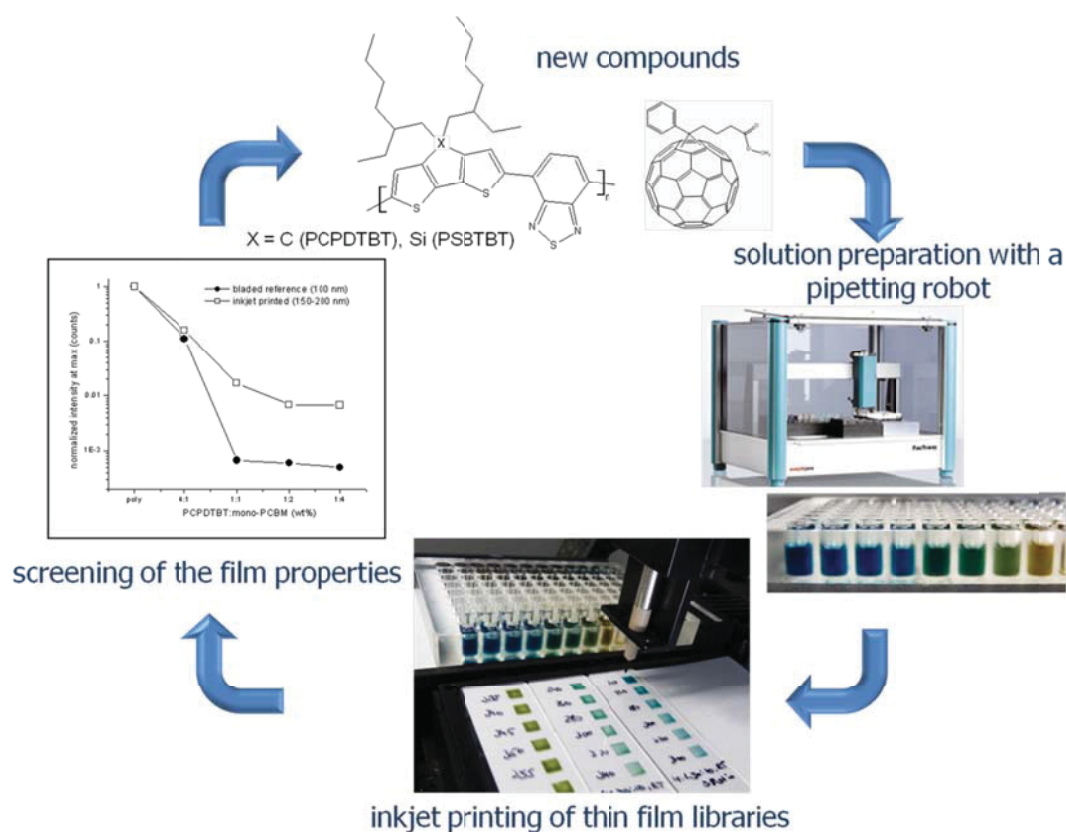


Figure 2.3 Schematic representation of a combinatorial screening workflow including inkjet printing for the preparation of thin polymer film libraries.

By incorporating inkjet printing into a combinatorial workflow, a significant step can be realized towards a fast screening of important materials properties for applications like OLEDs and OPVs. A systematic investigation of inkjet printed thin-film libraries was demonstrated for PPE-PPV libraries with variations in the polymer side groups, which led to significant changes in the optical properties.^[44] For OPVs combinatorial inkjet printing led to optimized solar cells with power conversion efficiencies up to 2.9%.^[19,33]

Inkjet printing can bridge the gap between polymer synthesis and solid-state property evaluation, since the technique opens the way to an automatic preparation of thin-film libraries of polymers, blends and composites with a systematic variation of parameters, such as chemical composition or thickness. When novel compounds are to be processed *via* inkjet printing, an optimization of film properties needs to be performed for each material.^[45,46]

3 Fluid characteristics of π -conjugated polymer inks

Parts of this chapter have been published/will be published: 2) A. Teichler, J. Perelaer, U. S. Schubert, *Macromol. Chem. Phys.* **2013**, *214*, 547-555. 3) A. Teichler, J. Perelaer, F. Kretschmer, M. D. Hager, U. S. Schubert, *Macromol. Chem. Phys.* **2013**, *214*, 664-672. 4) A. Teichler, Z. Shu, A. Wild, C. Bader, J. Nowotny, G. Kirchner, S. Harkema, J. Perelaer, U. S. Schubert, *Eur. Polym. J.* **2013**, DOI:10.1016/j.eurpolymj.2013.03.031.

Since the final film quality depends not only on the drying behavior of the solvents, but also on a stable and reproducible droplet formation during the printing process, the fluid characteristics are very important. Using inkjet printing as film formation method the polymer ink needs to fulfill certain criteria. Besides surface tension and viscosity, the boiling point of the solvent is an important issue for a reproducible droplet formation. All experiments in this thesis are performed using an Autrodop system from microdrop Technologies. Drop-on-demand (DoD) piezo-based printheads are used that have an inner nozzle diameter of 70 μm . Using this setup, inks within a viscosity range of 0.4 to 20 mPas are processable. Typical drop diameters generated by the used nozzle are, depending on the solvent, in the range between 60 and 70 μm , which corresponds to drop volumes of 115 to 180 pL.

Since not every solution forms stable and accurate droplets by means of inkjet printing the Z -number was developed, which is a characteristic fluid parameter that takes important fluid properties into account. The Z -number predicts the printability of an ink and is, therefore, important in order to evaluate the applicability of a solution in the inkjet printing process using a specific nozzle diameter. The Z -number

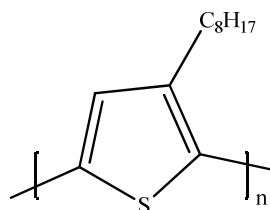
$$Z = \frac{(d\rho\gamma)^{1/2}}{\eta}$$

is dependent on the nozzle diameter d , the density ρ , the surface tension γ and the viscosity η .^[47] It was reported that limitations in printability occur if the Z -number is either lower than 2 or higher than 14,^[48] whereas other groups found a reproducible printability using inks with Z -numbers >60 .^[49] Limitations in printability are encountered for high viscosities (low Z -numbers) and satellite formation (high Z -numbers).^[50]

The influence of fluid properties is demonstrated by three examples using different π -conjugated polymers. The first section shows a systematical investigation of solvent systems characterized by different surface tensions, viscosities as well as boiling points. Secondly, the influence of different monomer contents in a terpolymer library on fluid properties and

printability is discussed. Finally, it is demonstrated that similar ink characteristics result in comparable droplet formations although different π -conjugated polymers are used.

As a first example, the π -conjugated polymer poly(3-octylthiophene) **1** (P3OT, Scheme 3.1), which belongs to the currently most applied polymer class (polythiophenes) in the field of organic electronics,^[51,52] was used to investigate a variation of solute properties.



1

Scheme 3.1 Schematic representation of the π -conjugated polymer P3OT **1** ($M_n = 34,000$ g/mol, regioregularity (RR) >98.5%).

Various solvent systems were used that have on the one hand a systematically increased difference in the boiling point and on the other hand comparable boiling points but different viscosities and surface tensions. By following this approach, a systematic evaluation of correlations between ink characteristics and printability were revealed. The boiling points of the used solvents need to be high enough to ensure a stable droplet formation over a longer time period. Too low boiling points lead to a faster evaporation at the nozzle tip, which causes nozzle clogging. Three solvents were selected as main solvents that covered a broad range of boiling points (bp): toluene (bp 110 °C), *p*-xylene (bp 138 °C) and 1,3,5-trimethylbenzene (1,3,5-TMB, bp 165 °C). Non-chlorinated aromatic solvents with boiling points between 136 °C and 293 °C were selected as *co*-solvents, which resulted in a boiling point difference between main and *co*-solvent solvent of at least 18 K (Table 3.1).

To obtain insights in the effect of ink properties to the printing quality, surface tensions, densities and viscosities of all P3OT inks were measured and the corresponding Z-numbers were calculated (see Table 3.1). The surface tensions and viscosities were measured to be in a range of 18 to 26 mN/m and 0.747 to 1.011 mPas, respectively, and are in an inkjet printable regime. The viscosity is mainly determined by the main solvent and was therefore found to increase in the following order: toluene < *p*-xylene < 1,3,5-TMB. The corresponding Z-number decreases with increased viscosity and was found to be between 53 and 36.

Table 3.1 Ink characteristics of **1** (4 mg/mL) in solvent systems with different boiling points.

Solvent system (90/10)	Boiling point [°C]	γ [mN/m]	ρ [g/cm³]	η [mPas]	Z-number
toluene/ethylbenzene	110/136	25.5	0.868	0.752	52.3
toluene/ <i>o</i> -xylene	110/144	25.6	0.869	0.785	50.3
toluene/ <i>iso</i> -propylbenzene	110/153	22.4	0.867	0.769	47.9
toluene/propylbenzene	110/159	25.0	0.867	0.760	51.3
toluene/1,3,5-TMB	110/165	25.9	0.867	0.747	53.1
toluene/1,2,4-TMB	110/170	24.9	0.868	0.757	51.4
toluene/1,2,3-TMB	110/176	25.4	0.877	0.771	51.2
toluene/butylbenzene	110/183	23.1	0.867	0.788	47.5
toluene/pentylbenzene	110/205	25.3	0.867	0.790	49.6
toluene/hexylbenzene	110/226	25.5	0.867	0.845	46.6
toluene/octylbenzene	110/261	22.5	0.867	0.839	44.0
toluene/nonylbenzene	110/282	25.8	0.864	0.849	46.5
toluene/decylbenzene	110/293	25.9	0.866	0.851	46.6
<i>p</i> -xylene/propylbenzene	138/159	25.4	0.863	0.849	45.4
<i>p</i> -xylene/1,3,5-TMB	138/165	23.7	0.862	0.800	47.7
<i>p</i> -xylene/1,2,4-TMB	138/170	23.5	0.863	0.838	43.7
<i>p</i> -xylene/1,2,3-TMB	138/176	25.5	0.866	0.832	45.4
<i>p</i> -xylene/butylbenzene	138/183	23.4	0.862	0.842	43.6
<i>p</i> -xylene/pentylbenzene	138/205	25.5	0.862	0.902	45.5
<i>p</i> -xylene/hexylbenzene	138/226	25.7	0.862	0.894	44.0
<i>p</i> -xylene/octylbenzene	138/261	25.9	0.862	0.912	43.3
<i>p</i> -xylene/nonylbenzene	138/282	25.9	0.862	0.920	43.0
<i>p</i> -xylene/decylbenzene	138/293	25.6	0.862	0.917	42.9
1,3,5-TMB/butylbenzene	165/183	21.3	0.865	0.933	38.9
1,3,5-TMB/pentylbenzene	165/205	21.6	0.865	0.948	38.1
1,3,5-TMB/hexylbenzene	165/226	24.8	0.865	0.981	39.5
1,3,5-TMB/octylbenzene	165/261	25.1	0.865	0.996	39.1
1,3,5-TMB/nonylbenzene	165/282	25.6	0.865	1.011	38.9
1,3,5-TMB/decylbenzene	165/293	25.8	0.865	0.998	39.6

In this study no printing limitations based on different Z -numbers were identified. Although satellite droplets were observed for inks with a high Z -number, an in-flight merging of the satellite droplet with the main droplet was revealed for all tested inks. Additionally, no nozzle clogging was obtained, indicating that the boiling points were high enough to ensure a stable droplet formation over a longer time period by applying similar printing conditions of 60 to 70 V and 30 to 35 μ s for pulse voltage and pulse length, respectively.

Secondly, to evaluate correlations between polymer structures, molar masses and printability a polymer library consisting of eight terpolymers with systematically varied composition was investigated. The low bandgap polymer library poly(diketopyrrolopyrrole-*co*-benzothiadiazole-*co*-fluorene) (P(DPP-*co*-BTD-*co*-F)) is characterized by systematically varying contents of the DPP and BTD moieties, while keeping the fluorene content constant (Figure 3.1). The resulting polymer compositions of polymers **2** to **9** and their corresponding molecular characteristics are summarized in Table 3.2.

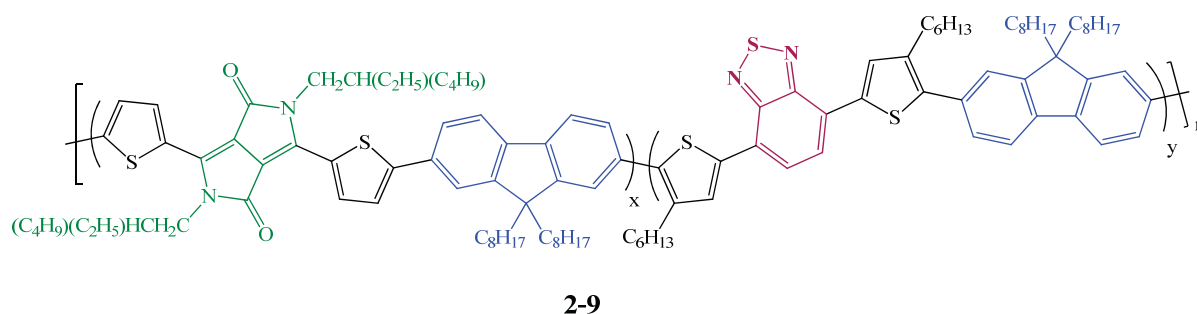


Figure 3.1 Schematic representation of the terpolymers P(DPP-*co*-BTD-*co*-F) **2** to **9**. For a detailed composition see Table 3.2.

Trends in surface tensions, viscosities, densities and Z -numbers were investigated, but no relationships between the different parameters could be identified (Table 3.2). The expected trend of increasing viscosity with increasing molar mass was not observed for this polymer library, because there are too many parameters of influence, such as a changing polymer composition combined with changes in rigidity of the chains and the variations in the molar mass. As not every single parameter can be addressed separately it is difficult to reveal such correlations. At this point, it can be concluded that the DPP unit affects the ink viscosity significantly, whereas the effect of the BTD seems to be less significant; a continuous increase of the ink's viscosity was observed with increasing DPP content in the polymer when a composition of DPP/BTD/F 50/50/100 is exceeded. In contrast, an increasing BTD content

shows no clear dependence on the polymer composition. Instead, the molar mass seems to influence the ink viscosity at low DPP contents, since polymer **2**, which has the lowest M_n , exhibits a significant low viscosity. As a conclusion, correlations between polymer composition and ink properties are too complex to elucidate for the current investigated polymer library.

Table 3.2 Composition, molar mass and fluid properties of terpolymers P(DPP-co-BTD-co-F) **2** to **9** in toluene/*o*-DCB 90/10 (5 mg/mL).

	DPP	BTD	F	M_n [g/mol]	M_w [g/mol]	PDI	γ [mN/m]	ρ [g/cm ³]	η [mPas]	Z- number
2	0	100	100	8,400	18,000	2.12	33.0	0.910	0.698	65.7
3	40	60	100	37,000	93,000	2.52	29.7	0.911	0.942	46.2
4	50	50	100	37,000	81,000	2.20	34.5	0.910	0.966	48.5
5	60	40	100	19,000	44,000	2.35	33.4	0.911	0.852	54.2
6	70	30	100	25,000	54,000	2.18	34.6	0.911	0.916	51.3
7	80	20	100	25,000	56,000	2.24	33.8	0.911	0.942	49.3
8	90	10	100	31,000	68,000	2.22	32.5	0.911	1.013	44.9
9	100	0	100	26,000	56,000	2.15	34.6	0.910	1.058	44.4

As a third example, three different conjugated polymers poly(flourene-phenylene) PFP **10**, poly(phenylene-vinylene) PPV **11** and poly(phenylene-vinylene)-poly(phenylene-ethynylene) PPE-PPV **12**, (Figure 3.2), which can be employed as emissive materials for OLED devices, were investigated.

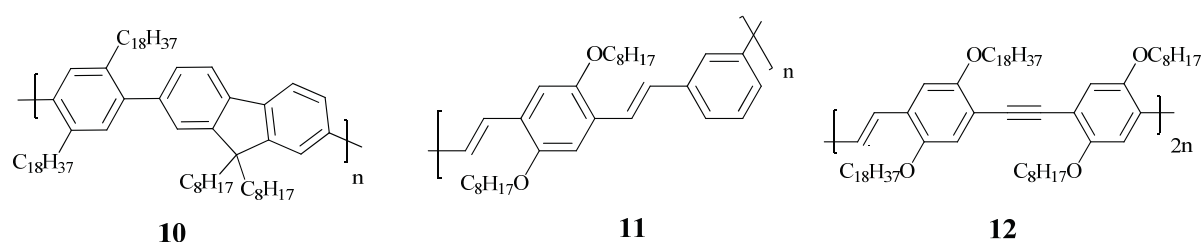


Figure 3.2 Schematic representation of PFP **10**, PPV **11** and PPE-PPV **12**.

The polymers reveal tuned polymeric structures and different molar masses. For all three polymers the same solvent system (toluene/*o*-DCB 90/10) and a concentration of 4 mg/mL was used. The surface tensions and densities were similar for all inks (Table 3.3). The viscosities of the three different polymer solutions differ slightly from each other, which follows the trend of the molar mass of the polymers: polymer **11** (0.70 mPas) < polymer **12** (0.72 mPas) < polymer **10** (0.76 mPas). These results are in agreement with the finding of De

Gans *et al.*, who studied the effect of different molar masses of polystyrene to the ink viscosity.^[30] The *Z*-numbers were calculated to be between 18 and 20. Again, no satellite formation was observed and, thus, the inks were stable to be inkjet printed using the same printing settings (75 V, 35 μ s).

Table 3.3 Polymer and ink properties of **10**, **11** and **12** in the solvent system toluene/*o*-DCB (4 mg/mL).

	M_n [g/mol]	M_w [g/mol]	PDI	γ [mN/m]	ρ [g/cm ³]	η [mPas]	<i>Z</i> - number
10	14,200	29,700	2.09	31.1	0.915	0.76	18.6
11	5,100	9,500	1.86	31.1	0.916	0.70	20.2
12	8,600	33,970	3.95	31.2	0.917	0.72	19.6

As a conclusion of this section, all tested soluble π -conjugated polymers revealed a stable and reproducible droplet formation by using solvent systems that are applicable for organic electronics. Although high *Z*-numbers were observed, droplet formation without satellite formation was achieved. At this point no limitations for a reproducible droplet formation were observed concerning the fluid characteristics.

4 Influence of process conditions to the quality of inkjet printed films

Parts of this chapter have been published/will be published: 3) A. Teichler, J. Perelaer, F. Kretschmer, M. D. Hager, U. S. Schubert, *Macromol. Chem. Phys.* **2013**, *214*, 664-672. 4) A. Teichler, Z. Shu, A. Wild, C. Bader, J. Nowotny, G. Kirchner, S. Harkema, J. Perelaer, U. S. Schubert, *Eur. Polym. J.* **2013**, DOI:10.1016/j.eurpolymj.2013.03.031.

In order to gain insights into the interaction of different printing and drying properties, each processing parameter needs to be addressed separately. To reveal relationships between all parameters, a systematical investigation is required, which can be realized by using a screening approach by means of 2-dimensional film libraries. The dot spacing, which is the center-to-center distance of two adjacent droplets, has a crucial effect on the film formation. Low dot spacings result in the deposition of more material and also cause a longer film drying. On the other hand, too high dot spacings prevent an efficient coalescence of the deposited droplets and lead to the formation of lines or even single droplets. Due to the good wetting of the applied polymer inks used here (contact angles $<10^\circ$ on glass substrates), an efficient merging of the droplets on the substrate occurs, resulting in a continuous film formation. As a consequence, it was possible to apply a wide range of dot spacings (80 to 220 μm).

Since all other investigated parameters are also dependent on the applied dot spacing, a 2-dimensional screening was performed. The effect of the dot spacing can therefore be found in the different parts that discuss the thin-film optimization experiments.

As a second processing parameter, the concentration of the polymer in the ink reveals not only a significant influence on the final film thickness, but also on the film quality. To study the effect of the concentration polymer **4** was investigated using different ink concentrations (3 mg/mL, 5 mg/mL and 7 mg/mL) and three solvent systems (chlorobenzene (CB)/*ortho*-dichlorobenzene (*o*-DCB), *o*-xylene/*o*-DCB and toluene/*o*-DCB, all in a ratio of 90/10, respectively). The solvents were carefully chosen to match the applicability in the inkjet printing process as well as in OPVs.^[7,53] Table 4.1 summarizes the obtained film thicknesses and surface roughnesses for the best obtained film homogeneity using the respective inks.

Table 4.1 Film properties of **4** inkjet printed from different solvent systems using altered concentrations.

Solvent system (90/10)	c [mg/mL]	Dot spacing [μm]	Film thickness [nm]	Surface roughness	
				[nm]	[%]
CB/ <i>o</i> -DCB	3	160	40	7	18
	5	140	120	30	25
	7	140	190	40	21
<i>o</i> -xylene/ <i>o</i> -DCB	3	180	30	23	77
	5	180	40	10	25
	7	160	170	18	11
toluene/ <i>o</i> -DCB	3	160	65	8	12
	5	140	155	13	8
	7	120	215	14	7

Printing from CB/*o*-DCB and *o*-xylene/*o*-DCB leads to an inhomogeneous film formation for all concentrations. The solvent system toluene/*o*-DCB represents the most suitable solvent to produce films of polymer **4** with an adequate homogeneity (surface roughness <10%) using a concentration of 5 mg/mL (Figure 4.1). A lower concentration (3 mg/mL) does not result in homogenous films, indicated by the significant line formation even at smaller dot spacings. Inkjet printed films applying a concentration of 7 mg/mL revealed a high homogeneity but too high film thicknesses for the application in organic electronics. A film thickness between 100 and 200 nm for the active layer is required.^[54] Therefore, a concentration of 5 mg/mL is applicable due to the achieved layer thicknesses of 155 nm, whereas 215 nm thick films were obtained for the concentration of 7 mg/mL.

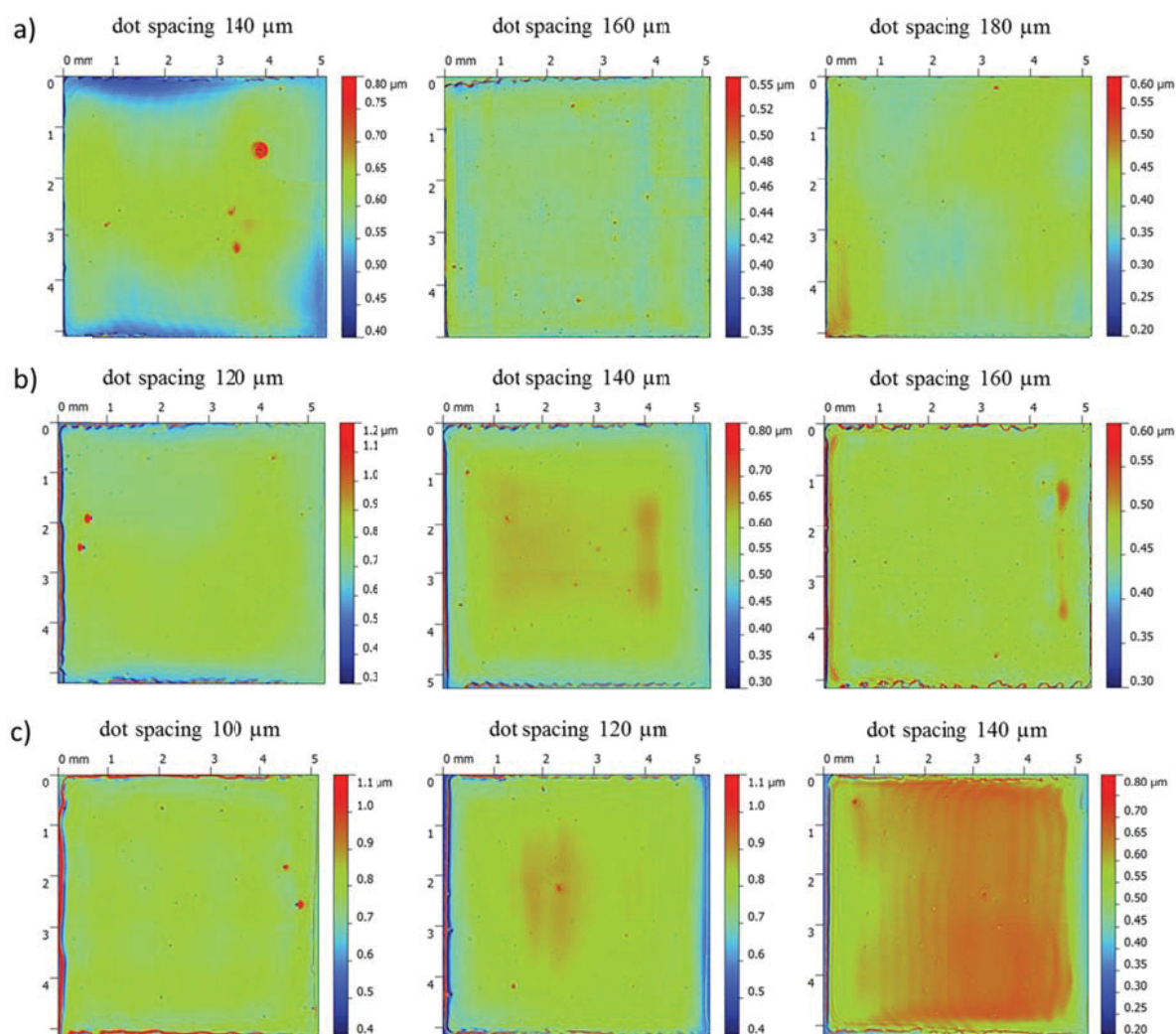


Figure 4.1 Optical profiler images of inkjet printed films of polymer **4** using the solvent system toluene/*o*-DCB in a ratio of 90/10 and a concentration of 3 mg/mL (a), 5 mg/mL (b) and 7 mg/mL (c).

A challenge of single nozzle inkjet printing is the variation of film sizes. In particular, the variation of the film size is not trivial since the drying behavior strongly depends on the amount of applied material and the drying time. For the inkjet printing process, the deposited material starts drying already during the printing of the entire film. Since the films were produced by printing lines next to each other, which subsequently merge into a continuous feature, the length of a line and, as a consequence, the time until the next line is printed, is crucial to control the film formation properties.

Figure 4.2 combines the investigation of two challenges, film thickness and film size requirements, for polymer **3**, printed from toluene/*o*-DCB. Film sizes of 5 mm × 5 mm and 20 mm × 20 mm as well as toluene/*o*-DCB ratios of 90/10 (Figure 4.2a) and 70/30 (Figure 4.2b) were investigated, respectively.

For toluene/*o*-DCB 90/10 and a film size of 5 mm × 5 mm a dot spacing of 100 μm is favorable (film thickness 250 nm) due to a decrease in film quality for higher drop-to-drop distances (Figure 4.2a, left). For larger film sizes, the control over the film quality is more demanding (Figure 4.2a, right). One reason is the increased drying time of each printed line before the adjacent line is printed. As described before, the film quality is thereby dependent on the size of the film as well as the solvent's boiling point. For a film size of 20 mm × 20 mm line formation occurs during drying at high dot spacings. For low dot spacings an increased uniformity (100 μm) but a too high film thickness (350 nm) was observed.

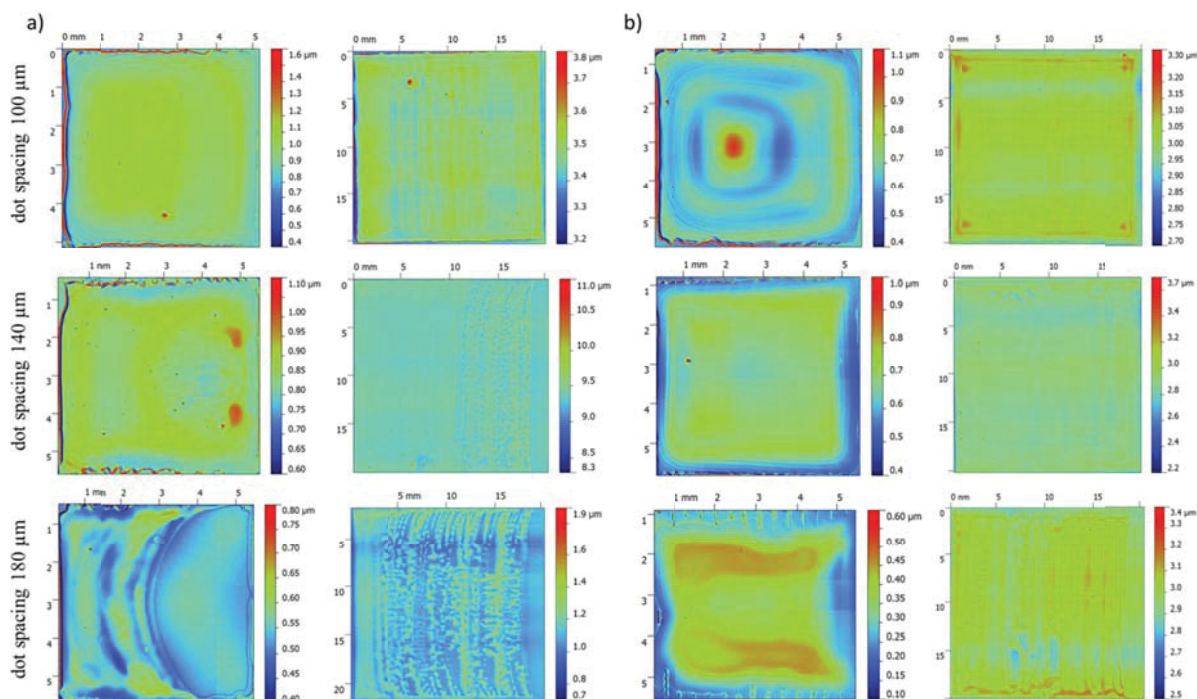


Figure 4.2 Optical profiler images of inkjet printed films of polymer 3 (3 mg/mL) using the solvent system toluene/*o*-DCB in ratios of 90/10 (a) and 70/30 (b) by volume in a film size of 5 mm × 5 mm (left) and 20 mm × 20 mm (right).

If an aimed application of the inkjet printed layers requires a lower film thickness than the film thickness found for an optimal film formation, different approaches can be used to reduce the layer thickness: i) increasing the dot spacing, ii) decreasing the ink concentration and iii) increasing the amount of the high boiling solvent. The first two points lead to a reduction of the deposited material and, hence, result in a lower film thickness. The third option introduces a longer drying of the deposited material, which leads to a more homogeneous drying of the printed films.

Using a *co*-solvent content of 30 vol.% for the solvent system toluene/*o*-DCB (Figure 4.2b) a film thickness of 130 nm was obtained for a film size of 5 mm × 5 mm and a thickness of 100 nm for 20 mm × 20 mm for dot spacings of 140 μm, respectively. In contrast, by using a solvent ratio of 50/50 the drying of the film is very slow, leading to a multiple ring-like drying pattern. As a result, non-uniform films are observed for both film sizes. Additional investigations for a film size of 10 mm × 10 mm confirm that an increase of the *co*-solvent content to a ratio of 70/30 improves the film quality at lower film thicknesses (170 nm).

It can be concluded that for an increased film size an increased content of the high boiling solvent leads to an improved control over the film formation. It is noticeable that not only thinner films can be prepared but also an improved film formation is observed. Hence, the approach of increasing the boiling point of the applied solvent represents a good alternative to reveal thinner as well as larger thin films with a homogeneous film formation.

In order to improve the drying pattern, an increase of the printing velocity could reduce the observed line formation when large film sizes or low high boiling point contents are used. Since a single printed drop dries within a few seconds a large printing velocity is preferred. For a print head velocity of 1 mm/s the droplets show a good merging within the line but adjacent lines are not able to coalesce (Figure 4.3a). In contrast, a printing velocity of 30 mm/s reveals an inaccurate droplet positioning due to a high air flow caused by the high printing speed (Figure 4.3b). In order to ensure a fast but accurate printing, a velocity of 20 mm/s was found as an optimal printing speed (Figure 4.3c).

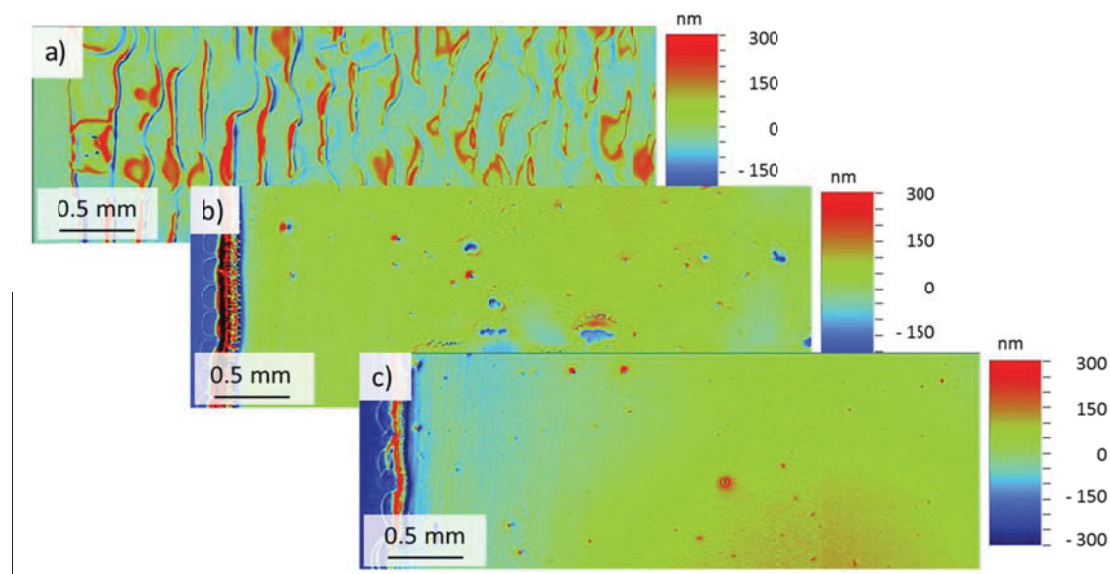


Figure 4.3 Optical profiler images of inkjet printed films using toluene/*o*-DCB (90/10) and printing velocities of 1 mm/s (a), 30 mm/s (b) and 20 mm/s (c).

5 Thin-film optimization by selective modification of the solvent system

Parts of this chapter have been published: 2) A. Teichler, J. Perelaer, U. S. Schubert, *Macromol. Chem. Phys.* **2013**, *214*, 547-555.

A systematic investigation of the effect of the solvent's boiling point to the film quality was investigated for polymer **1**, using solvents with systematically varied boiling points (Table 5.1). In order to evaluate relationships between ink properties and film homogeneity, the inks were printed and surface topographies as well as surface roughnesses were measured by using interferometry techniques. The film thicknesses and surface roughnesses R_a for the main solvents toluene, *p*-xylene and 1,3,5-TMB are summarized in Table 5.1.

A significant influence of the *co*-solvent's boiling point to the resulting film homogeneity was observed. For toluene as a main solvent it was found that a *co*-solvent with a low boiling point, like ethylbenzene (bp 136 °C), is not suitable for a smooth film formation (surface roughness R_a 96.2%). The small boiling point difference between the two solvents caused the deposited material to dry too quickly, which resulted in non-homogeneous films (Figure 5.1a). When using this solvent system and a wide range of dot spacings, *i.e.* with a varied amount of deposited material, no continuous films were formed. Instead, individual lines were observed for all dot spacings, suggesting that the characteristic line-by-line deposition of inkjet printing takes too long to create a continuous film.

When using a solvent system with a higher boiling *co*-solvent, for example pentylbenzene (bp 205 °C), continuous films with improved film formation qualities were observed with a surface roughness R_a of 24% of the film thickness (Figure 5.1b). A dot spacing of 130 μm represents the optimum amount of deposited material (Figure 5.1b, middle); a lower dot spacing (80 μm) leads to irregularities due to too much deposited ink (Figure 5.1b, left), whereas higher dot spacings (180 μm) lead to the formation of lines and to an increased surface roughness (Figure 5.1b, right).

Table 5.1 Film properties of **1** inkjet printed from solvent systems with different boiling points (4 mg/mL).

Solvent system (90/10)	Boiling point [°C]	Film thickness [nm]	Surface roughness R_a	
			[nm]	[%]
toluene/ethylbenzene	110/136	105	101	96.2
toluene/ <i>o</i> -xylene	110/144	85	81	95.3
toluene/ <i>iso</i> -propylbenzene	110/153	70	58	82.9
toluene/propylbenzene	110/159	80	51	63.8
toluene/1,3,5-TMB	110/165	80	55	68.8
toluene/1,2,4-TMB	110/170	75	35	46.7
toluene/1,2,3-TMB	110/176	75	31	41.3
toluene/butylbenzene	110/183	70	23	32.9
toluene/pentylbenzene	110/205	75	18	24.0
toluene/hexylbenzene	110/226	70	25	35.7
toluene/octylbenzene	110/261	65	28	43.1
toluene/nonylbenzene	110/282	60	32	53.3
toluene/decylbenzene	110/293	55	24	43.6
<i>p</i> -xylene/propylbenzene	138/159	100	78	78.0
<i>p</i> -xylene/1,3,5-TMB	138/165	100	62	62.0
<i>p</i> -xylene/1,2,4-TMB	138/170	90	59	65.6
<i>p</i> -xylene/1,2,3-TMB	138/176	85	24	28.2
<i>p</i> -xylene/butylbenzene	138/183	100	24	24.0
<i>p</i> -xylene/pentylbenzene	138/205	95	12	12.6
<i>p</i> -xylene/hexylbenzene	138/226	80	10	12.5
<i>p</i> -xylene/octylbenzene	138/261	70	15	21.4
<i>p</i> -xylene/nonylbenzene	138/282	80	19	23.8
<i>p</i> -xylene/decylbenzene	138/293	80	23	28.8
1,3,5-TMB/butylbenzene	165/183	90	36	40.0
1,3,5-TMB/pentylbenzene	165/205	90	17	18.9
1,3,5-TMB/hexylbenzene	165/226	90	12	13.3
1,3,5-TMB/octylbenzene	165/261	85	5	5.9
1,3,5-TMB/nonylbenzene	165/282	90	9	10.0
1,3,5-TMB/decylbenzene	165/293	80	8	10.0

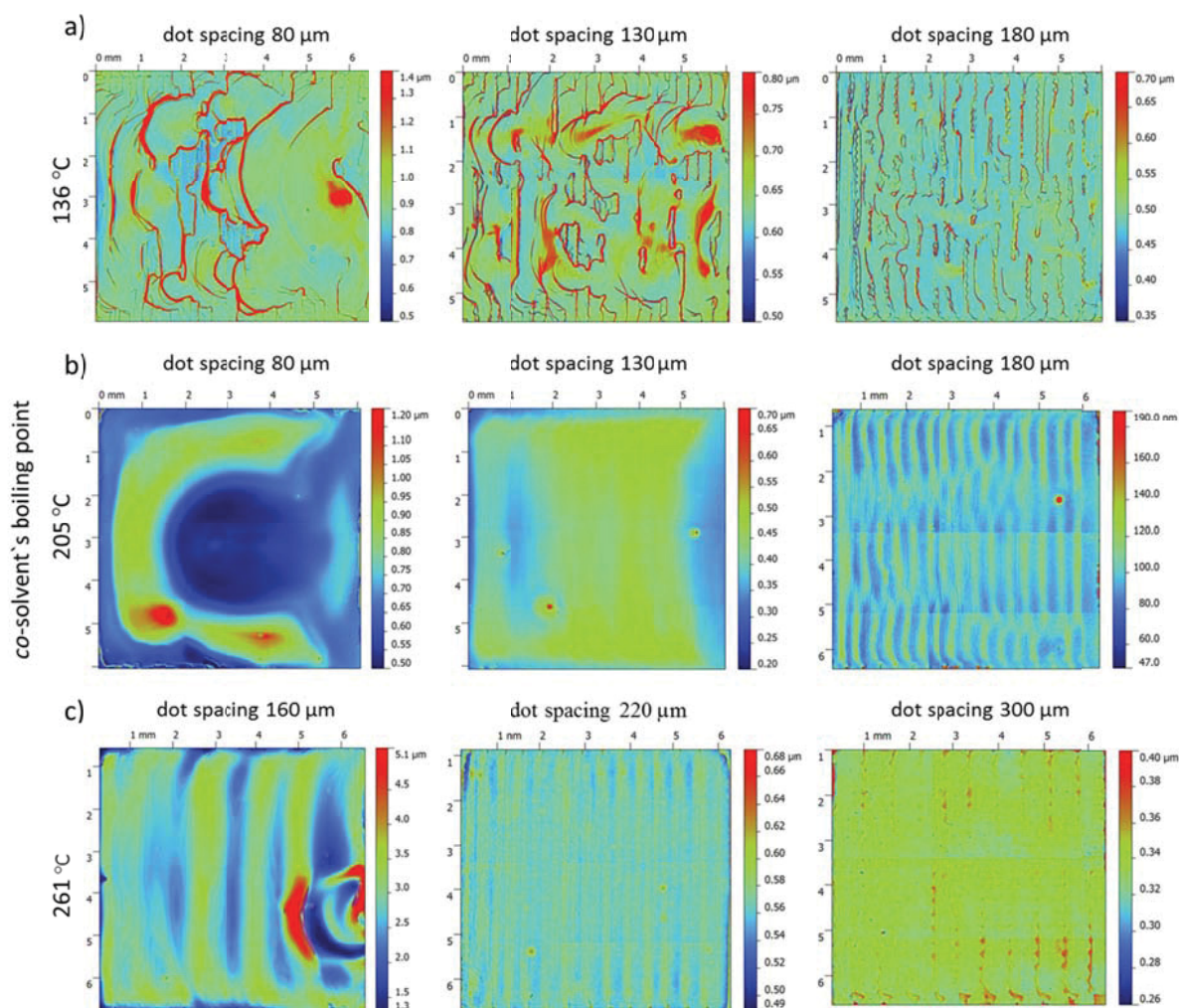


Figure 5.1 Optical profiler images of inkjet printed films of polymer **1** (4 mg/mL) using toluene as main solvent and as *co*-solvent ethylbenzene (a), pentylbenzene (b) and octylbenzene (c) in a ratio of 90/10.

With a further increase of the *co*-solvent's boiling point the surface roughness increases using a *co*-solvent with a boiling point >226 °C (Figure 5.1c, Table 5.1). In this case, the drying takes too long and the material forms an irregular film surface, which is due to multiple drying steps that lead to a ring-like pattern or to the formation of lines (Figure 5.1c).

In order to confirm the results found for toluene, two other main solvents, *p*-xylene and 1,3,5-TMB, were investigated. For *p*-xylene the *co*-solvent hexylbenzene with a boiling point of 226 °C was found to result in the best film quality with a surface roughness R_a of 10 nm (12.5%, Table 5.1). For 1,3,5-TMB the *co*-solvent octylbenzene (bp 261 °C) revealed best film formation properties with a surface roughness R_a of 5 nm (6%, Table 5.1). For lower or higher boiling point solvents, increased surface roughnesses were again observed.

When comparing the three main solvents, it was found that the boiling point difference between the main and the *co*-solvent has a crucial effect on the film formation quality. Figure 5.2 shows that an optimal boiling point difference between main and *co*-solvent exists, which ensures the lowest surface roughness. As found here, the most favorable boiling point difference is between 90 and 100 °C. In addition, Figure 5.2 reveals that an increased boiling point of the main solvent (toluene < *p*-xylene < 1,3,5-TMB) results in lower surface roughnesses even if there is only a smaller difference in boiling point between the main solvent and the *co*-solvent. Therefore, a higher boiling main solvent tolerates a broader range of boiling point differences for a good film formation. In this study the solvent system 1,3,5-trimethylbenzene/octylbenzene represents the best solvent system with an optimal film formation and the smallest roughness for **1** ($R_a = 5$ nm).

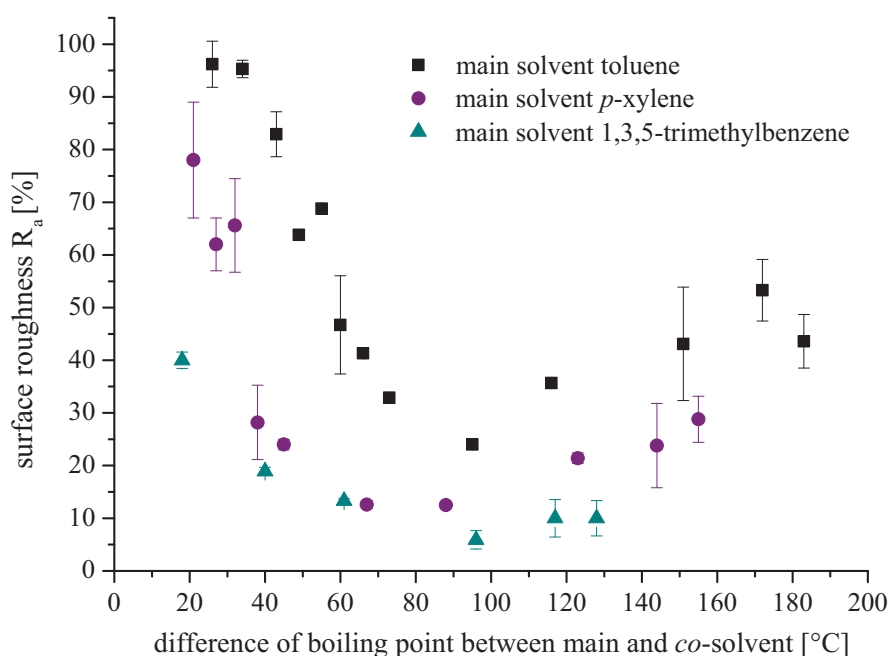


Figure 5.2 Surface roughness R_a vs. boiling point difference between main and *co*-solvent for inkjet printed films of polymer **1** (4 mg/mL). The ratio main/*co*-solvent is 90/10 v/v.

To identify the potential of the newly found solvent system, the solvent systems toluene/*ortho*-dichlorobenzene (*o*-DCB) and chlorobenzene/*o*-DCB, which are frequently used in other reports, were investigated.^[7,39] Both solvent systems revealed a surface roughness R_a of >25 nm and a decreased film homogeneity in comparison to the solvent system 1,3,5-TMB/octylbenzene. Hence, the latter solvent system represents a significant improvement for a smooth film formation by means of inkjet printing.

To proof, if the new solvent system is also suitable for other classes of π -conjugated polymers, the P(DPP-*co*-BTD-*co*-F) **4** and the PPV **11** were tested concerning their film formation characteristics using 1,3,5-TMB/octylbenzene as solvent system. The investigations showed that the solvent system is suitable to reach surface roughnesses R_a of 6 nm and 8 nm for **4** and **11**, respectively. It is therefore believed that for the applicability of a certain solvent system in the inkjet printing process, the solubility of the polymer is the most critical issue. All polymers revealed a good solubility, due to side-chains attached to the polymer backbone.

As a conclusion, it was shown that the choice of solvent system is crucial to reveal homogeneous layers as well as applicable film thicknesses. Both film properties can be tuned by the solvent's boiling points as well as the solvent system ratio. A good alternative to change the concentration of an ink in order to reveal thinner as well as more homogeneous films is the approach of increasing the boiling point of the ink by:

- i) the choice of the main solvent;
- ii) the choice of the *co*-solvent;
- iii) the main solvent/*co*-solvent ratio.

The optimization of inkjet printed thin films is dependent on a variety of parameters that need to be screened systematically. Factors of influence are mainly determined by the drying speed and the amount of deposited material. To tune the quality of inkjet printed films, the solvent/solvent system, concentration, dot spacing and substrate temperature need to be chosen carefully. Figure 5.3 depicts an overview of the most important parameters, which reveal an influence to the quality of inkjet printed films. The optical profiler images show how each parameter affects the film formation. In order to optimize the thin-film formation, a balance needs to be found between the influences of each parameter. However, other parameters like the surface tension and the viscosity of the solvent system do not show a significant effect to the observed film formation properties in the investigated range.

Since the parameters affect each other and cannot be studied individually the findings here stress the importance of a combinatorial screening of film properties for varying ink characteristics. Moreover, optimal processing parameters cannot be easily predicted by a simple investigation of selected ink properties; a systematic investigation of materials, processing conditions as well as resulting film properties is required. By using inkjet printing, this process can be performed in a fast and simple manner with small amounts of materials.

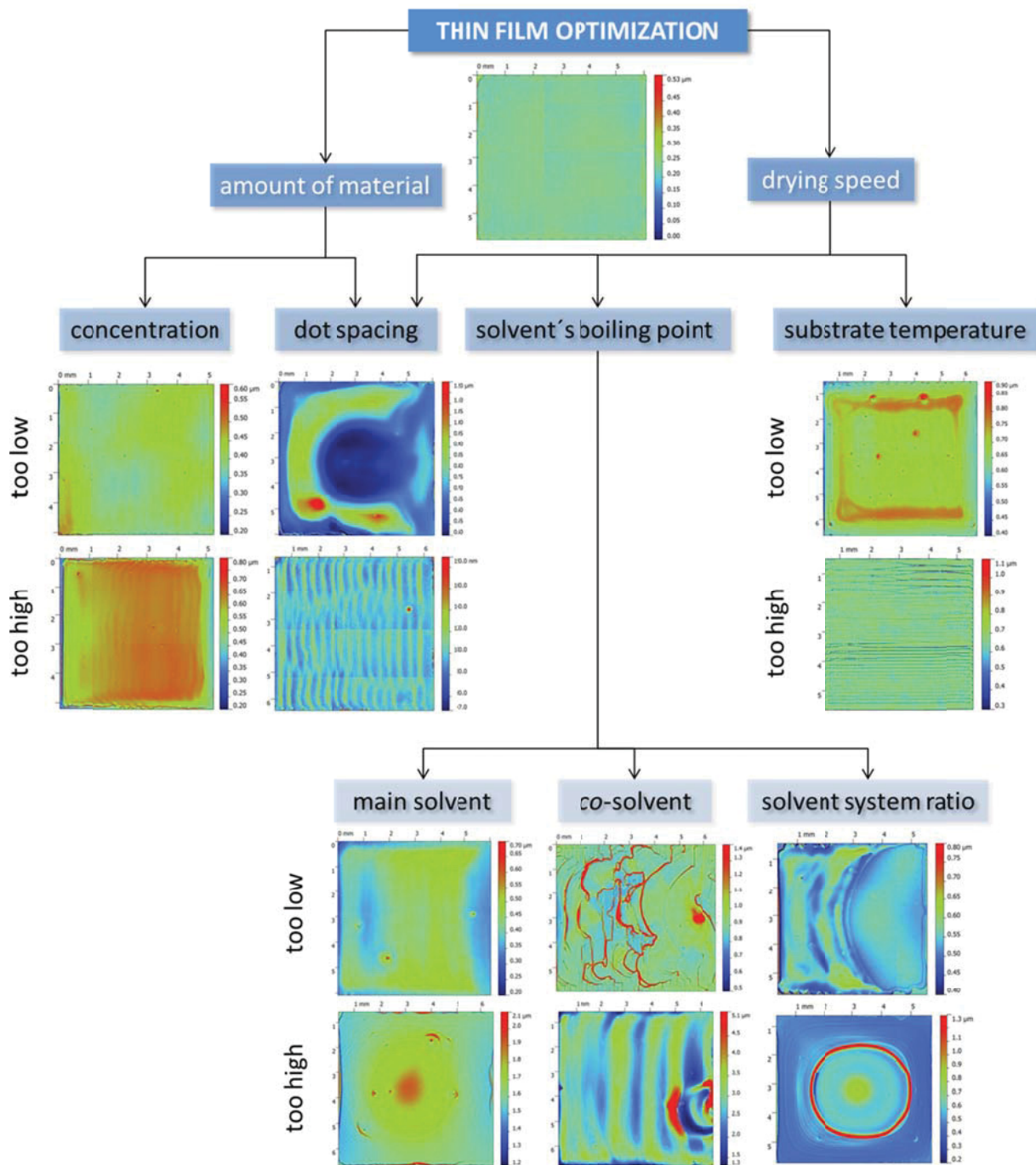


Figure 5.3 Overview of the most important parameters that influence the quality of inkjet printed films, including optimization pathways for a homogeneous film formation.

6 Screening of π -conjugated polymers for organic photovoltaics

Parts of this chapter have been published/will be published: 3) A. Teichler, J. Perelaer, F. Kretschmer, M. D. Hager, U. S. Schubert, *Macromol. Chem. Phys.* **2013**, 214, 664-672. 5) A. Teichler, S. Hölzer, J. Nowotny, J. Perelaer, S. Hoepfner, F. Kretschmer, C. Bader, M. D. Hager, U. S. Schubert, *ACS Comb. Sci.*, accepted.

A well investigated polymer for OPV applications is poly(3-hexylthiophene) (P3HT). Currently, power conversion efficiencies of up to 5% have been reported using this polymer.^[14] However, polythiophenes are limited in their photon harvesting properties since their absorption does not match the maximum photon flux of the solar spectrum.^[55] Improved photon harvesting characteristics are obtained by donor-acceptor polymers that consist of multiple building units that match different absorption regions of the solar spectrum.^[56] Well-known building units for such polymers are, for example, diketopyrrolopyrrole (DPP), benzothiadiazole (BTD) and fluorene (F). The beneficial properties, including the narrow bandgap of the DPP moiety,^[57] good photovoltaic properties of BTD^[58] and easy tailoring characteristics of F,^[59] can be combined into a single donor-acceptor polymer. Such polymers reveal a low bandgap and favorable optical properties such as a broad absorption up to 750 nm.^[60]

A polymer library that consists of a new polymer class, poly(diketopyrrolopyrrole-*co*-benzothiadiazole-*co*-fluorene) (P(DPP-*co*-BTD-*co*-F)), with varying amounts of the DPP and BTD moieties, was investigated systematically using inkjet printing. The effect of polymer composition, different solvents and solvent systems to the optical properties of inkjet printed films was studied.

Figure 6.1 represents the chemical structure of the P(DPP-*co*-BTD-*co*-F) library including their composition. A detailed representation of the polymer characteristics (M_n , PDI) can be found in Table 3.2. Furthermore, an image of an inkjet printed polymer library is depicted, wherein the polymer composition and the effect of the applied dot spacing were screened on a single substrate.

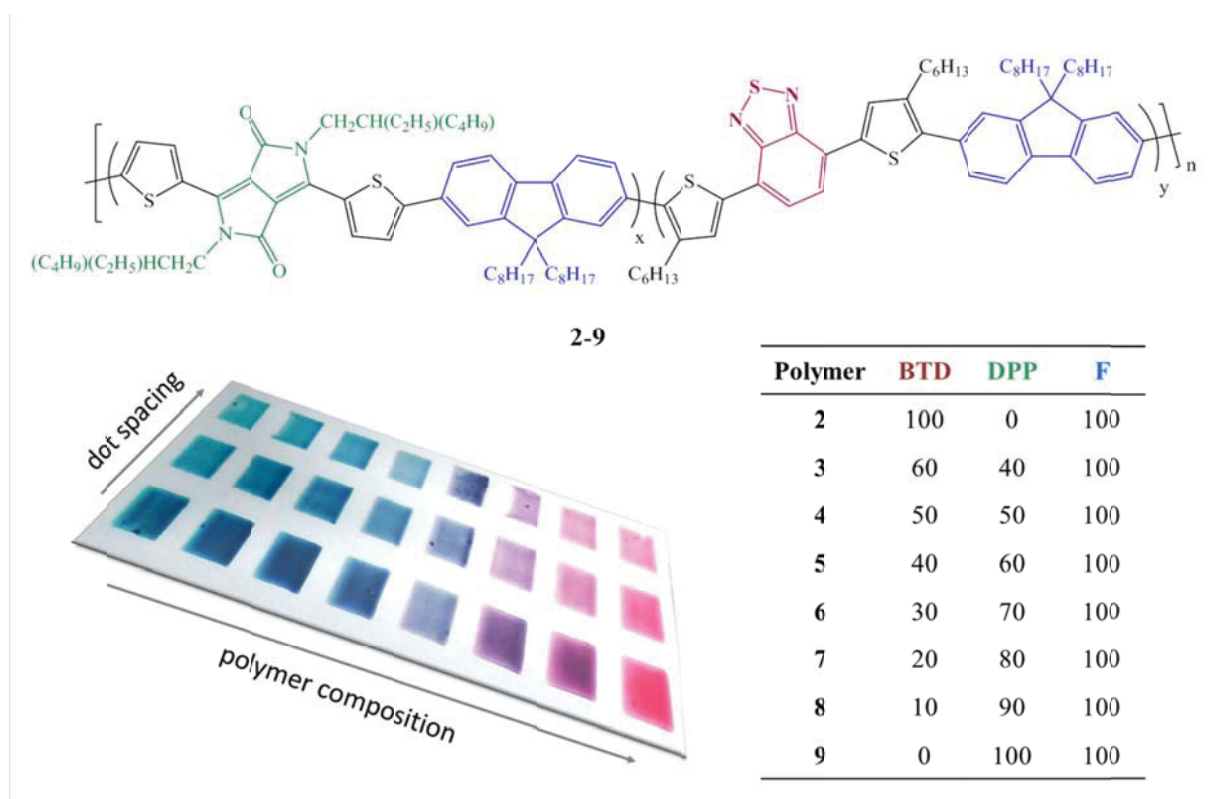


Figure 6.1 Overview of the composition of the P(DPP-co-BTD-co-F) library. Image of the inkjet printed polymers 2-9 in dependence of the dot spacing.

In Chapter 4 the film formation of this polymer library was presented for polymer 4. However, not only the homogeneity of the printed films determine the quality of the final organic devices, but also the optical properties of the films. First of all, the effect of the three different solvent systems toluene/*o*-DCB, CB/*o*-DCB and *o*-xylene/*o*-DCB (with a solvent ratio of 90/10) to the absorption and emission characteristics of inkjet printed films of polymer 4 was investigated (Figure 6.2). It can be seen that the use of the solvent system toluene/*o*-DCB results in the best properties: the intensity of the absorption bands at 530 nm and 660 nm for toluene/*o*-DCB is significantly increased (compared to the short wavelength absorption at 350 nm) in comparison to the other two solvent systems. In particular, an increased absorption at higher wavelengths is preferred for the application in OPVs.^[61] The emission band at 694 nm is observed for all three solvent systems. The shoulder at 750 nm, which represents an indication for interactions between the polymer chains, is independent on the choice of solvent system. The absorption and emission spectra shown in Figure 6.2a represent the optical characteristics of inkjet printed films by using an identical dot spacing (140 μ m), which results for all three solvent systems in different film thicknesses: 155 nm for toluene/*o*-DCB, 120 nm for CB/*o*-DCB and 100 nm for *o*-xylene/*o*-DCB. For the first two solvent systems, the applied dot spacing represents the best film formation, whereas for the

latter one, an optimal film formation could not be revealed at any dot spacing due to a strong agglomeration, *i.e.* the films have a higher surface roughness. The absorption of a π -conjugated polymer is dependent on the dot spacing, *i.e.* film thickness (Figure 6.2b). For polymer **4** an increase in intensity with decreasing dot spacing is revealed and the absorption peaks at 600 nm and 660 nm are more pronounced. Therefore, the optimal processing conditions, such as the dot spacing and the solvent system, reveal an influence on the optical properties of π -conjugated polymer films.

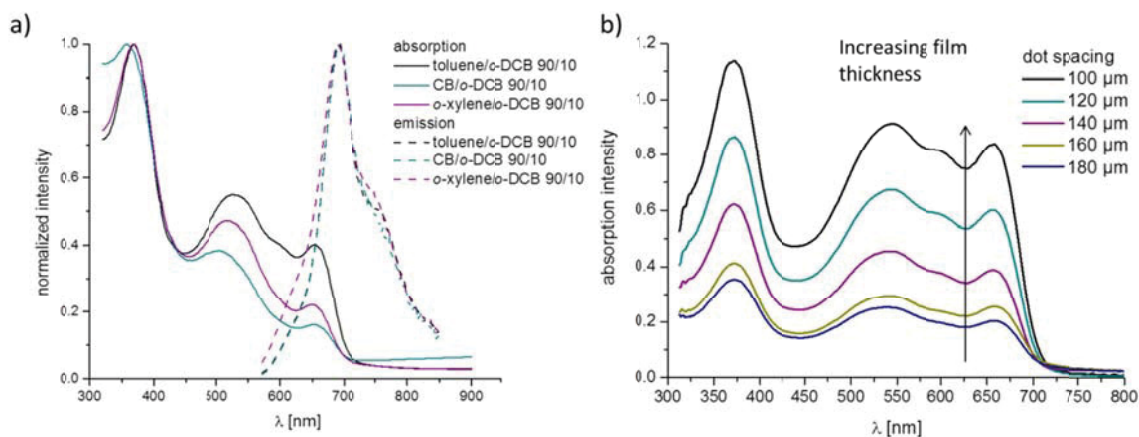


Figure 6.2 Optical properties of polymer **4** by using different solvent systems (a) as well as different dot spacings (b).

Since the drying time of a wet π -conjugated polymer film strongly influences the absorption behavior of the dried film, the influence of the toluene/*o*-DCB ratio was investigated for polymer **3** (Figure 6.3). A higher *o*-DCB content, which leads to a longer drying time, revealed only a slight increase of the absorption intensity at 540 nm and 660 nm for the ratios 70/30 and 50/50. The emission characteristics are equal for the three solvent ratios. Therefore, the change of the solvent system ratio has only a minor influence.

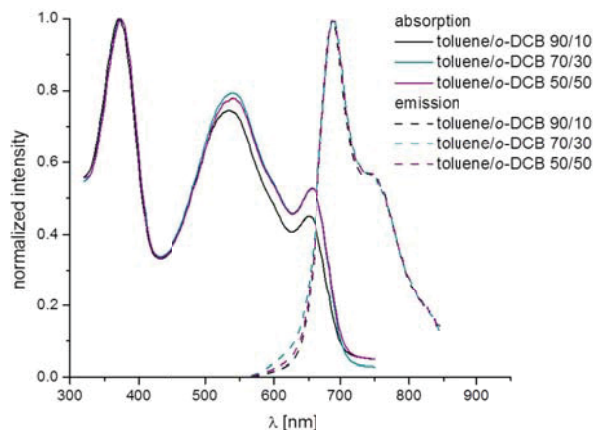


Figure 6.3 Optical properties of inkjet printed films of polymer **3** by using different solvent ratios.

The absorption and emission characteristics of all eight P(DPP-co-BTD-co-F) polymers **2** to **9** in solution and as inkjet printed films are depicted in Figure 6.4 and summarized in Table 6.1. Polymer **2**, which exhibits only the building units F and BTD, has in solution two absorption peaks at 350 nm and 510 nm. By incorporating a DPP unit, the polymer absorption exhibits two more peaks at approximately 590 nm and 640 nm. With increased DPP content the intensity of the absorption peak at 640 nm increases and red-shifts to 655 nm. At the same time, since the BTD-content is decreasing, the absorption peak at around 510 nm decreases. As a result of the red-shifted absorption with increasing DPP-content, the optical bandgap of the polymers decreases from 2.12 eV for polymer **2** to 1.80 eV for polymer **9**. In the inkjet printed films, the polymers show a clear red-shift in absorption (~ 9 to 18 nm) in comparison to their solutions, which is attributed to a further planarization of the polymer backbone in the films.^[62] As a result, the optical bandgaps of the polymers in the films are reduced: from 1.98 eV for **2** to 1.70 eV for **9**. As for the absorption, the emission of the polymer library depends on the polymer composition. Polymer **2** reveals a single emission peak at 640 nm in solution, which is shifted to 662 nm in the film. With increasing DPP content the main emission peak with a high wavelength-shoulder is located at 660 nm, shifting to 676 nm. In the film, the emission is clearly red-shifted by 20 to 36 nm and the intensity of the higher wavelength shoulder is increased with increasing DPP content.

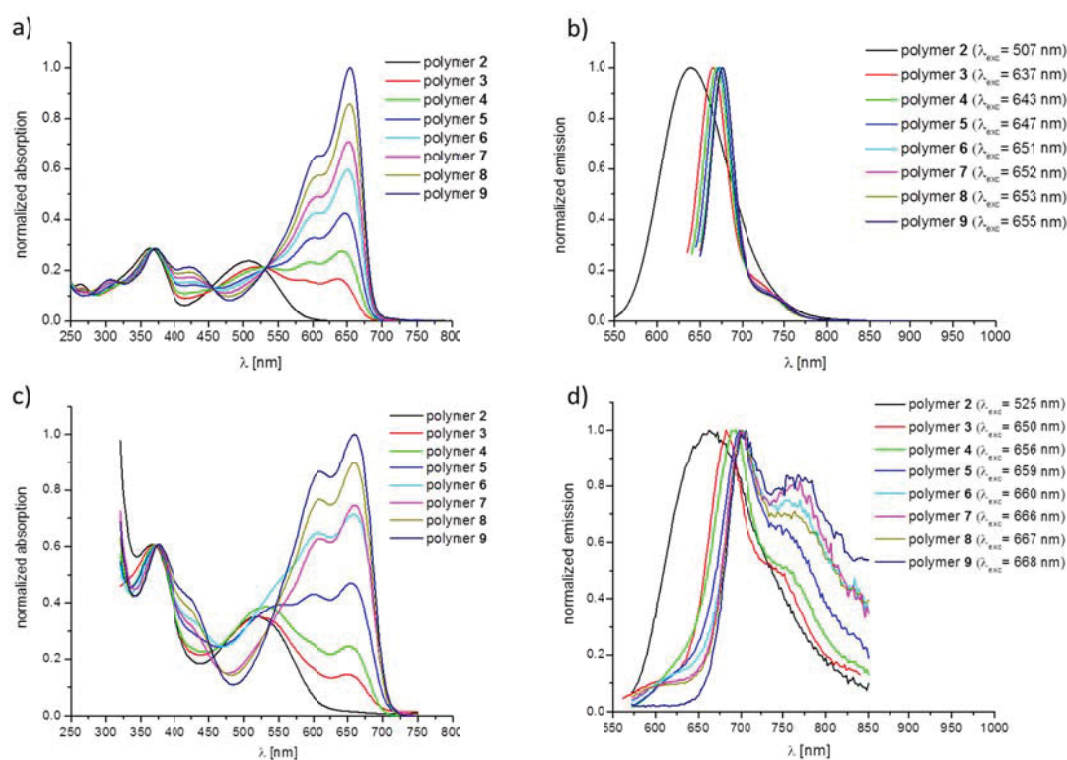


Figure 6.4 Absorption (a,c) and emission (b,d) spectra of polymers **2** to **9** in solution (a,b) and as inkjet printed films (c,d).

Table 6.1 Absorption and emission characteristics of polymers **2-9** in solution and as inkjet printed films.

Polymer	$\lambda_{\text{abs, sol.}}$ [nm]	$\lambda_{\text{PL, sol.}}$ [nm]	$E_{\text{g, sol.}}$ [eV]	$\lambda_{\text{abs, film}}$ [nm]	$\lambda_{\text{PL, film}}$ [nm]	$E_{\text{g, film}}$ [eV]
2	507	639	2.12	525	662	1.98
3	637	662	1.82	650	682	1.78
4	643	667	1.82	656	694	1.80
5	647	670	1.81	659	698	1.75
6	651	675	1.81	660	700	1.75
7	652	676	1.81	666	700	1.74
8	653	676	1.81	667	702	1.70
9	655	676	1.80	668	704	1.68

A straight forward approach to increase the absorption range of an inkjet printed polymer film is blending of two polymers with different absorption behaviors. Improved performances of organic solar cell devices have been reported in literature by using a ternary active layer of polymer/polymer/fullerene^[63,64] or polymer/small molecule/fullerene.^[65] Thereby, the fullerene derivatives act as electron acceptor and the polymer as electron donor.

In order to optimize the absorption of the active layer materials, the blend system consisting of poly(3-octylthiophene) (P3OT) **1** and P(DPP-*co*-F) **9** was investigated according to film formation and optical behavior.

Figure 6.5a shows the absorption spectra for the mixtures of **1** and **9** in solution. The peak at around 450 nm is assigned to **1** and the peaks at 376 nm, 430 nm, 608 nm and 660 nm to **9**, respectively. After inkjet printing (Figure 6.5b), the UV-Vis spectra show a significant broadening in the region of 650 to 750 nm, by adding a small fraction of **9**, leading to an overall absorption range between 350 nm and 750 nm. The absorption peaks of the film are in comparison to the solution behavior more structured as well as red-shifted. The blend ratio **1/9** 60/40 shows the broadest and most intense absorption of the investigated blends. Hence, this ratio was used for further investigations.

The absorption spectrum of **1** in the solid state is characterized by polythiophene interchain interactions that lead to a more ordered phase of the polymer and, hence, to a lower bandgap.^[59] It is worth notable that the specific P3OT interchain interaction in the solid state (550 nm, 610 nm) is still observed when mixed with **9**. Thus, it can be assumed that the addition of **9** does not interrupt the formation of highly ordered thiophene crystals.

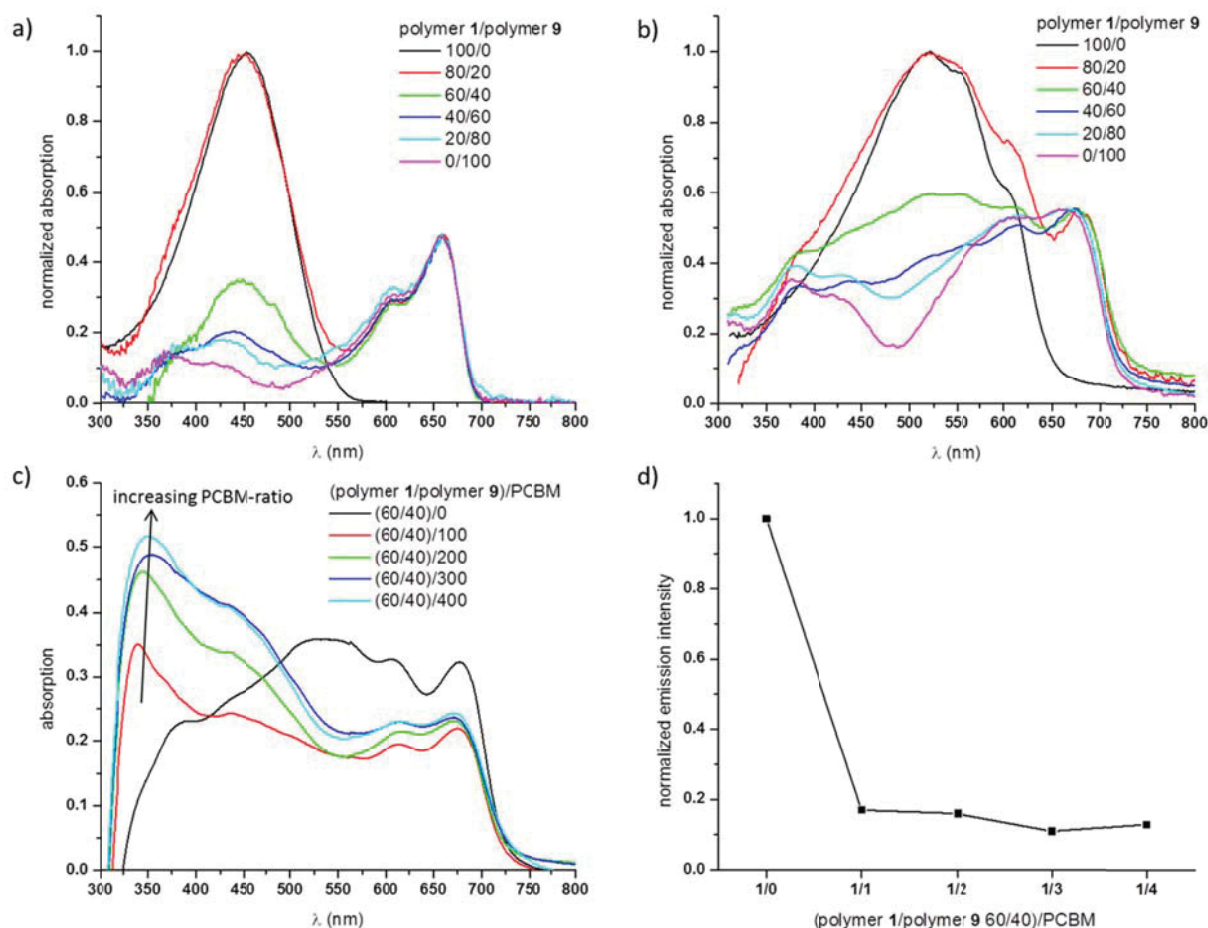


Figure 6.5 Absorption spectra of binary **1/9** mixture in solution (**a**) and as inkjet printed films (**b**). Absorption (**c**) and normalized emission intensity (**d**) of inkjet printed films of the ternary blends (**1/9**)/PCBM with a **1/9** ratio of 60/40.

Ternary blends were prepared from the **1/9** 60/40 mixtures by adding mono(1-[3-(methoxycarbonyl)propyl]-1-phenyl)-[6,6] C_{61} (PCBM) as electron-accepting unit, which is commonly used in active layers of organic solar cells.^[54] The polymer blend/PCBM ratios of 1/1, 1/2, 1/3 and 1/4 were inkjet printed and investigated according to their film formation behavior and optical properties. The absorption spectra of the polymer blend **1/9** 60/40 in the mixture with different amounts of PCBM are shown in Figure 6.5c. The intensity of the absorption peak at 320 nm is increasing with higher PCBM contents. The polymer absorption peaks reveal a slight blue shift upon addition of PCBM.

A quick indication of effective mixing and charge separation within the active layer can be given by measuring the photoluminescence quenching of the ternary blends. A high quenching of the emission was found for all investigated (**1/9**)/PCBM blends. The maximum quenching was observed for a ratio of (**1/9**)/PCBM (40/60)/300 (Figure 6.5d), indicating an appropriate charge transfer in the blend film.

However, the morphology affects the charge transport through the active layer significantly and is crucial for an evaluation of applicable polymer/fullerene blends or active layer preparation conditions for OPVs.^[59] For this purpose, atomic force microscopy (AFM) measurements were performed on selected blends. For the binary polymer/fullerene blends **1**/PCBM 1/1 (Figure 6.6a,d) and **9**/PCBM 1/3 (Figure 6.6b,e) smooth film surfaces with a surface roughness R_a of 1 nm are obtained. The inkjet printed film of **9**/PCBM shows a good phase separation, which is reported to be a suitable active layer morphology.^[66]

1/PCBM films prepared by inkjet printing from CB/*o*-DCB revealed fibrillar domains of P3OT that represent a highly ordered self-organization of the chains (Figure 6.6d). The morphology observed for the as-printed film is comparative to spin-coated films after annealing or additive addition.^[66,67] Post-processing annealing methods, like thermal or solvent annealing, in order to reorganize the polythiophene chains into the preferred fibrillar structure, which result in improved charge transport properties are reported in literature. As shown here, P3OT reveals self-organized domains in the blend with PCBM already in the as-inkjet printed films prepared at room temperature. The reason for the differences in film formation characteristics can be explained by the use of different film preparation techniques. When using conditions that cause a slow film drying, *e.g.* by inkjet printing, the polythiophene chains are able to form highly ordered structures during drying of the film. In contrast, when the drying proceeds too fast, *e.g.* by using spin-coating, the formation of the thermodynamically preferred crystalline polythiophene phases cannot take place.

AFM measurements of the ternary blend (**1**/**9**)/PCBM (60/40)/300 (Figure 6.6c,f) reveal a smooth (surface roughness R_a 1 nm) and well mixed layer morphology. The typical main chain crystals of the P3OT, which are observed in the binary **1**/PCBM blend, were not observed in the ternary blend films. This is in agreement with the findings of the absorption spectra of the (**1**/**9**)/PCBM blend, where only weak signals, which correspond to the P3OT interchain interactions, were found. In contrast, the band structure of **1** was observed in the absorption spectra of the binary blend **1**/**9** 60/40. Hence interchain interactions of **1** should also occur in **1**/**9** blends. As a result, the interruption of the self-organization of P3OT is only observed in the ternary blend film. Although improved absorption characteristics of the ternary blend films are observed, morphological investigations reveal an un-preferred P3OT morphology in comparison to the binary **1**/PCBM mixture. To answer the question whether the successful mixing of two polymers with PCBM in a ternary blend reveals an enhanced solar cell performance, solar cell characteristics need to be measured, which is planned for the near future.

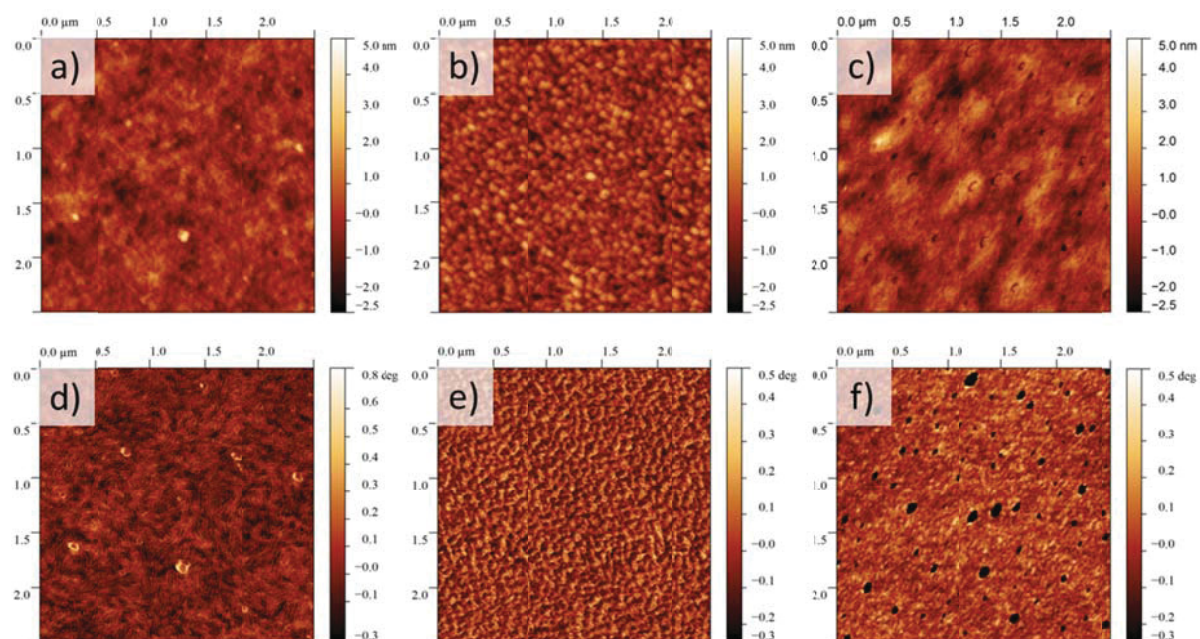


Figure 6.6 AFM height (top) and phase (bottom) images of inkjet printed films of 1/PCBM 1/1 (a,d), 9/PCBM 1/3 (b,e), and (1/9)/PCBM (60/40)/300 (c,f).

Since not only optical film characteristics but also morphological properties are important for an evaluation of promising donor/acceptor blends for solar cells, the combinatorial screening workflow presented here can only limit the amount of samples to be tested, but cannot provide a selection of one best donor/acceptor combination. Since morphological investigations represent a serious bottleneck for a fast and efficient screening procedure, the combinatorial screening workflow is of high importance, since it reduces the amount of samples significantly.

7 Inkjet printing towards organic light emitting diodes

Parts of this chapter have been published/will be published: 4) A. Teichler, Z. Shu, A. Wild, C. Bader, J. Nowotny, G. Kirchner, S. Harkema, J. Perelaer, U. S. Schubert, *Eur. Polym. J.* **2013**, DOI:10.1016/j.eurpolymj.2013.03.031. 6) A. Wild, A. Teichler, C.-L. Ho, X.-Z. Wang, H. Zhan, F. Schlütter, A. Winter, M. D. Hager, W.-Y. Wong, U. S. Schubert, *J. Mater. Chem. C* **2013**, *1*, 1812-1822. 7) A. Wild, A. Teichler, C. v. d. Ehe, A. Winter, M. D. Hager, B. Yao, B. Zhang, Z. Xie, W.-Y. Wong, U. S. Schubert, *Macromol. Chem. Phys.* **2013**, DOI:10.1002/macp.201300003.

Besides the control of the optical properties of inkjet printed thin films by the processing conditions, another strategy is to tailor the chemistry of the polymers. The electroluminescence emission color of π -conjugated polymers is mainly determined by the chromophore, which is defined by the chemical structure as well as the conjugation length of the polymer backbone.^[67] The introduction of donor-acceptor dyes favors the formation of the energetically less stable quinoid structure, which leads to a lower energy absorption and emission maxima. Moreover, to fine-tune the emission color, the conjugation length of the polymer can be varied by *ortho* or *meta* connection of the monomeric units, enabling a hypsochromic shift of the emission wavelength. In general, the tunable band gap allows the synthesis of π -conjugated polymers with customized optical properties.^[68]

By the chemical tailoring, three π -conjugated polymers with red, green and blue (RGB) emission colors are prepared for OLED applications. Different polymer structures were utilized, including a poly(fluorene-phenylene) **10**, a poly(phenylene-vinylene) (PPV) **11** and a poly(phenylene-ethynylene)-poly(phenylene-vinylene) (PPE-PPV) **12** copolymer (Figure 7.1).

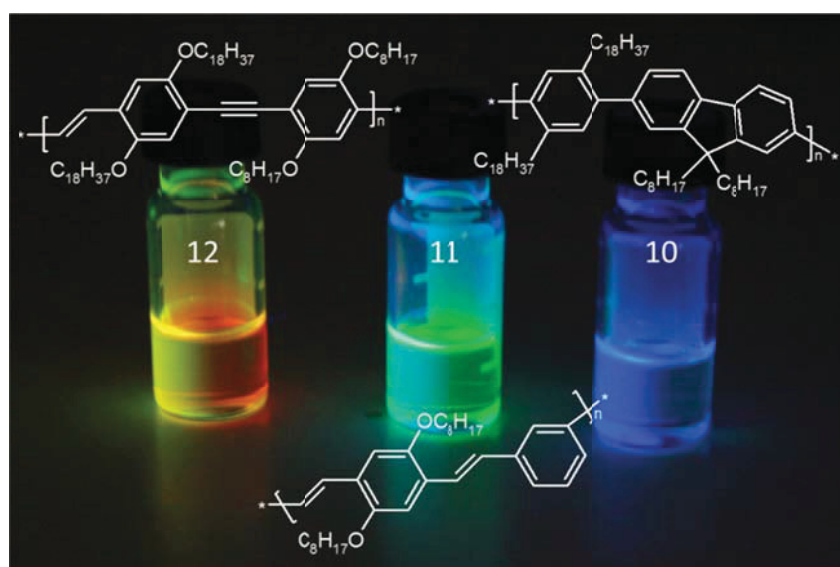


Figure 7.1 Schematic representation of the chemical structures of polymers **10**, **11** and **12** as well as photograph of the polymer inks (excited at 366 nm).

For the fabrication of emissive layers for OLED devices by inkjet printing, the polymers **10**, **11** and **12** were dissolved in the solvent system toluene/*ortho*-dichlorobenzene (*o*-DCB) with varying concentrations. A film thickness of approximately 80 nm is required to achieve good light emitting efficiencies.^[69] Different ink concentrations (3 to 8 mg/mL) were tested for their film formation behavior, resulting film thickness as well as film roughness for polymer **12**. A concentration of 4 mg/mL was observed as optimal ink parameter since the surface roughness shows a local minimum of 10 nm at a film thickness of 80 nm. The optimal ink parameters found for polymer **12** were successfully applied to the polymers **10** and **11**, since all inks have similar fluid properties and, as a result, equal printing characteristics. Figure 7.2 shows optical profiler images of optimized inkjet printed films of the polymers **10**, **11** and **12** revealing a homogeneous film formation. For the polymers **10** and **11** a dot spacing of 120 μm yielded a film thickness of approximately 72 nm and 80 nm, respectively. Indicated by the cross-sections, the homogeneity of the inkjet printed films of **10** and **11** is improved compared to polymer **12**.

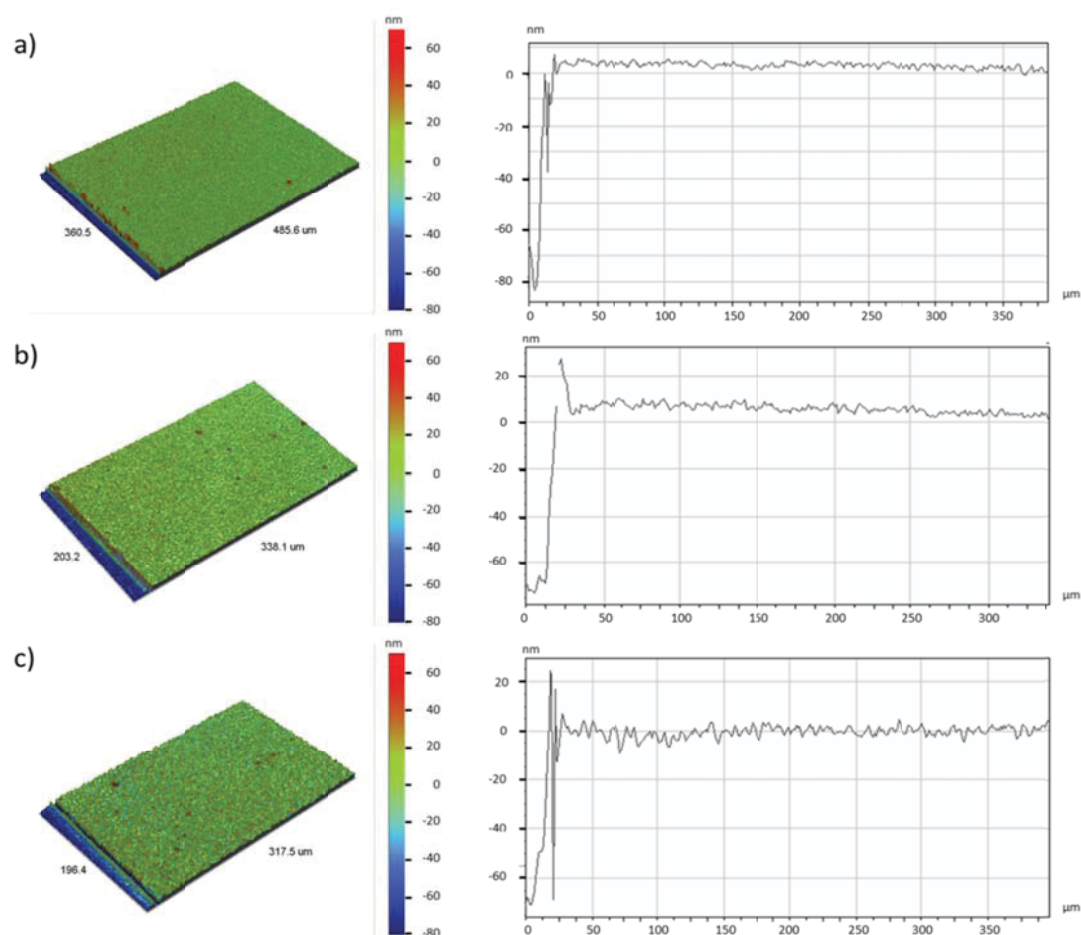


Figure 7.2 Optical profiler images (left) and corresponding cross-sections (right) of thin films inkjet printed from optimized ink and printing conditions (4 mg/mL, toluene/*o*-DCB 90/10): polymer **10** (a), polymer **11** (b) and polymer **12** (c).

As a result, the optimized ink properties found for **12** can be easily transferred to the other two polymers, yielding a high control over film formation even for different polymer classes. One reason for this observation might be the high solubility of all three polymers in the solvent system, which ensures a good printability and a stable droplet formation.

The absorption and emission spectra of the solutions and inkjet printed thin films of all three polymers are shown in Figure 7.3 and the optical properties are summarized in Table 7.1. A printed film of polymer **10** shows two absorption peaks at 370 nm and 383 nm revealing an optical bandgap of 3.04 eV. Photoluminescence is observed in the blue region at 413 nm with a shoulder at around 435 nm. Compared to the solution, the film exhibits two main absorption peaks, indicating that solid state aggregation occurs.^[70] Polymer **11** absorbs in the solid state at 416 nm and emits at 504 nm with a shoulder at 536 nm. As a result, polymer **11** has a bandgap of 2.61 eV and an emission in the green region. For polymer **12**, an absorption wavelength at 470 nm and emission wavelengths at 560 nm and 578 nm were observed revealing an orange-red emitting polymer with a bandgap of 2.35 eV. A pronounced shoulder at higher wavelengths could be observed in the absorption spectra of the solid state, indicating that aggregation formation occurs during film drying. Whereas polymer **12** has in solution a single main emission peak with a small shoulder, two emission peaks are observed in the solid state. All three polymers reveal in the solid state a red-shifted absorption in comparison to solution, which is more pronounced in the PPE-PPV-based polymer **12** than in the fluorene-based polymer **10**.^[70]

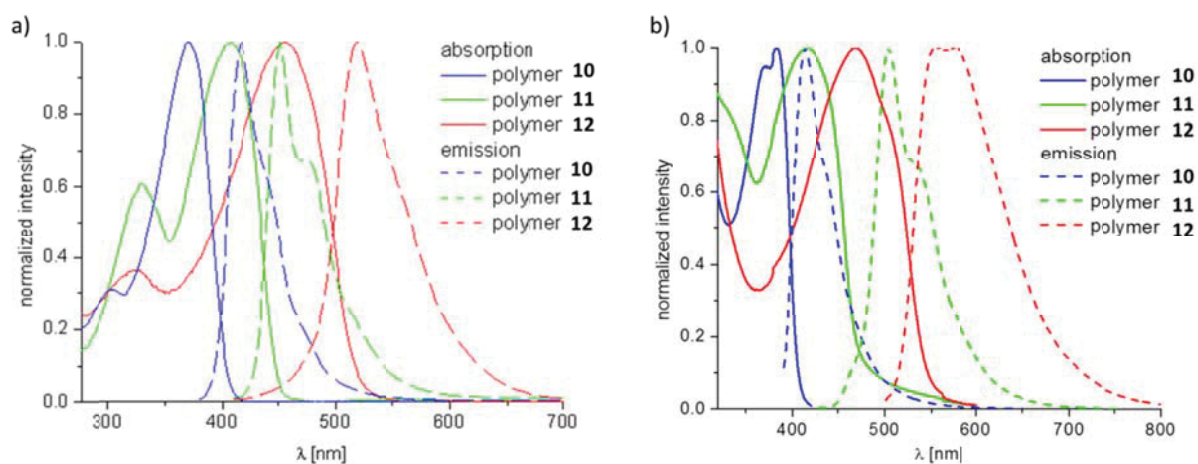


Figure 7.3 Absorption and emission of polymers **10**, **11** and **12** in solution (a) and as inkjet printed films (b) prepared from toluene/*o*-DCB 90/10 (4 mg/mL).

Table 7.1 Absorption and emission characteristics of polymers **10**, **11** and **12** in solution and as inkjet printed films.

	$\lambda_{\text{abs, sol}}$ [nm]	$E_{\text{g, sol}}$ [eV]	$\lambda_{\text{PL, sol}}$ [nm]	Φ_{PL}	$\lambda_{\text{abs, film}}$ [nm]	$E_{\text{g, film}}$ [eV]	$\lambda_{\text{PL, film}}$ [nm]	Film thickness [nm]
10	372	3.08	417	0.71	370, 383	3.05	413, 435 (s)	72
11	408	2.77	452	0.80	416	2.58	504, 536 (s)	80
12	455	2.40	519	0.48	470	2.28	560, 578	80

OLEDs with a size of 1 mm × 1 mm were prepared by using the optimized printing conditions found for each polymer. Figure 7.4a shows the output spectra of the red and green OLED device including the optical appearance of the film homogeneity during electrical excitation. The OLED of polymer **11** shows electroluminescence at 505 nm with a shoulder at 530 nm, which is comparable with the photoluminescence characteristics of the polymer. The OLED of polymer **12** reveals a broad output spectrum with a maximum intensity at 585 nm. Both polymer OLEDs show a relative good homogeneity during electrical excitation. In contrast, the OLEDs of polymer **10** display no light output since the polymer layer is short cut upon an increased voltage. The J-V curves of the OLEDs of polymer **11** and **12** reveal that light is emitted at relative high voltages (> 10 V), whereas polymer **11** requires less electrical consumption than the OLED of polymer **12** (Figure 7.4b).

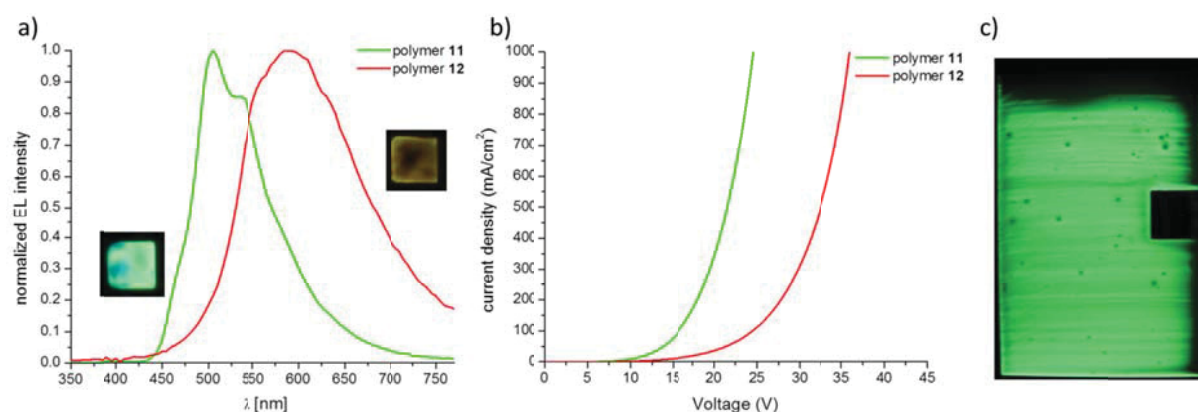


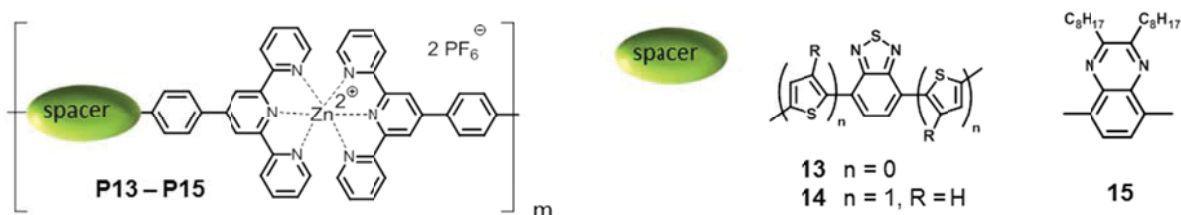
Figure 7.4 Output spectra and photographs of the (1 mm × 1 mm) OLED devices using a driving current and voltage of 5 mA and 19.8 V for polymer **11** and 5 mA and 32.1 V for polymer **12** (a). J-V curves of the OLED devices (1 mm × 1 mm) (b) and photograph of a 20 mm × 30 mm OLED of polymer **11** (c).

When printing the OLEDs with a size of 20 mm × 30 mm, a limitation of inkjet printing is encountered using a single nozzle print head. As the films are prepared by a line-by-line deposition, the size of an inkjet printed film is crucial for the drying process, since the lines start to dry before printing of the entire film is completed. The resulting film formation

of polymer **11** (Figure 7.4c) reveals a clear line formation, leading to a decreased film homogeneity and emission quality. A multi-nozzle print head would decrease the preparation time and, as a consequence, improve the film quality.

Besides RGB, white organic light emitting materials are of interest both in the scientific and industrial communities, due to their great potential in lighting applications and as back-lights in liquid-crystal displays. Usually, the white light results from a simultaneous emission of red, green and blue chromophores or of two complementary colors, *e.g.* orange and blue.^[71] A library of Zn^{II} *bisterpyridine* coordination polymers with a central dye moiety, surrounded by thiophene donors was assembled in order to tune emission colors towards white light emitting layers. A large number of donor-based π -conjugated *bisterpyridines* was published until now, however, the reported absorption and emission maxima are most often in the region of $\lambda_{\text{abs}} = 400$ nm and $\lambda_{\text{PL}} = 450$ to 470 nm, respectively.^[72] In contrast to metal-free conjugated polymers, there are only a few examples of donor-acceptor-based *bisterpyridines* reaching emission maxima of $\lambda_{\text{PL}} > 550$ nm.^[73] For OLED devices, however, materials emitting in the red region ($\lambda_{\text{EL}} \sim 650$ nm) are required as well.

The systematic modification of the dye and the conjugation length in the Zn^{II} *bisterpyridine* coordination polymers enabled the tuning of the absorption and emission maxima. The green-emitting polymer **13** ($\lambda_{\text{PL}} = 503$ nm) and the red-emitting polymer **14** ($\lambda_{\text{PL}} = 606$ nm), both based on a 2,1,3-benzothiadiazole system, and the blue-emitting quinoxaline-containing *bisterpyridine* **15** ($\lambda_{\text{PL}} = 424$ nm) were utilized in the inkjet printing process (Scheme 7.1).



Scheme 7.1 Schematic representation of the chemical structures of Zn^{II} *bisterpyridine* polymers.

In order to avoid the preparation of different mixtures of the three polymers for the tuning of film emission color, the single colors were printed separately on top of each other. This printing procedure represents a material-efficient as well as variable approach.^[74] The assembly of statistical copolymers and thereby a homogeneous film formation was ensured by printing a solvent layer after the last layer. The kinetic lability of the Zn^{II} *bisterpyridine*

complex ($t_{1/2} < 0.1$ min) in solution state allows, thereby, the reorganization and formation of statistical copolymers within the printed films. The combinatorial, two-dimensional variation of multiple parameters revealed that a solvent system of DMF/acetophenone (90/10), a concentration of 5 mg/mL and a substrate temperature of 50 °C represented suitable settings to print *bisterpyridine* Zn^{II} coordination polymers.^[75] Using these parameters, homogeneous films of the pure blue, green and red polymers were printed.

The amount of deposited material in the inkjet printing process can be easily varied by the dot spacing. The films of pure polymers were printed with a dot spacing of 90 μm , resulting in the most homogeneous film formation and a film thickness of approximately 300 nm. All other compound ratios could be realized by adjusting the dot spacing accordingly. To enable an efficient process, the printing sequence was maintained, starting from blue followed by green, red, and a subsequent layer of pure solvent. Figure 7.5 depicts typical optical profiler images of the work flow for the printing of a film consisting of layers of **15** (blue) and **14** (red) in a ratio of 80/20. After printing the bottom layer (blue, dot spacing 100 μm), the red layer was printed with a dot spacing of 200 μm . Due to this high dot spacing, the resulting film quality is very low (Figure 7.5b). However, after an additional layer of pure solvent (dot spacing 90 μm), a homogeneous film was obtained (Figure 7.5c).

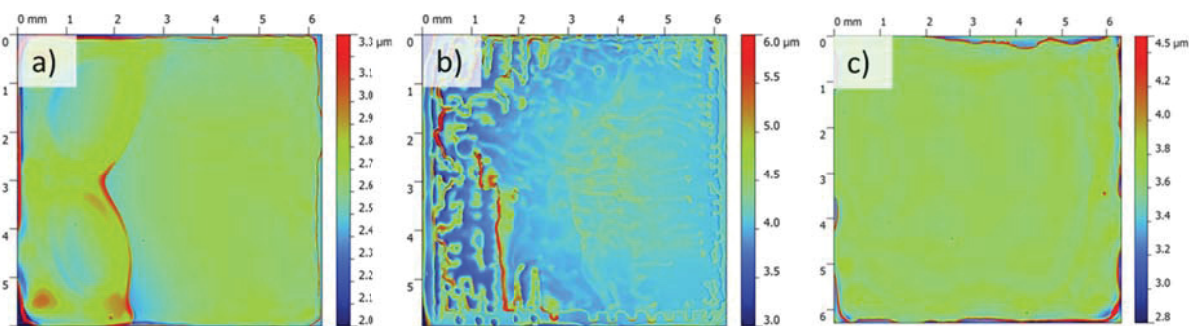


Figure 7.5 Optical profiler images after printing of (a) **15** (dot spacing 100 μm), (b) **14** (dot spacing 200 μm) and (c) solvent (dot spacing 90 μm) on top of each other.

Figure 7.6b shows a picture of the inkjet printed films, excited at $\lambda_{\text{ex}} = 365$ nm, corresponding to the mixing triangle depicted in Figure 7.6a. The corners of this triangle represent the pure polymers **13** (G, F12), **14** (R, A7) and **15** (B, A12), whereas the borders are mixtures of two polymers. The six films in the middle are composed of all three polymers. The polymer ratio was varied in 20% steps. The emission spectra of the BGR films (Figure 7.6c) reveal tunable emission colors of the inkjet printed films. The CIE coordinates of each column of the mixing triangle follow a line, enabling the estimation of the color of unknown mixtures (Figure 7.6d).

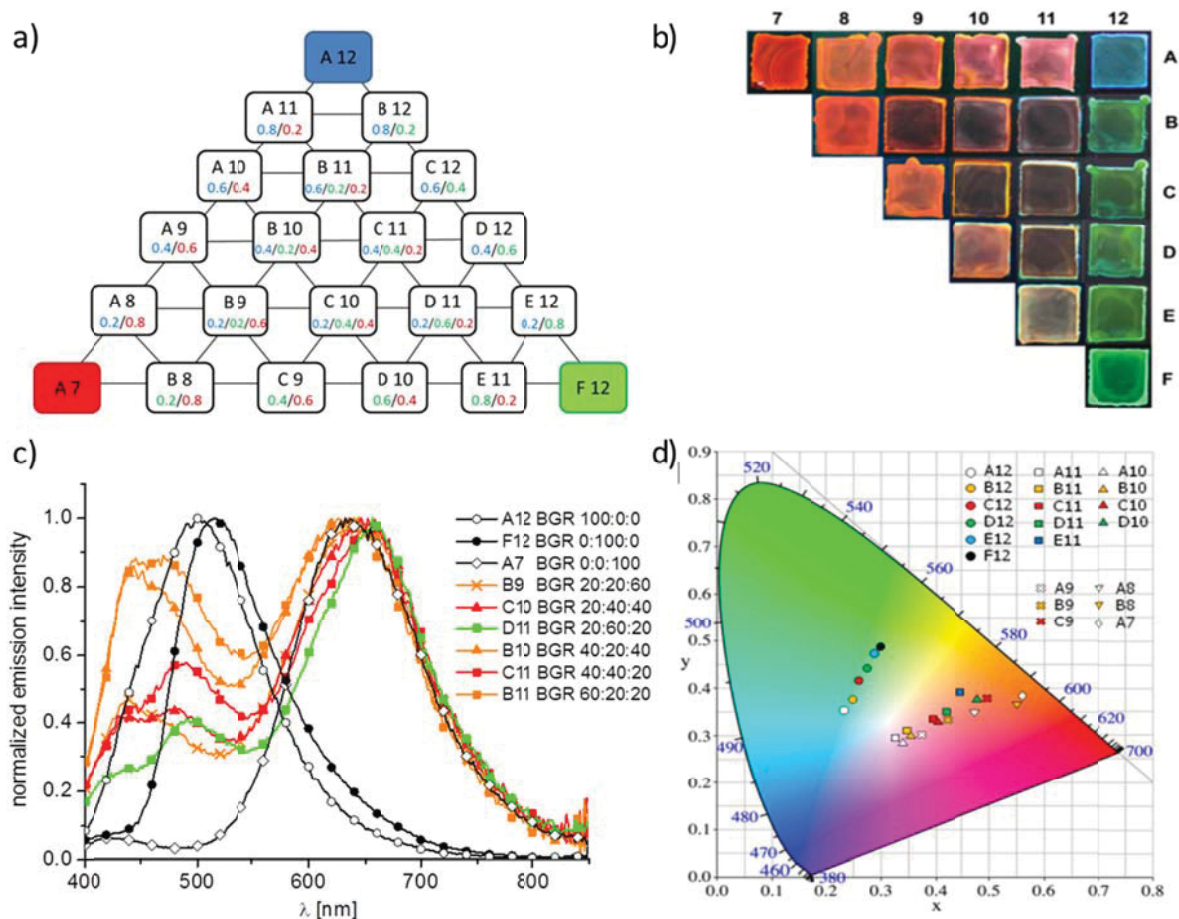


Figure 7.6 Mixing triangle (a), picture of the inkjet printed films (6 mm \times 6 mm each, $\lambda_{\text{ex}} = 365$ nm) (b), emission spectra of the inkjet printed films of BGR (c) and the position of the photoluminescence in the CIE space (d).

In order to prove, if homogeneous copolymers are formed, the film BGR 20/40/40 was prepared, while using a different printing order. Additionally, the emission spectra of these films were compared with metallo-copolymer ones of the same composition, which were prepared beforehand and printed at once (Figure 7.7a). For that reason, i) the ink of the homopolymers **15**, **13** and **14** (20/40/40) were mixed in a closed vial and ii) a copolymer with the respective monomer ratio was prepared analogous to the homopolymers. The emission spectra are only slightly influenced by the printing order and also the films of the premixed homo- and the copolymer displays similar emission behavior (Figure 7.7a). Since, inkjet printing reveals a reproducibility value of 96 to 99% a minor variation between the emission spectra needs to be tolerated.^[30] Thereby, the concept of metallo-copolymerization by inkjet printing was proven.

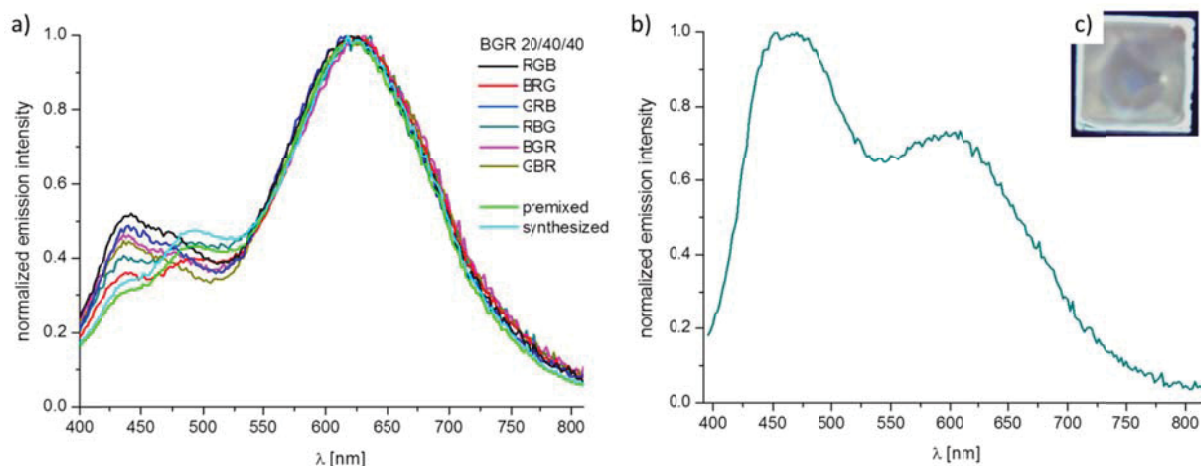


Figure 7.7 Emission spectra of the film C10 printed in different order in comparison to premixed polymer (film, $\lambda_{\text{ex}} = 365$ nm) (a). Emission spectrum (b) and picture (c) of the inkjet printed film of BGR 80/10/10 ($\lambda_{\text{ex}} = 365$ nm).

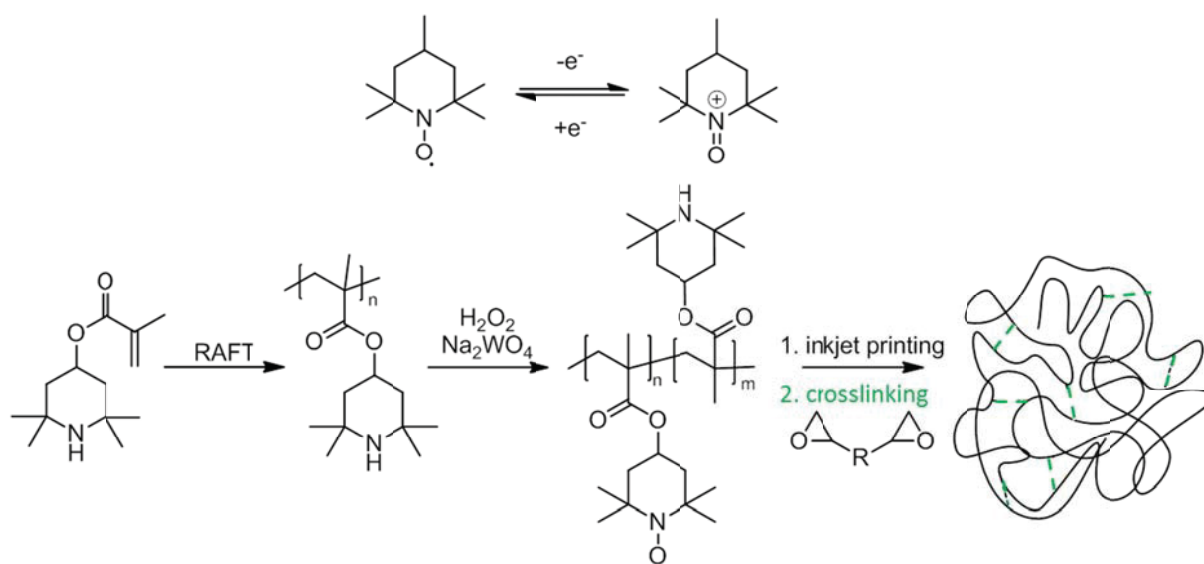
Finally, the possibility to assemble a white emitting film was investigated. According to the CIE graph depicted in Figure 7.6d, the aimed white color is located between the films A12 (100/0/0) and B11 (60/20/20). Therefore, a film using a polymer ratio of 80/10/10 was printed. The respective emission spectrum ($\lambda_{\text{ex}} = 365$ nm) shows a broad emission over the visible region with a maximum in the blue ($\lambda_{\text{PL}} = 452$ nm) and the orange/red ($\lambda_{\text{PL}} = 608$ nm) region (Figure 7.7b,c). The resulting CIE coordinates of $x = 0.311$ and $y = 0.307$ confirm the white color perception.

Further investigations regarding improved processability of Zn^{II} bisterpyridine coordination polymers *via* solvent-based film preparation techniques at room temperature triggered the introduction of polymeric side chains (poly(styrene) or poly(methacrylate)). As a result, improved solubility in a variety of organic solvents could be observed, which leads to an enhanced control over the film formation. Homogeneous films of the metallo-polymers with a surface roughness < 10 nm could be produced *via* inkjet printing by using the solvent system CB/*o*DCB 90/10.

8 Inkjet printing of organic electrodes for radical batteries

Parts of this chapter have been published/will be published: 8) T. Janoschka, A. Teichler, A. Krieg, M. D. Hager, U. S. Schubert, *J. Polym. Sci., Part A: Polym. Chem.* **2012**, *50*, 1395. 9) T. Janoschka, A. Teichler, B. Häupler, T. Jähnert, M. D. Hager, U. S. Schubert, *Adv. Energy Mater.* **2013**, DOI 10.1002/aenm.201300036.

For mobile applications, batteries need to be lightweight, flexible, thin and easily to be produced. In this context, printing technology paves the way for the cost efficient manufacturing of flexible batteries. While most batteries rely on metal based electrode materials, which often show unwanted environmental issues, the rapidly evolving class of organic radical batteries (ORB) employs organic polymers as active electrode material.^[76,77] ORB make use of an environmentally favorable polymer that carries redoxactive stable radicals, such as 2,2,6,6-tetramethylpiperidine-1-oxyl (TEMPO), Scheme 8.1.



Scheme 8.1 Schematic representation of the reversible redox reaction of a TEMPO radical (top). Schematic representation of the synthesis of radical polymer poly(2,2,6,6-tetramethylpiperidinyloxy-4-yl methacrylate) (PTMA), oxidation, and subsequent thermal crosslinking with a multifunctional epoxide (bottom).

Simple, solution-based processing techniques like spin-coating^[78] and doctor blading^[79] are generally employed for the fabrication of ORB electrodes. The disadvantages of such techniques are their tendency to waste much of the material as well as the inflexibility in shape and size of the electrode layout. Advanced processing techniques such as inkjet printing can greatly improve the manufacturing of organic radical battery electrodes.

For the electrode design, the polymer needs to be highly soluble in solvents, which are suitable for the inkjet printing process. On the other hand, the polymer has to be insoluble in

the electrolyte solution (*e.g.*, organic carbonates) employed in the assembled device. Electroactive radical polymers are processable *via* inkjet printing, if the requirement in good solubility, *i.e.*, a low molar mass is given. In order to avoid the solubility of the polymer film in the electrolyte solution, the inkjet printed film needs to be crosslinked afterwards. Therefore, a simple crosslinking approach was applied.

The TEMPO radical based polymer poly(2,2,6,6-tetramethylpiperidinyloxy-4-yl methacrylate) (PTMA), is commonly prepared from the monomer 2,2,6,6-tetramethylpiperidin-4-yl methacrylate by free radical polymerization and subsequent oxidation of amine bearing pre-polymer in order to form the redoxactive TEMPO radical polymer. If the oxidation step by hydrogen peroxide^[80] is incomplete a *co*-polymer is obtained (Scheme 8.1). The amino moieties, which are not oxidized to the nitroxide radicals, can therefore be used for further functionalization or crosslinking. Multifunctional epoxides (Scheme 8.1) were chosen as crosslinking agent. Since the polymer shows good thermal stability ($T_g = 160\text{ }^\circ\text{C}$), the crosslinking could easily be initiated by thermal treatment.

For ORB-electrodes, the ink has to contain besides the electroactive polymer a conductive additive as well. Additives, such as graphite^[81] are commonly used in literature. For inkjet printing, these materials proved to be unsuitable, as they cause clogging of the printing nozzle (inner diameter 70 μm). Carbon nanopowder, a material of much lower particle size (< 50 nm), was found to be suitable in the inkjet printing process.

PTMA is well soluble in many solvents, including dichloromethane, toluene, *N,N*-dimethylformamid (DMF), *o*-DCB, and *N*-methyl-2-pyrrolidone (NMP). Several combinations of these solvents were tested, whereas DMF was found to be most suitable, because it not only dissolves PTMA but also forms stable dispersions of the carbon nanopowder. Since inkjet printing from a single solvent causes the preferential accumulation of the ink material at the rim of a dried film, a *co*-solvent (NMP) in a content of 10 vol.% was added to the ink. As a result, the material is homogeneously distributed all over the film. Besides the active polymer and the conductive additive the crosslinking agent is the most important component of the ink. To ensure a high degree of crosslinking tetraphenylethane glycidyl ether was chosen, as it can react with up to four amine units. As films inkjet printed from the described ink caused the formation of brittle films, which peel off in the electrolyte solution, a plasticizer (ethylenecarbonate (EC)) was used. Upon addition of EC to the prescribed ink in an amount of 5 vol.%, a homogeneous and stable film was formed.

In order to study the stability of the inkjet printed electrodes, half-cells were built and charged/discharged repeatedly. The experiments were carried out in a temperature controlled cell at 30 °C employing a three electrode setup (Ag/AgCl reference electrode, platinum counter electrode, printed working electrode).

Inks that did not contain a crosslinking agent revealed a fast decrease in charge storage capacity. After only two cycles no active polymer was left. The stability of the electrode was enhanced by crosslinking the electrode using the optimized procedure described above. About 75% of the initial capacity was retained after 150 charging/discharging cycles (Figure 8.1). The decline can be attributed to a slow degradation of the electrode due to active polymer being washed out of the polymer composite. Increasing the amount of epoxide-crosslinker as well as using PTMA with up to 40% of free amine groups (60% oxidized to form TEMPO) did not result in a significantly improved stability. As the carbon nanopowder appears to be hindering the crosslinking process, epoxidized carbon nanopowder was prepared by reacting the powder with *m*-chloroperoxybenzoic acid.^[82] The epoxidized carbon can react with the free amine groups of the PTMA polymer and act as crosslinking agent itself, covalently linking the active polymer to the insoluble conductive additive. Thereby an increased cycling stability was achieved (Figure 8.1). After a slight increase of the charge storage capacity within the first cycles due to wetting/activation of the electrode the initial capacity was retained even after 150 cycles.

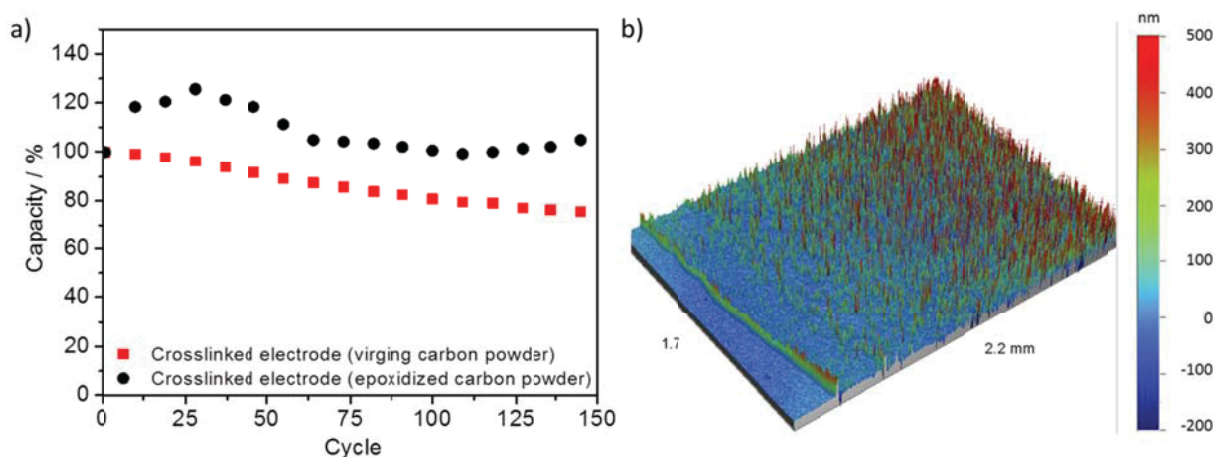


Figure 8.1 Charging/discharging curves of inkjet printed electrode (a). Optical profiler image of an inkjet printed electrode (b).

In summary, a reactive inkjet printing strategy for the manufacturing of printed electrodes used in organic radical batteries was developed. This technique might be of interest for the manufacturing of patterned, flexible organic radical batteries used in battery-powered smart cards.

9 Summary

In order to evaluate the potential of inkjet printing as film preparation technique, which can be employed for active layer materials in organic electronic devices, a detailed understanding of this preparation technique is required. Drying processes and the resulting film morphologies need to be well understood. This thesis provides an overview of methodical investigations of ink characteristics, printing conditions and final film properties. In particular, the possibility to integrate inkjet printing into a combinatorial screening workflow evolves inkjet printing to a notable method for an efficient screening of new materials for organic electronics applications like organic photovoltaics (OPVs), organic light emitting diodes (OLEDs) and organic radical batteries (ORBs, Figure 9.1).

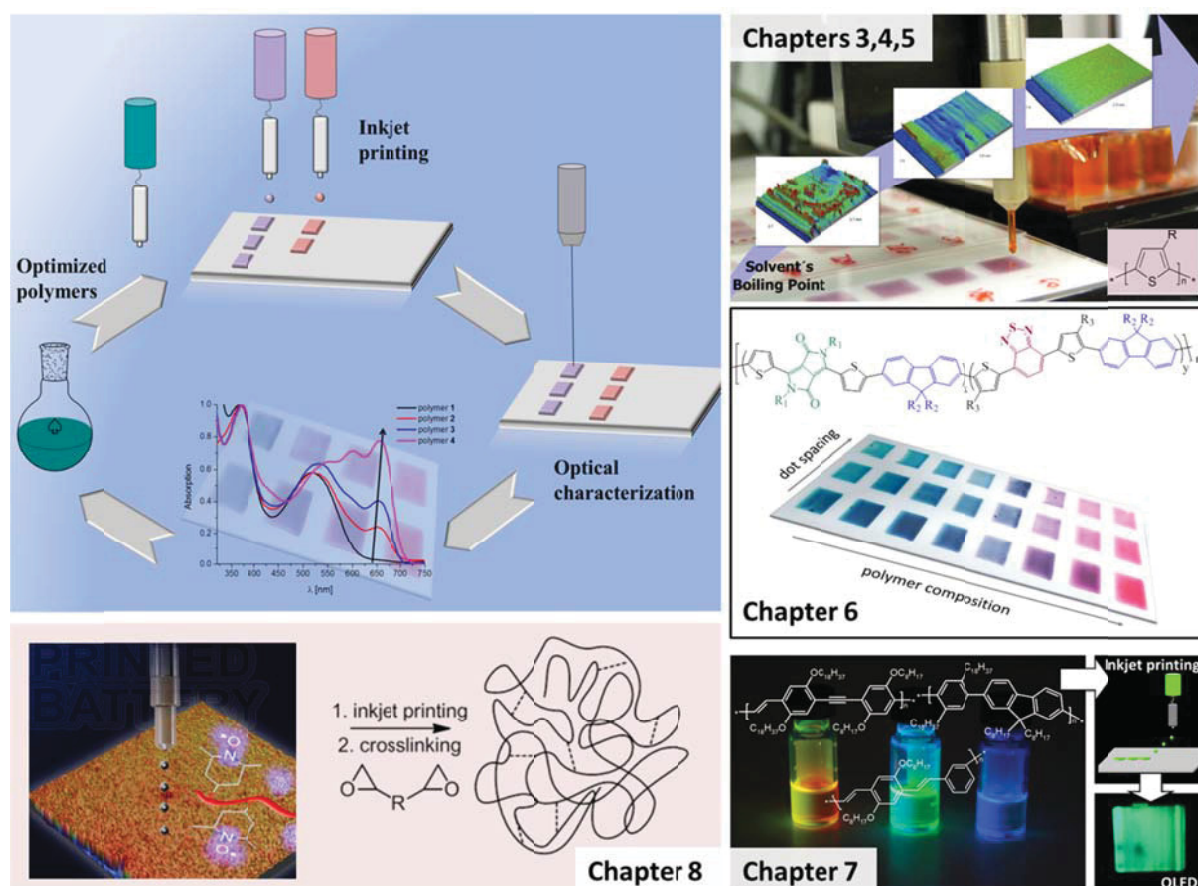


Figure 9.1 Overview of the content of the chapters presented in this thesis.

Fluid characteristics like surface tension, viscosity and contact angle of π -conjugated polymer inks are investigated, since these parameters reveal a crucial effect on the applicability of materials in the inkjet printing process. In the investigated concentration range (3 to 8 mg/mL) no limitations for a reproducible droplet formation were observed for the π -

conjugated polymers concerning the mentioned fluid characteristics. In contrast, the processing conditions reveal a superior influence on the quality of inkjet printed films. Factors of influence are mainly determined by the drying speed and the amount of deposited material. To tune the quality of inkjet printed films the solvent/solvent system, concentration, dot spacing and substrate temperature need to be chosen carefully. Optimal parameter values range between 120 to 160 μm for the dot spacing, 4 to 5 mg/mL for the concentration and 20 mm/s for the printing velocity, respectively. A critical parameter for the application of a single nozzle print head is the film size. Uniform films could be easily prepared in dimensions up to 8 mm \times 8 mm. Using larger film sizes a line formation is observed, which is an indication for a too fast drying before the entire film is printed. For an increased film size, a higher content of the high boiling solvent leads to an improved control over the film formation. Using solvent ratios of toluene/*ortho*-dichlorobenzene 70/30 instead of 90/10 resulted not only in thinner films, but also in lower surface roughnesses. As most important factor, the boiling point of the applied solvent system shows a significant effect towards the thin-film optimization. The choice of the solvent system is crucial to reveal homogeneous layers as well as applicable film thicknesses. Both film properties can be tuned by the solvent's boiling points as well as the solvent system ratio. Optimal solvent parameters are the following:

- i) boiling point (bp) of the main solvent: $110\text{ }^\circ\text{C} < \text{bp} < 170\text{ }^\circ\text{C}$;
- ii) boiling point of the *co*-solvent, *i.e.* difference between main and *co*-solvent: 90 to 100 $^\circ\text{C}$;
- iii) main solvent/*co*-solvent ratio: 90/10 to 70/30.

With the obtained overview of film drying characteristics functional polymers were screened with regard to their potential application in organic electronic devices. The optical and morphological properties of a π -conjugated terpolymer library are screened, whereas optimal processing conditions resulted in films with a broad absorption behavior between 350 and 750 nm as well as a well-segregated nano-morphology. By applying the combinatorial screening workflow optimal compound combinations either for polymer/fullerene or polymer/polymer/fullerene blends were revealed, which need to be tested for every single polymer. As a consequence, best processing conditions as well as materials were discovered for an application in OPVs. Using this approach, the immense number of potential polymers and processing parameter could be reduced in a material- and time-efficient manner.

Following a similar strategy, red, green and blue emitting polymers were employed in OLEDs in order to test the potential of single materials or the assembly of a white emitting layer. Finally, polymers containing organic radical moieties were investigated with regard to the development of environmentally friendly electrode materials for ORBs. A reactive inkjet printing approach was developed in order to produce stable electrode films.

The overview of film-quality-influencing parameters using inkjet printing provided in this work leads to an improved understanding of the effect of single ink or processing parameters to the final film properties and stress the importance of a combinatorial screening approach. As a result, inkjet printing can bridge the gap between polymer synthesis and solid-state property evaluation, since the technique opens the way to an automatic preparation of thin-film libraries of polymers, blends and composites with a systematic variation of parameters, such as chemical composition or thickness. Up to now, it was not possible to build high-efficient organic electronic devices from the optimized materials and the developed processing conditions due to the limited applicability of film sizes using a single-nozzle print head. Therefore, future challenges include the transfer of the gained knowledge to other inkjet printing systems and materials, in order to apply inkjet printing in an industry-relevant roll-to-roll process.

10 Zusammenfassung

Um das Potential des Tintenstrahldrucks als Filmpräparationsmethode zu beurteilen, welche für den Schichtaufbau von aktiven Polymeren in der organischen Elektronik zur Anwendung kommt, ist ein detailliertes Verständnis dieser Filmpräparationsmethode notwendig. Trocknungsprozesse und die resultierenden Filmmorphologien müssen verstanden werden. Die vorliegende Arbeit bietet einen Überblick über systematische Untersuchungen und Beziehungen von Tinteneigenschaften, Prozessbedingungen und Filmcharakteristika. Durch den Einsatz des Tintenstrahldrucks in einen kombinatorischen Arbeitsablauf verfügt diese Methode über entscheidende Vorteile gegenüber anderen Filmpräparationsmethoden hinsichtlich effizienten Prüfens neuer Materialien für die organische Elektronik, wie organische Solarzellen, organische Leuchtdioden und organische Radikalbatterien (Abbildung 10.1).

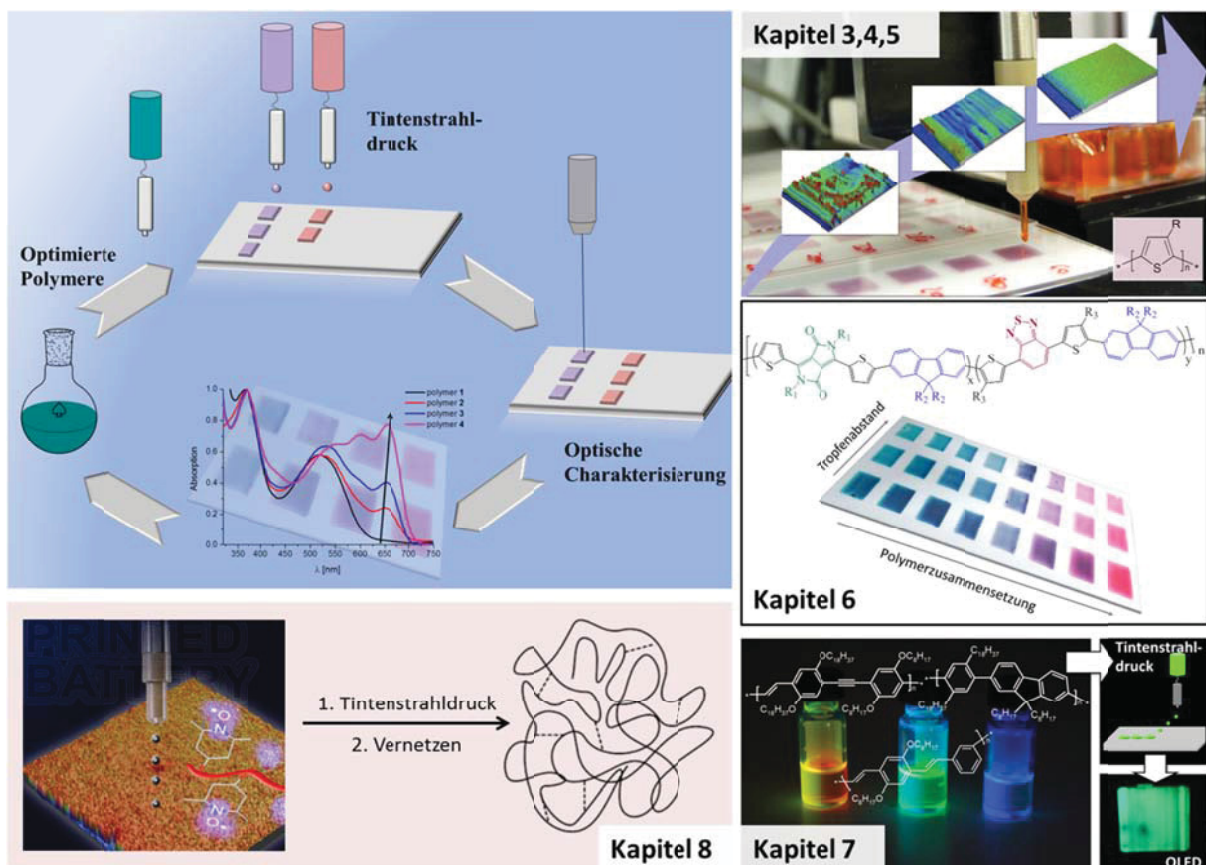


Abbildung 10.1 Überblick über die Inhalte der Kapitel dieser Arbeit.

Die Eigenschaften der Polymertinten wie Oberflächenspannungen, Viskositäten und Kontaktwinkel wurden untersucht, da diese Parameter die Eignung von Materialien für das Tintenstrahldrucken entscheidend bestimmen. Im untersuchten Konzentrationsbereich (3 bis 8 mg/mL) wurden keine Einschränkungen in der Verarbeitbarkeit der untersuchten π -konjugierten Polymere aufgrund instabiler Tropfenbildung beobachtet. Anders als die Tinteneigenschaften zeigten die Prozessparameter einen entscheidenden Einfluss auf die Qualität der gedruckten Schichten. Einflussfaktoren sind hauptsächlich einhergehend mit der Trocknungsgeschwindigkeit der gedruckten Filme sowie die Menge an aufgebrachtem Material. Um die Homogenität der hergestellten Schichten zu verbessern müssen das Lösungsmittel/Lösungsmittelsystem, die Konzentration, der Tropfenabstand sowie die Substrattemperatur systematisch ausgewählt werden. Optimale Werte der Verarbeitungsparameter liegen zwischen 120 und 160 μm für den Tropfenabstand, 4 bis 5 mg/mL für die Konzentration und 20 mm/s für die Druckgeschwindigkeit. Ein kritischer Prozessparameter für die Anwendung der Polymertinten unter Verwendung eines Ein-Düsen-Druckkopfes ist die Filmgröße. Homogene Schichten konnten problemlos bis zu einer Größe von 8 mm \times 8 mm hergestellt werden. Jedoch wurde bei größeren Filmabmessungen Linienbildung beobachtet, welche charakteristisch für ein zu schnelles Trocknen des gedruckten Materials ist. Für größere Filme führt eine Erhöhung des Gehaltes an hochsiedendem Lösungsmittel im Lösungsmittelgemisch zu einer Verlängerung der Trocknungszeit und damit zur Verbesserung der Schichthomogenität. Bei der Nutzung eines Lösungsmittelverhältnisses von 70/30 anstelle von 90/10 für das System Toluol/*ortho*-Dichlorbenzol konnte eine höhere Kontrolle über den Trocknungsprozess der gedruckten Schichten erreicht werden. Nicht nur die Oberflächenrauigkeit konnte verringert werden, sondern auch dünnere Schichten konnten durch die Anwendung höherer Tropfenabstände hergestellt werden. Wichtigster Einflussfaktor für die Kontrolle und Optimierung der Filmbildung mittels Tintenstrahldruckens ist somit der Verdampfungspunkt des Lösungsmittels. Die Wahl des Lösungsmittels bestimmt sowohl die Homogenität als auch die Dicke der Schichten und stellt somit das wichtigste Kriterium für die Anwendung der Filme in organischen Elektronikbauteilen dar. Der Verdampfungspunkt der Tinte kann im Druckprozess kontrolliert werden durch:

- Verdampfungspunkt (K_p) des Hauptlösungsmittels: $110\text{ }^\circ\text{C} < K_p < 170\text{ }^\circ\text{C}$;
- Verdampfungspunkt des Co-Lösungsmittels, *i.e.* Differenz zwischen Haupt- und Co-Lösungsmittel: 90 bis 100 $^\circ\text{C}$;
- Verhältnis zwischen Haupt- und Co-Lösungsmittel: 90/10 bis 70/30.

Mit dem erhaltenen Wissen über wichtige Einflussfaktoren für eine homogene Filmpräparation konnten funktionelle Polymere hinsichtlich ihrer potentiellen Anwendung in organischen Elektronikbauteilen untersucht werden. Die optischen als auch morphologischen Eigenschaften einer π -konjugierten Terpolymerbibliothek wurden erforscht. Optimale Prozessbedingungen resultierten dabei in Schichten hoher Homogenität mit einem breiten Absorptionsspektrum zwischen 350 und 750 nm. Durch die Herstellung und Untersuchung der Schichten konnten mittels des kombinatorischen Arbeitsablaufes auch binäre Polymer/Fulleren sowie ternäre Polymer/Polymer/Fulleren Mischungen hinsichtlich ihrer filmbildenden Eigenschaften und ihres Absorptionsverhaltens untersucht werden. Somit konnten mittels Tintenstrahldruckens verbesserte Prozessbedingungen für organische Solarzellen sowie neue potentielle Materialien systematisch und effizient untersucht sowie evaluiert werden. Mit Hilfe dieser Methode wurden ebenfalls rot-, blau- und grün-emittierende Polymere für die Anwendung in organischen Leuchtdioden hinsichtlich ihrer Verwendung als Einzelmaterial oder als weißlicht-emittierende Schicht untersucht. Letztendlich wurden Polymere, die organische Radikaleinheiten tragen, im Druckprozess angewendet und somit ihre Prozessierbarkeit als umweltfreundliche Elektroden für organische Radikalbatterien bewiesen. Stabile Elektroden konnten so durch reaktives Tintenstrahldrucken hergestellt werden.

Diese Arbeit bietet einen Überblick über die wesentlichen Parameter, die die Filmbildung mittels des Tintenstrahldrucks beeinflussen. Somit kann der Einfluss verschiedener Tinten- als auch Prozesseigenschaften auf die resultierenden Filmeigenschaften besser verstanden und auf neue Materialien angewendet werden. Zudem wird der Vorteil eines kombinatorischen Arbeitsprozesses durch zeit- und materialeffizientes Arbeiten deutlich. Die Herstellung von Dünnschicht-Bibliotheken von Polymeren und Mischungen mittels systematischer Variation von chemischen Material- oder resultierenden Filmeigenschaften schließt die Lücke zwischen Polymersynthese und der Untersuchung der Schichteigenschaften. Leider war es bisher nicht möglich, hocheffiziente organische Elektronikbauteile unter Verwendung der optimierten Material- sowie Prozesseigenschaften herzustellen, da die genutzten Instrumente mit nur einer Düse nur für kleine Filmdimensionen anwendbar ist. Deshalb müssen sich zukünftige Untersuchungen auf die Anwendung des erworbenen Wissens über den Druckprozess auf industrierelevante Rolle-zu-Rolle-Methoden beziehen.

References

- [1] F. C. Krebs, T. Tromholt, M. Jørgensen, *Nanoscale* **2010**, *2*, 873-886.
- [2] L. S. Hung, C. H. Chen, *Mat. Sci. Eng. R* **2002**, *39*, 143-222.
- [3] A. Facchetti, *Chem. Mater.* **2011**, *23*, 733-758.
- [4] F. C. Krebs, *Sol. Energ. Mat. Sol. C.* **2009**, *93*, 394-412.
- [5] P. Dutta, Y. Xie, M. Kumar, M. Rathi, P. Ahrenkiel, D. Galipeau, Q. Q. Qiao, V. Bommisetty, *J. Photon. Energy* **2011**, *1*, 011124.
- [6] S. Nilsson, A. Bernasik, A. Budkowski, E. Moons, *Macromolecules* **2007**, *40*, 8291-8301.
- [7] A. Teichler, R. Eckardt, S. Hoepfener, C. Friebe, J. Perelaer, A. Senes, M. Morana, C. J. Brabec, U. S. Schubert, *Adv. Energy Mater.* **2011**, *1*, 105-114.
- [8] H. M. Haverinen, R. A. Myllyla, G. E. Jabbour, *Appl. Phys. Lett.* **2009**, *94*, 0731081-0731083.
- [9] M. Sanyal, B. Schmidt-Hansberg, M. F. G. Klein, A. Colsmann, C. Munuera, A. Vorobiev, U. Lemmer, W. Schabel, H. Dosch, E. Barrena, *Adv. Energy Mater.* **2011**, *1*, 363-367.
- [10] Y. H. Chang, S. R. Tseng, C. Y. Chen, H. F. Meng, E. C. Chen, S. F. Horng, C. S. Hsu, *Org. Electron.* **2009**, *10*, 741-746.
- [11] F. C. Krebs, *Sol. Energ. Mat. Sol. C.* **2009**, *93*, 465-475.
- [12] S. E. Shaheen, R. Radspinner, N. Peyghambarian, G. E. Jabbour, *Appl. Phys. Lett.* **2001**, *79*, 2996-2998.
- [13] B. Derby, *Annu. Rev. Mater. Res.* **2010**, *40*, 395-414.
- [14] L. Y. Wong, R. Q. Png, F. B. S. Silva, L. L. Chua, D. V. M. Repaka, Shi-Chen, X. Y. Gao, L. Ke, S. J. Chua, A. T. S. Wee, P. K. H. Ho, *Langmuir* **2010**, *26*, 15494-15507.
- [15] M. T. Dang, G. Wantz, H. Bejbouji, M. Urien, O. J. Dautel, L. Vignau, L. Hirsch, *Sol. Energ. Mat. Sol. C.* **2011**, *95*, 3408-3418.
- [16] B. J. de Gans, P. C. Duineveld, U. S. Schubert, *Adv. Mater.* **2004**, *16*, 203-213.
- [17] B. J. de Gans, U. S. Schubert, *Macromol. Rapid Commun.* **2003**, *24*, 659-666.
- [18] R. D. Deegan, *Phys. Rev. E* **2000**, *61*, 475-485.
- [19] C. N. Hoth, P. Schilinsky, S. A. Choulis, C. J. Brabec, *Nano Lett.* **2008**, *8*, 2806-2813.
- [20] J. S. Yu, I. Kim, J. S. Kim, J. Jo, T. T. Larsen-Olsen, R. Søndergaard, M. Hosel, D. Angmo, M. Jørgensen, F. C. Krebs, *Nanoscale* **2012**, *4*, 6032-6040.
- [21] M. Barret, S. Sanaur, P. Collot, *Org. Electron.* **2008**, *9*, 1093-1100.
- [22] K. J. Baeg, D. Khim, J. H. Kim, M. Kang, I. K. You, D. Y. Kim, Y. Y. Noh, *Org. Electron.* **2011**, *12*, 634-640.
- [23] Y. Yoshioka, P. D. Calvert, G. E. Jabbour, *Macromol. Rapid Commun.* **2005**, *26*, 238-246.
- [24] E. Tekin, E. Holder, D. Kozodaev, U. S. Schubert, *Adv. Funct. Mater.* **2007**, *17*, 277-284.
- [25] C. N. Hoth, S. A. Choulis, P. Schilinsky, C. J. Brabec, *J. Mater. Chem.* **2009**, *19*, 5398-5404.
- [26] H. Do, M. Reinhard, H. Vogeler, A. Puetz, M. F. G. Klein, W. Schabel, A. Colsmann, U. Lemmer, *Thin Solid Films* **2009**, *517*, 5900-5902.
- [27] C. J. Brabec, S. Gowrisanker, J. J. M. Halls, D. Laird, S. J. Jia, S. P. Williams, *Adv. Mater.* **2010**, *22*, 3839-3856.
- [28] B. Schmidt-Hansberg, M. Sanyal, N. Grossiord, Y. Galagan, M. Baunach, M. F. G. Klein, A. Colsmann, P. Scharfer, U. Lemmer, H. Dosch, J. Michels, E. Barrena, W. Schabel, *Sol. Energ. Mat. Sol. C.* **2012**, *96*, 195-201.
- [29] A. Lange, M. Wegener, C. Boeffel, B. Fischer, A. Wedel, D. Neher, *Sol. Energ. Mat. Sol. C.* **2010**, *94*, 1816-1821.

- [30] B. J. de Gans, U. S. Schubert, *Langmuir* **2004**, *20*, 7789-7793.
- [31] B. J. de Gans, E. Kazancioglu, W. Meyer, U. S. Schubert, *Macromol. Rapid Commun.* **2004**, *25*, 292-296.
- [32] S. H. Ko, H. Pan, C. P. Grigoropoulos, C. K. Luscombe, J. M. J. Frechet, D. Poulidakos, *Nanotechnology* **2007**, *18*, 3452021-3452028.
- [33] V. Marin, E. Holder, M. M. Wienk, E. Tekin, D. Kozodaev, U. S. Schubert, *Macromol. Rapid Commun.* **2005**, *26*, 319-324.
- [34] J. S. Park, J. P. Kim, C. Song, M. Lee, *Displays* **2010**, *31*, 164-167.
- [35] D. Soltman, V. Subramanian, *Langmuir* **2008**, *24*, 2224-2231.
- [36] Y. Oh, J. Kim, Y. J. Yoon, H. Kim, H. G. Yoon, S. N. Lee, J. Kim, *Curr. Appl. Phys.* **2011**, *11*, S359-S363.
- [37] E. Tekin, B. J. de Gans, U. S. Schubert, *J. Mater. Chem.* **2004**, *14*, 2627-2632.
- [38] H. Hu, R. G. Larson, *J. Phys. Chem. B* **2006**, *110*, 7090-7094.
- [39] A. Teichler, R. Eckardt, C. Friebe, J. Perelaer, U. S. Schubert, *Thin Solid Films* **2011**, *519*, 3695-3702.
- [40] S. van Bavel, E. Sourty, G. de With, K. Frolic, J. Loos, *Macromolecules* **2009**, *42*, 7396-7403.
- [41] T. Aernouts, T. Aleksandrov, C. Giroto, J. Genoe, J. Poortmans, *Appl. Phys. Lett.* **2008**, *92*, 0333061-0333063.
- [42] A. Calabrese, A. Pellegrino, R. Po, A. Savoini, F. Tinti, N. Camaioni, *Sol. Energ. Mat. Sol. C.* **2011**, *95*, 3428-3432.
- [43] T. Wang, A. D. F. Dunbar, P. A. Staniec, A. J. Pearson, P. E. Hopkinson, J. E. MacDonald, S. Lilliu, C. Pizzey, N. J. Terrill, A. M. Donald, A. J. Ryan, R. A. L. Jones, D. G. Lidzey, *Soft Matter* **2010**, *6*, 4128-4134.
- [44] E. Tekin, H. Wijlaars, E. Holder, D. A. M. Egbe, U. S. Schubert, *J. Mater. Chem.* **2006**, *16*, 4294-4298.
- [45] H. Q. Zhang, R. Hoogenboom, M. A. R. Meier, U. S. Schubert, *Meas. Sci. Technol.* **2005**, *16*, 203-211.
- [46] R. Hoogenboom, M. A. R. Meier, U. S. Schubert, *Macromol. Rapid Commun.* **2003**, *24*, 16-32.
- [47] J. E. Fromm, *IBM J. Res. Dev.* **1984**, *28*, 322-333.
- [48] D. Jang, D. Kim, J. Moon, *Langmuir* **2009**, *25*, 2629-2635.
- [49] J. Perelaer, P. J. Smith, M. M. P. Wijnen, E. van den Bosch, R. Eckardt, P. H. J. M. Ketelaars, U. S. Schubert, *Macromol. Chem. Phys.* **2009**, *210*, 387-393.
- [50] B. Derby, *Annu. Rev. Mater. Res.* **2010**, *40*, 395-414.
- [51] Y. Kim, S. Cook, S. M. Tuladhar, S. A. Choulis, J. Nelson, J. R. Durrant, D. D. C. Bradley, M. Giles, I. McCulloch, C. S. Ha, M. Ree, *Nat. Mater.* **2006**, *5*, 197-203.
- [52] J. S. Liu, E. Sheina, T. Kowalewski, R. D. McCullough, *Angew. Chem. Int. Ed.* **2002**, *41*, 329-332.
- [53] A. J. Moule, K. Meerholz, *Adv. Mater.* **2008**, *20*, 240-245.
- [54] S. Günes, H. Neugebauer, N. S. Sariciftci, *Chem. Rev.* **2007**, *107*, 1324-1338.
- [55] D. Muehlbacher, M. Scharber, M. Morana, Z. G. Zhu, D. Waller, R. Gaudiana, C. Brabec, *Adv. Mater.* **2006**, *18*, 2884-2889.
- [56] J. Roncali, *Macromol. Rapid Commun.* **2007**, *28*, 1761-1775.
- [57] C. Zhuoying, M. J. Lee, R. S. Ashraf, Y. Gu, S. Albert-Seifried, M. M. Nielsen, B. Schroeder, T. D. Anthopoulos, M. Heeney, I. McCulloch, H. Sirringhaus, *Adv. Mater.* **2012**, *24*, 647-652.
- [58] L. E. Poander, L. Pandey, S. Barlow, P. Tiwari, C. Risko, B. Kippelen, J. L. Bredas, S. R. Marder, *J. Phys. Chem. C* **2011**, *115*, 23149-23163.
- [59] E. Bundgaard, F. C. Krebs, *Sol. Energ. Mat. Sol. C.* **2007**, *91*, 954-985.

- [60] F. Kretschmer, M. D. Hager, U. S. Schubert, *in preparation*.
- [61] T. Ameri, G. Dennler, C. Waldauf, H. Azimi, A. Seemann, K. Forberich, J. Hauch, M. Scharber, K. Hingerl, C. J. Brabec, *Adv. Funct. Mater.* **2010**, *20*, 1592-1598.
- [62] I. F. Perepichka, S. Roquet, P. Leriche, J. M. Raimundo, P. Frere, J. Roncali, *Chem. - Eur. J.* **2006**, *12*, 2960-2966.
- [63] H. Kim, M. Shin, Y. Kim, *J. Phys. Chem. C* **2009**, *113*, 1620-1623.
- [64] Y. Kim, M. Shin, H. Kim, Y. Ha, C. S. Ha, *J. Phys. D: Appl. Phys.* **2008**, *41*, 2251011-2251015.
- [65] J. H. Huang, M. Velusamy, K. C. Ho, J. T. Lin, C. W. Chu, *J. Mater. Chem.* **2010**, *20*, 2820-2825.
- [66] L. J. Huo, J. H. Hou, H. Y. Chen, S. Q. Zhang, Y. Jiang, T. L. Chen, Y. Yang, *Macromolecules* **2009**, *42*, 6564-6571.
- [67] Y. J. Cheng, S. H. Yang, C. S. Hsu, *Chem. Rev.* **2009**, *109*, 5868-5923.
- [68] J. Roncali, P. Frere, P. Blanchard, R. de Bettignies, M. Turbiez, S. Roquet, P. Leriche, Y. Nicolas, *Thin Solid Films* **2006**, *511*, 567-575.
- [69] R. H. Friend, R. W. Gymer, A. B. Holmes, J. H. Burroughes, R. N. Marks, C. Taliani, D. D. C. Bradley, D. A. Dos Santos, J. L. Bredas, M. Logdlund, W. R. Salaneck, *Nature* **1999**, *397*, 121-128.
- [70] T. Q. Nguyen, V. Doan, B. J. Schwartz, *J. Chem. Phys.* **1999**, *110*, 4068-4078.
- [71] N. T. Kalyani, S. J. Dhoble, *Renew. Sust. Energ. Rev.* **2012**, *16*, 2696-2723.
- [72] A. Wild, A. Winter, F. Schluetter, U. S. Schubert, *Chem. Soc. Rev.* **2011**, *40*, 1459-1511.
- [73] A. Wild, A. Winter, M. D. Hager, U. S. Schubert, *Analyst* **2012**, *137*, 2333-2337.
- [74] E. Tekin, P. J. Smith, U. S. Schubert, *Soft Matter* **2008**, *4*, 703-713.
- [75] C. Friebe, A. Wild, J. Perelaer, U. S. Schubert, *Macromol. Rapid Commun.* **2012**, *33*, 503-509.
- [76] T. Janoschka, A. Teichler, A. Krieg, M. D. Hager, U. S. Schubert, *J. Polym. Sci., Part A: Polym. Chem.* **2012**, *50*, 1394-1407.
- [77] K. Nakahara, K. Oyaizu, H. Nishide, *Chem. Lett.* **2011**, *40*, 222-227.
- [78] K. Koshika, N. Sano, K. Oyaizu, H. Nishide, *Macromol. Chem. Phys.* **2009**, *210*, 1989-1995.
- [79] Y. Y. Cheng, C. C. Li, J. T. Lee, *Electrochim. Acta* **2012**, *66*, 332-339.
- [80] Y. Kim, C. Jo, J. Lee, C. W. Lee, S. Yoon, *J. Mater. Chem.* **2012**, *22*, 1453-1458.
- [81] K. Nakahara, S. Iwasa, M. Satoh, Y. Morioka, J. Iriyama, M. Suguro, E. Hasegawa, *Chem. Phys. Lett.* **2002**, *359*, 351-354.
- [82] W. Yuan, M. B. Chan-Park, *ACS Appl. Mater. Interfaces* **2012**, *4*, 2065-2073.

Publication list

Refereed publications in scientific journals

1. Anke Teichler, Rebecca Eckardt, Stephanie Hoepfner, Christian Friebe, Jolke Perelaer, Alessia Senes, Mauro Morana, Christoph J. Brabec, Ulrich S. Schubert, *Adv. Energy Mater.* **2011**, *1*, 105-114.
“Combinatorial screening of polymer/fullerene blends for organic solar cells by inkjet printing”
2. Anke Teichler, Rebecca Eckardt, Christian Friebe, Jolke Perelaer, Ulrich S. Schubert, *Thin Solid Films* **2011**, *519*, 3695-3702.
“Film formation properties of inkjet printed poly(phenylene-ethynylene)-poly(phenylene-vinylene)s”
3. Alexander M. Breul, Christian Pietsch, Roberto Menzel, Johann Schaefer, Anke Teichler, Martin D. Hager, Jürgen Popp, Benjamin Dietzek, Rainer Beckert, Ulrich S. Schubert, *Eur. Polym. J.* **2012**, *48*, 1339-1347.
“Blue emitting side-chain pendant 4-hydroxy-1,3-thiazoles in polystyrenes synthesized by RAFT polymerization”
4. Tobias Janoschka, Anke Teichler, Andreas Krieg, Martin D. Hager, Ulrich S. Schubert, *J. Polym. Sci., Part A: Polym. Chem.* **2012**, *50*, 1394-1407.
“Polymerization of free secondary amine bearing monomers by RAFT polymerization and other controlled radical techniques”
5. Alexander M. Breul, Johann Schaefer, George M. Pavlov, Anke Teichler, Stephanie Hoepfner, Christine Weber, Jürgen Nowotny, Lars Blankenburg, Jürgen Popp, Martin D. Hager, Benjamin Dietzek, Ulrich S. Schubert, *J. Polym. Sci., Part A: Polym. Chem.* **2012**, *50*, 3192-3205.
“Synthesis and characterization of polymethacrylates containing conjugated oligo(phenylene ethynylene)s as side chains”

6. Sebastian Wünscher, Steffi Stumpf, Anke Teichler, Oliver Pabst, Jolke Perelaer, Erik Beckert, Ulrich S. Schubert, *J. Mater. Chem.* **2012**, *22*, 24569-24576.
“Localized atmospheric plasma sintering of inkjet printed silver nanoparticles”

7. Andreas Wild, Anke Teichler, Cheuk-Lam Ho, Xing-Zhu Wang, Hongmei Zhan, Florian Schlütter, Andreas Winter, Martin D. Hager, Wai-Yeung Wong, Ulrich S. Schubert, *J. Mater. Chem. C* **2013**, *1*, 1812-1822.
“Formation of dynamic metallo-polymers by inkjet printing: Towards white-emitting materials”

8. Anke Teichler, Jolke Perelaer, Ulrich S. Schubert, *Macromol. Chem. Phys.* **2013**, *214*, 547-555.
“Screening of film formation qualities of various solvent systems for π -conjugated polymers via combinatorial inkjet printing”

9. Anke Teichler, Jolke Perelaer, Florian Kretschmer, Martin D. Hager, Ulrich S. Schubert, *Macromol. Chem. Phys.* **2013**, *214*, 664-672.
“Systematic investigation of a novel low-bandgap terpolymer library via inkjet printing: Influence of ink properties and processing conditions”

10. Anke Teichler, Jolke Perelaer, Ulrich S. Schubert, *J. Mater. Chem. C* **2013**, *1*, 1910-1925.
“Inkjet printing of organic electronics – Comparison of deposition techniques and classification of state-of-the-art developments”

11. Anke Teichler, Zhe Shu, Andreas Wild, Cornelia Bader, Jürgen Nowotny, Gerwin Kirchner, Stephan Harkema, Jolke Perelaer, Ulrich S. Schubert, *Eur. Polym. J.* **2013**, *49*, 2186-2195.
“Inkjet printing of chemically tailored light-emitting polymers”

12. Anke Teichler, Stefan Hölzer, Jürgen Nowotny, Jolke Perelaer, Stephanie Hoepfener, Florian Kretschmer, Cornelia Bader, Martin D. Hager, Ulrich S. Schubert, *ACS Comb. Sci.* **2013**, *15*, 410-418.
“Combinatorial screening of inkjet printed ternary blends for organic electronics – Absorption behavior and morphology”
13. Tobias Janoschka, Anke Teichler, Bernhard Häupler, Thomas Jähnert, Martin D. Hager, Ulrich S. Schubert, *Adv. Energy Mater.* **2013**, *3*, 1025-1028.
“Reactive inkjet printing of organic radical batteries”
14. Andreas Wild, Anke Teichler, Christian von der Ehe, Andreas Winter, Martin D. Hager, Bing Yao, Baohua Zhang, Zhieyuan Xie, Wai-Yeung Wong, Ulrich S. Schubert, *Macromol. Chem. Phys.* **2013**, *214*, 1072-1080.
“Zn^{II} Bisterpyridine metallopolymers: Improved processability by the introduction of polymeric side chains”,
15. Markus J. Barthel, Tobias Rudolph, Anke Teichler, Renzo Paulus, Jürgen Vitz, Stephanie Hoepfener, Martin D. Hager, Felix H. Schacher, Ulrich S. Schubert, *Adv. Funct. Mater.* **2013**, DOI:10.1002/adfm201300469.
“Self-healing materials via reversible crosslinking of poly(ethylene oxide)-*block*-poly(furfuryl glycidyl ether) (PEO-*b*-PFGE) block copolymer films”

Book chapter

1. Anke Teichler, Jolke Perelaer, Ulrich S. Schubert, in *Inkjet-based Micromanufacturing* (Ed. J. Korvink, P. J. Smith, D.-Y. Shin, O. Brand, G. K. Fedder, C. Hierold, O. Tabata), Wiley-VCH Verlag GmbH & Co. KGaA, Weinheim, **2012**, pp. 19-39.
“Combinatorial screening of materials using inkjet printing as a patterning technique”

Oral presentations

1. Anke Teichler, Rebecca Eckardt, Jolke Perelaer, Ulrich S. Schubert
Printing Future Days, 02.-05. November 2009, Chemnitz, Germany
“Inkjet printing of thin film libraries of PPE-PPVs”
2. Anke Teichler
High-throughput Experimentation Programme Review Meeting of the Dutch Polymer Institute (DPI), 07. December 2009, Jena, Germany
“Functional materials for plastic electronics: Inkjet Printing and detailed optical property investigation”
3. Anke Teichler
High-throughput Experimentation Programme Review Meeting of the Dutch Polymer Institute (DPI), 22. April 2010, Eindhoven, The Netherlands
“Functional materials for plastic electronics: Inkjet Printing and detailed optical property investigation”
4. Anke Teichler
High-throughput Experimentation Programme Review Meeting of the Dutch Polymer Institute (DPI), 13. September 2010, Darmstadt, Germany
“Inkjet printing of conjugated polymers: Expanding polymer absorption for organic solar cell applications using a combinatorial approach”
5. Anke Teichler
High-throughput Experimentation Programme Review Meeting of the Dutch Polymer Institute (DPI), 15. June 2011, Darmstadt, Germany
“Combinatorial screening of new conjugated polymers for organic solar cell applications”

6. Anke Teichler, Rebecca Eckardt, Stephanie Hoepfener, Christian Friebe, Jolke Perelaer, Ulrich S. Schubert
Printing Future Days, 07.-10. November 2011, Chemnitz, Germany
“Combinatorial screening of polymer/fullerene blends for solar cells by inkjet printing”

7. Anke Teichler, Jolke Perelaer
High-throughput Experimentation Programme Review Meeting of the Dutch Polymer Institute (DPI), 06. June 2012, Darmstadt, Germany
“Combinatorial inkjet printing and new sintering techniques”

8. Anke Teichler, Jolke Perelaer
High-throughput Experimentation Programme Review Meeting of the Dutch Polymer Institute (DPI), 03. December 2012, Jena, Germany
“Inkjet printing of functional devices”

Poster presentations

1. Anke Teichler, Rebecca Eckardt, Stephanie Hoepfener, Christian Friebe, Jolke Perelaer, Ulrich S. Schubert
Annual Meeting of the Dutch Polymer Institute (DPI), 16. November 2010, Bergen op Zoom, The Netherlands
“Combinatorial screening of polymer/fullerene blends for solar cells by inkjet printing”

2. Anke Teichler, Rebecca Eckardt, Stephanie Hoepfener, Christian Friebe, Jolke Perelaer, Ulrich S. Schubert
Bayreuth Polymer Symposium, 11.-13. September 2011, Bayreuth, Germany
“Combinatorial screening of polymer/fullerene blends for solar cells by inkjet printing”

3. Anke Teichler, Sebastian Wünscher, Zhe Shu, Florian Kretschmer, Jolke Perelaer, Ulrich S. Schubert
Annual Meeting of the Dutch Polymer Institute (DPI), 15. November 2011, Zeist, The Netherlands
“Inkjet printing of functional materials”

4. Anke Teichler, Zhe Shu, Florian Kretschmer, Jolke Perelaer, Ulrich S. Schubert
Annual Meeting of the Dutch Polymer Institute (DPI), 13. November 2012, Zeist, The Netherlands
“Inkjet printing of conjugated polymers”

Curriculum vitae



- 02/10/1984 Born in Wolfen, Germany
- 08/91 – 06/95 Public Elementary School Thalheim, Germany
- 08/95 – 06/04 Anne-Frank-Gymnasium Sandersdorf, Germany
Degree: General qualification for university entrance
- 10/04 – 10/09 Friedrich Schiller University Jena, Germany
Student of chemistry, equivalence: M.Sc.
- 01/09 – 03/09 Eindhoven University of Technology, The Netherlands
Guest researcher as part of the diploma thesis in the group of Prof. Ulrich S. Schubert
- 11/08 – 10/09 Friedrich Schiller University Jena, Germany
Diploma student at the Laboratory of Organic and Macromolecular Chemistry (IOMC) in the group of Prof. Ulrich S. Schubert
- Since 11/09 Friedrich Schiller University Jena, Germany
Ph.D. student at the Laboratory of Organic and Macromolecular Chemistry (IOMC) in the group of Prof. Ulrich S. Schubert

Jena, den ____ 2013

Acknowledgement/Danksagung

Zu guter Letzt möchte ich all denen danken, die mir in den letzten Jahren zur Seite gestanden haben und ohne die diese Arbeit nicht möglich gewesen wäre.

An erster Stelle möchte ich meinem wissenschaftlichen Betreuer Prof. Dr. Ulrich S. Schubert für die Möglichkeit danken, meine Doktorarbeit in seiner Gruppe anfertigen zu dürfen. Die Freiheit an verschiedenen interessanten Themen zu arbeiten, sowie die Vielzahl an unterschiedlichen Charakteren in der Gruppe haben eine sehr gute Arbeitsatmosphäre geschaffen.

I would like to thank the DPI for providing the funding for my employment. The cluster meetings were a good possibility to present and discuss latest results.

Jolke Perelaer, my direct supervisor, I thank you for improving my written English in nicely readable texts. Otherwise my weird writing style might not be understood from others.

Andy Wild, Florian Kretschmer und Cornelia Bader möchte ich dafür danken, dass meine Arbeit durch eure Polymere, die ihr mir zur Verfügung gestellt habt, stets leuchtend bunt war. Andy, ich danke dir für die tolle Zusammenarbeit, die schon viele Früchte getragen hat. Ich hatte selten so gut druckbare Polymere. Tobias Janoschka, ich danke auch dir für die Polymere, die du extra trotz anfänglicher Schwierigkeiten für das Inkjet Printing hergestellt hast. Schwarz und weiß sind ja auch irgendwie Farben, aber über deine Polymere habe ich mich nicht immer gefreut.

Jürgen Nowotny, dir gilt Dank für die optische Charakterisierung unserer gedruckten Filme, wann immer unsere Geräte streikten oder für die Charakterisierung nicht ausreichten. Stefan Hölzer und Stephanie Höppener danke ich für die AFM-Messungen und anschließender Interpretation. Auch wenn es zu Beginn große Probleme mit der Klebrigkeit der Filme gab, konnten letztendlich doch viele aussagekräftige AFM-Bilder entstehen.

I would like to thank my master students Zhe Shu and Lan Wang for their good work in the field of OLEDs and OPVs, respectively. I enjoyed being your supervisor since I learned as well a lot from you guys. I hope you enjoyed the time as well and I wish you all the best for your future.

Renzo Paulus and Jürgen Vitz are acknowledged for their great help, whenever there was a problem with equipment and computers. Thank you both for keeping everything running; otherwise I would have thrown something out of the window. Furthermore, thank you a lot for the secure driving between Jena and the Netherlands or Darmstadt. Aber nicht zu

unterschätzen sind auch die administrativen Anlaufstellen. Ich danke Anja Helbig, Tanja Wagner und Sylvia Braunsdorf, die stets ein offenes Ohr für die kleineren und größeren Erledigungen hatten.

Ein wichtiger Teil dieser Arbeit bestand auch im Testen der gedruckten Filme als aktive Schicht in organischen Bauteilen. Ich möchte vor allem Olesia Synooka, Maik Bärenklau und Harald Hoppe von der TU Ilmenau für die Kooperation danken, die es ermöglichte aus unseren gedruckten Filmen Solarzellen zu bauen. Danke für die fortwährende Unterstützung, auch wenn die Ergebnisse sehr ernüchternd waren. I will acknowledge as well Gerwin Kirchner and Stephan Harkema from the Holst Center (The Netherlands) for the possibility to build OLEDs from our printed films. Michael Flämmich and Norbert Danz (Fraunhofer Institute for Applied Optics and Precision Engineering, Jena, Germany) are acknowledged for using their optical characterization setup for the testing of OLED devices.

For valuable discussions I thank all members of the inkjet and P4E meetings, in particular Sebastian Wünscher, Martin Hager, Tobias Janoschka, Stefan Hölzer, Andy Wild, Florian Kretschmer, Lan Wang, Zhe Shu, Oliver Pabst, David Pretzel, Martijn van Dongen, Franziska Wolf, Daniel Schmidt and Falk Kemper.

Even though it was mostly crowded and chaotic in the lab 3.20 I would like to thank Sebastian, Lan, Franziska and Shu for the nice atmosphere. I enjoyed the time in the lab very much, since we shared not only the worry about experiments that did not work out, but also good conversations and music. Da ja Laborarbeit nicht alles ist, sondern auch Büroarbeit getan werden muss, möchte ich mich auch bei meinen Bürokollegen Markus, Andreas und Pietscher bedanken. Ich habe die Zeit in einem Männerbüro sehr genossen und wir hatten immer sehr viel Spaß, auch wenn ihr vor allem meine Montagslaunen ertragen musstet. Danke Andreas für die besonders herausragenden Musikstücke, die die lästige Schreibtischarbeit gleich viel leichter gemacht haben. Tobi und Nicole, meine neuen Bürokollegen, euch wünsche ich in diesem Büro ebenso viel Spaß.

Schließlich möchte ich mich bei all denen bedanken, die dafür gesorgt haben, dass Arbeit nicht nur Arbeit ist, und auch ihre Freizeit mit mir geteilt haben: Sebastian, Matthias, Sofia, Andreas, Stefan, Markus, BANja, Torsten, Tobi, Katrin, Antje, Pietscher, Alex, Kempfi, Christine, Renzo, Tobi, Chris und Erik. Die vielen Grill- und Glühweinabende, Geburtstagsfeten, Kanufahrten (Danke Sofia!) und Mexikaner-Essen boten gelungene Abwechslungen, die ich nie vergessen werde. Sogar ein ganzes Wochenende in Steinheid

haben wir überlebt ohne uns die Köpfe einzuschlagen. Auch wenn ich an dieser Stelle nicht allen im Einzelnen danken kann, möchte ich doch wenigstens an einige von euch ein paar Worte richten. Zu aller erst, großer Dank gilt Sebastian. Danke, dass mit dir endlich ein Lichtblick in die Inkjet-Gruppe kam. Trotz unterschiedlicher Themen hatten wir doch viele hilfreiche Diskussionen, auch wenn unser gemeinsames Projekt leider nicht zu realisieren war. Vielen Dank auch für das kritische Lesen dieser Arbeit. Ich hoffe, du kannst dir die Freude an der Arbeit (trotz meiner Abwesenheit) erhalten. Danke für deine Freundschaft und die Dauerreservierung für deinen Couch-Schlafplatz. Ich danke dir Matthias, meinem „Herbergsvater“, dass ihr immer einen Schlafplatz zur Verfügung habt. Euer wunderbares Frühstück kann locker mit dem Stilbruch konkurrieren. Vielen Dank für deine schonungslosen, aber ehrlichen Kommentare. Andreas, die Zeit mit dir im Büro war sehr unterhaltsam und es wurde nie langweilig. Ich hoffe, auch einmal meinen Namen in der Danksagung deiner Arbeit lesen zu dürfen. In der Zwischenzeit hoffe ich, Sofia verpasst dir ordentliche Motivationsschübe. In diesem Zuge wünsche ich dir Sofia noch viel Durchhaltevermögen. Behalte dir deine stets fröhliche und wunderbar direkte Art! Danke dir Markus für den unvergesslichen Rom-Trip. Ich wünsche dir und Claudia eine wundervolle Zukunft, ob in Italien oder Deutschland. Und nicht zu vergessen, einen lieben Dank an alle tatkräftigen Umzugshelfer (Andreas, Pietscher, Matthias, Sebastian). Ich hoffe, ich kann auf euch auch in Zukunft zählen, auch wenn sich meine Adresse noch viele Male ändern sollte und wir Dachgeschosswohnungen (ohne Aufzug) bevorzugen. In diesem Zuge möchte ich mich bei Stefan (und Dörte) für die interessante Stadtführung durch Halle bedanken. Ich danke euch allen für eure Freundschaft, die aus den letzten Jahren eine unvergessliche Zeit gemacht hat. Ich wünsche euch allen noch viel Schaffenskraft und hoffe, dass man sich dann und wann mal wieder sieht; und wenn ich dafür extra umziehen muss und eure Hilfe gebraucht wird....

Zu guter Letzt; großer Dank gebührt meiner Familie, die mir in jeglicher Hinsicht zur Seite gestanden hat.

Declaration of authorship/Selbstständigkeitserklärung

Ich erkläre, dass ich die vorliegende Arbeit selbstständig und unter Verwendung der angegebenen Hilfsmittel, persönlichen Mitteilungen und Quellen angefertigt habe.

I certify that the work presented here is, to the best of my knowledge and belief, original and the result of my own investigations, except as acknowledged, and has not been submitted, either in part or whole, for a degree at this or any other university.

Jena, den ____ 2013

List of abbreviations

AFM	atomic force microscopy
bp	boiling point
BTD	benzothiadiazole
CB	chlorobenzene
CIE	Commission internationale de l'éclairage (Normfarbensystem)
d	inner nozzle diameter
ρ	density
DPP	diketopyrrolopyrrole
DMF	<i>N,N</i> -dimethylformamid
DoD	drop-on-demand
F	fluorene
ITO	indium-tin-oxide
J	current-density
M_n	number average molar mass
M_w	weight average molar mass
NMP	<i>N</i> -methyl-2-pyrrolidon
<i>o</i> -DCB	<i>ortho</i> -dichlorobenzene
OLED	organic light emitting diodes
OPV	organic photovoltaics
ORB	organic radical battery
OTFT	organic thin film transistor

LIST OF ABBREVIATIONS

PCBM	mono(1-[3-(methoxycarbonyl)propyl]-1-phenyl)-[6,6]C ₆₁
PDI	polydispersity index
PDPP- <i>co</i> -BTD- <i>co</i> -F	poly(diketopyrrolopyrrole- <i>co</i> -benzothiadiazole- <i>co</i> -fluorene)
PFP	poly(fluorene-phenylene)
P3HT	poly(3-hexylthiophene)
P3OT	poly(3-octylthiophene)
PPV	poly(phenylene-vinylene)
PPE-PPV	poly(phenylene-ethynylene)-poly(phenylene-vinylene)
PTMA	poly(2,2,6,6-tetramethylpiperidinyloxy-4-yl methacrylate)
R _a	surface roughness (average roughness)
R2R	roll-to-roll
RR	regioregularity
γ	surface tension
TMB	trimethylbenzene
TEMPO	2,2,6,6-tetramethylpiperidine-1-oxyl

Publications

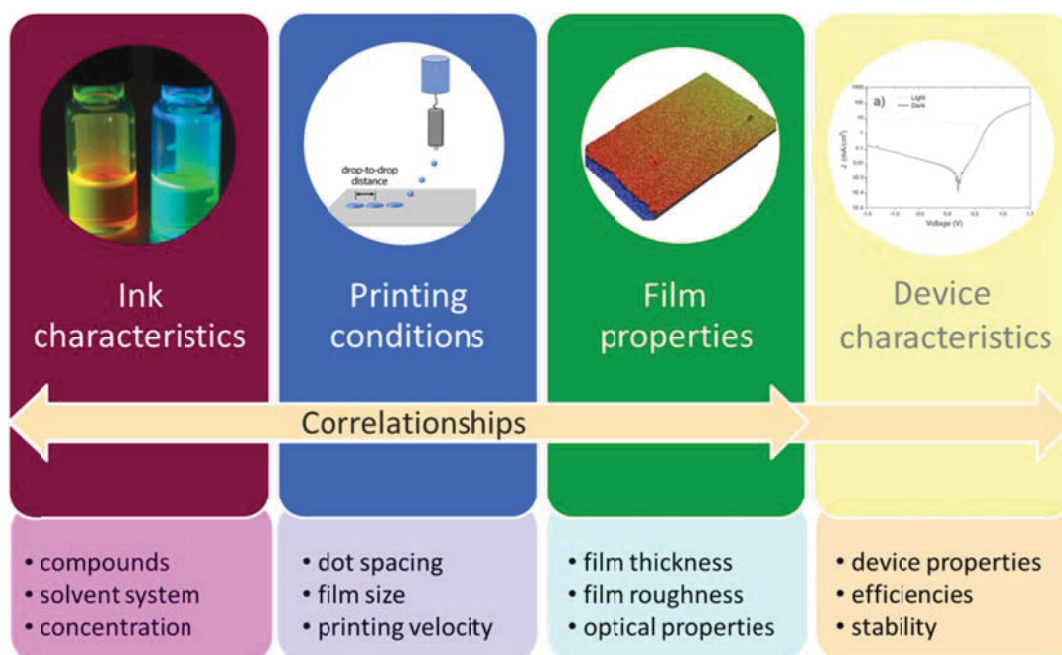
- 1) Reproduced from *J. Mater. Chem. C* **2013**, *1*, 1910-1925 with permission from the Royal Society of Chemistry.
- 2) Reproduced by permission of John Wiley & Sons Ltd., UK. Copyright 2013 WILEY-VCH GmbH & Co. KGaA, Weinheim.
- 3) Reproduced by permission of John Wiley & Sons Ltd., UK. Copyright 2013 WILEY-VCH GmbH & Co. KGaA, Weinheim.
- 4) Reproduced from *Eur. Polym. J.* **2013**, DOI:10.1016/j.eurpolymj.2013.03.031. with permission of Elsevier B.V. Copyright 2013.
- 5) Reproduced with permission from *ACS Comb. Sci.*, in press. Unpublished work copyright 2013 American Chemical Society.
- 6) Reproduced from *J. Mater. Chem. C* **2013**, *1*, 1812-1822 with permission from the Royal Society of Chemistry.
- 7) Reproduced by permission of John Wiley & Sons Ltd., UK. Copyright 2013 WILEY-VCH GmbH & Co. KGaA, Weinheim.
- 8) Reproduced by permission of John Wiley & Sons Ltd., UK. Copyright 2012 WILEY-VCH GmbH & Co. KGaA, Weinheim.
- 9) Reproduced by permission of John Wiley & Sons Ltd., UK. Copyright 2013 WILEY-VCH GmbH & Co. KGaA, Weinheim.

Publication 1

“Inkjet Printing of Organic Electronics – Comparison of Deposition Techniques and Classification of State-of-the-art Developments”

Anke Teichler, Jolke Perelaer, Ulrich S. Schubert

J. Mater. Chem. C **2013**, *1*, 1910-1925.



Inkjet printing of organic electronics – comparison of deposition techniques and state-of-the-art developments

Cite this: *J. Mater. Chem. C*, 2013, **1**, 1910

Anke Teichler,^{abc} Jolke Perelaer^{abc} and Ulrich S. Schubert^{*abc}

Inkjet printing represents a solution dispensing technique that is characterized by its non-contact, material-efficient and reproducible processing. This critical review discusses the use of inkjet printing for organic electronics with a focus on the applicability as well as the drying behavior. The nascent inkjet printing technique is compared to commonly used solution deposition methods, like spin-coating and doctor blading. Basic drying principles of inkjet printed features are understood and fundamental correlations between processing properties and film characteristics can be drawn. It is, however, a long way to gain a full understanding of the complete drying process, since the process conditions as well as the ink properties correlate in a complex relation with the final device properties. Nevertheless, inkjet printing has the potential to evolve as one of the most promising film preparation techniques in the future and has already been applied successfully in combinatorial screening workflows and for the preparation of organic solar cell devices.

Received 23rd September 2012
Accepted 17th December 2012

DOI: 10.1039/c2tc00255h

www.rsc.org/MaterialsC

1 Introduction

For the preparation of conventional inorganic electronics, vacuum and photolithography techniques are used for a roll-to-

roll (R2R) processing, which are cost-intensive and rather rigid processing methods. The introduction of a digital, non-contact and mask-less solution processing technique at R2R velocity would significantly reduce the total costs for the production of (organic) electronic devices.¹ In the field of organic electronics, applicable fabrication processes benefit from the solubility of the organic conductors, e.g. conjugated polymers or small molecules, in organic solvents.² An enhanced solubility of the conjugated polymers is obtained by attaching side chains to the

^aLaboratory of Organic and Macromolecular Chemistry (IOMC), Humboldtstraße 10, 07743 Jena, Germany. E-mail: ulrich.schubert@uni-jena.de

^bJena Center for Soft Matter (JCSM), Friedrich-Schiller-University Jena, Philosophenweg 7, 07743 Jena, Germany

^cDutch Polymer Institute (DPI), P.O. Box 513, 5600 MB Eindhoven, The Netherlands



Anke Teichler was born in 1984 in Wolfen (Germany) and studied chemistry at the Friedrich-Schiller-University Jena (Germany). After research activities at the Eindhoven University of Technology (The Netherlands), she obtained her MSc degree in chemistry in 2009. As a PhD student she is continuing her studies in combinatorial inkjet printing of functional polymers under the supervision of Prof. Ulrich S. Schubert in Jena.



Jolke Perelaer obtained his masters in organometallic chemistry with Prof. Dr G. van Koten at the University of Utrecht in the Netherlands in 2004. In 2009 he finished his PhD within the group of Prof. Dr U. S. Schubert at the Eindhoven University of Technology in the Netherlands with the focus on the preparation of (conductive) microstructures via inkjet printing and embossing techniques. He continued his work with Prof. Dr U. S. Schubert as a project manager of the inkjet-group at the Friedrich-Schiller-University in Jena, Germany. The topics include printed electronics, combinatorial materials screening and printed bio-materials.

polymer backbone. This enables a cost-effective processing *via* solution deposition methods, although the molecular packaging of the polymers may be affected by the addition of bulky side chains.³ On account of this, the chemical tailoring of polymers shows an influence on the polymer characteristics, including charge carrier mobilities as well as morphological and optical properties of the processed films.⁴ In addition, the application of various processing conditions can influence the film characteristics, including the thickness, the homogeneity and the optical behavior. Therefore, each preparation method requires an optimization of the processing parameters with the focus on the application of the processed layers.

The efforts and challenges of optimizing the applied solution deposition techniques to be addressed in the field of organic electronics are of particular interest for organic photovoltaics (OPVs). This research area shows the potential of specific film formation techniques for an efficient and reliable processing. On the other hand, however, also challenges arise that need to be solved, including the drying mechanisms and film formation characteristics. Since not only surface characteristics of the deposited films can be tuned by different applied solution and processing conditions, but also an optimized nano-morphology of the active layer is of importance; OPVs represent the significance of optimized preparation settings. Organic solar cells can be classified by their active layer architecture as layered or bulk heterojunction solar cells, where the donor (*e.g.* polymer) and acceptor (*e.g.* fullerene derivative) materials are either deposited as separate layers or from a mixture as one layer, respectively.⁵ The latter architecture is favored due to an improved charge generation assigned to an increased contact area when the donor and acceptor materials are mixed. For the preparation of bulk heterojunction organic solar cells the nano-morphology, which is strongly dependent on different applied processing methods and conditions, is crucial. As a consequence, the discussion on the drying properties and the thin film optimization is represented here using the example of OPVs.

Krebs pointed out that for further developments of organic solar cells it is necessary to evaluate besides the efficiency

values, also the long-term device stability as well as the processing techniques.⁶ All three aspects need to be assessed in order to develop organic solar cells that can compete on the current photovoltaic market (Fig. 1). In recent research, high-efficiency values have surpassed each other, and currently the highest reported efficiency for a single layer bulk heterojunction solar cell is 7.4%⁷ and for a tandem solar cell 8.6%.⁸ Recently, Heliatek reported an efficiency of 10.7%⁹ for its organic tandem solar cell, confirming that OPVs can reach efficiencies >10%¹⁰ for single layer solar cells and >15%¹¹ for tandem cells. The advancement of efficiency over recent years was realized by improving the properties of photoactive materials, like benzo-dithiophene,⁷ as well as by the development of new material geometries, like poly(3-hexylthiophen-2,5-diyl) (P3HT) nanowires.¹²

The second factor, *i.e.* the importance of a long-term stability of the organic solar cells, has not been frequently addressed by researchers; only a few reports discuss the stability of complete devices over a longer time period¹³ and the classification of conjugated polymers according to their degradation rate.¹⁴

For the third factor, *i.e.* the device preparation techniques, research is mainly focused on spin-coating, while a few groups use other solution deposition methods, like inkjet printing or doctor blading. The main reason is that spin-coating is characterized by an easy handling and fast processing. However, spin-coating is not able to be used in an automated fabrication and cannot pattern a substrate selectively. Inkjet printing is, in contrast to spin-coating, able to pattern in an automated and variability manner.¹⁵ Inkjet printing and doctor blading reveal a complex drying behavior of the printed features. Inkjet printing, however, shows many advantages, like a non-contact, mask-less and combinatorial processing, wherein hundreds of different materials – or better ink compositions – can be screened, while consuming little amounts of materials as well as generating a low amount of waste. Inkjet printing has been used as an



Ulrich S. Schubert was born in Tübingen (Germany) in 1969. He studied chemistry in Frankfurt and Bayreuth (both Germany) and the Virginia Commonwealth University, Richmond (USA). His PhD studies were performed at the Universities of Bayreuth and South Florida/Tampa. After postdoctoral training with J.-M. Lehn at the University in Strasbourg (France), he moved to the TU München (Germany) and

obtained his Habilitation in 1999. In 1999–2000 he was a professor at the Center for NanoScience, University of Munich (Germany), and in 2000–2007 Full-Professor at TU Eindhoven. Currently he holds a chair at the Friedrich-Schiller-University Jena (Germany).

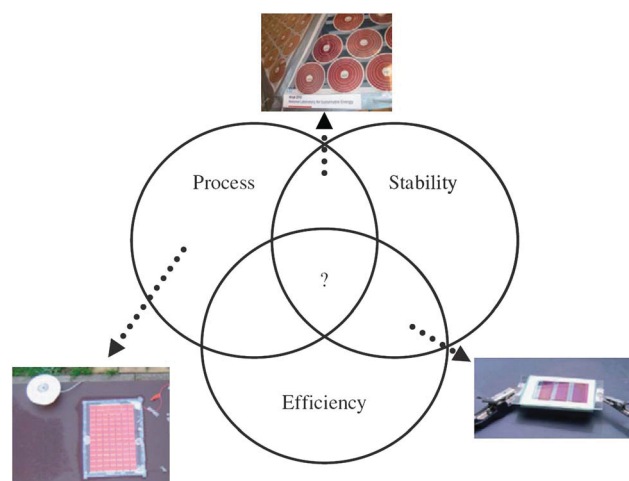


Fig. 1 Schematic representation of the three key factors that need to be optimized for a competitive development of organic solar cells for commercial applications. Reprinted from F. C. Krebs, Fabrication and processing of polymer solar cells: a review of printing and coating techniques, *Sol. Energy Mater. Sol. Cells*, **93**, 394–412, Copyright 2012, with permission from Elsevier.⁶

on-demand, digital patterning as well as film forming technique in several printed electronics applications, including organic thin film transistors (OTFTs),^{16,17} organic light emitting diodes (OLEDs)^{18,19} and organic photovoltaics (OPVs).^{20,21} Inkjet printing was also used for applying light emitting quantum dots,²² silver electrodes¹ and chemical sensors.²³

Besides spin-coating and inkjet printing, solution deposition techniques, like doctor blading²⁴ and screen printing,²⁵ were also used for the fabrication of OPVs. However, all patterning techniques require a continuous development in order to produce efficient devices in a reproducible R2R manner.

This contribution is divided into five sections. After an introduction, various common solution processing techniques, including spin-coating, doctor blading and screen printing, will be discussed regarding their film formation characteristics. In the next section, advantages and challenges of the inkjet printing process will be discussed, with the focus on the application of inkjet printed layers for organic solar cells. The fourth section presents a direct comparison and a critical classification of film preparation conditions and final film properties for spin-coating, doctor blading and inkjet printing. It is discussed that a comparison of these processing techniques in terms of applied solvents or processing temperatures cannot (yet) be done. Instead, inkjet printing requires different processing conditions to yield optimal layer properties. For the evaluation of the quality and resulting device efficiencies little research is reported so far in the field of inkjet printing. Therefore, a critical overview about challenges and possibilities that will arise with the use of inkjet printing is given in the fifth section, which evaluates inkjet printing as one of the prospective applied solution deposition techniques for organic electronics.

2 Common solution processing techniques

Favorable techniques are characterized by low processing costs as well as low materials consumption, but there is a clear difference between lab scale methods and R2R processes. For both types of processing the sizes of the final devices, the processing speeds as well as the possibility to use flexible substrates represent important factors. Whereas lab scale methods are sufficient for fundamental studies, R2R processes are required for the up-scaling of OPVs production.

In order to address advantages and disadvantages of inkjet printing for the preparation of organic solar cells and to gain an overview of the challenges and possibilities of this technique, other solution deposition processes are also discussed here. A selection of techniques will be highlighted that are frequently reported in the current literature. Moreover, a detailed discussion on the drying behavior and the film formation characteristics will be presented. A detailed technical summary of a few preparation methods with the main focus on R2R processes was recently presented by Krebs.⁶

In the research area of organic photovoltaics the interaction between working principles and processing conditions is not yet fully understood. Despite the many published studies that show improvements and new developments, the fundamental

correlations between processing conditions and the utilized polymers for organic solar cells are not elucidated. Once a good process is found for a donor–acceptor, *i.e.* a polymer–fullerene blend, it does not automatically imply that it will also work for other donor–acceptor combinations in a similar way, or sometimes at all. Every polymer (class) requires therefore a special processing and post-production treatment to perform well as a donor material. The reason why several methods are currently discussed in the literature is based on the fact that different active layer materials require different processing methods and conditions for an optimized device performance. A selection of these processing techniques that are used as lab-scale processes for fundamental studies, including spin-coating, doctor blading and screen printing, will be described in the following sections and compared to inkjet printing.

2.1 Spin-coating

Spin-coating is an often discussed processing technique in the open literature. The reasons can be found in the ease of handling, reproducibility and applicability of a wide variety of materials. First of all, the process of spin-coating is characterized by a high simplicity and by the easy deposition of the solute material onto a rotating substrate (Fig. 2). This technique reveals homogeneous films in a very reproducible way with little investments for the equipment. However, a significant disadvantage is the one-by-one operation of this technique. Only one substrate can be coated at a time and it needs to be changed manually when moving to the next substrate. Therefore, a fast and automated processing is not possible with this technique, which is the reason why spin-coating is not applicable for a R2R processing. Secondly, most of the applied material (>90%) is wasted due to the ejection of solution from the substrate during rotation.²² Although only a little amount of material is required for the preparation of a spin-coated film, the high waste consumption is a clear drawback of this technique.⁶

During spin-coating centrifugal forces induce a strong sheering of the coating solution. Due to a radial flow most of the material is ejected and the film becomes thinner until equilibrium is reached, which is determined by the spin speed and the

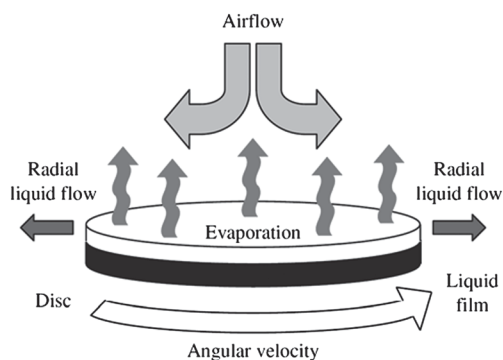


Fig. 2 Schematic representation of the film preparation technique spin-coating. Reprinted from F. C. Krebs, Fabrication and processing of polymer solar cells: a review of printing and coating techniques, *Sol. Energy Mater. Sol. Cells*, **93**, 394–412, Copyright 2012, with permission from Elsevier.⁶

increase in solution viscosity. The final film thickness, which can be adjusted by the solute concentration and the applied spin speed, is reached when the solvent is evaporated.²⁶ The film thickness increases with increasing concentration as well as with decreasing spin speed. It was found that solvents with a higher vapor pressure result in thicker films than solvents with lower volatilities, while using the same concentration for the coating solution.²⁷

When applying spin-coated polymer films in electronic devices, relationships between coating parameters and the final device characteristics can be evaluated. For spin-coated films these correlations are well understood for organic field-effect transistors (OFETs), organic light emitting diodes (OLEDs) and organic photovoltaics (OPVs).

The morphology of a spin-coated layer is, besides the processing conditions, dependent on the solvent. It is known that polymers in solution tend to aggregate above a certain concentration and that this behavior is strongly influenced by the polymer class. For example, at concentrations below 0.4% the polymer poly[2-methoxy-5-(2'-ethyl-hexyloxy)-1,4-phenylene vinylene] (MEH-PPV) shows no aggregation, while it is highly aggregated at concentrations >1%.²⁸ It was discussed by Shi *et al.* that the morphology of MEH-PPV films can be varied in the region between these two concentrations for loose aggregation (CLA) by changing the spin speed. By using low concentrations the loose polymer chains tend to stretch due to the effective radial flow, resulting in films that show absorption at higher wavelengths due to an improved packing of the polymer chains and enhanced conjugation. In contrast, when coating from highly concentrated solutions, the radial flow is not strong enough to break the polymer aggregates, which results in a coiled polymer chain with a reduced conjugation and, as a consequence, absorption at lower wavelengths is observed.²⁸ Subsequently, the optical and electronic properties can be tuned by preparing thin films from solutions having the prescribed intermediate concentration, which is also dependent on the molar mass of the polymer and the solvent.

Furthermore, by screening thin film properties of spin-coated polymer layers it was found that the emission color of spin-coated films depends on the drying time. At lower spin speeds and, thus, with a longer drying time, the polymer coils are entangled and the formation of interchain species is preferred, which leads to a red-shift as well as to additional aggregation peaks at higher wavelengths in the emission spectra.²⁹

For the investigation of field-effect mobilities of conjugated polymers, *e.g.* of P3HT, in spin-coated films, it was discussed that the boiling point of the processing solvent represents another critical processing parameter due to the resulting drying time of the processed films.³⁰ Whereas low-boiling solvents lead to a drying within seconds, high-boiling solvents increased the drying time to a few minutes, which was found to be sufficient for the self-organization of the polymer into the thermodynamically favored structure and for improved electrical properties. As a result, the microstructure of P3HT can be controlled by the choice of solvent, as high-boiling solvents lead to a higher degree of P3HT crystallization. A comparison

between spin-coated and drop-cast films was performed by Larsen and coworkers using the same processing solvent.²⁷ Drop-casting resulted in higher charge carrier mobilities than spin-coating, which was caused by the longer drying times for drop-cast films. Hence, film morphologies as well as electrical properties can be tuned by different drying speeds originating from the preparation method itself.

In addition, DeLongchamp *et al.* investigated the orientation of P3HT chains as a function of the spin speed. The authors discussed the relationship between the obtained crystal structure and the drying speed at varied spin velocities. With increased spin speed, the orientation of P3HT changes from edge-on to plane-on orientations (Fig. 3).³¹ Therefore, not only the crystallinity of P3HT is affected by the drying speed, but also the orientation distribution of the polymer chains.³²

For the preparation of solution-processed active layers in OPVs, spin-coating is currently the most frequently reported technique in the literature to obtain thin and homogeneous films with a well segregated film morphology. It was found for spin-coating of P3HT/[6,6]-phenyl-C₆₁-butyric acid methyl ester (PCBM) mixtures that slower drying results in improved solar cell performances due to an increased hole-mobility of the P3HT polymer.³³ Therefore, a higher boiling solvent, for example *ortho*-dichlorobenzene (*o*DCB), is preferred over lower boiling solvents, like chloroform. This approach revealed balanced charge carrier mobilities for P3HT and PCBM, leading to a more optimized charge transport in the solar cell. Li *et al.* investigated OPV performances of spin-coated P3HT/PCBM films as a function of the drying time. Improved solar cell characteristics were found when the films were dried very slowly (~20 minutes) and, as a result, the external quantum efficiency (EQE) is 65%, whereas a fast evaporation of the solvent (~20 seconds) revealed an EQE of only 19%, resulting in power conversion efficiencies (PCEs) of 3.5% and 1.4%, respectively (Fig. 4).³⁴ The authors discussed that P3HT is highly ordered due to the slow drying, showing enhanced optical as well as charge carrier mobilities, which leads to a balanced charge transport in the active layer.

Recently, Dang *et al.* studied the role of the used solvents for spin-coating P3HT/PCBM blends. Six different solvents with different boiling points, ranging from 61 to 214 °C, were investigated (see Fig. 5a).³⁵ A red-shifted and strongly structured absorption of the P3HT/PCBM layer was observed with increasing boiling point of the processing solvent, which is consistent with earlier reports.³⁰ Although a rough film surface

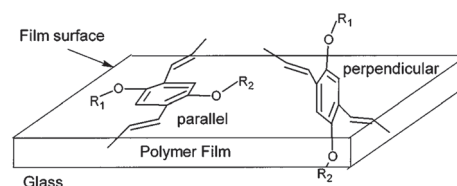


Fig. 3 Schematic representation of edge-on (perpendicular) and plane-on (parallel) orientation of P3HT onto a substrate. Reprinted with permission from Y. Shi, J. Liu and Y. Yang, *J. Appl. Phys.*, 2000, **87**, 4254–4263. Copyright 2012, American Institute of Physics.²⁹

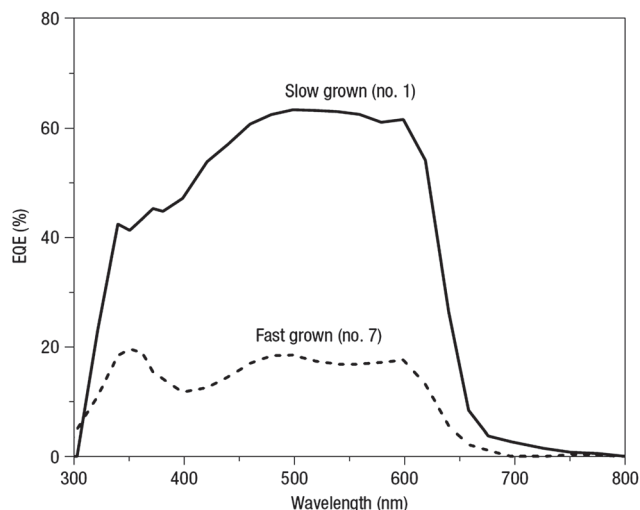


Fig. 4 External quantum efficiencies of P3HT/PCBM films produced by slow and fast drying processes. Reprinted with permission from Macmillan Publishers Ltd: Nature Materials, G. Li, V. Shrotriya, J. S. Huang, Y. Yao, T. Moriarty, K. Emery and Y. Yang, *Nat. Mater.*, 2005, **4**, 864–868, Copyright 2012.³⁴

is observed when using solvents with a boiling point above 150 °C, a clear phase separation was observed, which led to increased solar cell efficiencies (Fig. 5b). This study shows that within a used processing method, the choice of the applied solvent has a significant effect on the resulting film absorption and morphology. Layer properties must therefore be optimized by the correct choice of solvent as well as the processing conditions.

Another approach for improving the morphology of an active layer is to use a post-processing treatment. The crystalline polymer P3HT showed enhanced chain packaging after thermal annealing of the prepared film. Treat *et al.* reported highly efficient OPVs built from P3HT/PCBM due to an increased P3HT-crystallinity and improved photoconversion efficiencies upon thermal treatment.³⁶ For amorphous polymers it was recently reported that improved morphologies and efficiencies were obtained by adding a small amount of 1,8-octanedithiol, which has a relatively high boiling point as well as a selective solubility for polymers and fullerenes.³⁷

2.2 Doctor blading

As a second lab-scale technique, doctor blading is used for the preparation of the active layer for organic solar cells. With this method, a well-defined film thickness can be obtained by moving a sharp plate at a fixed distance over the substrate to be coated (Fig. 6). A disadvantage of this contact deposition technique is the large amount of waste that remains on the sharp plate after processing. Doctor blading is similar to spin-coating, in terms of cost-effectiveness and complexity, but is much slower in terms of processing.⁶

For doctor blading, as well as for inkjet printing, which will be discussed in a later section, the wetting behavior of the coating solution is an important factor. For a good wetting, which results in a good film formation, the surface tension of the coating solution needs to be lower than the substrate surface energy.³⁸ The homogeneity of bladed films depends on the solute concentration and the coating speed.³⁹ Wang *et al.* identified three different stages during the drying of a doctor bladed film. After a fast evaporation step of the solvent, until a solute content of approximately 50%, a rapid crystallization takes place, followed by a slow evaporation and a slow crystallization.⁴⁰

Schmidt-Hansberg and coworkers investigated the optical properties of P3HT/PCBM films prepared by doctor blading from *o*DCB as a function of the drying speed. The authors reported that a more featured and red-shifted absorption is obtained upon a slow drying process.³⁹ At reduced coating temperatures, a slow drying was observed for doctor bladed P3HT/PCBM films prepared from chlorobenzene, which resulted in a preferred morphology due to slower crystallization

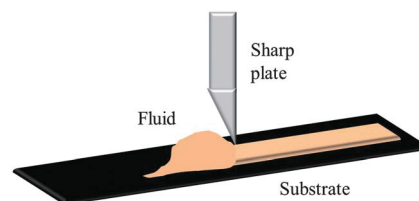


Fig. 6 Schematic representation of the doctor blading process.

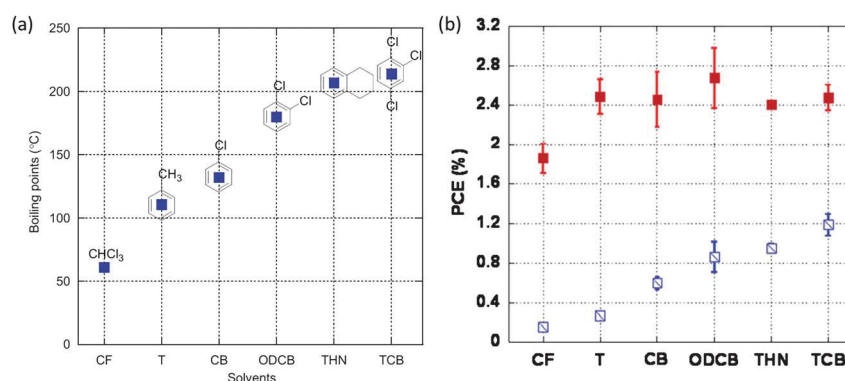


Fig. 5 (a) Chemical structure and boiling points of the different solvents investigated for P3HT/PCBM spin-coated films. (b) Power conversion efficiencies of solar cells prepared from the six different solvents as prepared (open symbols) and annealed (closed symbols). Reprinted from M. T. Dang *et al.*, Polymeric solar cells based on P3HT:PCBM: role of the casting solvent, *Sol. Energy Mater. Sol.*, **95**, 3408–3418, Copyright 2012, with permission from Elsevier.³⁵

kinetics. Despite a longer drying time, the obtained films revealed a rough film surface. At increased temperatures, a stronger phase separation was observed attended by a decreasing surface roughness.²⁴ Subsequently, improved solar cell performances were achieved by decreasing the substrate temperature, which resulted in a PCE of 2.1% at 15 °C.⁴¹ Other research groups, however, obtained different results; for the same polymer/fullerene system, but with different solvents, including toluene and tetralin, an optimum substrate temperature of 60 °C was found to reveal a high efficiency. Toluene and tetralin resulted in a PCE of 3.8%⁴² and 3.3%,⁴³ respectively. Both solvents, toluene (bp 110 °C) and tetralin (bp 205 °C), have a significant difference in their boiling points that cause different drying speeds of the bladed films.

Therefore, it can be concluded that an optimum layer morphology is not only dependent on the drying speed, but also on the used solvents as well as the resulting rheological properties. These findings indicate that a prediction of best processing parameters cannot be given at this point, and further investigations are required to understand the influence of the processing conditions for this particular coating technique.

Knife-over-edge coating is the R2R equivalent to doctor blading, where the knife is stationary and the substrate is moving during coating. By using this technique, smooth films were obtained in a reasonable production time by transferring the know-how obtained from doctor blading to this process.⁶

2.3 Screen printing

As a third technique, screen printing has been reported for the preparation of the active layers for solar cells. This technique forces the ink through a screen by applying pressure with a squeegee (Fig. 7)⁴⁴ and results in the formation of homogeneous films. However, large film thicknesses and long drying times are observed. This method is highly R2R compatible by using a rotational screen printer, but additional costs arise, for example, when changing the printing layout, which requires a unique screen and needs to be changed every time the layout changes. The inks entail a high viscosity and more waste is produced during processing; the material remains on the screen and the squeegee after processing.

Krebs *et al.* showed that the R2R production of flexible organic solar cells is possible by screen printing.²⁵ Using this technique, the devices were able to be prepared in large scale as

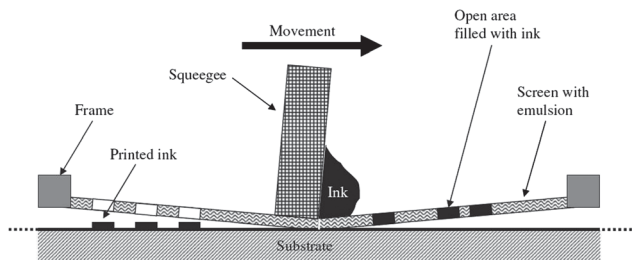


Fig. 7 Schematic representation of the film preparation technique screen printing. Reprinted from F. C. Krebs, Fabrication and processing of polymer solar cells: a review of printing and coating techniques, *Sol. Energy Mater. Sol.*, **93**, 394–412, Copyright 2012, with permission from Elsevier.⁶

well as under ambient conditions. Furthermore, the exclusion of the expensive indium-tin-oxide (ITO) ensured the demonstration of a cost-effective and green processing.² A major drawback of this technique is the lack of possibilities for morphology as well as film thickness optimization, which results in low OPV efficiencies.

3 Inkjet printing – control of features morphology

For a detailed understanding of the preparation techniques as well as to evaluate whether inkjet printing has the potential for producing high-efficiency solar cells, the drying processes and resulting film morphologies need to be well understood. This will be further discussed in this section for inkjet printed droplets, lines and films. The requirements and characteristics of the droplet generation as well as the impact of the droplets on the substrate were reviewed elsewhere.^{45,46} Here, the focus will be on drying processes and the resulting film properties.

3.1 Inkjet printing characteristics

Inkjet printing represents an accurate and reproducible film preparation technique, which relies on the formation of individual droplets that are ejected from a nozzle. The subsequent drop coalescence at the substrate depends on the dot spacing, which is defined as the center-to-center distance between two adjacent droplets, and forms the final printing patterns (Fig. 8). The ejected sub-nanoliter droplets have a diameter approximately equal to the size of the nozzle orifice and can be slightly adjusted by the operating conditions.⁴⁷

Inkjet printing has not yet attracted as much interest as spin-coating for the preparation of OPVs, which can be ascribed to a more complex film preparation and drying process. For inkjet printing, all solute parameters have a significant influence on the preparation of the printed patterns, which makes the ink development crucial. Important factors include the ink viscosity and surface tension as well as the nozzle diameter. Compared to other solution processing techniques, inkjet printing is characterized by high material efficiency; only small amounts of materials are required and only a little waste is produced. Inkjet printing allows an instant change of the printing pattern by the printer software. Therefore, no masks or lithography steps are

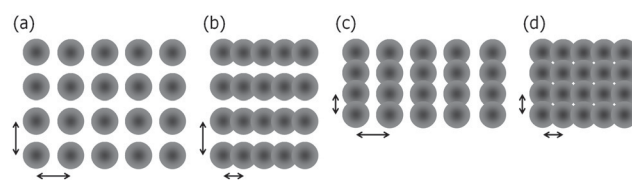


Fig. 8 Schematic representation of variations in dot spacing, indicated by the arrow: (a) single droplets when the dot spacing in the x- and y-direction is larger than the droplet diameter on the substrate, (b) horizontal lines when the dot spacing in the x-direction is reduced and (c) vertical lines for a reduced dot spacing in the y-direction. Continuous films (d) are formed when in both x- and y-directions the dot spacings are smaller than the droplet diameter on the substrate. Reprinted with permission from ref. 50.

required, which decreases the processing costs significantly. Depending on the number of operating nozzles (1 to 128 for lab scale inkjet printers) the printing speed can be varied. By means of inkjet printing, features with a thickness of several tens of nanometers up to multiple tens of micrometers can be produced in a reproducible manner.^{48,49} When using multiple nozzles and print heads, a high speed production of thin films can be performed. However, up to now, no reports are available in the open literature that discuss inkjet printing as a R2R coating technique.

For a lab scale technique, which provides fundamental knowledge, a combinatorial screening of materials and parameters is crucial to assure reproducibility as well as reliability. A large number of printing parameters influences the morphology and homogeneity of active layers, and it is not possible to investigate each single parameter individually and in a decent amount of time.⁵¹ Not only process-depending parameters, like the dot spacing for inkjet printing, need to be optimized, but also the solvent/solute parameters, like the used solvent(s) and concentration. Several studies report the optimization of single parameters: concentration,⁵² solvent system,²⁰ blend ratio,⁵³ dot spacing,⁵⁴ and substrate temperature,⁴⁰ but in most cases a combinatorial screening was not performed, which leaves possible synergies between the parameters undiscovered. Consequently, the results are difficult to compare. Therefore, a large number of crucial parameters need to be evaluated in a systematic screening in order to identify the optimal parameters for the used film preparation technique.

Renz *et al.* showed a multiparametric optimization of spin-coated P3HT/PCBM films by the variation of PCBM content, spin time and annealing time.⁵⁵ This study shows a comprehensive optimization of the mentioned parameters with respect

to their morphological properties and, most importantly, solar cell characteristics. With the subsequent investigation how each variation of the parameters affects the solar cell results, a screening is given, which is only limited by the non-automated processing *via* spin-coating.

In contrast, inkjet printing allows a fast, easy and reproducible screening of compound libraries, for example, of conjugated polymers,⁵⁶ CdTe nanoparticles,⁵⁷ as well as of polymer/fullerene blends for OPVs.⁵⁸ Teichler *et al.* presented a screening workflow that included the ink preparation with a pipetting robot, the thin-film library preparation by using inkjet printing and the characterization of the produced compound libraries by using high-throughput analytical tools, including UV/vis plate readers (Fig. 9).²⁰ Hereby, a complete combinatorial screening of solute properties and their influence on the thin-film properties of the inkjet printed films was introduced. Subsequently, structure–property relationships were evaluated that lead to optimized processing conditions for the used polymer/fullerene combinations as well as to the elucidation of synergies that may exist between different parameters.

3.2 Drying processes

Not only the solution properties, like the solvent and the concentration, have an effect on the rheological properties of the coating solution, but also the used coating process itself has an influence on the final film characteristics.⁵⁹ As concluded from the previous section, the processing time has a significant effect on the final morphology. The drying time is determined by the boiling point of the used solvent and the applied processing technique. Whereas spin-coating is seen as being a fast drying method, doctor blading and inkjet printing are

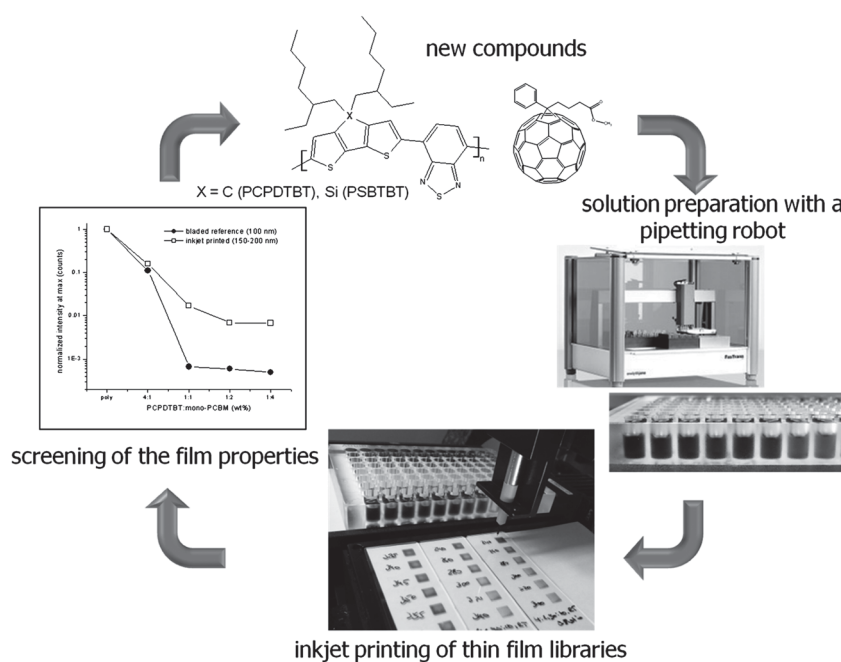


Fig. 9 Schematic representation of a combinatorial screening workflow including inkjet printing for the preparation of thin polymer film libraries. Reprinted with permission from ref. 20, Copyright 2012, Wiley-VCH Verlag GmbH & CoKGaA.

techniques where the film drying proceeds at a longer time scale. Therefore, by choosing one of the latter preparation techniques, one has to take into account that the best working conditions, like solvents and concentrations that show a good film forming performance, cannot be adapted easily to another processing technique. In fact, the control over the obtained morphology represents a complicated interaction between various parameters and cannot be predicted easily.

In the previous section, the importance of the drying speed of the prepared films was discussed for spin-coating and doctor blading. The drying speed is also crucial for a successful inkjet printing procedure. Individual inkjet printed sub-nanoliter droplets dry in a fraction of a second, while the drying speed of an inkjet printed film strongly depends on the thickness of the film and, hence, the number of placed droplets. In this case, the drying of a film may take several minutes, which explains why inkjet printing is characterized as a slow drying process in contrast to spin-coating. The following section will discuss the detailed analysis of the drying and solidification behavior of different printing solutions and their influence on the morphology of the final features.

Coffee drop effect. One of the main challenges in the inkjet printing process is to gain control over the resulting film homogeneity during drying. A complete understanding of processes taking place in a drying droplet is very complex, and the coffee drop effect and Marangoni flow are both considered to be important factors. Therefore, a prediction of the resulting film characteristics is at this point rather difficult and strongly depends on the system as well as the features' size. The so-called coffee-drop-effect,⁶⁰ which describes the accumulation of solute material at the rim of a drying droplet, is a result of an inhomogeneous evaporation of the solvent and of a pinned contact line (Fig. 10a).⁶¹ Several mechanisms have been reported to minimize the coffee-drop-effect and mostly rely on the controlled evaporation of the solvent.

First, coffee rings can be reduced by an increased vapor pressure around the drying feature. Kajiya *et al.* showed that an enhanced drying pattern was obtained by exposing the drying droplet to an increased solvent vapor.⁶² Furthermore,

Park *et al.* found that for this so-called solvent vapor, annealing a high-boiling solvent with a high surface tension is required to improve the rearrangement of the deposited material.⁶³

As a second solution to the coffee-drop effect, a more feasible approach is suggested by printing from a solvent mixture, in which the main solvent has a lower boiling point and a higher surface tension than the co-solvent.⁶⁴ Typically, the minor component of the solvent mixture is added in a few tens of volume percentages.⁶¹ During the drying of the printed feature, *i.e.* a droplet, a line or a film, the low boiling solvent evaporates first at the contact line, which leads to an outward flow of the solvent carrying solute towards the edge. Therefore, the addition of the high-boiling solvent strongly reduces the evaporation of the solvent at the edges, since the amount of high-boiling solvent is here locally higher than that of the low-boiling solvent. At the same time, a surface tension gradient is induced in the printed feature that leads to an inward flow of material – the so-called Marangoni flow.⁶⁵ A resulting circulation of the material leads to a homogeneous material distribution (Fig. 10b).

Finally, the drying speed of a printed feature can be controlled by creating a temperature difference between the ink and the surface. By increasing the substrate temperature from 25 to 60 °C for the inkjet printing of an aqueous poly(3,4-ethylenedioxy-thiophene):polystyrenesulfonic acid (PEDOT:PSS) ink, an improved drying pattern and a reduction of the droplet width from 100 μm to 65 μm were observed by Zhou *et al.*, which were explained by the reduced time for a complete spreading.⁶⁶ It is believed that an increased substrate temperature stimulates solvent evaporation, which reduces the in-flight droplet diameter as well as the impact diameter at the substrate, and, as a consequence, the spreading of the droplet.⁶⁷ However, other reports that used other materials revealed the appearance of drying inhomogeneities when the substrate temperature was set too high.^{54,68} Therefore, the substrate temperature needs to be carefully screened for each ink and substrate combination in order to form homogeneous surfaces.

Controlling line and film formation. When droplets are inkjet printed close to each other, lines or films are formed upon drop coalescence that show a more complex dependence on the printing parameters. In the case of printing lines, the dot spacing, or drop-to-drop distance, of the droplets results in different line morphologies, as shown in Fig. 11. When the dot spacing is chosen too small, bulging effects, as depicted in Fig. 11a, will appear due to too much deposited material, whereas a large dot spacing results in scalloped but continuous lines (Fig. 11c) or individual droplets (Fig. 11d). Only when the dot spacing is optimized are homogeneous and continuous lines formed (Fig. 11b).⁶¹

However, the dot spacing is just one of the factors that determine the quality of inkjet printed lines or films. In fact, many parameters have an influence on the film formation, including the solute concentration, the solvent as well as the substrate temperature. All parameters require an optimization for each polymer class to reveal homogeneous features.

Teichler *et al.* discussed the elucidation of optimized film qualities by the preparation of a poly(phenylene-ethynylene)-poly(phenylene-vinylene) (PPE-PPV) library. The best film

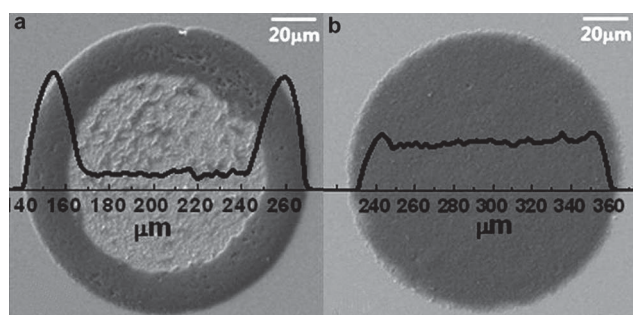


Fig. 10 Scanning electron microscopy images and surface profiles of aluminum oxide droplets inkjet printed from (a) the single solvent water and (b) a solvent mixture of water and dimethylformamide in the ratio of 90/10. Reprinted from Y. Oh *et al.*, Inkjet printing of Al(2)O(3) dots, lines, and films: from uniform dots to uniform films, *Curr. Appl. Phys.*, **11**, S359–S363, Copyright 2012, with permission from Elsevier.⁶¹

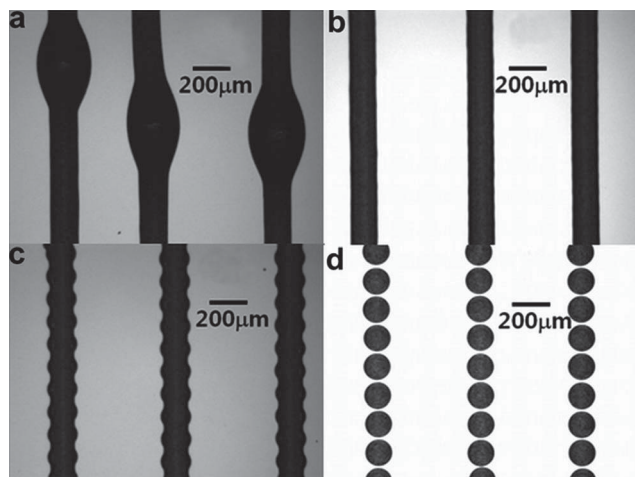


Fig. 11 Morphologies of inkjet printed lines obtained by the variation of dot spacing: (a) bulges, (b) homogeneous lines, (c) scalloped lines and (d) individual droplets. Reprinted from Y. Oh *et al.*, Inkjet printing of Al(2)O(3) dots, lines, and films: from uniform dots to uniform films, *Curr. Appl. Phys.*, **11**, S359–S363, Copyright 2012, with permission from Elsevier.⁶¹

quality was observed for a concentration of 4 mg mL^{-1} , a solvent system of toluene/*o*DCB 90/10 and inkjet printing at ambient conditions.⁵⁴ A faster drying, induced either by a reduction of the high boiling solvent *o*DCB or by an increased substrate temperature, led to a reduction of the film homogeneity. Furthermore, an increase in the solute concentration does not show a positive effect on the film quality. The report demonstrates that optimized processing conditions can be revealed easily by using inkjet printing. However, a simple prediction of the best printing parameters has not been given so far.

At this point, it is worth mentioning that printing conditions, which result in the best film homogeneity, are not automatically the best printing parameters for a desired application. For instance, inkjet printing performed from a specific solution results in a homogeneous film with a typical film thickness, but the properties of the inkjet printed features are strongly dependent on the layer thickness. For example, a red-shifted polymer emission as well as a change in the shape of the emission peaks was found for thicker films, indicating more pronounced inter-chain interactions.^{56,69} Furthermore, another discrepancy arises when the obtained film thickness that shows the best film quality is too thick for a desired application. In particular, the active layers for solar cells should have a thickness between 100 and 200 nm.⁵ However, the approach to vary the dot spacing to adjust for the required film thickness may not result in homogeneous layers. Therefore, ink properties, like the concentration, need to be changed and, consequently, a new ink has to be developed, which again requires optimization of the printing parameters. The elucidation of best layer as well as application properties represents a complex interaction between the solution and the printing characteristics that, in addition, needs to be adjusted for the desired application of the inkjet printed feature. Preferably, a combinatorial screening of each parameter is then performed to identify synergies between multiple parameters as well as to speed up the investigation.

The importance of the solvent system used in the inkjet printing process on the film properties of semi-crystalline TIPS-pentacene was recently reported by Madec *et al.*⁷⁰ The authors found a significant change in morphology as well as a strong increased hole-mobility due to an increased crystallinity simply by adding 10% of a higher boiling solvent to the main solvent. Furthermore, Chung *et al.* performed inkjet printing of TIPS-pentacene from the high boiling solvent propylene glycol methyl ether acetate (PEGMEA, bp 145 °C) and found charge carrier mobilities similar to those for drop-casting, but significantly higher than for spin-coating.⁷¹ This result indicates that a slower drying process reveals an improved material crystallinity.

Moreover, for the active layer of an organic solar cell the solvent and the drying time play a critical role, since only a well-segregated nano-morphology leads to a high PCE. Therefore, an optimum drying time of the processed layers exists; too short (long) drying times would lead to too little (much) segregated morphologies. Aernouts and coworkers reported the preparation of P3HT/PCBM solar cells, where the active layer was inkjet printed from a mixture of chlorobenzene and tetralin in a volume ratio of 1 : 1.⁵² Different solute concentrations (1, 2 and 3 wt%) were investigated for their film formation properties. It was found that an increased concentration led to a film formation with a higher surface roughness. The authors did not further study the processing or ink parameters. Hence, the obtained power conversion efficiency of 1.4% represents the performance of a not fully optimized inkjet printed device.

Another approach was presented by Lange *et al.*,⁷² who used a solvent system consisting of relatively high boiling solvents (chlorobenzene, trichlorobenzene) for the inkjet printing of P3HT/PCBM layers. To stimulate solvent evaporation, the authors used subsequent heating, which resulted in a reduced drying time. Therefore, a fast drying of the films (<30 seconds) was achieved, resulting in well-segregated morphologies and efficiencies of 2.4%, which are similar to spin-coating (2.6%). Neophytou *et al.* showed that heating during processing improved the performance of P3HT/PCBM solar cells from 1.5% (substrate temperature 34 °C) to 2.7% (substrate temperature 42 °C).²¹

Finally, Eom and coworkers added 1,8-octanedithiol to the ink. This resulted in efficiencies of 3.7% due to a morphology tuning by the ability of 1,8-octanedithiol for a selective solubility of one of the active layer materials. In addition to the prepared P3HT/PCBM layers, also the PEDOT:PSS layer was inkjet printed for these devices.⁷³

This section showed that by means of inkjet printing a controlled and reproducible material deposition is possible. Despite the fact that over recent years significant progress was made to improve the understanding of the drying behavior of inkjet printed features, further investigation on the effects of processing conditions on layer properties is required.

4 Direct comparison of applied processes and film characteristics

Many reports in the open literature discuss different processing techniques in order to achieve optimized device properties and efficiencies, but only a few reports allow a direct comparison

between different coating techniques. From reports discussing, for example, spin-coating or inkjet printing, a rough overview is provided on challenges and possibilities for a single process, while mainly the donor/acceptor system P3HT/PCBM is used. A direct comparison of the methods, where the same operators as well as the same characterization tools are used, is, however, preferred. Following this approach, a better analogy of current classifications as well as future developments can be drawn.

Wong and coworkers investigated the charge carrier mobilities and related morphological properties of inkjet printed, drop-cast and spin-coated P3HT films, prepared from a chlorobenzene solution (Fig. 12).⁵⁹ The authors found a remarkable difference in the resulting film properties depending on the preparation method. The highest crystallinity was observed for the inkjet printed films, whereas spin-coating resulted in the lowest crystallinity. Low root-mean-square (rms)-roughnesses for drop-cast and spin-coated films revealed an improved contact to the underlying surface, in contrast to the rough inkjet printed films. Hence, improved charge carrier mobilities were

obtained only for spin-coated and drop-cast films. The study shows a significant difference in the resulting morphologies depending on the preparation method. Therefore, different drying kinetics as well as processing properties significantly affect the film formation and the nano-morphology. Furthermore, the study showed that an optimized degree of crystallinity of P3HT results in high charge carrier mobilities as well as smooth film surfaces. It was assumed by the authors that a too long drying time of the relatively thick inkjet printed P3HT film (1.7 μm) leads to a too high crystallinity, whereas a thinner inkjet printed film may reveal improved film characteristics due to a shorter drying time.

For the preparation of efficient P3HT/PCBM organic solar cells, Hoth *et al.* optimized the ink and processing properties for the respective applied preparation technique. The authors investigated polymer solar cells with inkjet printed and doctor bladed active layers (Fig. 13).⁷⁴ The processing conditions of doctor bladed samples were transferred to the inkjet printing process, but, unfortunately, this transfer of parameters was

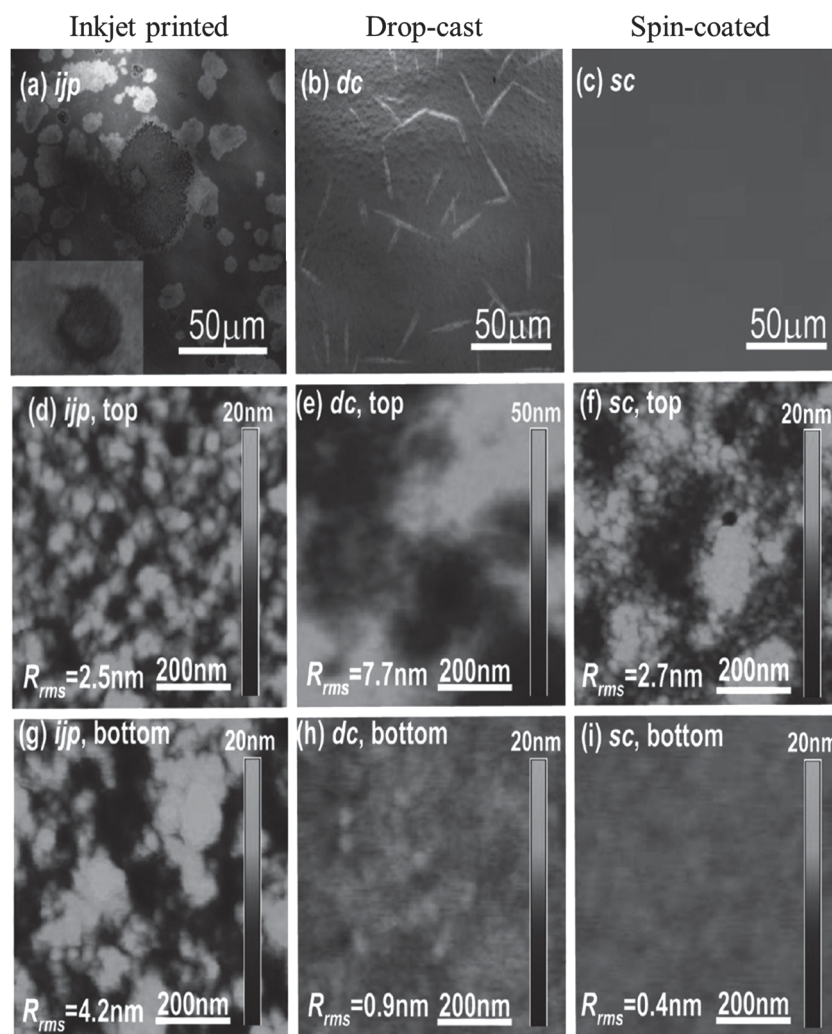


Fig. 12 Optical micrographs (a–c) and AFM images (d–i) of inkjet printed (a, d, g), drop-cast (b, e, h) and spin-coated (c, f, i) P3HT films prepared from chlorobenzene. Reprinted with permission from L. Y. Wong, R. Q. Png, F. B. S. Silva, L. L. Chua, D. V. M. Repaka, Shi-Chen, X. Y. Gao, L. Ke, S. J. Chua, A. T. S. Wee and P. K. H. Ho, *Langmuir*, 2010, **26**, 15494–15507. Copyright 2012 American Chemical Society.⁵⁹

found to be much more complex. Whereas for doctor blading highly regioregular (RR, 98%) P3HT showed the best performances, the preparation of inkjet printed films from the same solvent system was not possible in a simple manner due to a too fast gelation of P3HT and, subsequently, an increase in solution viscosity (Fig. 13a). For doctor blading the ink's viscosity had no significant influence on the processability, but inkjet printing requires a low viscosity (<100 mPa s).⁷⁵ Therefore, P3HT with a lower RR, which shows a slower gelation time, was used for inkjet printing and resulted in more homogeneous films (Fig. 13b). Furthermore, the authors found a strong dependence of the substrate temperature during processing on the film homogeneity. For doctor blading a plate temperature of 60 °C

showed the best results, while inkjet printing resulted in strong inhomogeneities when printing above 40 °C. First printing trials were performed with a single solvent (tetralin, bp 204 °C), which revealed a long drying time of the prepared films and, as a consequence, led to rough film surfaces as well as to a strong demixing of P3HT and PCBM. The authors have therefore developed a solvent system consisting of 68% *ortho*-dichlorobenzene (bp 179 °C) and 32% mesitylene (bp 165 °C), which revealed a reduced drying time as well as an improved film formation. By using this solvent mixture the surface roughness was lowered, the morphology was enhanced and the overall solar cell results were improved (Fig. 13d). The solar cells with an inkjet printed active layer of 96% RR P3HT/PCBM revealed

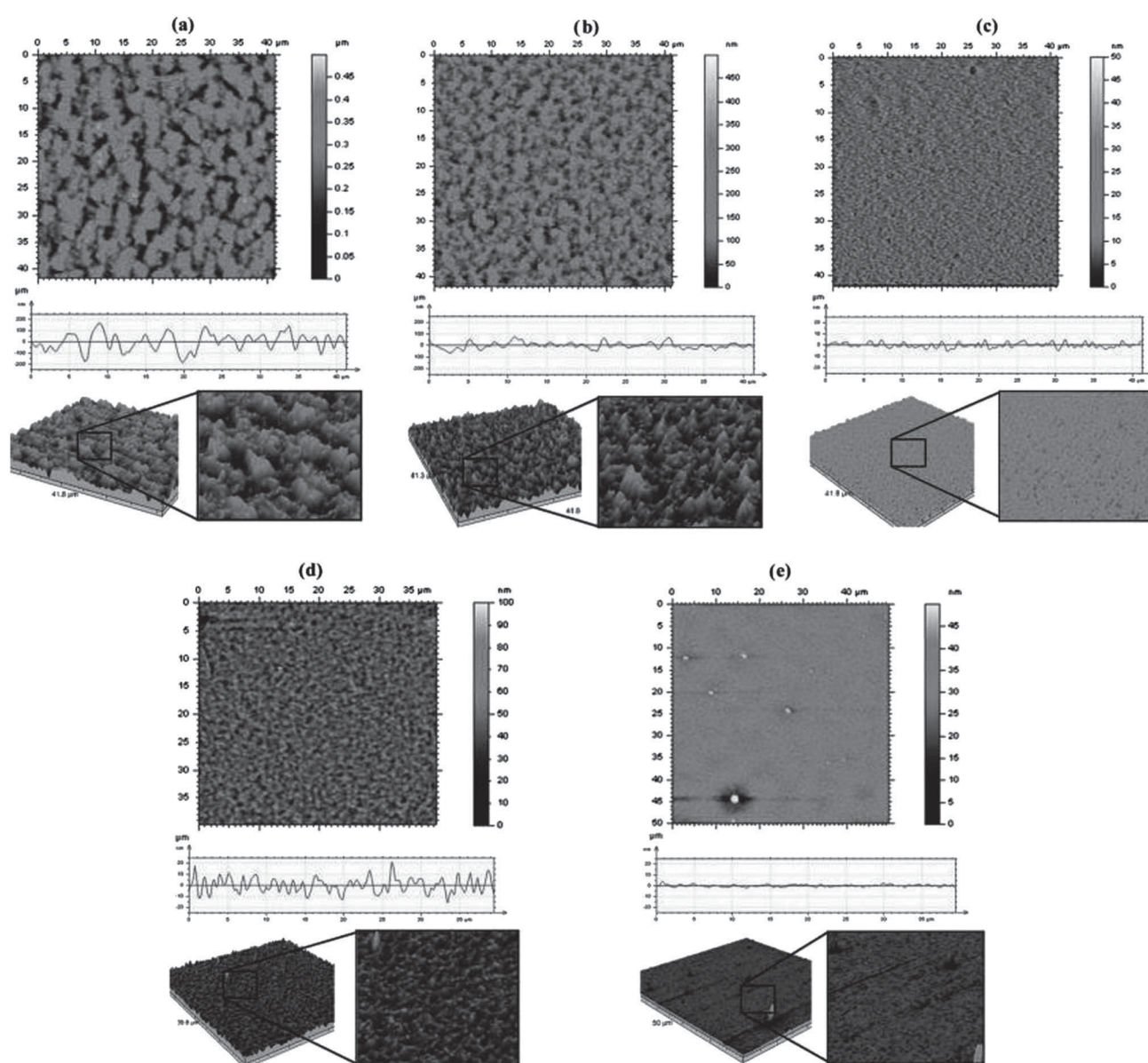


Fig. 13 Atomic force microscopy images of (a) inkjet printed RR-98.5%-P3HT/PCBM films prepared from tetralin, (b) inkjet printed RR-93%-P3HT/PCBM films prepared from tetralin, (c) doctor bladed RR-93%-P3HT/PCBM films prepared from tetralin, (d) inkjet printed RR-96%-P3HT/PCBM films prepared from oDCB/mesitylene and (e) doctor bladed RR-96%-P3HT/PCBM films prepared from oDCB/mesitylene. Reprinted with permission from C. N. Hoth, P. Schilinsky, S. A. Choulis and C. J. Brabec, *Nano Lett.*, 2008, **8**, 2806–2813. Copyright 2012 American Chemical Society.⁴³

an efficiency of 3.5%, which was a little lower than the efficiencies obtained with doctor bladed devices (4.1%, Fig. 13e). The authors explained the small difference by a higher surface roughness for the inkjet printed compared to the doctor bladed devices.⁷⁴

Jung *et al.* described the preparation of inkjet printed P3HT/PCBM solar cells using a single solvent. The authors did not mention problems that typically occur during printing from a single solvent, *i.e.* the formation of a coffee drop and low overall film homogeneity. The authors revealed relatively high efficiencies of 3.8% when using chlorobenzene (bp 132 °C) and 3.6% for *o*DCB (bp 179 °C) by optimizing the dot spacing of the deposited droplets. The lower values for the higher boiling *o*DCB were attributed to a longer film drying time. In contrast, the spin-coated reference devices yielded slightly higher device efficiencies for the higher boiling *o*DCB, but lower efficiencies for the lower boiling chlorobenzene.⁷⁶ This was attributed to the discrepancy between the drying rate requirements for the different deposition methods, as was described in a previous section. The lower boiling point solvent chlorobenzene seems to be more suitable for a slow drying process such as inkjet printing, whereas the higher boiling point solvent *o*DCB leads to improved results for spin-coated devices. Hence, both cases may result in optimal overall drying rates, depending on the processing techniques.

The results in this section confirm that a simple prediction of the resulting film morphology is not possible by easily switching the processing methods while using the same solute as well as processing conditions. A summary of applied film deposition techniques, processing techniques and device efficiencies reached is provided in Table 1. Since this review is focused on inkjet printing, data for spin-coating and doctor blading are provided for the purpose of comparison. Note that optimized PCE for spin-coated films exceeds 5%.⁷⁷ The values

reported here represent only a direct comparison of processing conditions and process. Each preparation method needs a separate optimization for the applied solution as well as for the desired application; whereas inkjet printing requires a faster film drying for efficient solar cell performances, the spin-coating process prefers a slow film drying.⁴³ Moreover, the current literature focuses mainly on the donor-acceptor combination P3HT/PCBM, while other systems may potentially show different results.

5 Discussion

In the previous sections the drying characteristics and resulting film properties of different film preparation methods were discussed. It was shown that the control of the film morphology depends on the used preparation technique. The characteristics of organic semiconductor layers, *e.g.* charge carrier mobilities, optical and morphological properties, significantly depend on the molecular ordering of the polymer in the dried film, which can be tuned as a function of the film forming process as well as fabrication conditions. Whereas for spin-coating the correlations between processing parameters and layer properties are relatively well understood, there is much work to be done in order to fully understand the general drying kinetics for the inkjet printing process.

To form a complete picture of the advantages and drawbacks of the inkjet printing method as well as to elucidate potential developments of this process, an overview of properties and challenges is summarized in Fig. 14.

An attractive issue when using inkjet printing is that only a little amount of the materials is required and, due to a low waste production, inkjet printing is characterized as a material-efficient technique. Due to the fact that inkjet printing is an additive technique, there is no limitation for the used

Table 1 PCE of P3HT/PCBM solar cells processed by different techniques and conditions

Processing technique	RR P3HT [%]	Solvent	Processing temp. [°C]	Thermal annealing	PCE [%]	Ref.
Spin-coating	N/A	Toluene	RT	—	0.3	35
Spin-coating	N/A	CB	RT	—	0.7	35
Spin-coating	N/A	<i>o</i> DCB	RT	—	0.8	35
Spin-coating	N/A	CB/trichlorobenzene	RT	130 °C	2.6	72
Doctor blading	N/A	DCB	15	—	2.1	41
Doctor blading	N/A	DCB	40	—	0.9	41
Doctor blading	N/A	Toluene	RT	140 °C/20 min	3.5	42
Doctor blading	N/A	Toluene	60	140 °C/20 min	3.8	42
Doctor blading	93	Tetralin	60	140 °C/10 min	3.3	43
Doctor blading	96	<i>o</i> DCB/mesitylene 68/32	40	140 °C/10 min	4.1	43
Doctor blading	96	<i>o</i> DCB/mesitylene 68/32	40	140 °C/10 min	4.1	43
Inkjet printing	N/A	CB/trichlorobenzene	N/A	130 °C	2.4	72
Inkjet printing	95	<i>o</i> DCB	34 °C	140 °C/15 min	1.5	21
Inkjet printing	95	<i>o</i> DCB	42 °C	140 °C/15 min	2.7	21
Inkjet printing	N/A	CB	RT	—	2.0	73
Inkjet printing	N/A	CB/ <i>o</i> DCB 95/5	RT	—	3.4	73
Inkjet printing	98.5	<i>o</i> DCB/mesitylene 68/32	40	140 °C/10 min	0.1	74
Inkjet printing	98.5	Tetralin	40	140 °C/10 min	0.7	74
Inkjet printing	93	Tetralin	40	140 °C/10 min	1.3	74
Inkjet printing	96	<i>o</i> DCB/mesitylene 68/32	40	140 °C/10 min	3.5	74
Inkjet printing	N/A	CB	RT	90 °C/10 min	3.6	76
Inkjet printing	N/A	<i>o</i> DCB	RT	90 °C/10 min	3.8	76

substrates, and flexible, curved substrates can be used besides rigid, planar surfaces. Therefore, inkjet printing can be easily applied for the fabrication of flexible devices. However, the solute properties, *i.e.* solvent, viscosity and surface tension, are more critical parameters for applicability in the inkjet printing process, in contrast to spin-coating. Furthermore, inkjet printing can be used in a combinatorial screening workflow to characterize materials and thin-film properties. This approach significantly accelerates the materials research.

Depending on the chosen inkjet printer system, there is a specific window for a useable surface tension, viscosity and density of the ink. Fromm predicted the successful printing of an ink when the Z-number, which depends on the nozzle orifice d , the surface tension γ , the density ρ and the viscosity η , is greater than 2.⁷⁸ Some studies report a printability only in the range $2 < Z < 14$,⁷⁹ while other studies confirm printability of fluids with $Z > 60$.⁶⁷ In practice, however, the lower limit is determined by the viscosity that dissipates the pressure pulse,¹⁵ whereas the upper limit represents the formation of satellite droplets.⁸⁰ Furthermore, systems where the Z-number is much larger than 10 are printable as long as the formed satellites merge with the main droplet. The main factor that appeared to affect an ink's printability is its vapor pressure, with unstable droplets and no droplets being produced for solvents with vapor pressures higher than approximately 13 kPa. As soon as significant solvent evaporation takes place at the nozzle orifice, nozzle clogging may occur and printing is disturbed.

Besides the ink's rather small working window, a second challenge of the inkjet printing process is the ink's wetting behavior on the substrate. For thin film preparation, a good wetting behavior, hence a low contact angle of the ink with the underlying substrate, is preferred. Despite the fact that film size and thickness can be easily varied by changing the number of

deposited droplets, the drying control of different film sizes is very complicated. Applying the solute and the printing parameters, which were found to be the optimized values for small films, does not automatically result in a good film formation for increased film sizes.

A third challenge is the dependence of the size of the device on its final efficiency. All reported efficiencies in the open literature are small, lab-scale produced devices. However, by increasing the film size, for example, from 0.04 to 1 cm², device parameters, like the fill factor (FF) and the power conversion efficiency (PCE), significantly decrease.⁸¹

Other effects, such as the drying kinetics and the fluid flow within a drying droplet, are at this moment not fully understood and not able to be controlled. Therefore, it is difficult to predict the final film formation using inkjet printing. All these factors show the importance of evolving complete knowledge and, subsequently, controlling the drying processes that take place in an inkjet printed film.

When inkjet printing is applied for bulk heterojunction solar cells, the preparation and optimization are very complicated, since both the processing techniques as well as the solution properties affect the final device efficiency. For instance, it is not clear whether the surface roughness or the nano-morphology is the main limiting factor for the power conversion efficiency. This knowledge is, however, crucial for the choice of processing parameters, as a high boiling solvent leads to an increased surface roughness. It is noticeable that in the literature, contradicting results are reported, for example on the effect of the substrate temperature during coating.^{54,66} Up to now no general guideline was found for an optimized device efficiency, since most of the research groups change only a single (or at best a few) parameters out of many. At this point, a combinatorial screening would lead to more comparable results and better insight.

Most of the reported results indicated a correlation between the drying speed, either induced by the solvents or by the applied methods, and the device characteristics.^{35,59} However, it was also reported that not only do the drying kinetics influence the resulting film properties, but also the type of solvents, independent of the boiling point.^{42,43} Zhang *et al.* investigated the use of a solvent mixture, consisting of a main solvent chloroform and a co-solvent (xylene, toluene or chlorobenzene).⁸² From the discussions above, a general improvement of the spin-coated polyfluorene (PF)/PCBM layers was expected since the three co-solvents increase the boiling point of the solvent mixture significantly. Instead, only chlorobenzene showed improved OPV characteristics, whereas the other two co-solvents revealed a reduction of PCEs due to the formation of pronounced domains and increased surface roughnesses. The optimized parameters cannot be transferred easily to other polymer/fullerene combinations, since every compound solution has different rheological and, as a consequence, drying properties. P3HT is a semi-crystalline polymer, whereas processing dependent studies for more amorphous polymers, such as PF, are not available to such an extent.

Furthermore, polymer-polymer combinations have been used in OPVs to broaden the absorption spectrum and, as a

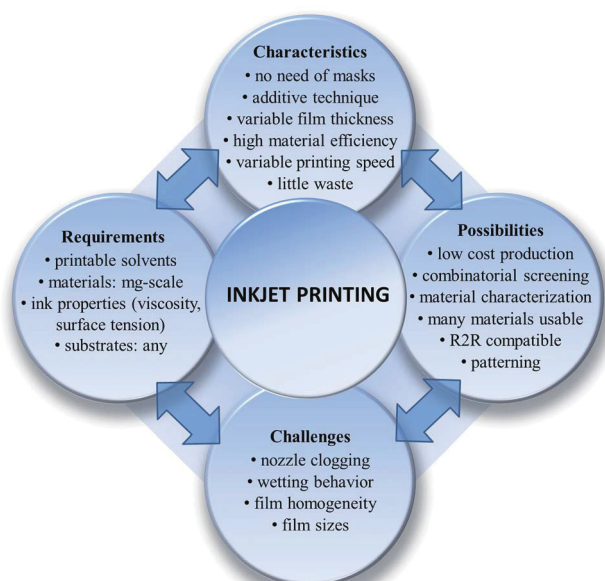


Fig. 14 Schematic representation of characteristics, requirements, possibilities and challenges of the inkjet printing process.

consequence, to improve the efficiency of the solar cell. The combination of materials results in a more complex drying behavior compared to a single polymer system.⁵ Since polymers tend to segregate in solution, a fast drying of the prepared layer is preferred, otherwise the polymers are not well mixed in the final active layer and charge generation cannot take place. Arias *et al.* found enhanced morphological properties by using spin-coating compared to doctor blading by applying a lower boiling solvent as well as by increasing the substrate temperature during the fabrication of a polyfluorene blend, which contradicts the P3HT processing properties, as discussed in a previous section.⁸³

In the near future one more challenge remains, which is to investigate more environmentally friendly solvents. Schmidt-Hansberg and coworkers investigated the replacement of the common solvents used for OPVs with non-halogenated solvent mixtures in doctor bladed films.⁸⁴ It was found that indane in combination with toluene represents a suitable replacement for the common chlorinated solvents, resulting in good absorption behaviors as well as a high polymer crystallinity. Furthermore, a combination of acetophenone and mesitylene was proven to be a good solvent system for spin-coated films in order to replace oDCB in OPV preparation.⁸⁵

The advantages of inkjet printing demonstrate that the required efforts are profitable, because inkjet printing can emerge as a material-efficient, cost-effective and R2R-compatible patterning technique. However, for the application of inkjet printing in a commercially available device there are many challenges to overcome, which is the reason why inkjet printing up to now has mainly been used in a scientific research environment.

6 Conclusion

This review discussed different printing and coating techniques applied for organic electronics. Since the nano-morphological structure of solar cell active layers, which can be significantly tuned by applied parameters, can be correlated directly to the device efficiency, the effect of processing conditions was discussed in particular for OPVs. The emphasis was on the drying characteristics of the preparation techniques. The relatively new and nascent technology of inkjet printing was compared to spin-coating and doctor blading – the latter two are currently the most commonly used preparation techniques for active layers in organic electronics. It was shown that film properties strongly depend on the drying time, which is influenced by the used solvent as well as by the processing technique itself. Spin-coating was found to give good layer properties when using solvents with a high boiling point, whereas in the slow drying processing of inkjet printing, solvents with a lower boiling point are preferred. On the other hand, the interplay between the drying kinetics and film properties is more complicated.

The analysis of the drying characteristics of the different preparation methods showed that basic principles are well understood, but that there is not yet a complete understanding of drying behaviors and resulting film characteristics. A prediction of layer properties when using a combination of ink

and processing method is currently not possible, but it needs to be a major aim for further research in order to gain a complete understanding of the morphological properties as well as to evolve the ability to transfer existing knowledge to new materials. Different ways to control the drying process *via* the variation of preparation characteristics as well as tuning the drying speed of the as-prepared films were shown.

From a current point of view, none of the processing methods is considered to be the best for the preparation of OPVs in order to produce homogeneous layers with an optimal nano-morphology. Spin-coating is a well developed technique that reaches the highest reported efficiencies, but is not characterized by a material-efficient or R2R-compatible processing method. In contrast, inkjet printing is able to produce devices with sufficient efficiencies in a reproducible and material efficient manner. Inkjet printing has proven to be highly useful for the preparation of single lab devices and is a promising technique for R2R processing, but clearly needs more optimization to produce devices in larger numbers as well as in size and in a reproducible way.

In summary, inkjet printing is promising as a material-efficient and non-contact deposition process tool. In the field of organic electronics, in particular OPV, the state of research is increasing, but behind other solution deposition methods like spin-coating. Optimal processing parameters, like solvent or substrate temperature, cannot be transferred easily to other solution processing methods. At this point it is therefore clear that the fabrication of organic solar cell devices may use different preparation methods for each individual layer. For more efficient fabrication, R2R processing is preferred, since multiple processing techniques can be easily applied in sequence.

Inkjet printing, however, can bridge the gap between polymer synthesis and solid-state or surface property evaluation, since the technique opens the way to the automatic preparation of thin-film libraries of polymers, polymer blends and composites, with a systematic variation of parameters such as chemical composition or thickness. When novel compounds are to be processed *via* inkjet printing, an optimization of film properties needs to be performed by the use of a combinatorial screening for each individual parameter that influences the homogeneity.

Acknowledgements

The authors thank the DPI (project #620, technology area HTE) as well as the European Community's Seventh Framework Programme (FP7/2007-2013) under grant agreement no. 248816 for financial support.

References

- 1 J. Perelaer, P. J. Smith, D. Mager, D. Soltman, S. K. Volkman, V. Subramanian, J. G. Korvink and U. S. Schubert, *J. Mater. Chem.*, 2010, **20**, 8446–8453.
- 2 F. C. Krebs, *Org. Electron.*, 2009, **10**, 761–768.

- 3 S. W. Ko, E. T. Hoke, L. Pandey, S. H. Hong, R. Mondal, C. Risko, Y. P. Yi, R. Noriega, M. D. McGehee, J. L. Bredas, A. Salleo and Z. A. Bao, *J. Am. Chem. Soc.*, 2012, **134**, 5222–5232.
- 4 H. N. Tsao and K. Muellen, *Chem. Soc. Rev.*, 2010, **39**, 2372–2386.
- 5 S. Guenes, H. Neugebauer and N. S. Sariciftci, *Chem. Rev.*, 2007, **107**, 1324–1338.
- 6 F. C. Krebs, *Sol. Energy Mater. Sol. Cells*, 2009, **93**, 394–412.
- 7 Y. Y. Liang, Z. Xu, J. B. Xia, S. T. Tsai, Y. Wu, G. Li, C. Ray and L. P. Yu, *Adv. Mater.*, 2010, **22**, E135–E138.
- 8 L. T. Dou, J. B. You, J. Yang, C. C. Chen, Y. J. He, S. Murase, T. Moriarty, K. Emery, G. Li and Y. Yang, *Nat. Photonics*, 2012, **6**, 180–185.
- 9 <http://www.heliatek.com>, accessed 22 June 2012.
- 10 M. C. Scharber, D. Wuhlbacher, M. Koppe, P. Denk, C. Waldauf, A. J. Heeger and C. L. Brabec, *Adv. Mater.*, 2006, **18**, 789–792.
- 11 G. Dennler, M. C. Scharber, T. Ameri, P. Denk, K. Forberich, C. Waldauf and C. J. Brabec, *Adv. Mater.*, 2008, **20**, 579–583.
- 12 A. H. Rice, R. Giridharagopal, S. X. Zheng, F. S. Ohuchi, D. S. Ginger and C. K. Luscombe, *ACS Nano*, 2011, **5**, 3132–3140.
- 13 J. A. Hauch, P. Schilinsky, S. A. Choulis, R. Childers, M. Biele and C. J. Brabec, *Sol. Energy Mater. Sol. Cells*, 2008, **92**, 727–731.
- 14 M. Jørgensen, K. Norrman, S. Gevorgyan, T. Tromholt, B. Andreasen and F. C. Krebs, *Adv. Mater.*, 2012, **24**, 580–612.
- 15 E. Tekin, P. J. Smith and U. S. Schubert, *Soft Matter*, 2008, **4**, 703–713.
- 16 M. Barret, S. Sanaur and P. Collot, *Org. Electron.*, 2008, **9**, 1093–1100.
- 17 K. J. Baeg, D. Khim, J. H. Kim, M. Kang, I. K. You, D. Y. Kim and Y. Y. Noh, *Org. Electron.*, 2011, **12**, 634–640.
- 18 Y. Yoshioka, P. D. Calvert and G. E. Jabbour, *Macromol. Rapid Commun.*, 2005, **26**, 238–246.
- 19 E. Tekin, E. Holder, D. Kozodaev and U. S. Schubert, *Adv. Funct. Mater.*, 2007, **17**, 277–284.
- 20 A. Teichler, R. Eckardt, S. Hoepfner, C. Friebe, J. Perelaer, A. Senes, M. Morana, C. J. Brabec and U. S. Schubert, *Adv. Energy Mater.*, 2011, **1**, 105–114.
- 21 M. Neophytou, W. Cambarau, F. Hermerschmidt, C. Waldauf, C. Christodoulou, R. Pacios and S. A. Choulis, *Microelectron. Eng.*, 2012, **95**, 102–106.
- 22 H. M. Haverinen, R. A. Myllyla and G. E. Jabbour, *Appl. Phys. Lett.*, 2009, **94**, 073108.
- 23 M. O'Toole, R. Shepherd, G. G. Wallace and D. Diamond, *Anal. Chim. Acta*, 2009, **652**, 308–314.
- 24 M. Sanyal, B. Schmidt-Hansberg, M. F. G. Klein, A. Colmann, C. Munuera, A. Vorobiev, U. Lemmer, W. Schabel, H. Dosch and E. Barrena, *Adv. Energy Mater.*, 2011, **1**, 363–367.
- 25 F. C. Krebs, M. Jørgensen, K. Norrman, O. Hagemann, J. Alstrup, T. D. Nielsen, J. Fyenbo, K. Larsen and J. Kristensen, *Sol. Energy Mater. Sol. Cells*, 2009, **93**, 422–441.
- 26 D. B. Hall, P. Underhill and J. M. Torkelson, *Polym. Eng. Sci.*, 1998, **38**, 2039–2045.
- 27 K. Norrman, A. Ghanbari-Siahkali and N. B. Larsen, *Annu. Rep. Prog. Chem., Sect. C: Phys. Chem.*, 2005, **101**, 174–201.
- 28 Y. Yang, Y. Shi, J. Liu and T.-F. Guo, in *Electronic and Optical Properties of Conjugated Molecular Systems in Condensed Phases*, ed. S. Hotta, Research Signpost, Kerala, 2003, pp. 307–354.
- 29 Y. Shi, J. Liu and Y. Yang, *J. Appl. Phys.*, 2000, **87**, 4254–4263.
- 30 J. F. Chang, B. Q. Sun, D. W. Breiby, M. M. Nielsen, T. I. Solling, M. Giles, I. McCulloch and H. Siringhaus, *Chem. Mater.*, 2004, **16**, 4772–4776.
- 31 D. M. DeLongchamp, B. M. Vogel, Y. Jung, M. C. Gurau, C. A. Richter, O. A. Kirillov, J. Obrzut, D. A. Fischer, S. Sambasivan, L. J. Richter and E. K. Lin, *Chem. Mater.*, 2005, **17**, 5610–5612.
- 32 H. C. Yang, T. J. Shin, L. Yang, K. Cho, C. Y. Ryu and Z. N. Bao, *Adv. Funct. Mater.*, 2005, **15**, 671–676.
- 33 V. D. Mihailetschi, H. X. Xie, B. de Boer, L. M. Popescu, J. C. Hummelen, P. W. M. Blom and L. J. A. Koster, *Appl. Phys. Lett.*, 2006, **89**, 012107.
- 34 G. Li, V. Shrotriya, J. S. Huang, Y. Yao, T. Moriarty, K. Emery and Y. Yang, *Nat. Mater.*, 2005, **4**, 864–868.
- 35 M. T. Dang, G. Wantz, H. Bejbouji, M. Urien, O. J. Dautel, L. Vignau and L. Hirsch, *Sol. Energy Mater. Sol. Cells*, 2011, **95**, 3408–3418.
- 36 N. D. Treat, C. G. Shuttle, M. F. Toney, C. J. Hawker and M. L. Chabinyc, *J. Mater. Chem.*, 2011, **21**, 15224–15231.
- 37 A. Pivrikas, H. Neugebauer and N. S. Sariciftci, *Sol. Energy*, 2011, **85**, 1226–1237.
- 38 S. J. Storfer, J. T. Dipiazza and R. E. Moran, *J. Coat. Technol.*, 1988, **60**, 37–43.
- 39 B. Schmidt-Hansberg, H. Do, A. Colmann, U. Lemmer and W. Schabel, *Eur. Phys. J. Spec. Top.*, 2009, **166**, 49–53.
- 40 T. Wang, A. D. F. Dunbar, P. A. Staniec, A. J. Pearson, P. E. Hopkinson, J. E. MacDonald, S. Lilliu, C. Pizzey, N. J. Terrill, A. M. Donald, A. J. Ryan, R. A. L. Jones and D. G. Lidzey, *Soft Matter*, 2010, **6**, 4128–4134.
- 41 B. Schmidt-Hansberg, M. Sanyal, M. F. G. Klein, M. Pfaff, N. Schnabel, S. Jaiser, A. Vorobiev, E. Mueller, A. Colmann, P. Scharfer, D. Gerthsen, U. Lemmer, E. Barrena and W. Schabel, *ACS Nano*, 2011, **5**, 8579–8590.
- 42 Y. H. Chang, S. R. Tseng, C. Y. Chen, H. F. Meng, E. C. Chen, S. F. Horng and C. S. Hsu, *Org. Electron.*, 2009, **10**, 741–746.
- 43 C. N. Hoth, P. Schilinsky, S. A. Choulis and C. J. Brabec, *Nano Lett.*, 2008, **8**, 2806–2813.
- 44 S. E. Shaheen, R. Radspinner, N. Peyghambarian and G. E. Jabbour, *Appl. Phys. Lett.*, 2001, **79**, 2996–2998.
- 45 B. Derby, *Annu. Rev. Mater. Res.*, 2010, **40**, 395–414.
- 46 B. J. de Gans, P. C. Duineveld and U. S. Schubert, *Adv. Mater.*, 2004, **16**, 203–213.
- 47 R. M. Verkouteren and J. R. Verkouteren, *Langmuir*, 2011, **27**, 9644–9653.
- 48 A. M. J. van den Berg, P. J. Smith, J. Perelaer, W. Schrof, S. Koltzenburg and U. S. Schubert, *Soft Matter*, 2007, **3**, 238–243.
- 49 E. Tekin, E. Holder, V. Marin, B. J. de Gans and U. S. Schubert, *Macromol. Rapid Commun.*, 2005, **26**, 293–297.

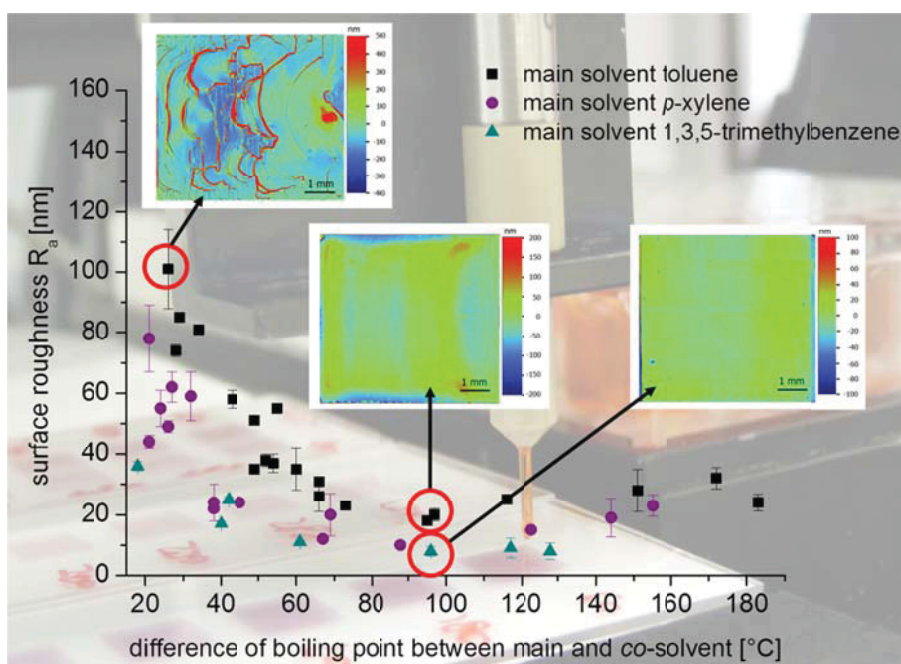
- 50 J. Perelaer, Eindhoven University of Technology, Eindhoven, 2009, *PhD Thesis*.
- 51 J. Peet, M. L. Senatore, A. J. Heeger and G. C. Bazan, *Adv. Mater.*, 2009, **21**, 1521–1527.
- 52 T. Aernouts, T. Aleksandrov, C. Girotto, J. Genoe and J. Poortmans, *Appl. Phys. Lett.*, 2008, **92**, 033306.
- 53 A. Calabrese, A. Pellegrino, R. Po, A. Savoini, F. Tinti and N. Camaioni, *Sol. Energy Mater. Sol. Cells*, 2011, **95**, 3428–3432.
- 54 A. Teichler, R. Eckardt, C. Friebe, J. Perelaer and U. S. Schubert, *Thin Solid Films*, 2011, **519**, 3695–3702.
- 55 J. A. Renz, T. Keller, M. Schneider, S. Shokhovets, K. D. Jandt, G. Gobsch and H. Hoppe, *Sol. Energy Mater. Sol. Cells*, 2009, **93**, 508–513.
- 56 E. Tekin, H. Wijlaars, E. Holder, D. A. M. Egbe and U. S. Schubert, *J. Mater. Chem.*, 2006, **16**, 4294–4298.
- 57 E. Tekin, P. J. Smith, S. Hoepfener, A. M. J. van den Berg, A. S. Susha, A. L. Rogach, J. Feldmann and U. S. Schubert, *Adv. Funct. Mater.*, 2007, **17**, 23–28.
- 58 V. Marin, E. Holder, M. M. Wienk, E. Tekin, D. Kozodaev and U. S. Schubert, *Macromol. Rapid Commun.*, 2005, **26**, 319–324.
- 59 L. Y. Wong, R. Q. Png, F. B. S. Silva, L. L. Chua, D. V. M. Repaka, Shi-Chen, X. Y. Gao, L. Ke, S. J. Chua, A. T. S. Wee and P. K. H. Ho, *Langmuir*, 2010, **26**, 15494–15507.
- 60 R. D. Deegan, *Phys. Rev. E: Stat. Phys., Plasmas, Fluids, Relat. Interdiscip. Top.*, 2000, **61**, 475–485.
- 61 Y. Oh, J. Kim, Y. J. Yoon, H. Kim, H. G. Yoon, S. N. Lee and J. Kim, *Curr. Appl. Phys.*, 2011, **11**, S359–S363.
- 62 T. Kajiya, W. Kobayashi, T. Okuzono and M. Doi, *Langmuir*, 2010, **26**, 10429–10432.
- 63 J. S. Park, J. P. Kim, C. Song and M. Lee, *Displays*, 2010, **31**, 164–167.
- 64 E. Tekin, B. J. de Gans and U. S. Schubert, *J. Mater. Chem.*, 2004, **14**, 2627–2632.
- 65 H. Hu and R. G. Larson, *J. Phys. Chem. B*, 2006, **110**, 7090–7094.
- 66 J. X. Zhou, J. Y. H. Fuh, H. T. Loh, Y. S. Wong, Y. S. Ng, J. J. Gray and S. J. Chua, *Int. J. Adv. Manuf. Tech.*, 2010, **48**, 243–250.
- 67 J. Perelaer, P. J. Smith, M. M. P. Wijnen, E. van den Bosch, R. Eckardt, P. H. J. M. Ketelaars and U. S. Schubert, *Macromol. Chem. Phys.*, 2009, **210**, 387–393.
- 68 J. Perelaer, B. J. de Gans and U. S. Schubert, *Adv. Mater.*, 2006, **18**, 2101–2104.
- 69 M. Wang, G. Z. Yang, M. Wang and T. X. Liu, *Polym. Adv. Technol.*, 2010, **21**, 381–385.
- 70 M. B. Madec, P. J. Smith, A. Malandraki, N. Wang, J. G. Korvink and S. G. Yeates, *J. Mater. Chem.*, 2010, **20**, 9155–9160.
- 71 S. Chung, J. Jang, J. Cho, C. Lee, S. K. Kwon and Y. Hong, *Jpn. J. Appl. Phys.*, 2011, **50**, 03CB05.
- 72 A. Lange, M. Wegener, C. Boeffel, B. Fischer, A. Wedel and D. Neher, *Sol. Energy Mater. Sol. Cells*, 2010, **94**, 1816–1821.
- 73 S. H. Eom, H. Park, S. H. Mujawar, S. C. Yoon, S. S. Kim, S. I. Na, S. J. Kang, D. Khim, D. Y. Kim and S. H. Lee, *Org. Electron.*, 2010, **11**, 1516–1522.
- 74 C. N. Hoth, S. A. Choulis, P. Schilinsky and C. J. Brabec, *J. Mater. Chem.*, 2009, **19**, 5398–5404.
- 75 <http://www.microdrop.de>, accessed 08 November 2012.
- 76 J. Jung, D. Kim, J. Lim, C. Lee and S. C. Yoon, *Jpn. J. Appl. Phys.*, 2010, **49**, 05EB03.
- 77 M. T. Dang, L. Hirsch and G. Wantz, *Adv. Mater.*, 2011, **23**, 3597–3602.
- 78 J. E. Fromm, *IBM J. Res. Dev.*, 1984, **28**, 322–333.
- 79 D. Jang, D. Kim and J. Moon, *Langmuir*, 2009, **25**, 2629–2635.
- 80 K. A. M. Seerden, N. Reis, J. R. G. Evans, P. S. Grant, J. W. Halloran and B. Derby, *J. Am. Ceram. Soc.*, 2001, **84**, 2514–2520.
- 81 A. Manor, E. A. Katz, T. Tromholt, B. Hirsch and F. C. Krebs, *J. Appl. Phys.*, 2011, **109**, 074508.
- 82 F. Zhang, S. Lacic, M. Svensson, M. R. Andersson and O. Inganäs, *Sol. Energy Mater. Sol. Cells*, 2006, **90**, 1607–1614.
- 83 A. C. Arias, J. D. MacKenzie, R. Stevenson, J. J. M. Halls, M. Inbasekaran, E. P. Woo, D. Richards and R. H. Friend, *Macromolecules*, 2001, **34**, 6005–6013.
- 84 B. Schmidt-Hansberg, M. Sanyal, N. Grossiord, Y. Galagan, M. Baunach, M. F. G. Klein, A. Colsmann, P. Scharfer, U. Lemmer, H. Dosch, J. Michels, E. Barrena and W. Schabel, *Sol. Energy Mater. Sol. Cells*, 2012, **96**, 195–201.
- 85 C. D. Park, T. A. Fleetham, J. Li and B. D. Vogt, *Org. Electron.*, 2011, **12**, 1465–1470.

Publication 2

“Screening of Film Formation Qualities of Various Solvent Systems for π -conjugated Polymers via Combinatorial Inkjet Printing”

Anke Teichler, Jolke Perelaer, Ulrich S. Schubert

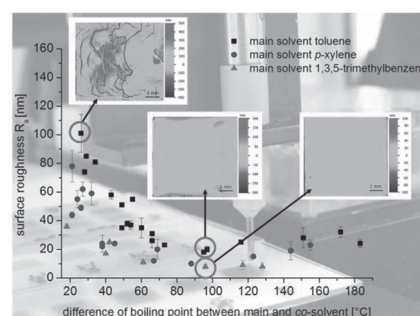
Macromol. Chem. Phys. **2013**, *214*, 547-555.



Screening of Film-Formation Qualities of Various Solvent Systems for π -Conjugated Polymers Via Combinatorial Inkjet Printing

Anke Teichler, Jolke Perelaer, Ulrich S. Schubert*

A systematic investigation of the relationships between the choice of solvent system and the film quality of inkjet printed π -conjugated polymer films is presented. Solution properties, such as surface tension and viscosity, have no effect on the final film quality, whereas the boiling point of the solvent and, more specifically, the difference in boiling point between the main and the co-solvent have a strong influence on the final film quality. New solvent systems are developed based on non-chlorinated, aromatic solvents that reveal homogeneous films when the difference in boiling point between the main and the co-solvent is between 90 and 100 °C.



1. Introduction

The research field of organic electronics has attracted great interest over the last years due to their light weight, flexibility, and cheap production. However, different challenging tasks need to be overcome in order to ensure inkjet printing to be a reliable processing technique; firstly, the development of the complete understanding of solution drying processes and, secondly, the identification of more environmental friendly alternatives for chlorinated solvents, which are commonly used as solvents in organic electronics.^[1,2] Chlorobenzene and *ortho*-dichlorobenzene are currently the most reported solvents, as they produce homogeneous films as well as an optimal nano-morphological structure of active layers for organic

photovoltaics (OPVs).^[3] The application of these solvents is not critical when utilizing lab-scale film-preparation techniques since the solvents are used only in small quantities. In contrast, in a roll-to-roll (R2R) process, where larger amounts of solvents are applied, the use of environmentally unfriendly solvents becomes critical.^[4] Therefore, novel solvents need to be investigated to ensure a greener processing for OPV applications, while maintaining a similar film morphology.^[5]

Among the diverse solution-deposition methods that are available for organic electronics,^[6,7] spin-coating has a clear supremacy over other techniques due to its simple processing conditions. The film formation characteristics are well understood for spin-coating,^[6] and this method is, therefore, a well-developed technique that offers an uncomplicated and fast experimentation procedure.^[8] However, spin-coating has clear disadvantages, including a high material waste and the lack of capability for an automatic process. In contrast, inkjet printing shows several advantages in comparison to other solution-deposition techniques, including a mask-free, drop-on-demand deposition, an efficient material handling, and the possibility for a combinatorial screening of potential materials and solvent systems.^[9,10] In particular, when using a combinatorial inkjet printing approach, many different materials or compound blends can be screened in parallel for their film formation characteristics as well as

A. Teichler, Dr. J. Perelaer, Prof. U. S. Schubert
Laboratory of Organic and Macromolecular Chemistry (IOMC),
Friedrich-Schiller-University Jena, Humboldtstraße 10,
07743 Jena, Germany
E-mail: ulrich.schubert@uni-jena.de
A. Teichler, Dr. J. Perelaer, Prof. U. S. Schubert
Jena Center for Soft Matter (JCSM), Friedrich-Schiller-
University Jena, Philosophenweg 7, 07743 Jena, Germany
A. Teichler, Dr. J. Perelaer, Prof. U. S. Schubert
Dutch Polymer Institute (DPI), P.O. Box 513, 5600 MB
Eindhoven, The Netherlands

thin-film properties.^[11,12] However, inkjet printing is limited to special solution properties, like a certain viscosity and surface tension window. In addition, the parameters that influence the drying of the deposited material are complex.^[12]

The main reason why inkjet printing is currently not well established in the field of organic electronics is the unpredictable final film formation, which is attributed to the complexity of the drying parameters and the incomplete basic investigations on the drying behavior of inkjet printed thin films.^[13,14] When alternative solvents for the chlorinated solvents are found, the basics of thin film drying processes need to be understood. The effects of several fluidic characteristics, such as the surface tension and the viscosity as well as the solvent system, have been discussed in literature.^[15] Furthermore, the choice of the processing solvent or solvent system represents a significant influence to the drying behavior of a printed feature. It was confirmed that a solvent mixture containing a lower boiling point main solvent and a higher boiling point co-solvent is required for inkjet printing in order to create homogeneous thin films and to suppress the so-called coffee-ring effect, which causes the material to concentrate at the rim of a droplet during drying.^[16] Several investigations on the influence of the solvent ratio between main and co-solvent to film surface homogeneities showed an optimal ratio of 90/10, whereas lower or higher contents of the high-boiling point solvent lead to non-homogeneous films as well as to increased surface roughnesses.^[11,12] In addition, Hu and Larson^[17] described the need of a co-solvent, which has, in addition to a higher boiling point, a lower surface tension than the main solvent. In this case, another material flow, called the Marangoni effect, is induced in the drying droplet leading to a homogeneous film formation.^[18]

The resulting film homogeneity is not only dependent on the drying of a printed feature but also on a stable and reproducible droplet formation. The latter two characteristics are described in literature as significantly influenced by the nozzle orifice as well as by the ink characteristics, including the surface tension, the viscosity, and the density. These parameters are combined in the dimensionless Z-number, which describes the printability of an ink by the use of a specific nozzle diameter.^[19] It was reported that limitations in printability occur, depending on the ink, if the Z-number is either lower than 2 or higher than 14,^[19] whereas other groups found a reproducible printability using inks with Z-numbers > 60.^[20]

In this contribution, a systematic investigation of ink properties, including the surface tension, the viscosity, and the solvent's boiling point, and their influence to the printability as well as to their film formation ability is presented by using a combinatorial inkjet printing approach. Therefore, only 80 mg of poly(3-octylthiophene) (P3OT)

and 0.5 mL of each solvent system were required for the preparation of the thin film library with 42 different solvent systems. A correlation between the ink properties and the surface roughness is evaluated.

2. Experimental Section

2.1. Materials

The polymer poly(3-octylthiophene) (P3OT) as well as all solvents were purchased from Sigma-Aldrich. The polymers poly(phenylene-vinylene) (PPV) and poly(diketopyrrolopyrrole-co-benzothiadiazole-co-fluorene) (poly(DPP-co-BTD-co-F)) were synthesized according to literature.^[21,22] The polymers were dissolved in the described solvent systems in a concentration of 4 mg mL⁻¹. After stirring overnight, the solutions were filtered using a syringe filter with a pore size of 0.45 μm.

2.2. Characterization

Surface tension and contact angles of the inks were investigated by the contact angle measurement system OCA 20 from Data-physics (Filderstedt, Germany). Density as well as viscosity measurements were performed using a DMA 02 density meter and a ball/capillary viscosimeter AMVn (Anton Paar, Graz, Austria), respectively. Surface topography as well as film thicknesses were measured using an optical profilometer Wyko NT9100 (Veeco, Mannheim, Germany).

2.3. Inkjet Printing

Inkjet printing was performed utilizing an Autodrop system from microdrop Technologies (Norderstedt, Germany). The printer was equipped with a piezo-based micropipette printhead with an inner diameter of 70 μm. A voltage of 60 to 80 V and a pulse width of 30 to 45 μs revealed a stable droplet formation for all inks. Microscope slides (3 in. × 1 in.) from Marienfeld (Lauda-Königshofen, Germany) were used as substrates. Cleaning of the substrates was done by rinsing with *iso*-propanol and drying with an air flow. The printed film size was 6 mm × 6 mm and the printing speed was set to 20 mm s⁻¹.

3. Results and Discussion

3.1. Ink Characteristics

A variation of solvent systems were chosen for the π-conjugated polymer poly(3-octylthiophene) (P3OT, Figure 1a) that have, on the one hand, a systematically increased difference in the boiling point of the individual solvents and, on the other hand, comparable boiling points, but different viscosities and surface tensions. By following this approach, a systematic evaluation of correlations between the ink characteristics and the film formation properties were revealed. Three solvents were

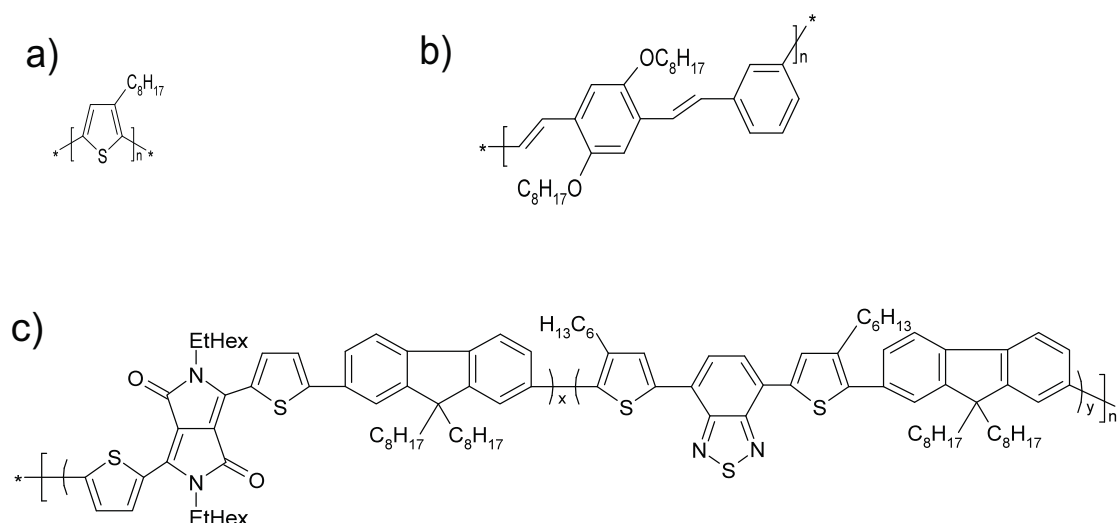


Figure 1. Schematic representation of the chemical structures of P₃OT (a), PPV (b), and poly(DPP-co-BTD-co-F) (c).

selected as main solvents that covered a broad range of boiling points (bp): toluene (bp 110 °C, Table 1), *p*-xylene (bp 138 °C, Table 2), and 1,3,5-trimethylbenzene (bp 165 °C, Table 3). Non-chlorinated aromatic solvents with

boiling points between 136 and 293 °C were selected as co-solvents, which resulted in a boiling-point difference of at least 18 K between the main and the co-solvent. In total, 42 different solvent systems were investigated: 20, 15, and

Table 1. Summary of the ink characteristics, including boiling point (bp), surface tension (γ), contact angle, density (ρ), viscosity (η), and Z-number, and film properties, including film thickness and roughness (R_a), of P₃OT using solvent systems with the main solvent toluene (90 vol%).

Co-solvent (10 vol%)	bp [°C]	γ [mN m ⁻¹]	Contact angle [°]	ρ [g cm ⁻³]	η [mPa s]	Z-number	Film thickness [nm]	Surface roughness R_a [nm]
Ethylbenzene	136	25.5	<10	0.868	0.752	52.3	105	101
<i>p</i> -Xylene	138	20.4	<10	0.867	0.751	46.9	85	74
<i>m</i> -Xylene	139	24.5	<10	0.867	0.754	51.1	85	80
<i>o</i> -Xylene	144	25.6	<10	0.869	0.785	50.3	85	81
<i>i</i> -Propylbenzene	153	22.4	<10	0.867	0.769	47.9	70	58
Propylbenzene	159	25.0	<10	0.867	0.760	51.3	80	51
3-Ethyltoluene	159	23.9	<10	0.868	0.771	49.4	80	35
4-Ethyltoluene	162	24.0	<10	0.867	0.753	50.7	75	38
2-Ethyltoluene	164	24.1	<10	0.869	0.773	49.5	85	37
1,3,5-Trimethylbenzene	165	25.9	<10	0.867	0.747	53.1	80	55
1,2,4-Trimethylbenzene	170	24.9	<10	0.868	0.757	51.4	75	35
1,2,3-Trimethylbenzene	176	25.4	<10	0.877	0.771	51.2	75	31
Indane	176	24.1	<10	0.877	0.806	47.7	80	26
Butylbenzene	183	23.1	<10	0.867	0.788	47.5	70	23
Pentylbenzene	205	25.3	<10	0.867	0.790	49.6	75	18
Tetralin	207	24.1	<10	0.878	0.808	47.6	75	20
Hexylbenzene	226	25.5	<10	0.867	0.845	46.6	70	25
Octylbenzene	261	22.5	<10	0.867	0.839	44.0	65	28
Nonylbenzene	282	25.8	<10	0.864	0.849	46.5	60	32
Decylbenzene	293	25.9	<10	0.866	0.851	46.6	55	24

Table 2. Summary of the ink characteristics, including boiling point (bp), surface tension (γ), contact angle, density (ρ), viscosity (η), and Z-number, and film properties, including film thickness and roughness (R_a), of P3OT using solvent systems with the main solvent *p*-xylene (90 vol%).

Co-solvent (10 vol%)	bp [°C]	γ [mN m ⁻¹]	Contact angle [°]	ρ [g cm ⁻³]	η [mPa s]	Z-number	Film thickness [nm]	Surface roughness R_a [nm]
Propylbenzene	159	25.4	<10	0.863	0.849	45.4	100	78
3-Ethyltoluene	159	25.4	<10	0.862	0.838	45.4	95	44
4-Ethyltoluene	162	23.8	<10	0.862	0.902	44.0	95	55
2-Ethyltoluene	164	25.6	<10	0.864	0.830	45.5	90	49
1,3,5-Trimethylbenzene	165	23.7	<10	0.862	0.800	47.7	100	62
1,2,4-Trimethylbenzene	170	23.5	<10	0.863	0.838	43.7	90	59
1,2,3-Trimethylbenzene	176	25.5	<10	0.866	0.832	45.4	85	24
Indane	176	26.1	<10	0.872	0.836	45.8	80	22
Butylbenzene	183	23.4	<10	0.862	0.842	43.6	100	24
Pentylbenzene	205	25.5	<10	0.862	0.902	45.5	95	12
Tetralin	207	20.2	<10	0.872	0.885	40.3	80	20
Hexylbenzene	226	25.7	<10	0.862	0.894	44.0	80	10
Octylbenzene	261	25.9	<10	0.862	0.912	43.3	70	15
Nonylbenzene	282	25.9	<10	0.862	0.920	43.0	80	19
Decylbenzene	293	25.6	<10	0.862	0.917	42.9	80	23

7 combinations using the main solvents toluene, *p*-xylene, and 1,3,5-trimethylbenzene, respectively.

Since the final film quality depends not only on the drying behavior of the solvents but also on a stable and reproducible droplet formation during the printing

process, the fluid characteristics are very important as well. To obtain insights in the effect of the ink properties to the printing quality, surface tensions and viscosities of all P3OT inks were measured and the corresponding Z-numbers were calculated (see Tables 1, 2, and 3). The surface

Table 3. Summary of the ink characteristics, including boiling point (bp), surface tension (γ), contact angle, density (ρ), viscosity (η), and Z-number, and film properties, including film thickness and roughness (R_a), of P3OT using solvent systems with the main solvent 1,3,5-trimethylbenzene (90 vol%).

Co-solvent (10 vol%)	bp [°C]	γ [mN m ⁻¹]	Contact angle [°]	ρ [g cm ⁻³]	η [mPa s]	Z-number	Film thickness [nm]	Surface roughness R_a [nm]
Butylbenzene	183	21.3	<10	0.865	0.933	38.9	90	36
Pentylbenzene	205	21.6	<10	0.865	0.948	38.1	90	17
Tetralin	207	20.2	<10	0.878	0.979	36.0	90	25
Hexylbenzene	226	24.8	<10	0.865	0.981	39.5	90	12
Octylbenzene	261	25.1	<10	0.865	0.996	39.1	85	8
Nonylbenzene	282	25.6	<10	0.865	1.011	38.9	90	9
Decylbenzene	293	25.8	<10	0.865	0.998	39.6	80	8
Butylbenzene	183	21.3	<10	0.865	0.933	38.9	90	36
Pentylbenzene	205	21.6	<10	0.865	0.948	38.1	90	17
Tetralin	207	20.2	<10	0.878	0.979	36.0	90	25
Hexylbenzene	226	24.8	<10	0.865	0.981	39.5	90	12
Octylbenzene	261	25.1	<10	0.865	0.996	39.1	85	8
Nonylbenzene	282	25.6	<10	0.865	1.011	38.9	90	9
Decylbenzene	293	25.8	<10	0.865	0.998	39.6	80	8

tensions and viscosities were measured to be in a range of 18–26 mN m⁻¹ and 0.747–1.011 mPas, respectively, and are in an inkjet printable regime.^[10] The viscosity is mainly determined by the main solvent and was therefore found to increase in the following order: toluene < *p*-xylene < 1,3,5-trimethylbenzene. The *Z*-number decreases with increased viscosity and was found to be between 53 and 36. In this study, no printing limitations based on different *Z*-numbers were identified. Although satellite droplets were observed for inks with a high *Z*-number, an in-flight merging of the satellite droplet with the main droplet was revealed for all tested inks. Additionally, no nozzle clogging was observed, indicating that the boiling points of the chosen solvents are high enough to ensure a stable droplet formation over a longer time period.

Furthermore, contact angle measurements were found to be below 10° on glass for all inks (see Tables 1, 2, 3), which ensures a good wetting on the substrate.^[23] Due to the good wetting of the inkjet printed droplets, a merging of the droplets on the substrate occurs, resulting in a continuous film formation even at higher dot spacings, which is the center-to-center distance between two adjacent droplets. As a consequence, a wide range of dot spacings (80–360 μm) were able to be screened for their resulting film homogeneity. In a later section, it is shown that not only a good spreading is a requirement for a good film formation at higher dot spacings, but also that the solvent's boiling point has a significant influence on the dot spacing range, where a homogeneous film is formed.

3.2. Film Formation

In order to evaluate relationships between ink properties and film homogeneity, the inks were inkjet printed and surface topographies as well as surface roughness were measured. The film thicknesses and surface roughnesses R_a of films with the best homogeneity for the main solvents toluene, *p*-xylene, and 1,3,5-trimethylbenzene are summarized in Table 1, 2, and 3, respectively. A significant influence of the co-solvent's boiling point to the resulting film homogeneity was found.

At first, toluene was used as a main solvent. It was observed that a co-solvent with a low boiling point, like ethylbenzene (bp 136 °C), was not found to be suitable for a smooth film formation. The small boiling point

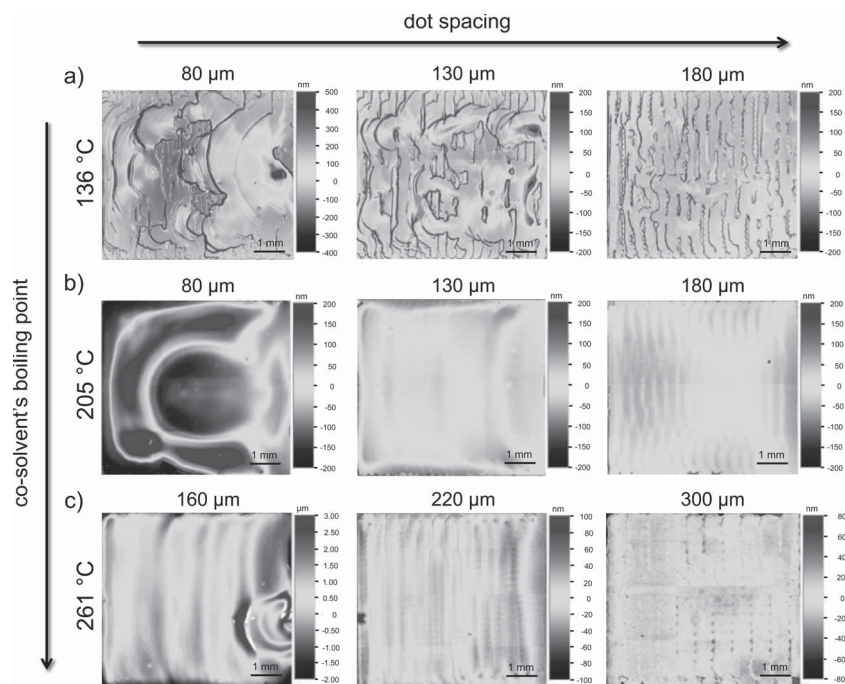


Figure 2. Optical-profiler images of inkjet printed P3OT films using toluene as the main solvent and ethylbenzene (a), pentylbenzene (b), and octylbenzene (c) as co-solvents, respectively.

difference between the two solvents caused the deposited material to dry too quickly and form non-homogeneous films. Figure 2a shows, from left to right, optical-profiler images of the inkjet printed films at dot spacings of 80, 130, and 180 μm, respectively. When using this solvent system and a wide range of dot spacings, that is, with varied amount of deposited material, no continuous film was formed. Instead, individual lines were observed for all dot spacings, suggesting that the characteristic line-by-line deposition of inkjet printing takes too long to create a continuous film. With decreased dot spacing, the amount of deposited material is increased and, consequently, the deposited material stays longer wet, which may lead to an improved film formation at lower dot spacings. However, with this solvent system, a reduction of the dot spacing did not result in improved film qualities. As a second method to reduce the printing time, an increase of the printing speed may lead to an improved film formation when using a lower co-solvent's boiling point.^[24] However, an increase of the printing velocity leads to an irregular droplet deposition accuracy, resulting in a decreased film homogeneity. Therefore, the printing speed was kept at 20 mm s⁻¹, which ensures a reproducible deposition accuracy at the highest velocity.

When using a solvent system with a higher boiling point of the co-solvent, for example, pentylbenzene (bp 205 °C), continuous films with an improved film-formation quality were observed with a surface roughness R_a

of 18 nm (Figure 2b). A dot spacing of 130 μm represents the optimum amount of deposited material (Figure 2b, middle) since a lower dot spacing (80 μm) lead to irregularities due to too much deposited material (Figure 2b, left), whereas higher dot spacings (180 μm) lead to the formation of lines and to an increased surface roughness (Figure 2b, right).

With a further increase of the co-solvent's boiling point, the range of dot spacings that are applicable for a continuous film formation increases; as a result of a longer drying time, the surface irregularities are smoothed. Figure 2c shows optical-profiler images of films inkjet printed from the solvent system toluene/octylbenzene, where dot spacings between 160 μm (left) and 300 μm (right) are used. It is observed that the surface roughness increases with increased boiling point of the co-solvent. In this case, the drying takes too long and the material is drying irregularly again; this time due to multiple drying steps that lead to a ring-like drying pattern or to the formation of stripes (Figure 2c).

In summary, when using the main solvent toluene, the co-solvent pentylbenzene with a boiling point of 205 $^{\circ}\text{C}$ revealed the smoothest film formation, whereas lower or higher boiling point solvents induced irregularities during drying. The choice of the co-solvent is therefore crucial for the film quality. However, other parameters, such as the surface tension and the viscosity of the co-solvent, show no significant influence to observed film formation properties. More precisely, among the 20 solvent combinations using toluene as main solvent, different co-solvents with the same or comparable boiling points, but different surface tensions or viscosities were tested (Table 1). Therefore, it is concluded here that the main parameter determining the final film homogeneity is the co-solvent's boiling point.

In order to confirm the results observed for toluene, two other main solvents, *p*-xylene and 1,3,5-trimethylbenzene, were investigated. For *p*-xylene, the co-solvent hexylbenzene with a boiling point of 226 $^{\circ}\text{C}$ was found to result in the highest film quality with a surface roughness R_a of 10 nm (Table 2, Figure S1, Supporting Information). For 1,3,5-trimethylbenzene, the co-solvent octylbenzene (bp 261 $^{\circ}\text{C}$) revealed the best film formation properties with a surface roughness R_a of 8 nm (Table 3, Figure S2, Supporting Information). By using lower or higher boiling point solvents, an increased surface roughness was observed.

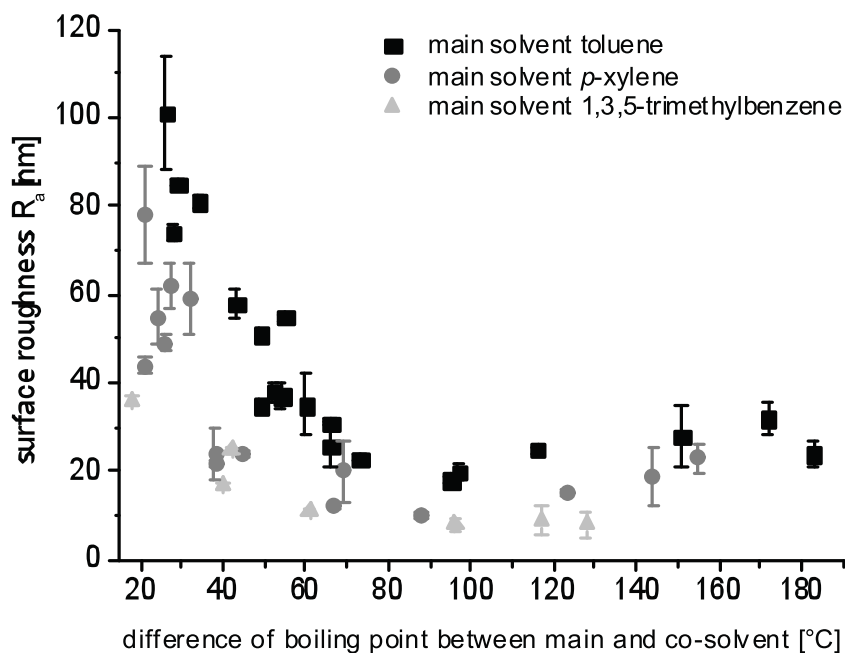


Figure 3. Surface roughness as function of boiling point difference between the main solvent and the co-solvent for inkjet printed P3OT films.

When comparing the three main solvents, it was found that the boiling point difference between the main and the co-solvent has a crucial effect on the film-formation quality. Figure 3 shows that an optimal boiling point difference between main and co-solvent exists, which ensures the lowest surface roughness. As found here, the most favorable boiling point difference between the main solvent and the co-solvent is between 90 and 100 $^{\circ}\text{C}$.

In addition, Figure 3 reveals that an increased boiling point of the main solvent (toluene < *p*-xylene < 1,3,5-trimethylbenzene) results in lower surface roughnesses even if there is only a small difference in boiling point between the main solvent and the co-solvent. Therefore, a higher boiling main solvent tolerates a broader range of boiling point differences for a good film formation. The optical-profiler images in Figure 4 demonstrate a significantly improved roughness when choosing a higher boiling main solvent; from 18 nm surface roughness for toluene (Figure 4a) to 8 nm for 1,3,5-trimethylbenzene (Figure 4c). The solvent system 1,3,5-trimethylbenzene/octylbenzene represents in this study the best solvent system with an optimal film formation and the smallest roughness for P3OT.

To compare the newly found solvent systems, the solvent systems toluene/*ortho*-dichlorobenzene and chlorobenzene/*ortho*-dichlorobenzene, which are frequently used in other reports,^[11,12] were used as reference (see Figure 5b and c). Both solvent systems revealed a surface roughness R_a of >25 nm and a decreased film homogeneity in comparison to the solvent system 1,3,5-trimethylbenzene/octylbenzene (Figure 5a). Hence,

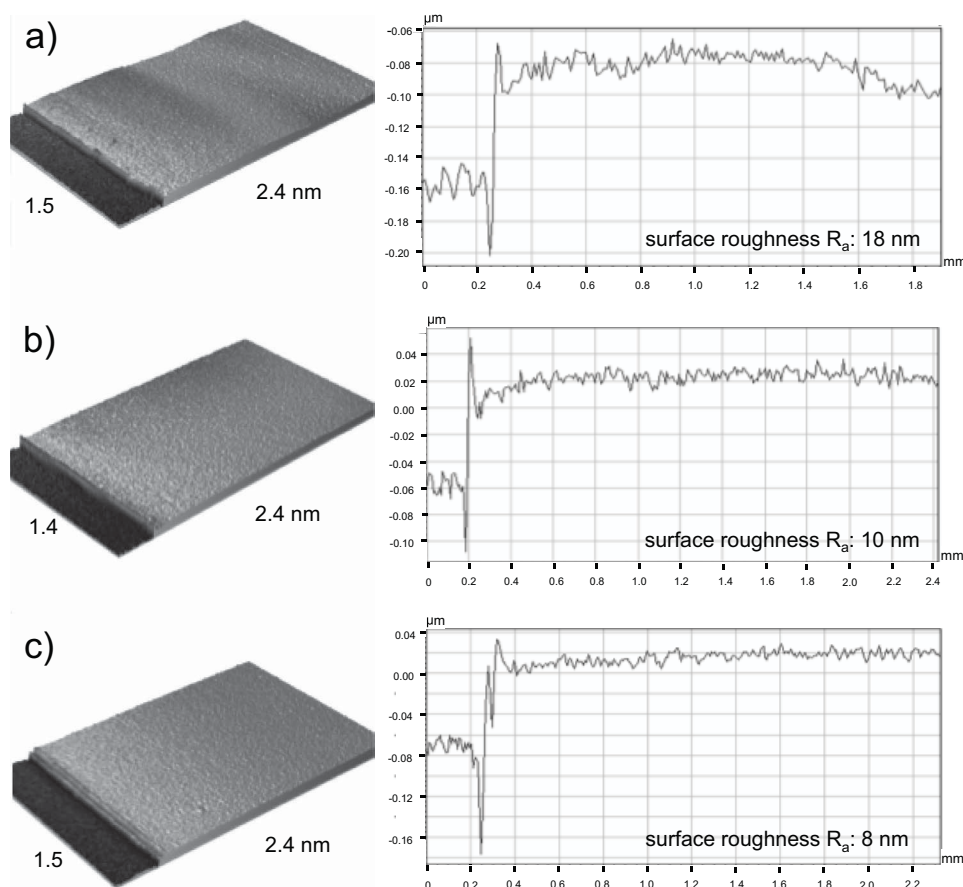


Figure 4. Optical-profiler images and corresponding cross-sections of inkjet printed P3OT films using the optimized solvent systems toluene/pentylbenzene (a), *p*-xylene/hexylbenzene (b), and 1,3,5-trimethylbenzene/octylbenzene (c).

the latter solvent system represents a significant improvement for a smooth film formation by inkjet printing.

Moreover, to prove if the new solvent system is also suitable for other classes of π -conjugated polymer, a PPV (Figure 1b) and a poly(DPP-*co*-BTD-*co*-F) (Figure 1c) were tested for their film formation characteristics using 1,3,5-trimethylbenzene/octylbenzene as solvent system. The investigations showed that the solvent system is suitable to reach surface roughnesses R_a of 6 and 8 nm for the poly(DPP-*co*-BTD-*co*-F) (Figure 5d) and PPV (Figure 5e), respectively. It is therefore believed that for the applicability of a certain solvent in the inkjet printing process the solubility of the polymer is the most critical issue. In this study, all three polymers revealed a good solubility due to side chains attached to the polymer backbone.

4. Conclusion

In this contribution, the combinatorial investigation of the film-formation quality for inkjet printed polymer films of more than 40 solvent systems was investigated. In order

to evaluate film quality influencing parameters, the solvent systems were systematically chosen. The resulting film homogeneities for the π -conjugated polymer P3OT showed that for a solvent system ratio of 90/10 an optimal boiling point difference between the lower boiling main solvent and the higher boiling co-solvent is between 90 and 100 °C. In general, a higher boiling point of the main solvent revealed more homogeneous thin films. The best solvent system was found to be a combination of 1,3,5-trimethylbenzene and octylbenzene, which resulted in homogeneous thin films with a roughness of 8 nm. The solvent system was found to be independent on the chosen polymer (class), as this solvent system was successfully used for creating homogeneous films with a low roughness with other π -conjugated polymers, including PPV and poly(DPP-*co*-BTD-*co*-F).

Furthermore, among the parameters that were screened, including surface tension, boiling point, contact angle, density, viscosity, and Z-number, it was found that only the boiling point difference between the main solvent and the co-solvent showed a significant influence on the film homogeneity and roughness.

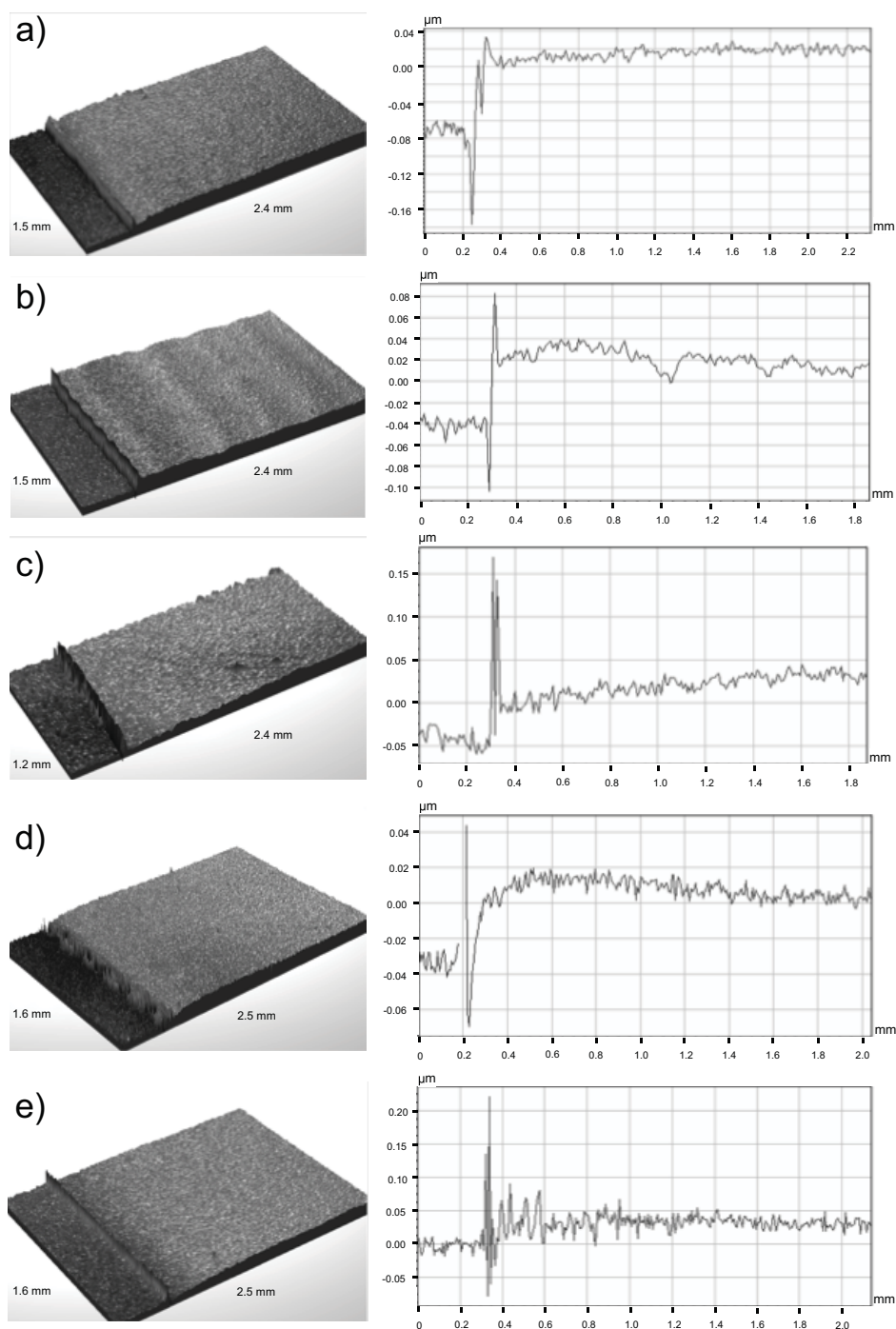


Figure 5. Optical-profiler images and corresponding cross-sections of inkjet printed P3OT films using the solvent systems 1,3,5-trimethylbenzene/octylbenzene (a), toluene/*ortho*-dichlorobenzene (b), and chlorobenzene/*ortho*-dichlorobenzene (c), as well as inkjet printed films of poly(DPP-co-BTD-co-F) (d) and PPV (e) using 1,3,5-trimethylbenzene/octylbenzene.

The newly developed solvent system has an obvious advantage over frequently used solvent systems with chlorinated solvents, in particular for safety issues when handling larger quantities of solvent, for example, when thinking of R2R processing. Moreover, the newly

developed solvent system revealed a lower film roughness than the chlorinated solvent systems.

A significant step toward an improved understanding of the basic film formation characteristics and toward a wider application of the inkjet printing process is

presented. Since the choice of the solvent systems affects not only the film-formation quality but is also crucial for the application of the polymer layer in organic electronics, because the solvent has an influence on, for example, charge mobility and nanomorphology,^[7,25,26] the influence of the solvent system to device performances need to be studied in the future.

Supporting Information

Supporting Information is available from the Wiley Online Library or from the author.

Acknowledgements: For financial support, the authors thank the Dutch Polymer Institute (DPI technology area HTE, project #620) as well as the European Community's Seventh Framework Program (FP7/2007-2013) under grant agreement no. 248816. Dr. Andreas Wild and Florian Kretschmer are acknowledged for the synthesis of the polymers PPV and poly(DPP-co-BTD-co-F), respectively.

Received: September 13, 2012; Published online: January 11, 2013; DOI: 10.1002/macp.201200547

Keywords: combinatorial screening; inkjet printing; π -conjugated polymers; solvent systems; thin-film libraries

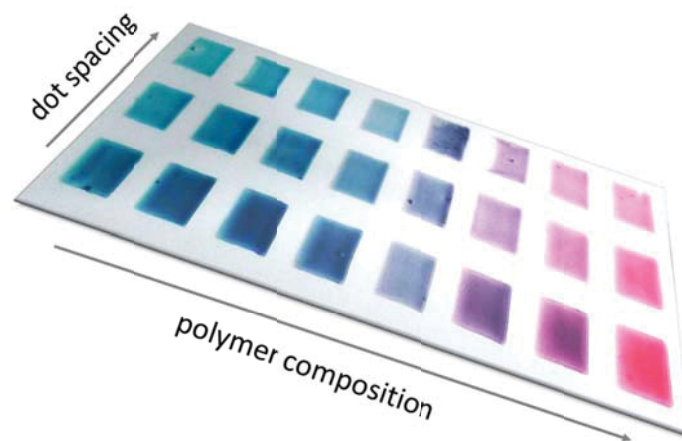
- [1] K. Sun, Y. J. Xia, J. Y. Ouyang, *Sol. Energy Mater. Sol. Cells* **2012**, *97*, 89.
- [2] S. Alem, T. Y. Chu, S. C. Tse, S. Wakim, J. P. Lu, R. Movileanu, Y. Tao, F. Belanger, D. Desilets, S. Beaupre, M. Leclerc, S. Rodman, D. Waller, R. Gaudiana, *Org. Electron.* **2011**, *12*, 1788.
- [3] S. van Bavel, S. Veenstra, J. Loos, *Macromol. Rapid Comm.* **2010**, *31*, 1835.
- [4] F. C. Krebs, T. Tromholt, M. Jorgensen, *Nanoscale* **2010**, *2*, 873.
- [5] B. Schmidt-Hansberg, M. Sanyal, N. Grossiord, Y. Galagan, M. Baunach, M. F. G. Klein, A. Colsmann, P. Scharfer, U. Lemmer, H. Dosch, J. Michels, E. Barrena, W. Schabel, *Sol. Energy Mater. Sol. Cells* **2012**, *96*, 195.
- [6] F. C. Krebs, *Sol. Energy Mater. Sol. Cells* **2009**, *93*, 394.
- [7] S. Günes, H. Neugebauer, N. S. Sariciftci, *Chem. Rev.* **2007**, *107*, 1324.
- [8] D. M. DeLongchamp, B. M. Vogel, Y. Jung, M. C. Gurau, C. A. Richter, O. A. Kirillov, J. Obrzut, D. A. Fischer, S. Sambasivan, L. J. Richter, E. K. Lin, *Chem. Mater.* **2005**, *17*, 5610.
- [9] B. J. de Gans, E. Kazancioglu, W. Meyer, U. S. Schubert, *Macromol. Rapid Comm.* **2004**, *25*, 292.
- [10] E. Tekin, P. J. Smith, U. S. Schubert, *Soft Matter* **2008**, *4*, 703.
- [11] A. Teichler, R. Eckardt, S. Hoepfener, C. Friebe, J. Perelaer, A. Senes, M. Morana, C. J. Brabec, U. S. Schubert, *Adv. Energy Mater.* **2011**, *1*, 105.
- [12] A. Teichler, R. Eckardt, C. Friebe, J. Perelaer, U. S. Schubert, *Thin Solid Films* **2011**, *519*, 3695.
- [13] M. Singh, H. M. Haverinen, P. Dhagat, G. E. Jabbour, *Adv. Mater.* **2010**, *22*, 673.
- [14] C. N. Hoth, P. Schilinsky, S. A. Choulis, C. J. Brabec, *Nano Lett.* **2008**, *8*, 2806.
- [15] B. Derby, *Annu. Rev. Mater. Res.* **2010**, *40*, 395.
- [16] R. D. Deegan, O. Bakajin, T. F. Dupont, G. Huber, S. R. Nagel, T. A. Witten, *Nature* **1997**, *389*, 827.
- [17] H. Hu, R. G. Larson, *J. Phys. Chem. B* **2006**, *110*, 7090.
- [18] Y. Oh, J. Kim, Y. J. Yoon, H. Kim, H. G. Yoon, S. N. Lee, J. Kim, *Curr. Appl. Phys.* **2011**, *11*, S359.
- [19] D. Jang, D. Kim, J. Moon, *Langmuir* **2009**, *25*, 2629.
- [20] J. Perelaer, P. J. Smith, M. M. P. Wijnens, E. van den Bosch, R. Eckardt, P. H. J. M. Ketelaars, U. S. Schubert, *Macromol. Chem. Phys.* **2009**, *210*, 387.
- [21] A. Teichler, Z. Shu, A. Wild, C. Bader, J. Nowotny, G. Kirchner, S. Harkema, J. Perelaer, U. S. Schubert, unpublished.
- [22] A. Teichler, J. Perelaer, F. Kretschmer, M. D. Hager, U. S. Schubert, *Macromol. Chem. Phys.* **2012**, DOI: 10.1002/macp.201200526.
- [23] E. Tekin, E. Holder, D. Kozodaev, U. S. Schubert, *Adv. Funct. Mater.* **2007**, *17*, 277.
- [24] E. Tekin, B. J. de Gans, U. S. Schubert, *J. Mater. Chem.* **2004**, *14*, 2627.
- [25] S. K. Jang, S. C. Gong, H. J. Chang, *Synth. Met.* **2012**, *162*, 426.
- [26] M. T. Dang, G. Wantz, H. Bejbouji, M. Urien, O. J. Dautel, L. Vignau, L. Hirsch, *Sol. Energy Mater. Sol. Cells* **2011**, *95*, 3408.

Publication 3

“Systematic Investigation of a Novel Low-Bandgap Terpolymer Library via Inkjet Printing: Influence of Ink Properties and Processing Conditions”

Anke Teichler, Jolke Perelaer, Florian Kretschmer, Martin D. Hager, Ulrich S. Schubert

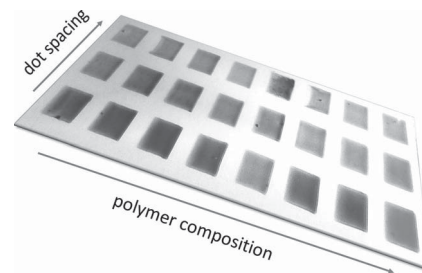
Macromol. Chem. Phys. **2013**, 214, 664-672.



Systematic Investigation of a Novel Low-Bandgap Terpolymer Library via Inkjet Printing: Influence of Ink Properties and Processing Conditions

Anke Teichler, Jolke Perelaer, Florian Kretschmer, Martin D. Hager, Ulrich S. Schubert*

The thin-film properties of a polymer library consisting of novel conjugated low-bandgap poly(diketopyrrolopyrrole-*co*-benzothiadiazole-*co*-fluorene) (poly(DPP-*co*-BTD-*co*-F)) polymers are investigated. The content of the monomer units in the copolymers is systematically varied. Structure–property relationships are obtained for the ink characteristics, the film formation qualities, and their optical properties. Toluene/*o*-DCB in a ratio 90/10 and a concentration of 5 mg mL⁻¹ is found to be a suitable solvent system for all polymers. The polymer compositions and the choice of solvent have a significant influence on the film properties. Inkjet printing is shown to be a suitable technique for the preparation of thin-film libraries that subsequently can be characterized by combinatorial screening tools.



1. Introduction

The number of new conjugated polymers that are synthesized for use in organic electronics, such as organic light-emitting diodes (OLEDs) or organic photovoltaics (OPVs), is rapidly growing.^[1] In order to investigate the compound

and thin-film properties of newly synthesized π -conjugated polymers, a rapid and combinatorial process is required to identify important structure–property relationships enabling the rational design of new materials with improved properties.^[2] For the preparation of thin films from solution, many printing techniques like gravure, flexo, screen, or inkjet printing, as well as coating techniques such as knife or slot die coating, are available.^[3] For the systematic investigation of thin-film properties, inkjet printing represents a versatile depositing technique, and has been implemented in a combinatorial workflow.^[4] As an additive technique, inkjet printing is characterized as a material-efficient film preparation method without the need of masks that requires only little amounts of materials and produces a minimal amount of waste, in contrast to other solution deposition methods, like spin-coating or doctor-blading.^[5]

Compared with the conventional fabrication of thin films, the drying mechanisms of inkjet printed films are not yet fully understood. The investigation of special

A. Teichler, Dr. J. Perelaer, F. Kretschmer, Dr. M. D. Hager, Prof. U. S. Schubert

Laboratory of Organic and Macromolecular Chemistry, Friedrich-Schiller-University Jena, Humboldtstraße 10, 07743 Jena, Germany

E-mail: ulrich.schubert@uni-jena.de

A. Teichler, Dr. J. Perelaer, F. Kretschmer, Dr. M. D. Hager, Prof. U. S. Schubert

Jena Center for Soft Matter (JCSM), Friedrich-Schiller-University Jena, Philosophenweg 7, 07743 Jena, Germany

A. Teichler, Dr. J. Perelaer, Dr. M. D. Hager, Prof. U. S. Schubert
Dutch Polymer Institute, P.O. Box 513, 5600 MB Eindhoven, The Netherlands

drying issues, like the coffee-ring effect^[6] and the Marangoni flow,^[7] represents the first steps toward a comprehensive understanding of the drying behavior of inkjet printed features, but a prediction of the final film characteristics of specific inks is not yet possible. The drying process is in contrast to other film formation techniques a very complex procedure, which is influenced by several parameters (e.g., temperature, solvent, concentration, and dot spacing). Although the effect of solution and processing properties is well investigated for spin-coating,^[8] the control of the film formation process is still a challenge for inkjet printing. As a consequence not only a systematic investigation of new compounds, but also a methodical screening of the most important processing parameters is required.

The integration of inkjet printing into a combinatorial screening workflow that incorporates solution preparation, film preparation, and thin-film investigation steps enables a fast and easy identification of optimal compound and processing parameters, which may have been undiscovered without using a combinatorial screening approach, as was reported recently for polymer/fullerene blends for organic solar cells.^[4,9] Crucial film preparation parameters, like the used solvent/co-solvent combination, the ink concentration, as well as the film thickness, have to be investigated for every single polymer class.^[10,11] Furthermore, also printing conditions, like dot spacing, film size, and substrate temperature are important parameters, as they initially determine the final film morphology. Recently, Krebs and co-workers^[12] investigated the effect of the film size to device efficiencies. The authors showed that the processing conditions that are currently applied for lab scale solar cells cannot be easily transferred for the fabrication of larger film sizes, since the solar cell performance decreases with increased film size. Therefore, the focus of investigations in the field of OPVs should move toward roll-to-roll (R2R) scalable processing. Inkjet printing is one suitable patterning technique for R2R processing; however, it requires a complete understanding of the film formation characteristics and the homogeneity influencing parameters. Hence, the design and application of a combinatorial screening workflow for the systematic investigation of each individual processing parameter could present an important step for an efficient development of new materials and devices.

Another reported material-efficient film preparation technique is differentially pumped slot die coating, where only 10 μL of ink was used to produce a solar cell in a combinatorial screening manner.^[13] Since every coating or printing technique is characterized by different processing conditions, different film optimization parameters need to be addressed. To the best of our knowledge, only inkjet printing and the slot die-coating technique are methods

that enable a time- and material-efficient screening of the large number of newly developed polymers. In order to identify the potential of these materials, a combinatorial screening approach, which allows a fast and efficient optimization and requires only little amounts of functional material, is of high importance.

A well-investigated polymer for OPV applications is poly(3-hexylthiophene) (P3HT). Currently, power conversion efficiencies of up to 5% have been reported using this polymer.^[14] However, polythiophenes are limited in their photon-harvesting properties since their absorption does not match the maximum photon flux of the solar spectrum.^[15] Improved photon-harvesting characteristics are obtained by donor-acceptor polymers, which consist of multiple building units that match different absorption regions of the solar spectrum.^[16] Well-known building units for such polymers are, for example, diketopyrrolopyrrole (DPP), benzothiadiazole (BTD), and fluorene (F). The beneficial properties, including the narrow bandgap of the DPP moiety,^[17] good photovoltaic properties of BTD,^[18] and easy tailoring characteristics of F,^[19] can be combined into a single donor-acceptor polymer. Such polymers revealed a low bandgap and favorable optical properties such as a broad absorption up to 750 nm.^[20]

In this contribution, a polymer library that consists of a new polymer class, poly(diketopyrrolopyrrole-co-benzothiadiazole-co-fluorene) (poly(DPP-co-BTD-co-F)), with varying compositions of the monomers DPP, BTD, and F is investigated systematically using inkjet printing. The film formation and the optical properties of these films were characterized. A combinatorial screening of thin-film properties of the library is shown, as well as insights into the effect of different solvents, solvent systems, polymer concentrations, and film sizes to the film drying characteristics are presented. Consequently, correlations between the polymer properties, that is, the influence of different monomer units, the resulting ink, and processing parameters, that is, film size, as well as film properties (homogeneity) can be revealed.

2. Experimental Section

2.1. Materials

The synthesis of the polymers **1** to **8** is described elsewhere.^[20] The solvents toluene, *o*-xylene, chlorobenzene (CB), and *ortho*-dichlorobenzene (*o*-DCB) were purchased from Sigma-Aldrich (Steinheim, Germany). The solutions were filtered before printing (pore size 1 μm) to prevent nozzle clogging. Microscope slides (3 inch \times 1 inch) from Marienfeld (Lauda-Königshofen, Germany) were used as substrates. The cleaning of the substrates was carried out by rinsing with *iso*-propanol and drying with an air flow.

2.2. Instrumentation

Surface tension and contact angles of the inks were investigated using the OCA 20 contact-angle measurement system from Data-physics (Filderstedt, Germany). Density and viscosity measurements were performed using a DMA 02 density meter and an AMVn ball/capillary viscosimeter (Anton Paar, Graz, Austria), respectively.

The inkjet printing experiments were carried out using an Autodrop system from microdrop Technologies (Norderstedt, Germany). The printer was equipped with a piezo-based micropipette printhead with an inner diameter of 70 μm . A voltage of 60–70 V and a pulse length of 30–35 μs revealed a stable droplet formation for all polymers in the applied solvent systems. The printing speed was set to 20 mm s^{-1} for all of the experiments. The thin-film libraries were printed in a microtiter plate pattern, that is, each film covers the position of a single well of a 96-well plate, to enable screening of the optical properties of the resulting films by using a UV-vis plate reader.

Surface topography and film thicknesses were measured using a Wyko NT9100 optical interferometric profiler (Veeco, Mannheim, Germany). A Tecan infinite M200 PRO UV-vis/fluorescence plate reader (Tecan, Crailsheim, Germany) was used to measure optical properties of the films.

3. Results and Discussion

3.1. Inkjet Printability and Film Formation

The polymer library poly(DPP-co-BTD-co-F) (Figure 1), which was investigated, is characterized by systematically varying contents of the DPP and BTD moieties, while keeping the fluorene content constant. The resulting polymer compositions of the polymers 1 to 8 and their corresponding molecular characteristics are summarized in Table 1.

At first, we sought to identify a suitable processing solvent followed by a favorable concentration to print from. For these experiments, polymer 3 was chosen to test the film formation since this polymer includes all three building units. Three ink concentrations (3, 5, and 7 mg mL^{-1}) and three solvent systems (chlorobenzene (CB)/*ortho*-dichlorobenzene (*o*-DCB), *o*-xylene/*o*-DCB, and toluene/*o*-DCB, all in a ratio of 90/10) were tested. The solvents were carefully chosen to match the applicability in the inkjet printing process^[4,10] as well as in OPVs.^[21,22] Subsequently, the film formation of polymer 3 was investigated

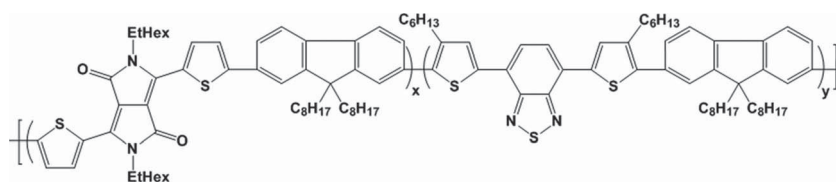


Figure 1. Schematic representation of the chemical structure of polymers 1 to 8. For detailed composition information and molecular characterization data see Table 1.

Table 1. Composition, molar masses, and PDI values of the polymers 1 to 8.

Polymer	BTD	DPP	F	\bar{M}_n [g mol ⁻¹]	\bar{M}_w [g mol ⁻¹]	PDI
1	100	0	100	8400	18 000	2.12
2	60	40	100	37 000	93 000	2.52
3	50	50	100	37 000	81 000	2.20
4	40	60	100	19 000	44 000	2.35
5	30	70	100	25 000	54 000	2.18
6	20	80	100	25 000	56 000	2.24
7	10	90	100	31 000	68 000	2.22
8	0	100	100	26 000	56 000	2.15

in a library of varying ink characteristics using the described solvent combinations and concentrations. Furthermore, different dot spacings (from 100 to 180 μm) were applied for each ink, which allows the evaluation of the film quality in a range of different film thicknesses.

As a first solvent system, polymer 3 was printed from CB/*o*-DCB (90/10) with a concentration of 5 mg mL^{-1} . It can be seen in Figure 2a that the drying of the solvent system does not result in homogeneous films at either of the dot spacings; rings of increased material concentrations can be seen over the film. An outward drying, which is observed mostly at higher dot spacings or higher concentrations (see Supporting Information, Figure S1b), leads to an inhomogeneous film formation. Although inkjet printed films from a concentration of 3 mg mL^{-1} (Supporting Information, Figure S1a) show an inward drying up to a dot spacing of 200 μm , an outward drying occurs for 5 mg mL^{-1} (Figure 2a) already at 140 μm and at 120 μm for 7 mg mL^{-1} (Supporting Information, Figure S1b), respectively. Hence, with increasing concentration the film formation using CB/*o*-DCB becomes more difficult and is limited to a smaller range of dot spacings. Moreover, a concentration of 3 mg mL^{-1} does not reveal a homogeneous film formation, as a result of too little amount of deposited material. Consequently, the solvent system CB/*o*-DCB is not suitable for the thin film preparation of the poly(DPP-co-BTD-co-F) library.

As a second solvent system *o*-xylene/*o*-DCB was investigated. Relatively homogeneous films were observed for concentrations of 5 mg mL^{-1} or higher (Figure 2b; and Supporting Information, Figure S2b, respectively), while a concentration of 3 mg mL^{-1} resulted in ring-shaped drying patterns (see Supporting Information, Figure S2a). However, a strong agglomeration was observed in the resulting films, which obviously hampers a good film surface uniformity.

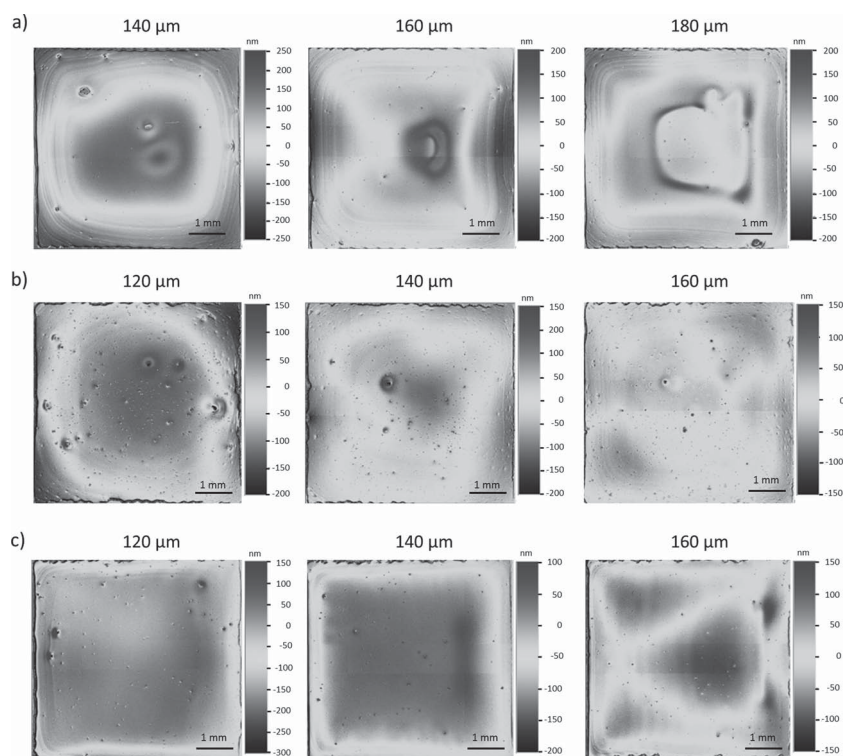


Figure 2. Optical profiler images of inkjet printed films of polymer **3** ($c = 5 \text{ mg mL}^{-1}$) using different solvent systems: a) CB/*o*-DCB 90/10, b) *o*-xylene/*o*-DCB 90/10, and c) toluene/*o*-DCB 90/10. From left to right the applied dot spacings are increasing.

As a result, *o*-xylene/*o*-DCB is also not applicable for the preparation of a homogeneous poly(DPP-*co*-BTD-*co*-F) film library.

Finally, toluene/*o*-DCB was used as a solvent system. It can be seen in Figure 2c that homogeneous films were obtained at a concentration of 5 mg mL^{-1} , up to dot spacings of $150 \mu\text{m}$. Although a lower concentration (3 mg mL^{-1} , Supporting Information, Figure S3a) does not result in homogenous films, indicated by the significant line formation even at smaller dot spacings, a higher concentration of 7 mg mL^{-1} reveals homogeneous films with dot spacings up to $150 \mu\text{m}$ (Supporting Information, Figure S3b).

From the selected solvents, it can be concluded that the solvent system toluene/*o*-DCB represents the most suitable solvent to produce films of polymer **3** with an adequate homogeneity. With respect to the required film thickness for organic electronics, which is below 200 nm ,^[23] a concentration of 5 mg mL^{-1} in toluene/*o*-DCB was chosen for further experiments due to the achieved layer thicknesses of 155 nm . In contrast, 215 nm thick films were obtained for the concentration of 7 mg mL^{-1} revealing a too high layer thickness (Supporting Information, Table S1, last column).

The next step was to prepare a thin-film library from all eight polymers with the optimized ink settings. It

was found that these settings indeed resulted in a homogeneous film formation for all eight polymers, as depicted in Figure 3. However, an optimization of the dot spacing is required to reveal the most homogeneous film formation, which may vary slightly from polymer to polymer due to their difference in molar mass and composition. Although polymer **3** showed the best film formation at $140 \mu\text{m}$, polymers **1** and **2** were processed by achieving optimal results with higher dot spacings (180 and $160 \mu\text{m}$, respectively) and polymers **4** to **8** with lower dot spacings (in the range 110 to $120 \mu\text{m}$). As a consequence, the film thicknesses obtained for the optimal printing conditions vary from 50 to 230 nm (Table 2, last column). Since an optimal active layer thickness is below 200 nm ,^[23] polymers **4**, **5**, and **6** revealed a too high film thickness using the prescribed settings. As a result of the applicability of a wider range of dot spacings by using toluene/*o*-DCB the film thickness of the polymers can be optimized. Here, the increase of the dot spacing to 120 and $140 \mu\text{m}$ leads to

a decrease in film thickness, whereas a good film quality was maintained (Table 2).

The variation in film formation of the different polymers can be ascribed to their varying ink properties (Table 3). In order to evaluate correlations among polymer structures, molar masses, surface tensions and viscosities, we tried to elucidate trends, but no relationships between the different parameters could be identified at this point. It is, for example, expected that the ink viscosity increases as the molar mass of the polymer increases.^[24] This trend cannot be observed for this copolymer library, since there are too many parameters of influence, such as a changing polymer composition combined with changes in rigidity of the chains and the variations in the molar mass. As not every single parameter can be addressed separately it is hard to reveal such correlations and trends. At this point, it can be concluded that the DPP unit affects the ink viscosity significantly, whereas the effect of the BTD seems to be less significant; a continuous increase of the ink's viscosity is observed with increasing DPP content in the polymer when a composition of DPP/BTD/F 50/50/100 is exceeded. In contrast, an increasing BTD content shows no clear dependence on the polymer composition. Instead, the molar mass seems to influence the ink viscosity at low DPP contents, since polymer **1**, which has the lowest \overline{M}_n , exhibits a significant low viscosity. As a conclusion at this

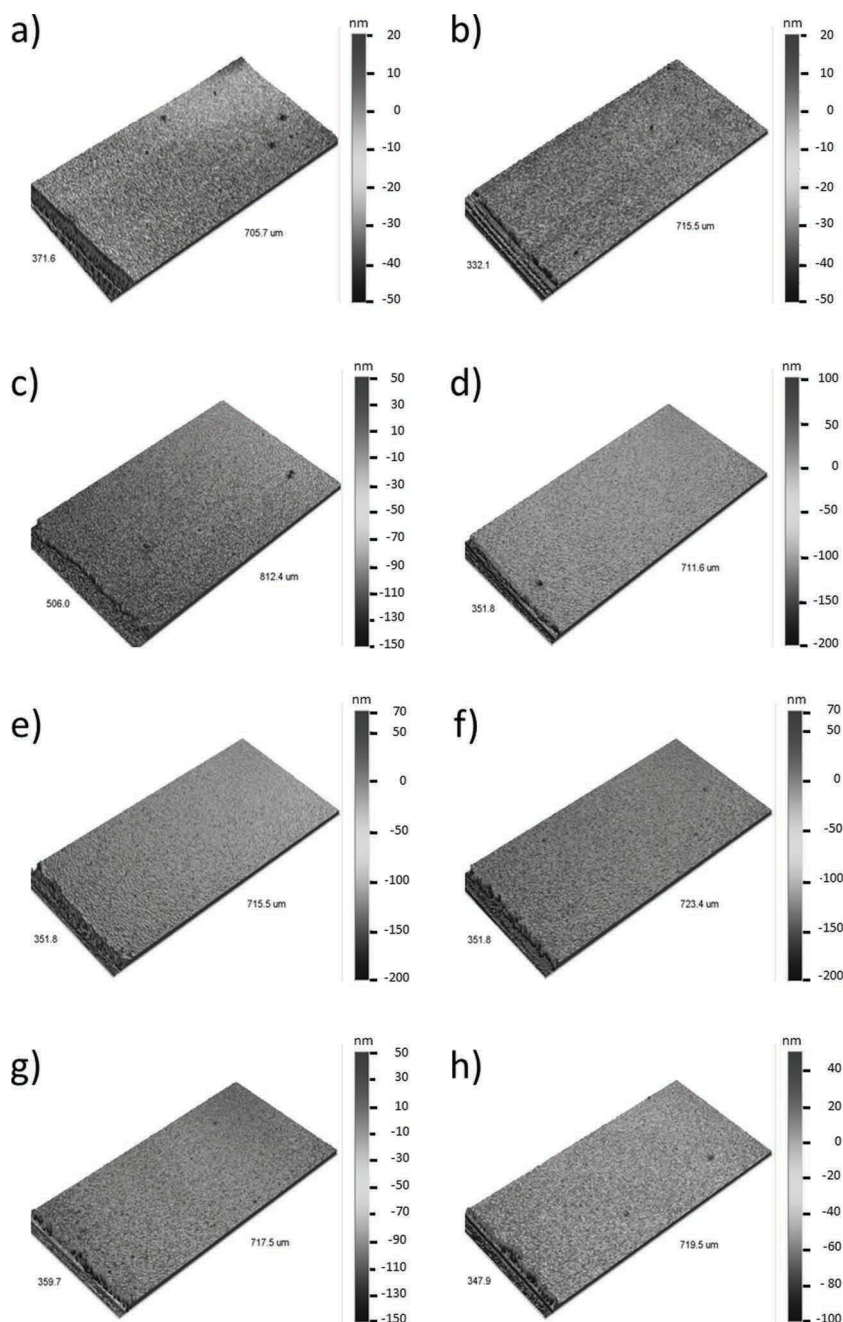


Figure 3. Optical profiler images of inkjet printed films using a concentration of 5 mg mL^{-1} and the solvent system toluene/*o*-DCB 90/10: a) polymer 1 (dot spacing $180 \text{ }\mu\text{m}$), b) polymer 2 (dot spacing $160 \text{ }\mu\text{m}$), c) polymer 3 (dot spacing $140 \text{ }\mu\text{m}$), d) polymer 4 (dot spacing $110 \text{ }\mu\text{m}$), e) polymer 5 (dot spacing $110 \text{ }\mu\text{m}$), f) polymer 6 (dot spacing $120 \text{ }\mu\text{m}$), g) polymer 7 (dot spacing $120 \text{ }\mu\text{m}$) and h) polymer 8 (dot spacing $120 \text{ }\mu\text{m}$).

point, correlations between ink characteristics and film properties are difficult to elucidate for the current investigated polymer library. These findings stress the importance of a combinatorial screening of film properties for varying ink characteristics because optimal processing parameter cannot be easily predicted by a simple investigation of selected ink properties. A systematic

investigation of materials, processing conditions, as well as resulting film properties is required. By using inkjet printing, this process can be performed in a fast and simple manner with small amounts of materials.

3.2. Film Thickness Versus Film Quality

By using inkjet printing as a film formation technique, challenges arise when the produced layer requires a certain film thickness or film size. For example, a processed ink is optimized according to the best film formation quality and the optimized printing conditions result in a certain film thickness. If this film thickness does not match the layer thickness necessities for a desired application, a variation in concentration and/or dot spacing may not always lead to comparable film formation qualities. A certain dot spacing interval is generally tolerated for the majority of polymer solutions, but if this interval is insufficient to reach the aimed film thickness, other printing parameters, like the ink properties (e.g., concentration), need to be changed. The same challenge arises when the application requires different film sizes. In particular for inkjet printing, the variation of the film size is not trivial since the drying behavior strongly depends on the amount of applied material and the drying time. For the inkjet printing process, the deposited material starts drying already during processing the entire film. Since inkjet printed layers were produced by printing lines next to each other, which subsequently merge into a continuous feature, the length of a line and, as a consequence, the time until the next line is printed, is crucial in order to control the film formation properties.

Figure 4 combines the investigation of the two described challenges, film thickness and film size requirements, for polymer 2, printed from toluene/*o*-DCB. Film sizes of $5 \text{ mm} \times 5 \text{ mm}$ and $20 \text{ mm} \times 20 \text{ mm}$ as well as toluene/*o*-DCB ratios of 90/10, 70/30, and 50/50 were investigated, respectively. The investigations were performed by using polymer 2 in a concentration of 3 mg mL^{-1} . This concentration was chosen since for the preparation of larger inkjet printed

Table 2. Film properties of the polymers 1 to 8 inkjet printed from toluene/*o*-DCB 90/10 at a concentration of 5 mg mL⁻¹.

Polymer	$\lambda_{\text{abs, film}}$ [nm]	$E_{\text{g, film}}$ [eV]	$\lambda_{\text{PL, film}}$ [nm]	Dot spacing [μm]	Film thickness [nm]
1	525	1.98	662	180	48 ± 6
2	650	1.78	682	160	66 ± 10
3	656	1.80	694	140	155 ± 13
4	659	1.75	698	110	234 ± 14
				120	190 ± 14
5	660	1.75	700	110	221 ± 9
				120	190 ± 12
6	666	1.74	700	120	219 ± 10
				140	180 ± 15
7	667	1.70	702	120	150 ± 9
8	668	1.68	704	120	114 ± 9

films a small dot spacing usually results in a good film quality, but also in a large film thickness. For this reason, a lower concentration of 3 mg mL⁻¹ was used here in order to reach lower layer thicknesses for a larger film size.

Figure 4a shows inkjet printed films in the size 5 mm × 5 mm (left) and 20 mm × 20 mm (right) prepared from toluene/*o*-DCB 90/10. Due to a decrease in film quality for higher drop-to-drop distances, a dot spacing of 100 μm is favorable for this solvent as it results in more homogeneous films with a film thickness of 250 nm for 5 mm × 5 mm. For larger film sizes, the control over the film quality is more difficult. One reason is the increased drying time of each printed line before a next line is printed next to the first dots. As described before, the film quality is thereby dependent on the size of the film as well as the solvent's boiling point. For a film size of 20 mm × 20 mm line formation occurs during drying at high dot spacings for the solvent system toluene/*o*-DCB 90/10. A dot spacing of 100 μm revealed an optimal film formation resulting in a high film thickness of approximately 350 nm.

As mentioned before, in this case the aimed application requires a lower film thickness. Different approaches can be used to reduce the layer thickness: i) increasing the dot spacing, ii) decreasing the ink concentration, and iii) increasing the amount of the high-boiling solvent. The first two points lead to a reduction of the deposited material and, hence, results in a lower film thickness. The third option introduces a longer drying of the deposited material, which leads to a more homogeneous drying of the printed films. As a result, a regular film formation can be obtained using higher dot spacings (140 μm) with the solvent mixture toluene/*o*-DCB 70/30 (Figure 4b). Furthermore, an increase in applicable dot spacings up to 150 μm is achieved. A film thickness of 130 nm was obtained for a film size of 5 mm × 5 mm and a thickness of 100 nm for 20 mm × 20 mm, respectively.

In addition, a solvent ratio of toluene/*o*-DCB 50/50 was tested to confirm constraints of the used approach. The solvent ratio 50/50 lead for both film sizes, 5 mm × 5 mm and 20 mm × 20 mm, to a strong decrease in film quality (Figure 4c). Using this solvent ratio, the drying of the film is very slow, leading to a multiple ring-like drying pattern. Additionally, investigations for a film size of 10 mm × 10 mm were performed (Supporting Information, Figure S4), confirming as well that an increase of the co-solvent content to a ratio of 70/30 improves the film quality at lower film thicknesses.

It can be concluded that for an increased film size an increased content of the high-boiling solvent leads to an improved control over the film formation. It is noticeable that not only thinner films can be prepared but also an improved film formation is observed. Hence, the approach of increasing the boiling point of the applied solvent represents a good alternative to reveal thinner as well as larger thin films with a homogeneous film formation. Since there is a limited window of applicable dot spacings, a reduction of the concentration leads for polymers usually to a decreased film quality.

Here, a straightforward approach of increasing the co-solvent content was proven as a good alternative. The

Table 3. Ink characteristics of the polymers 1 to 8.

Polymer	γ [mN m ⁻¹]	ρ [g cm ⁻³]	η [mPas]	Z-number	$\lambda_{\text{abs, sol.}}$ [nm]	$E_{\text{g, sol.}}$ [eV]	$\lambda_{\text{PL, sol.}}$ [nm]
1	33.0	0.910	0.698	65.7	507	2.12	639
2	29.7	0.911	0.942	46.2	637	1.82	662
3	34.5	0.910	0.966	48.5	643	1.82	667
4	33.4	0.911	0.852	54.2	647	1.81	670
5	34.6	0.911	0.916	51.3	651	1.81	675
6	33.8	0.911	0.942	49.3	652	1.81	676
7	32.5	0.911	1.013	44.9	653	1.81	676
8	34.6	0.910	1.058	44.4	655	1.80	676

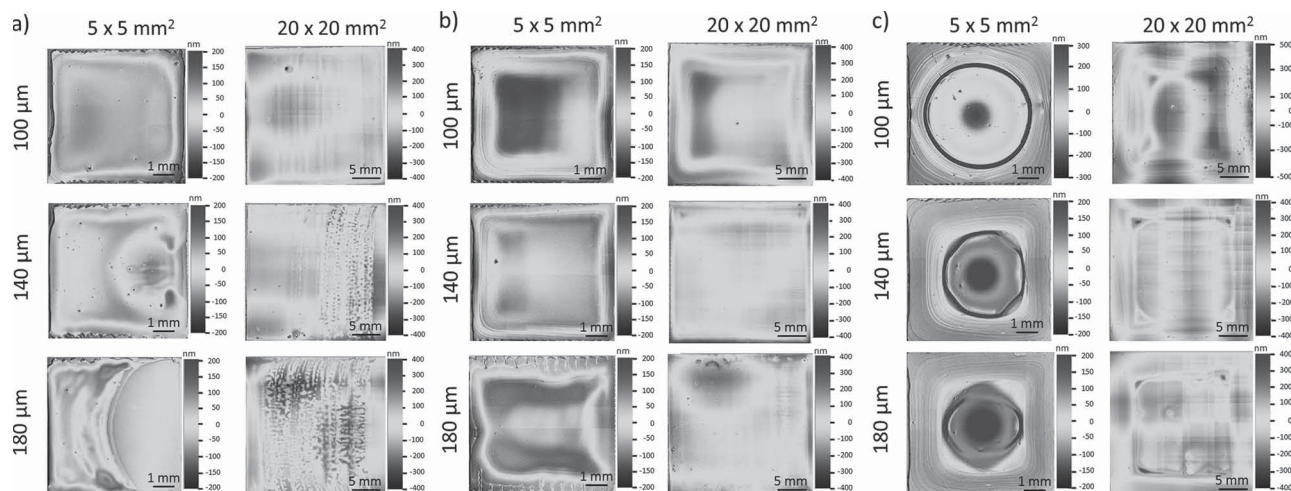


Figure 4. Optical profiler images of inkjet printed films of polymer **2** ($c = 3 \text{ mg mL}^{-1}$) processed by using toluene/*o*-DCB ratios 90/10 (a), 70/30 (b) and 50/50 (c). For each ratio, the films were prepared in the film sizes $5 \text{ mm} \times 5 \text{ mm}$ (left) and $20 \times 20 \text{ mm}$ (right).

preparation of even larger film sizes was, however, not performed since a single nozzle print-head was not seen as suitable for these experiments. For larger films than $20 \text{ mm} \times 20 \text{ mm}$, the use of a multi-nozzle print-head is preferred for a time-effective preparation.

3.3. Optical Properties

Not only the homogeneity and, as a consequence, the surface roughness of the printed films determines the quality of the final organic devices but also the optical properties of the films. First of all, the effect of the three different solvent systems toluene/*o*-DCB, CB/*o*-DCB, and *o*-xylene/*o*-DCB (with a solvent ratio of 90/10) to the absorption and emission characteristics of inkjet printed films of polymer **3** was investigated (Figure 5a). It can be seen that the use of the solvent system toluene/*o*-DCB results in the best properties: the intensity of the absorption bands at 530 and 660 nm for toluene/*o*-DCB is significantly increased (compared with the short wavelength absorption at 350 nm) in comparison to the other two solvent systems, which coincides with the results in the previous section for obtaining the best film formation. In particular, an increased absorption at higher wavelengths is preferred for the application in OPVs.^[25] An emission band at 694 nm is observed for all three solvent systems. The shoulder at 750 nm, which indicates more interactions between the polymer chains, is less dependent on the choice of solvent system.

Since the drying time of a wet π -conjugated polymer film strongly influences the absorption behavior of the dried film, the influence of the toluene/*o*-DCB ratio for polymer **2** was investigated (Figure 5b). An increased *o*-DCB content, which lead to an increased drying time, revealed only a slight increase of the absorption intensity at 540 and 660 nm for the ratios 70/30 and 50/50. All

other absorption and emission characteristics are equal for the three solvent ratios. Therefore, the change of the solvent system ratio causes only small modifications in the optical properties of polymer **2**.

The absorption and emission characteristics of the inkjet printed films of all eight polymers are depicted in Figure 5c and d, respectively, and in Table 2. Polymer **1**, which contains only the building units F and BTB, exhibits two absorption peaks at 370 and 520 nm. By incorporating a DPP building unit, the polymer absorption exhibits a third peak at approximately 660 nm. With increased DPP content, the intensity of the absorption peak at 660 nm increases and red-shifts to 668 nm. At the same time, since the BTB-content is decreasing, the absorption peak at around 520 nm decreases as well. As a result of the red-shifted absorption with increasing DPP-content, the optical bandgap of the polymers decreases from 1.98 eV for polymer **1** to 1.68 eV for polymer **8**. Therefore, the polymers show in the inkjet printed films a clear red-shift in absorption ($\approx 15 \text{ nm}$) in comparison to their solutions (Table 3), which is attributed to a further planarization of the polymer backbone in the films.^[26] The emission of the inkjet printed films of the polymer library depends on the polymer composition. Polymer **1** reveals a single emission peak at 662 nm, but shifts to longer wavelengths with the incorporation of DPP. Furthermore, a shoulder with increased intensity appears with addition of the DPP monomer in the copolymer.

4. Conclusion

In this contribution, the inkjet printability and selected thin film properties of a new polymer library consisting

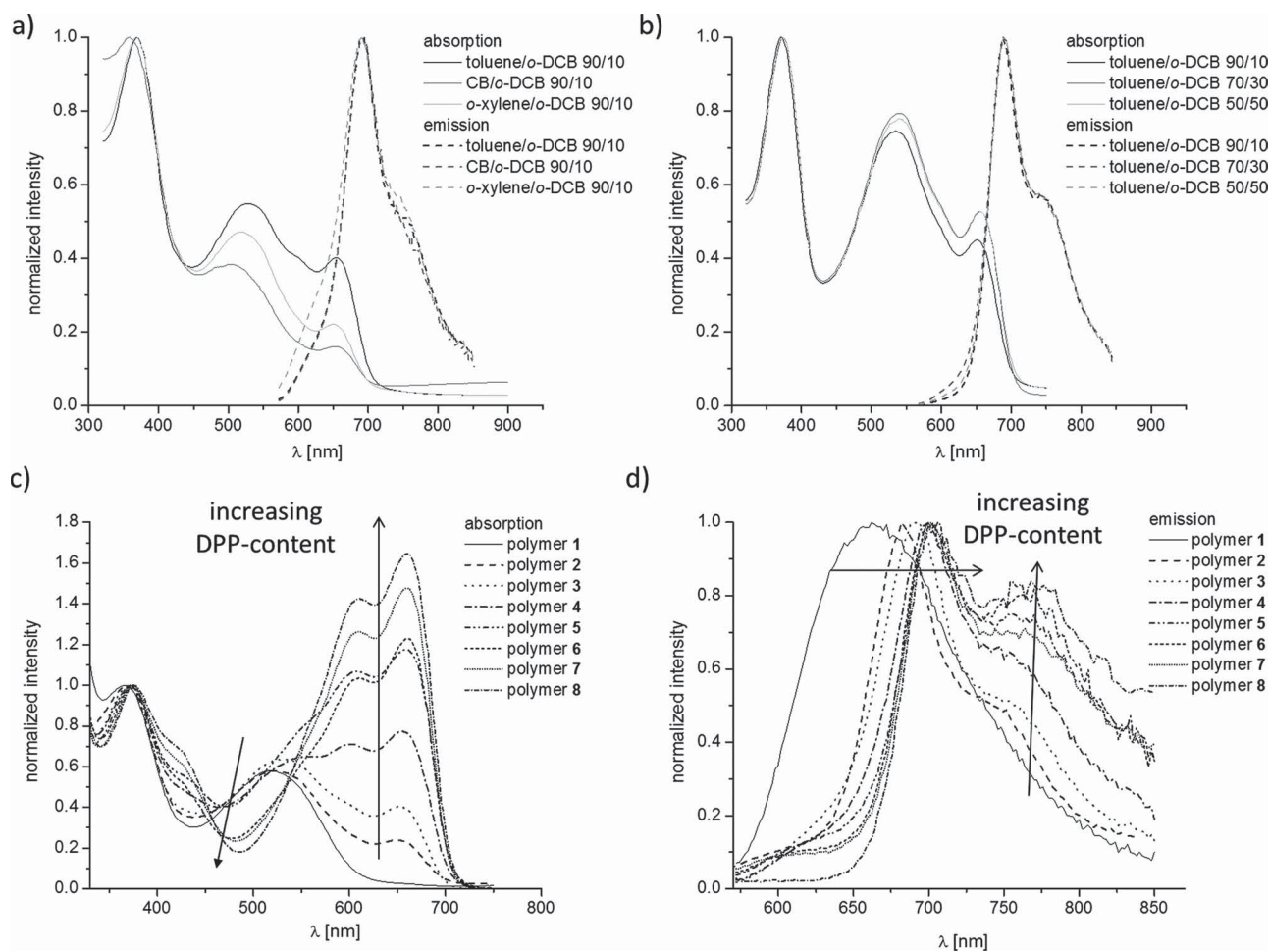


Figure 5. a) Normalized absorption and emission spectra of inkjet printed films of polymer **3** processed by the solvent systems toluene/*o*-DCB 90/10, CB/*o*-DCB 90/10, and *o*-xylene/*o*-DCB 90/10 (5 mg mL⁻¹). b) Normalized absorption and emission spectra of inkjet printed films of polymer **2** processed by the solvent system toluene/*o*-DCB in the ratios 90/10, 70/30, and 50/50 (5 mm × 5 mm, 3 mg mL⁻¹). c) Normalized absorption spectra of inkjet printed films of polymers **1** to **8** processed from toluene/*o*-DCB 90/10 (5 mg mL⁻¹). d) Normalized emission spectra of inkjet printed films of polymers **1** to **8** processed from toluene/*o*-DCB 90/10 (5 mg mL⁻¹).

of conjugated low-bandgap poly(diketopyrrolopyrrole-*co*-benzothiadiazole-*co*-fluorene) (poly(DPP-*co*-BTD-*co*-F)) polymers were investigated. Structure–property relationships between the polymer characteristics and the resulting thin film properties were obtained by the systematical variation of the monomer contents in the copolymers. In particular, the optical properties and film homogeneities were investigated. To accelerate the investigations, a combinatorial inkjet printing setup was used, whereby two-dimensional thin-film libraries were prepared to identify synergies between different properties, including solvent system, concentration, and film size.

It was found that a suitable solvent system for all polymers was toluene/*o*-DCB in a ratio 90/10 and a concentration of 5 mg mL⁻¹ when printing films of 5 mm × 5 mm. The polymer composition, that is, the DPP and BTD content, shows a significant influence on the film formation

characteristics as well as on the final film properties. When increasing the film size to 20 mm × 20 mm the solvent ratio had to be changed to 70/30 and the concentration to 3 mg mL⁻¹ to reveal homogeneous films with a film thickness of approximately 100 nm.

Inkjet printing has shown to be a suitable technique for the preparation of a thin-film library that can be easily characterized by combinatorial screening tools to elucidate correlations between the choice of solvent system, film formation qualities, and optical film properties. The use of the combinatorial screening workflow shows a high importance to identify materials and processing conditions that have the potential to yield highest solar cell efficiencies. Without the application of an efficient combinatorial screening approach, potentially record breaking polymers may have been undiscovered, simply because they were not efficiently screened.

Supporting Information

Supporting Information is available from the Wiley Online Library or from the author.

Acknowledgements: The authors would like to thank the Dutch Polymer Institute (DPI, technology area HTE, project #620) as well as the Thüringer Ministerium für Bildung, Wissenschaft und Kultur (Grant No. B 514-09049: PhotoMic) for financial support.

Received: September 1, 2012; Revised: October 16, 2012; Published online: January 17, 2013; DOI: 10.1002/macp.201200526

Keywords: combinatorial workflow; film-formation control; film size; inkjet printing; poly(DPP-co-BTD-co-F)

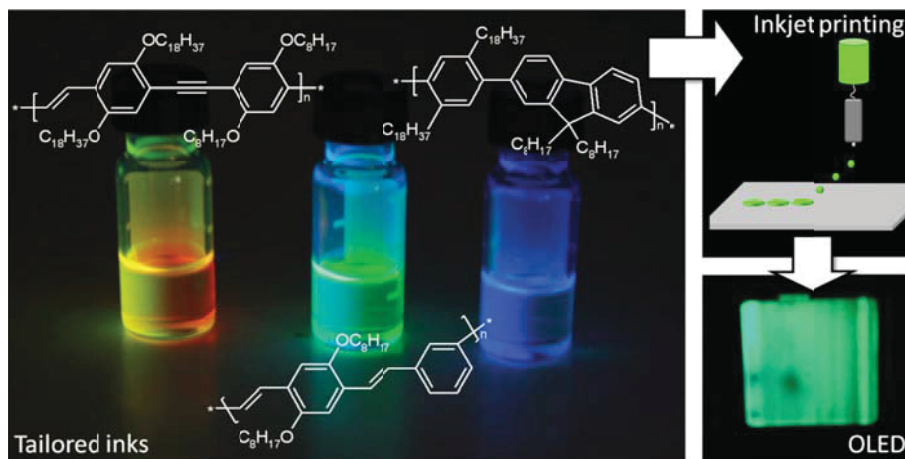
- [1] Y. Y. Liang, Z. Xu, J. B. Xia, S. T. Tsai, Y. Wu, G. Li, C. Ray, L. P. Yu, *Adv. Mater.* **2010**, *22*, E135.
- [2] E. Tekin, B. J. de Gans, U. S. Schubert, *J. Mater. Chem.* **2004**, *14*, 2627.
- [3] R. Søndergaard, M. Hoesel, D. Angmo, T. T. Larsen-Olsen, F. C. Krebs, *Mater. Today* **2012**, *15*, 36.
- [4] A. Teichler, R. Eckardt, S. Hoepfner, C. Friebe, J. Perelaer, A. Senes, M. Morana, C. J. Brabec, U. S. Schubert, *Adv. Energy Mater.* **2011**, *1*, 105.
- [5] M. Singh, H. M. Haverinen, P. Dhagat, G. E. Jabbour, *Adv. Mater.* **2010**, *22*, 673.
- [6] Y. Oh, J. Kim, Y. J. Yoon, H. Kim, H. G. Yoon, S. N. Lee, J. Kim, *Curr. Appl. Phys.* **2011**, *11*, S359.
- [7] H. Hu, R. G. Larson, *J. Phys. Chem. B* **2006**, *110*, 7090.
- [8] K. Norrman, A. Ghanbari-Siahkali, N. B. Larsen, *Annu. Rep. Prog. Chem., Sect. C* **2005**, *101*, 174.
- [9] V. Marin, E. Holder, M. M. Wienk, E. Tekin, D. Kozodaev, U. S. Schubert, *Macromol. Rapid Commun.* **2005**, *26*, 319.
- [10] A. Teichler, R. Eckardt, C. Friebe, J. Perelaer, U. S. Schubert, *Thin Solid Films* **2011**, *519*, 3695.
- [11] E. Tekin, H. Wijlaars, E. Holder, D. A. M. Egbe, U. S. Schubert, *J. Mater. Chem.* **2006**, *16*, 4294.
- [12] A. Manor, E. A. Katz, T. Tromholt, B. Hirsch, F. C. Krebs, *J. Appl. Phys.* **2011**, *109*, 074508.
- [13] J. Alstrup, M. Jørgensen, A. J. Medford, F. C. Krebs, *ACS Appl. Mater. Interfaces* **2010**, *2*, 2819.
- [14] M. T. Dang, L. Hirsch, G. Wantz, *Adv. Mater.* **2011**, *23*, 3597.
- [15] D. Muhlbacher, M. Scharber, M. Morana, Z. G. Zhu, D. Waller, R. Gaudiana, C. Brabec, *Adv. Mater.* **2006**, *18*, 2884.
- [16] J. Roncali, *Macromol. Rapid Commun.* **2007**, *28*, 1761.
- [17] C. Zhuoying, M. J. Lee, R. S. Ashraf, Y. Gu, S. Albert-Seifried, M. M. Nielsen, B. Schroeder, T. D. Anthopoulos, M. Heeney, I. McCulloch, H. Sirringhaus, *Adv. Mater.* **2012**, *24*, 647.
- [18] L. E. Poander, L. Pandey, S. Barlow, P. Tiwari, C. Risko, B. Kippelen, J. L. Bredas, S. R. Marder, *J. Phys. Chem. C* **2011**, *115*, 23149.
- [19] E. Bundgaard, F. C. Krebs, *Sol. Energy Mater. Sol. C* **2007**, *91*, 954.
- [20] F. Kretschmer, M. D. Hager, U. S. Schubert, *unpublished*.
- [21] C. Waldauf, M. Morana, P. Denk, P. Schilinsky, K. Coakley, S. A. Choulis, C. J. Brabec, *Appl. Phys. Lett.* **2006**, *89*, 233517.
- [22] M. T. Dang, G. Wantz, H. Bejbojji, M. Urien, O. J. Dautel, L. Vignau, L. Hirsch, *Sol. Energy Mater. Sol. C* **2011**, *95*, 3408.
- [23] S. Gunes, H. Neugebauer, N. S. Sariciftci, *Chem. Rev.* **2007**, *107*, 1324.
- [24] B. J. de Gans, U. S. Schubert, *Langmuir* **2004**, *20*, 7789.
- [25] T. Ameri, G. Dennler, C. Waldauf, H. Azimi, A. Seemann, K. Forberich, J. Hauch, M. Scharber, K. Hingerl, C. J. Brabec, *Adv. Funct. Mater.* **2010**, *20*, 1592.
- [26] I. F. Perepichka, S. Roquet, P. Leriche, J. M. Raimundo, P. Frere, J. Roncali, *Chem. Eur. J.* **2006**, *12*, 2960.

Publication 4

“Inkjet Printing of Chemically Tailored Light-Emitting Polymers”

Anke Teichler, Zhe Shu, Andreas Wild, Cornelia Bader, Jürgen Nowotny, Gerwin Kirchner,
Stephan Harkema, Jolke Perelaer, Ulrich S. Schubert

Eur. Polym. J. **2013**, *49*, 2186-2195.





Contents lists available at SciVerse ScienceDirect

European Polymer Journal

journal homepage: www.elsevier.com/locate/europolj

Inkjet printing of chemically tailored light-emitting polymers



Anke Teichler^{a,b,c,1}, Zhe Shu^{a,b,1}, Andreas Wild^{a,b,c}, Cornelia Bader^{a,b}, Jürgen Nowotny^{a,b}, Gerwin Kirchner^d, Stephan Harkema^d, Jolke Perelaer^{a,b,c,*}, Ulrich S. Schubert^{a,b,c,*}

^aLaboratory of Organic and Macromolecular Chemistry (IOMC), Friedrich Schiller University Jena, Humboldtstr. 10, 07743 Jena, Germany

^bJena Center for Soft Matter (JCSM), Friedrich Schiller University Jena, Philosophenweg 7, 07743 Jena, Germany

^cDutch Polymer Institute (DPI), P.O. Box 513, 5600 MB Eindhoven, The Netherlands

^dHolst Centre, High Tech Campus 31, 5656 AE Eindhoven, The Netherlands

ARTICLE INFO

Article history:

Received 3 January 2013

Received in revised form 20 March 2013

Accepted 23 March 2013

Available online 13 April 2013

Keywords:

 π -Conjugated polymers

Chemical tailoring

Inkjet printing

Thin-film libraries

Organic light emitting diode

ABSTRACT

For the implementation of the inkjet printing process in the fabrication of organic devices, like organic light emitting diodes (OLEDs), challenges such as the control over film formation need to be overcome in order to benefit from inkjet printing as a mask-free, material-efficient, non-contact and on-demand patterning technique. In this contribution, three different polymers with tailored properties were synthesized that reveal red, green and blue (RGB) emission colors. Film formation and thin-film properties were investigated in a combinatorial screening approach *via* inkjet printing. The solvent system toluene/*ortho*-dichlorobenzene revealed for all three polymers suitable film formation characteristics with final film thicknesses of 80 nm using a concentration of 4 mg/mL. Important relationships between polymer properties (molar mass), ink characteristics (viscosity) and film formation qualities (thickness, roughness) were identified. Finally, OLED devices were manufactured whereby the light emitting layers were inkjet printed using optimized processing conditions.

© 2013 Published by Elsevier Ltd.

1. Introduction

Organic electronic devices for lighting applications gain increasing popularity due to their light weight, flexibility as well as low processing costs. These characteristics can be ensured by an inexpensive solution processing, which preferably can be performed in a roll-to-roll (R2R) approach using flexible substrates [1]. A cost-effective processing requires solubility of the applied compounds in organic solvents. Only then, the expensive fabrication *via* vapor deposition, like applied for inorganic electronics, can be replaced by cost-effective solution fabrication

techniques. As a consequence organic electronics, such as organic light emitting diodes (OLEDs), can compete with inorganic devices, although their efficiencies are not yet as high as the efficiencies of the inorganic devices [2].

One of the most promising solution deposition techniques is inkjet printing, which is characterized by a precise and on-demand control of materials deposition due to a reproducible droplet formation. After ejection from the nozzle the droplets coalesce at the substrate, leading to the formation of a continuous film [3]. In order to produce homogeneous films many parameters that affect the final layer quality require an optimization. The influence of both the ink and the processing parameters was recently reported for poly(phenylene-ethynylene)-poly(phenylene-vinylene) (PPE-PPV) copolymers [4]. The control over film formation was achieved by the variation of ink concentration, solvent system, substrate temperature as well as drop-to-drop distance (dot spacing). Inkjet printed films

* Corresponding authors at: Laboratory of Organic and Macromolecular Chemistry (IOMC), Friedrich Schiller University Jena, Humboldtstr. 10, 07743 Jena, Germany. Tel.: +49 3641948200.

E-mail addresses: jolke.perelaer@uni-jena.de (J. Perelaer), ulrich.schubert@uni-jena.de (U.S. Schubert).

¹ These authors contributed equally for this work.

with a sufficient film quality were applied in organic electronics, such as OLEDs [5] and organic photovoltaics (OPV) [6]. Furthermore, inkjet printing enables a combinatorial screening of thin-film properties of polymer/fullerene layers for OPVs that strongly depend on the ink and the processing parameters [7]. Inkjet printing is, therefore, a suitable technique for the evaluation of synergies between ink and film properties. Characterized by an efficient materials handling both time and energy can be saved while using inkjet printing as a deposition technique.

The processing *via* solution deposition methods, like spin-coating or inkjet printing, is enabled by the attachment of side chains to the backbone of π -conjugated polymers, which enhances the solubility in organic solvents. In order to obtain homogeneous thin polymer films spin-coating is an often used patterning technique. The optical as well as morphological properties can be tuned as a function of polymer concentration, solvent, temperature and spin speed. Typically, a high concentration leads to a high aggregation of the polymer chains [8], while a red-shifted emission was obtained for lower spin speeds [9] and high boiling solvents result in a higher degree of crystallization [10].

In contrast to spin-coating, the control over the drying processes and the subsequent film formation is not yet fully understood for inkjet printed films. Although, inkjet printing shows some advantages over spin-coating, in particular a high material-efficiency, a low waste production and a mask-less, digital processing [7], it is currently not the preferred method to produce organic electronics, such as OLEDs [5,11]. Reasons can be found in the challenges that arise while using inkjet printing, such as the limitation to printable solvents and the control over the drying processes. The coffee-drop-effect [12] and the Marangoni flow [13] result in non-homogeneous drying patterns. An optimization of the ink as well as the processing parameters is required for each polymer class in order to identify optimal printing parameters for a specific application. Furthermore, not only the film formation properties, but also the optical characteristics of the layers are of importance when applying different processing parameters. It was found that the emission color of inkjet printed films is influenced by the layer thickness [14].

In order to make use of the beneficial properties of inkjet printing, control over the drying processes has to be obtained. The aim is to gain more insights into correlations between ink properties and film forming conditions. In this contribution, solution properties, inkjet printability and film formation characteristics of chemically tailored polymers is demonstrated. Different polymers were synthesized, including a poly(fluorene-phenylene), a poly(phenylene-vinylene) (PPV) and a poly(phenylene-ethynylene)-poly(phenylene-vinylene) (PPE-PPV) copolymer, in order to obtain red, green and blue (RGB) emission colors. Furthermore, the optimization of inkjet printed thin polymer films for OLED applications is presented. Inkjet printing allows here an acceleration of the thin-film optimization. Finally, optimized film forming settings were used to prepare the active layers for first OLED devices.

2. Experimental

2.1. Synthesis

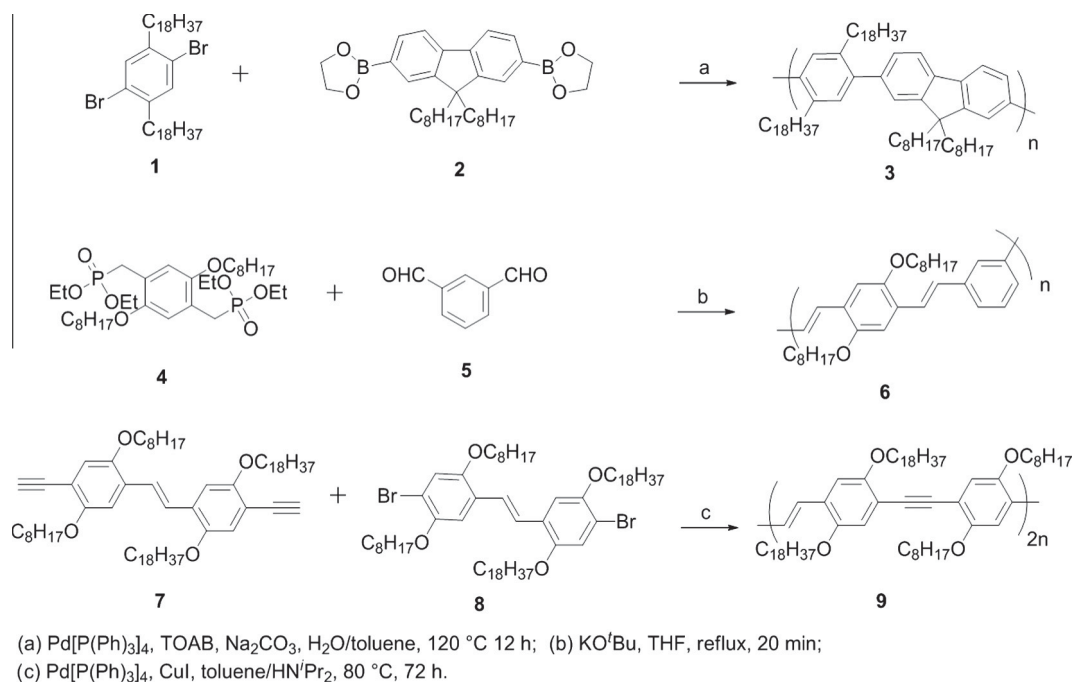
Solvents for synthesis were dried and distilled according to standard procedures and degassed by bubbling with nitrogen one hour prior to use. Isophthalaldehyde was purchased from Aldrich (97%) and recrystallized from toluene. Monomers **1**, **2**, **4**, **7** and **8** were synthesized in analogy to literature procedures [15–18]. A schematic representation of the synthesis of polymers **3**, **6** and **9** is given in Scheme 1.

The elemental analysis values of the π -conjugated polymers are not fitting, since the composition was, due to the high PDI values, calculated without taking into account the end groups. However, the identity of the substances and their polymeric nature was proven by ^1H NMR spectroscopy and size exclusion chromatography.

Synthesis of 3: **1** (318 mg, 0.6 mmol), **2** (445 mg, 0.6 mmol), Pd(PPh₃)₄ (7 mg, 1 mol%), tetraoctylammonium bromide (67 mg, 0.12 mmol) and a solution of 1.90 g Na₂CO₃ in 10 mL water were added to 25 mL toluene. The nitrogen-purged mixture was heated to gentle reflux. After no further change in the SEC trace was noted (12 h), the phases were separated and the organic phase was washed two times with water. Afterwards the solvent was removed under reduced pressure. The residue was dissolved in chloroform and precipitated in MeOH (1:20). The crude product was separated by filtration and Soxhlet extraction was conducted with heptane until no more oligomers dissolved. The remains were extracted with CHCl₃. The extract was concentrated under reduced pressure and precipitated in MeOH (1:20). The product was filtered off and dried to yield **3** as a white solid (483 mg, 0.49 mmol, 82%). Anal. Calcd for (C₇₁H₁₁₆)_n: C, 87.94%; H, 12.06%; N, 6.13%. Found: C, 87.52%; H, 11.71%.

^1H NMR (250 MHz, CD₂Cl₂): δ = 7.84 (b, FI-H), 7.81 (b, FI-H), 7.76 (b, FI-H), 7.65–7.59 (b, FI-H), 7.19 (b, Ph-H), 4.02 (b, CH₂), 2.07 (b, CH₂), 1.78 (b, CH₂), 1.55–1.00 (b, CH₂), 0.90–0.80 (b, CH₃).

Synthesis of 6: **4** (635 mg, 1.0 mmol) and **5** (134 mg, 1.0 mmol) were dissolved in toluene (20 mL), purged with nitrogen for 1 h and heated to 100 °C. KO^tBu (224 mg, 2.0 mmol) was added in small portions over a period of 20 min. Subsequently, benzaldehyde (212 mg, 2 mmol) was added to stop the reaction. After cooling to room temperature, the reaction mixture was neutralized with diluted aqueous HCl, the phases were separated and the organic phase was washed two times with water. Afterwards the solvent was removed under reduced pressure. The residue was dissolved in chloroform and precipitated in MeOH (1:20). The crude product was separated by filtration and Soxhlet extraction was conducted with heptane until no more oligomers dissolved. The remains were extracted with CHCl₃. The extract was concentrated under reduced pressure and precipitated in MeOH (1:20). The product was filtered off and dried to yield **6** as a yellow solid (364 mg, 0.79 mmol, 79%). Anal. Calcd for (C₃₂H₄₄O₂)_n: C, 83.43%; H, 9.63%. Found: C, 83.08%; H, 9.31%.



Scheme 1. Schematic representation of the synthesis of polymers **3**, **6** and **9**.

¹H NMR (250 MHz, CD₂Cl₂): δ = 7.69 (b), 7.60 (b), 7.53–7.48 (b), 7.43–7.34 (b), 7.27 (b), 7.21 (b), 4.11 (b, OCH₂), 1.92 (b, CH₂), 1.65–1.20 (b, CH₂), 0.88 (b, CH₃).

Synthesis of 9: **7** (2.0 g, 1.76 mmol), **8** (1.8 g, 1.76 mmol), Pd(PPh₃)₄ (82 mg, 0.07 mmol) and CuI (13 mg, 0.07 mmol) were dissolved in a solution of 40 mL toluene and 15 mL diisopropylamine. The mixture was purged with nitrogen for 30 min and subsequently heated to 80 °C for 72 h. Subsequently, the reaction mixture was filtered, the solution neutralized with aqueous HCl and dried with a Dean–Stark apparatus. Afterwards the solvent was reduced to 50 mL under reduced pressure and the solution precipitated in MeOH. The crude product was separated by filtration and Soxhlet extraction was conducted with MeOH until no more oligomers dissolved. The product was dried to yield **9** as a red solid (2.9 g, 0.49 mmol, 85%). Anal. Calcd for (C₁₃₆H₂₂₈O₈)_n: C, 82.03%; H, 11.54%. Found: C, 80.36%; H, 11.15%.

¹H NMR (250 MHz, CD₂Cl₂): δ = 7.52 (b), 7.46 (b), 7.17 (b), 7.02 (b), 4.05 (b, OCH₂), 1.88 (b, CH₂), 1.58–1.15 (b, CH₂), 0.87 (b, CH₃).

2.2. Instrumentation

2.2.1. Characterization

¹H NMR spectra were recorded on a Bruker AC 250 MHz spectrometer using the residual solvent resonance as an internal standard. Size exclusion chromatography (SEC) was measured on a Shimadzu system equipped with a SCL-10AV system controller, a LC-10AD pump, a DGU-14A Degasser, a RID-6A refractive index detector, a SIL-10AD auto sampler, and 3 mixed B (polymer lab) columns at room temperature. As eluent, THF was used at a flow

rate of 1 mL/min. The reported number average molar masses were calculated according to polystyrene standards. UV–Vis absorption spectra were recorded in 10^{−6} M CD₂Cl₂ solutions with an Analytik Jena SPECORD 250 (Jena, Germany) spectrometer. Solution emission spectra were measured with a Jasco FP-6500 spectrometer. Absolute quantum yields were determined by using a Hamamatsu C 10027 Photonic Multi-Channel Analyzer. Surface tension and contact angles of the inks were investigated on glass by the contact angle measurement system OCA 20 from Dataphysics (Filderstedt, Germany). Density as well as viscosity measurements were performed using a DMA 02 density meter and a ball/capillary viscosimeter AMVn (Anton Paar, Graz, Austria), respectively.

UV–Vis absorption spectra of the inkjet printed films were measured using a UV–Vis spectrometer Lambda 19 from Perkin Elmer. A fluorescence spectrometer HITACHI F-4500 was used to record the emission spectra of the inkjet printed polymer films. Surface topography as well as film thicknesses were measured using an optical interferometric profiler Wyko NT9100 (Veeco, Mannheim, Germany).

2.2.2. Inkjet printing

The polymers **3**, **6** and **9** were dissolved in a solvent mixture of toluene and *ortho*-dichlorobenzene (*o*-DCB) with varying concentrations. The solvents (toluene, *o*-DCB) were purchased from Sigma Aldrich and used without further purification. The polymer solutions were filtered before printing (pore size 1 μm) to prevent nozzle clogging. Microscope slides (3 × 1 in) from Marienfeld (Lauda-Königshofen, Germany) were used as substrates. The cleaning of the substrates was carried out by rinsing

with iso-propanol and drying with an air flow, followed by an oxygen plasma treatment for 5 min with a power of 240 Watt (Diener Electronic, Ebhausen, Germany). The inkjet printing was performed with an Autodrop system from microdrop Technologies (Norderstedt, Germany). The printer was equipped with a piezo-based micropipette print-head with an inner diameter of 70 μm . A voltage of 60 V and a pulse width of 35 μs revealed a stable droplet formation for all polymers in the solvent toluene/*o*-DCB 90/10 (v/v). The film size was usually 5 \times 5 mm² and the printing speed 20 mm/s.

2.2.3. OLED preparation

The OLEDs with the device structure glass substrate/ITO/PEDOT:PSS/active layer/cathode were fabricated at the Holst Centre Eindhoven (the Netherlands). In total 63 devices were prepared in three different sizes: 1 \times 1 mm², 3 \times 3 mm² and 20 \times 30 mm². A 100 nm thick PEDOT:PSS (Clevios AI VP 4083) layer was spin-coated on ITO/glass substrates and dried at 130 $^{\circ}\text{C}$. To pattern the PEDOT:PSS layer an ablation laser was used. The active polymer layers were subsequently inkjet printed using the optimized ink and printing conditions. The cathode materials Ba and Al were then evaporated through a shadow mask. Finally, the OLEDs were covered with a metal lid.

2.2.4. OLED characterization

The characterization of the devices was performed at the Fraunhofer IOF in Jena (Germany) using an optical fiber coupled calibrated spectrometer SD2000 from Ocean Optics for the detection of the output light spectra of the OLED devices. A YOKOGAWA GS610 source measure unit was used for an electrical power input in the constant current mode and for the *J*-*V* characterization. With this measurement set-up only the OLED devices in the size of 1 \times 1 mm² as well as 3 \times 3 mm² could be measured.

3. Results and discussion

3.1. Synthesis and characterization of the polymers

In order to tailor the emission color of the polymers, synthetic routes and known polymer structures were adapted from the literature. Phenylene-based polymers, in particular poly(fluorenes), were identified as the best candidates for blue emitting layers, because they exhibit high quantum yields, potential side-products are well-investigated and the synthesis *via* the Suzuki cross-coupling reaction is optimized [2]. For that reason poly-(fluorene-phenylene) **3** was synthesized by reacting the 1,4-dibromo-2,5-dioctadecylbenzene (**1**) and 2,2'-(9,9-dioctyl-9H-fluorene-2,7-diyl)bis(1,3,2-dioxaborolane) (**2**) (Scheme 1). The white polymer exhibits an intensive absorption maximum in the ultraviolet region ($\lambda_{\text{abs}} = 372$ nm), yielding in an intensive blue emission ($\lambda_{\text{PL}} = 417$ nm) with a quantum yield of $\Phi_{\text{PL}} = 0.71$ (Table 1, Fig. 1).

To assemble a green-emitting polymer poly(phenylene-vinylene) (PPV) copolymers were used here. It has been shown that thin films of PPV exhibit bright yellow-green

Table 1

Molar mass, PDI values and optical properties in solution of polymers **3**, **6** and **9**.

	λ_{abs} (nm)	E_g^a (eV)	λ_{PL}^b (nm)	Φ_{PL}	M_n^c (g/mol)	PDI
3	372	3.08	417	0.71	14,200	2.09
6	408	2.77	452	0.80	5,100	1.86
9	455	2.40	519	0.48	8,600	3.95

^a Calculated at 0.1 λ_{abs} .

^b Excited at λ_{abs} .

^c Calculated against poly(styrene) standard.

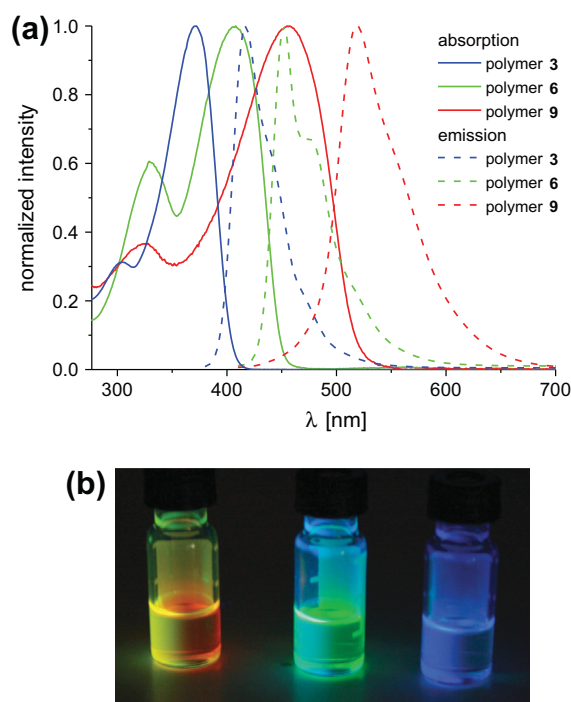


Fig. 1. (a) Absorption and emission of polymers **3**, **6** and **9** in solution, and (b) photograph of polymer inks (excited at 366 nm).

fluorescence with an emission maximum at $\lambda_{\text{PL}} = 551$ nm and a secondary peak at 2.4 eV (520 nm) [2]. However, unsubstituted PPV has a low solubility in organic solvents and is, therefore, difficult to process by a liquid processing technique, like inkjet printing. The substitution of PPV with alkoxy groups increases the solubility but, unfortunately, the band gap is reduced, leading to a significant red-shifted emission. When the phenylene units are connected to the *meta*- or *ortho*-position, the interruption of the conjugation in such polymers causes a blue-shift of the emission [19]. *Isophthalaldehyde* (**5**) was reacted with *bisphosphonate* (**4**) *via* Horner–Wadsworth–Emmons (HWE) reaction leading to the PPV **6** (Scheme 1). The short conjugation length in the polymer **6**, caused by the *meta*-linkage, lead to a yellow polymer, exhibiting a bright green emission ($\Phi_{\text{PL}} = 0.80$, $\lambda_{\text{PL}} = 452$ nm, Table 1).

In order to obtain polymers that have their emission wavelength in the red region of the spectrum, a further reduction of the band gap is required. A poly(phenylene-ethynylene)–poly(phenylene-vinylene) (PPE–PPV) was

synthesized. The presence of triple bonds in the structure results in a high level of planarity and, thereby, in a decrease of the band gap. The electroluminescence (EL) performance of PPEs is generally inferior to that of PPVs, but a combination of both units in one polymer backbone will combine the advantages, which leads to promising OLED materials [2]. The synthesis was performed by using a Sonogashira cross-coupling reaction of monomer **7** and **8** to yield polymer **9** as a red powder (Scheme 1). Polymer **9** exhibits in solution a PL maximum ($\Phi_{\text{PL}} = 0.48$) of $\lambda_{\text{PL}} = 519$ nm, representing an obvious bathochromic shift compared to the PPV **6** (Table 1).

3.2. Optimization of inkjet printed polymer films

For the fabrication of active layers for OLED devices by inkjet printing, the solubility and printability of the three polymers were first investigated. The polymers **3**, **6** and **9** were dissolved in the solvent system toluene/*ortho*-dichlorobenzene (*o*-DCB) with varying concentrations. All three polymers showed a good solubility with concentrations between 4 and 8 mg/mL in a solvent mixture of toluene/*o*-DCB 90/10.

Table 2 summarizes the properties of the three polymer inks. Since all polymers were dissolved in the same solvent system, the surface tension, density and contact angle were similar for all inks. The viscosities of the three different polymer solutions, however, differ slightly from each other, which follows the trend of the molar mass of the polymers: polymer **6** (0.70 mPa s) < polymer **9** (0.72 mPa s) < polymer **3** (0.76 mPa s). These results corroborate the findings of de Gans and Schubert, who studied the effect of different molar masses of polystyrene to the ink viscosity [20].

From the nozzle orifice d , the surface tension γ , the density ρ and the viscosity η of the polymer inks the Z -numbers, which assesses the printability of fluids, were calculated to be between 18 and 20. Although Jang et al. predicted that solutions with Z -numbers above 14 are not printable in a reliable way due to a satellite formation [21], other studies confirm printability of fluids with a high Z -number (>60) [22]. Here, we did not observe satellite formation and, thus, the inks were stable to be inkjet printed.

For the fabrication of the emissive layer of an OLED a film thickness of approximately 80 nm is required to achieve good light emitting efficiencies [23]. Different ink concentrations were tested for their film formation, film thickness as well as film roughness. First, the film formation of polymer **9** was investigated using varied

concentrations, as depicted in Fig. 2. Obviously, the film thickness depends on the ink concentration, but also the surface roughness, as depicted in Fig. 2e. For equal dot spacings the film thickness of the printed films increases with increasing concentration from 75 nm for 3 mg/mL to 290 nm for 8 mg/mL, respectively. The surface roughness shows a local minimum of 10 nm at 4 mg/mL, which corresponds to a film thickness of 120 nm. Although a film thickness of approximately 75 nm can be obtained for 3 mg/mL, a lower surface roughness is preferred for OLED applications since an improved contact quality between the OLED layers improves the charge injection into the active layer. A concentration of 4 mg/mL was, therefore, chosen for polymer **9** as optimal ink parameters. The film thickness of 120 nm, obtained with a dot spacing of 120 μm , was then reduced to 80 nm by increasing the dot spacing to 140 μm , leading to a reduced amount of deposited material, while the homogeneity of the resulting film was ensured.

The optimal ink parameters found for polymer **9** were successfully applied to the polymers **3** and **6**, since all inks have similar fluid properties and, as a result, equal printing characteristics. Fig. 3a–c shows optical profiler images of optimized inkjet printed films of the polymers **3**, **6** and **9**, respectively, revealing a homogeneous film formation. For the polymers **3** and **6** a dot spacing of 120 μm yielded a film thickness of approximately 72 nm and 80 nm. Indicated by the cross-sections in Fig. 3, the homogeneity of the inkjet printed films of polymer **3** and **6** is improved compared to polymer **9**. These results confirm that the optimized ink properties found for polymer **9** can be easily transferred to the other two polymers, yielding a high control over film formation even for different polymer classes. One reason for this may be the high solubility of all three polymers in the solvent system, which ensures a good printability and a stable droplet formation.

In summary, since the ink characteristics like viscosity and surface tension are comparable for all three polymer systems the droplet formation processes and film forming conditions are comparable. Although all three polymers reveal different chemical structures equal printing conditions could be applied, which represents an important step towards accelerated film formation conditions. Up to now, optimal printing conditions needed to be screened for each single polymer separately. For the polymers used here, the solvent system seems to mainly influence the ink characteristics (for the applied concentration). Therefore, significant steps towards a predictable film formation as well as insights into the film formation process by using

Table 2

Properties of inks and inkjet printed films of the polymers **3**, **6** and **9** (4 mg/mL, toluene/*o*-DCB 90/10).

	γ (mN/m)	ρ^a (g/cm ³)	η^a (mPa s)	Contact angle ^b (°)	Z - number	$\lambda_{\text{abs, film}}$ (nm)	$E_{\text{g, film}}$ ^c (eV)	$\lambda_{\text{PL, film}}$ ^d (nm)	Film thickness (nm)
3	31.1	0.915	0.76	<10	18.6	370,383	3.05	413,435 s	72
6	31.1	0.916	0.70	<10	20.2	416	2.58	504,536 s	80
9	31.2	0.917	0.72	<10	19.6	470	2.28	560,578	80

^a Measured at 20 °C.

^b On glass.

^c Calculated at 0.1 λ_{abs} .

^d Excited at λ_{abs} .

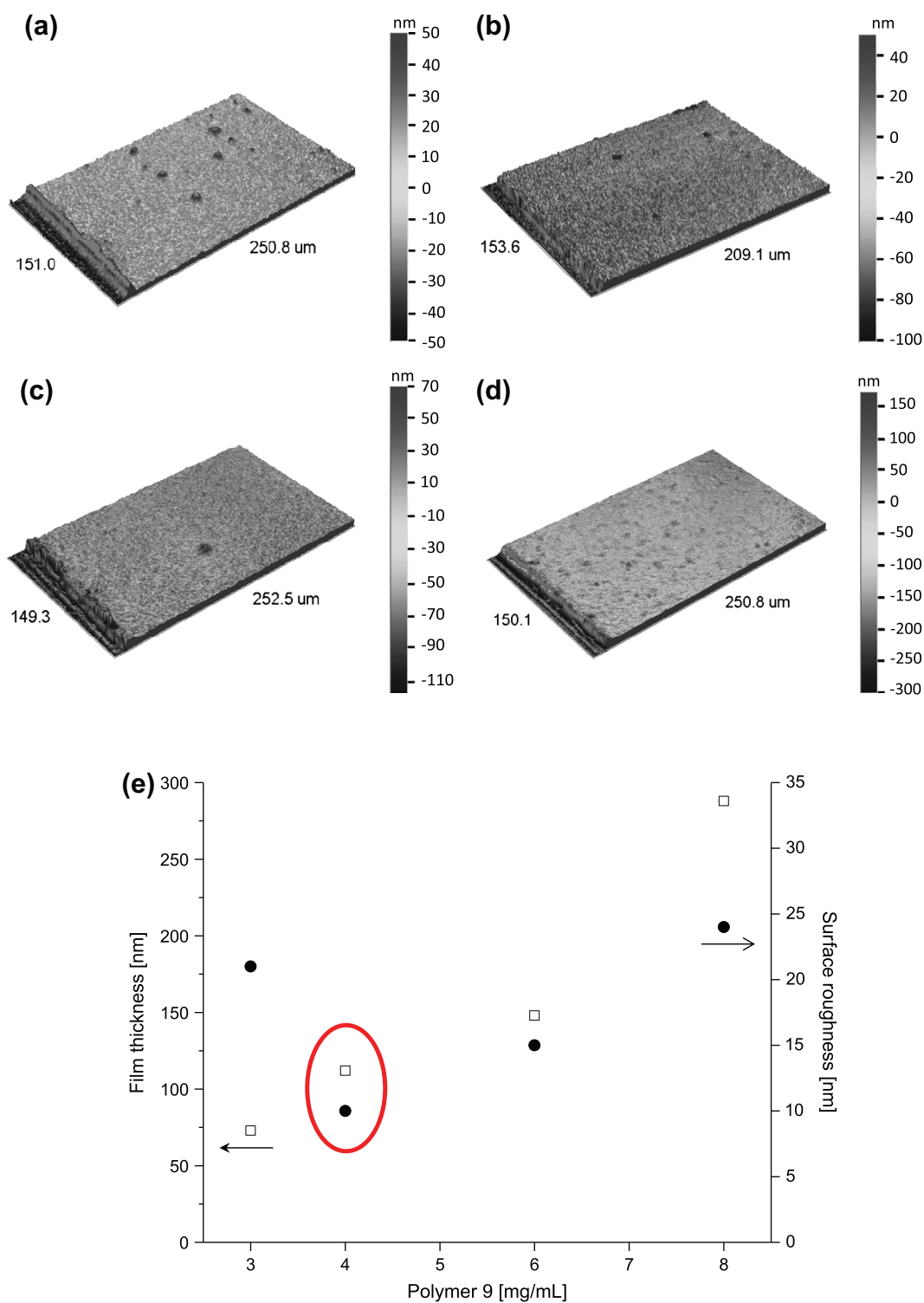


Fig. 2. Optical profiler images of inkjet printed films of polymer **9**, obtained with equal dot spacing from a toluene/*o*-DCB 90/10 mixture with concentrations of (a) 3 mg/mL, (b) 4 mg/mL, (c) 6 mg/mL and (d) 8 mg/mL, respectively. (e) Film thicknesses (squares) and film roughnesses (circles) of the layers prepared from different concentrations. The highlighted concentration of 4 mg/mL represents the optimum between aimed film thickness and best film formation properties.

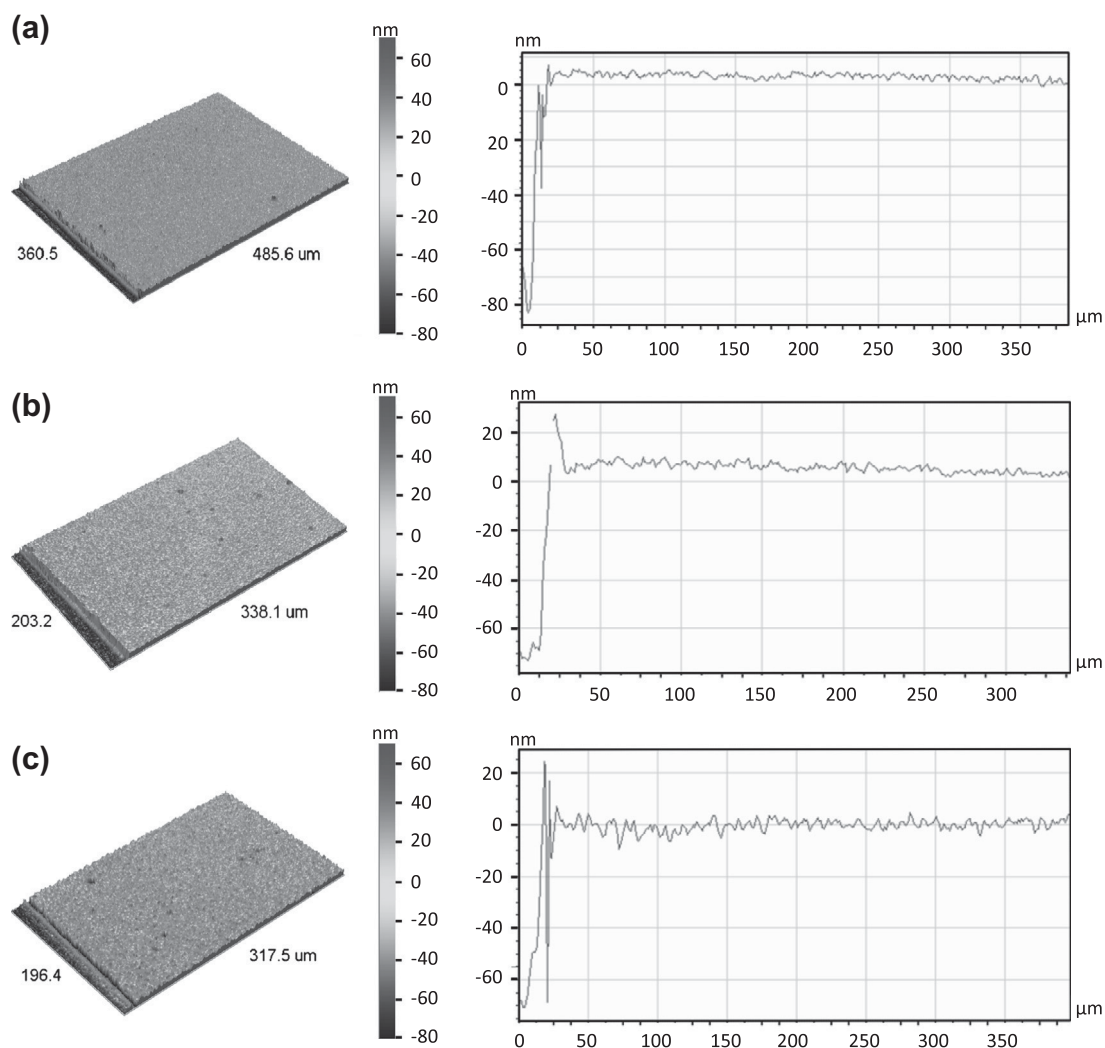


Fig. 3. Optical profiler images (left) and corresponding cross-sections (right) of thin films inkjet printed from optimized ink and printing conditions (4 mg/mL, toluene/*o*-DCB 90/10): (a) polymer **3** (dot spacing 120 μm), (b) polymer **6** (dot spacing 120 μm), and (c) polymer **9** (dot spacing 140 μm).

inkjet printing are revealed. Although polymer **9** showed the highest film roughness, further improvements could, however, not be achieved, even not by optimizing other parameters, like the solvent ratio, the substrate temperature and the printing speed. A lower or higher content of the high boiling solvent (toluene/*o*-DCB 95/5, 85/15) did not result in improved layer roughnesses. A printing speed of 20 mm/s was found to reveal an optimal film formation using the highest possible processing speed. A too low printing speed (e.g. 1 mm/s) results in an irregular drying pattern, since the drying of the printed material takes place before the entire film is printed. In contrast, when printing faster than 20 mm/s leads to a low printing accuracy. Furthermore, the inkjet printing experiments were performed at room temperature, because an increased substrate temperature revealed a too fast drying and, subsequently, a decreased film homogeneity. Although optical properties of π -conjugated polymer layers can vary depending on the used processing conditions, the focus here was on the

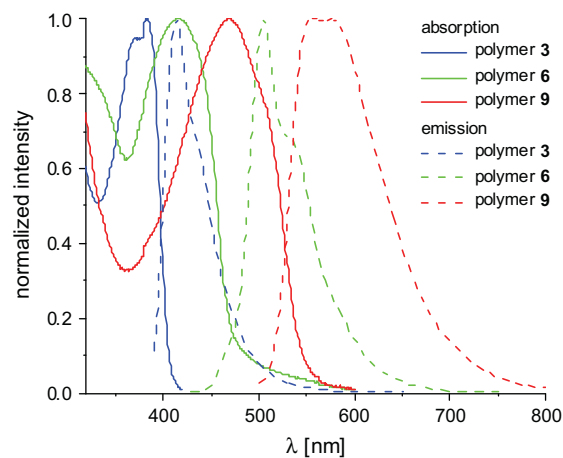


Fig. 4. Absorption and emission of polymers **3**, **6** and **9** as inkjet printed films from toluene/*o*-DCB 90/10 (4 mg/mL).

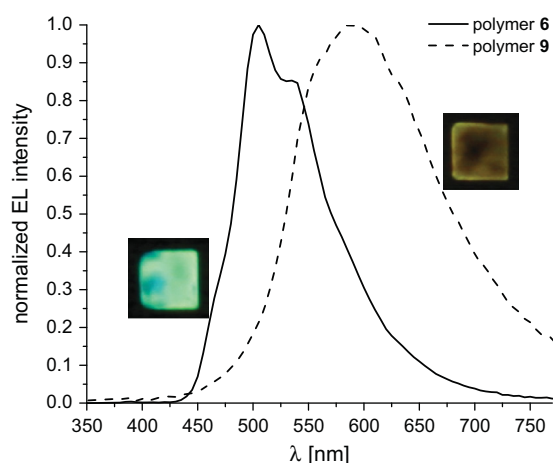


Fig. 5. Output spectra and photographs of the ($1 \times 1 \text{ mm}^2$) OLED devices using a driving current and voltage of 5 mA and 19.8 V for polymer **6** and 5 mA and 32.1 V for polymer **9**.

optimization of film thickness as well as film roughness requirements since a uniform emission is a key factor for the applications of OLEDs.

3.3. Characterization of inkjet printed polymer films

The absorption and emission spectra of the inkjet printed thin-films of all three polymers are shown in Fig. 4 and the optical properties are summarized in Table 2. Polymer **3** shows in the film two absorption peaks at 370 nm and 383 nm revealing an optical bandgap of 3.04 eV. Photoluminescence is observed in the blue region at 413 nm with a shoulder at around 435 nm. Compared to the solution, the film exhibits two main absorption peaks, indicating that solid state aggregation occurs [24]. Polymer **6** absorbs at 416 nm and emits at 504 nm with a shoulder at 536 nm. As a result, polymer **6** has a bandgap of 2.61 eV and an emission in the green region. According to the red-shifted absorption and emission in the inkjet printed film in comparison to solution, a planarization of the backbone

occurred in the solid state. Due to absence of additional peaks or shoulders aggregation of polymer **6** is not observed in the solid state. For polymer **9** an absorption wavelength at 470 nm and an emission wavelengths at 560 nm and 578 nm were observed revealing an orange-red emitting polymer with a bandgap of 2.35 eV. A pronounced shoulder at higher wavelengths could be observed in the absorption spectra of the solid state, indicating that aggregation formation occurs during film drying. Whereas polymer **9** has in solution a single main emission peak with a small shoulder, two emission peaks are observed in the solid state. All three polymers reveal in the inkjet printed films a red-shifted absorption in comparison to solution. Hence, a planarization of the polymer backbone takes place during film drying, which is more pronounced in the PPE-PPV-based polymer **9** than in the fluorene-based polymer **3** [24].

Inkjet printing is in comparison to other film preparation techniques like the commonly used spin-coating process known as being a slow film drying method. As a result aggregation of conjugated polymers might be favored. Indeed, improved crystallization and enhanced charge transport properties were observed, for e.g. polythiophenes, by using inkjet printing [25].

3.4. OLED characterization

OLEDs with a size of $1 \times 1 \text{ mm}^2$ and $3 \times 3 \text{ mm}^2$ were prepared by using the optimized printing conditions found for each polymer. Fig. 5 shows the output spectra of the red and green OLED device ($1 \times 1 \text{ mm}^2$) including the optical appearance of the film homogeneity during electrical excitation. The OLED of polymer **6** shows electroluminescence at 505 nm with a shoulder at 530 nm, which is comparable with the photoluminescence of polymer **6**. The OLED of polymer **9** reveals a broad output spectrum with a maximum intensity at 585 nm. Both polymer OLEDs show a relative good homogeneity during electrical excitation. In contrast, the OLEDs of polymer **3** display no light output since the polymer layer is short cut upon an increased

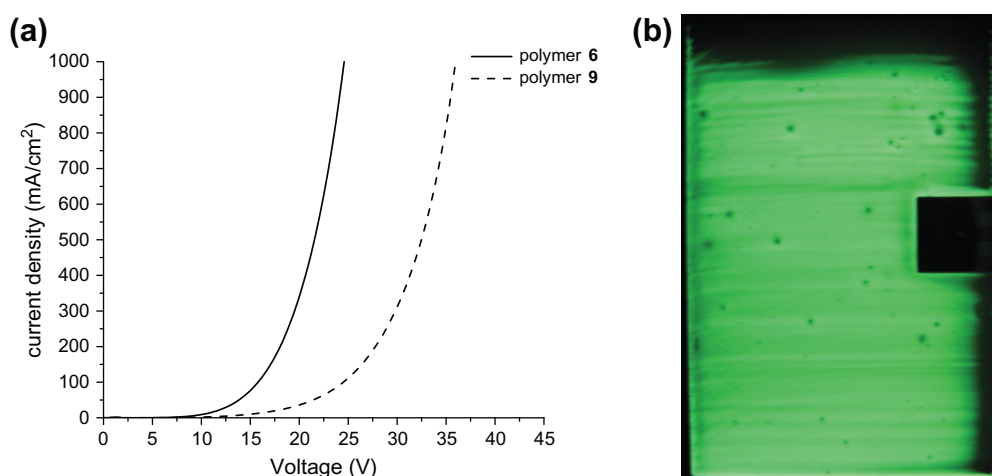


Fig. 6. J–V curves of the OLED devices ($1 \times 1 \text{ mm}^2$) of polymer **6** and **9** (a), and photograph of a $20 \times 30 \text{ mm}^2$ OLED of polymer **6** (b).

voltage. Since blue-emitting polymers like polymer **3** have a large bandgap a poor charge injection is observed and a high energy is required for an efficient light emission. In addition, poly(fluorenes) are known for their fast degradation during oxygen and light exposure [26]. Both reasons lead to the fast degradation of the blue OLED. An improved performance of polymer **3** may be revealed by handling the material under nitrogen atmosphere.

The J - V curves of the OLEDs of polymer **6** and **9** show that light is emitted at relative high voltages (>10 V), whereas polymer **6** requires less electrical consumption than the OLED of polymer **9** (Fig. 6a).

Output spectra and J - V curves of OLEDs with the size of 3×3 mm² are depicted in SI Fig. 1 for polymers **6** and **9**. The electroluminescence spectra of these devices are also similar to the polymer photoluminescence spectra, indicating that the output light is mainly determined by the polymer characteristics. Turn-on voltages for the devices of 3×3 mm² are as well above 10 V, whereas the blue emitting OLED of polymer **3** is not stable.

When printing the OLEDs with a size of 20×30 mm² a limitation of inkjet printing is observed when using a single nozzle print head. As the films are prepared by a line-by-line deposition, the size of an inkjet printed film is crucial for the drying process, since the lines start to dry before printing of the entire film is completed. The resulting film formation of polymer **6**, as depicted in Fig. 6b, reveals a clear line formation, leading to a decreased film homogeneity and quality. A multi-nozzle print head would decrease the preparation time and, as a consequence, improve the film quality.

These results confirm that the synthesized polymers require an optimization to obtain efficient, stable and colour-pure OLED devices. Only in this case, working OLEDs can be successfully prepared. By using inkjet printing, new polymers can be screened in a significant more efficient manner to elucidate important relationships between polymer characteristics, processing conditions and film forming properties. The OLEDs that were here reported were prepared and characterized under lab conditions, since the focus is set on the screening of film formation characteristics. Obviously, for a better performance handling under nitrogen atmosphere is preferred.

4. Conclusions

In this contribution, three conjugated polymers were chemically engineered to be used as red, green and blue light emitting materials for organic light emitting diodes (OLEDs). The polymers were processed via inkjet printing in order to reveal optimal conditions to produce homogeneous thin films with a thickness below 100 nm. Using inkjet printing as a combinatorial screening method, it was found that a concentration of 4 mg/mL in the solvent system toluene/*o*-DCB revealed homogeneous films of approximately 80 nm for all three polymers. The polymer inks have a similar Z -number of approximately 19, which resulted in a similar printing behavior without satellite formation. Finally, red and green light emitting diodes were

successfully prepared by inkjet printing the emissive polymers.

The results obtained here represent a significant step towards a controlled and predictable film formation by means of inkjet printing for OLED applications. Using the combinatorial inkjet printing approach novel materials can be screened in an efficient manner and candidates for a potential OLED application can be easily identified. In the near future, a parallel printing of the three different inks may be possible using a multi-nozzle system, which will allow a speed-up of processing.

Acknowledgements

For financial support the authors thank the DPI (Project #620, technology area HTE) as well as the European Community's Seventh Framework Programme (FP7/2007-2013) under Grant Agreement No. 248816. Furthermore, Dr. Michael Flämmich and Dr. Norbert Danz (Fraunhofer Institute for Applied Optics and Precision Engineering, Jena, Germany) are greatly acknowledged for using their optical characterization setup.

References

- [1] Krebs FC. Fabrication and processing of polymer solar cells: a review of printing and coating techniques. *Sol Energy Mater Sol C* 2009;93(4):394–412.
- [2] Grimsdale AC, Chan KL, Martin RE, Jokisz PG, Holmes AB. Synthesis of light-emitting conjugated polymers for applications in electroluminescent devices. *Chem Rev* 2009;109(3):897–1091.
- [3] Singh M, Haverinen HM, Dhagat P, Jabbour GE. Inkjet printing-process and its applications. *Adv Mater* 2010;22(6):673–85.
- [4] Teichler A, Eckardt R, Friebe C, Perelaer J, Schubert US. Film formation properties of inkjet printed poly(phenylene-ethynylene)-poly(phenylene-vinylene)s. *Thin Solid Films* 2011; 519(11): 3695–702.
- [5] Villani F, Vacca P, Nenna G, Valentino O, Burrasca G, Fasolino T, et al. Inkjet printed polymer layer on flexible substrate for OLED applications. *J Phys Chem C* 2009;113(30):13398–402.
- [6] Marin V, Holder E, Wienk MM, Tekin E, Kozodaev D, Schubert US. Ink-jet printing of electron donor/acceptor blends: towards bulk heterojunction solar cells. *Macromol Rapid Commun* 2005; 26(4):319–24.
- [7] Teichler A, Eckardt R, Hoepfener S, Friebe C, Perelaer J, Senes A, et al. Combinatorial screening of polymer: fullerene blends for organic solar cells by inkjet printing. *Adv Energy Mater* 2011;1:105–14.
- [8] Yang Y, Shi Y, Liu J, Guo T-F. The control of morphology and the morphological dependence of device electrical and optical properties in polymer electronics. In: Hotta S, editor. *Electronic and optical properties of conjugated molecular systems in condensed phases*. Kerala: Research Signpost; 2003. p. 307–54.
- [9] Shi Y, Liu J, Yang Y. Device performance and polymer morphology in polymer light emitting diodes: the control of thin film morphology and device quantum efficiency. *J Appl Phys* 2000;87(9):4254–63.
- [10] Chang JF, Sun BQ, Breiby DW, Nielsen MM, Solling TI, Giles M, et al. Enhanced mobility of poly(3-hexylthiophene) transistors by spin-coating from high-boiling-point solvents. *Chem Mater* 2004;16(23): 4772–6.
- [11] Tekin E, Holder E, Kozodaev D, Schubert US. Controlled pattern formation of poly [2-methoxy-5(2'-ethylhexyloxy)-1,4-phenylenevinylene] (MEH-PPV) by ink-jet printing. *Adv Funct Mater* 2007;17(2):277–84.
- [12] Oh Y, Kim J, Yoon YJ, Kim H, Yoon HG, Lee SN, et al. Inkjet printing of Al(2)O(3) dots, lines, and films: from uniform dots to uniform films. *Curr Appl Phys* 2011;11(3):S359–63.
- [13] Hu H, Larson RG. Marangoni effect reverses coffee-ring depositions. *J Phys Chem B* 2006;110(14):7090–4.
- [14] Tekin E, Wijlaars H, Holder E, Egbe DAM, Schubert US. Film thickness dependency of the emission colors of PPE-PPVs in inkjet printed libraries. *J Mater Chem* 2006;16(44):4294–8.

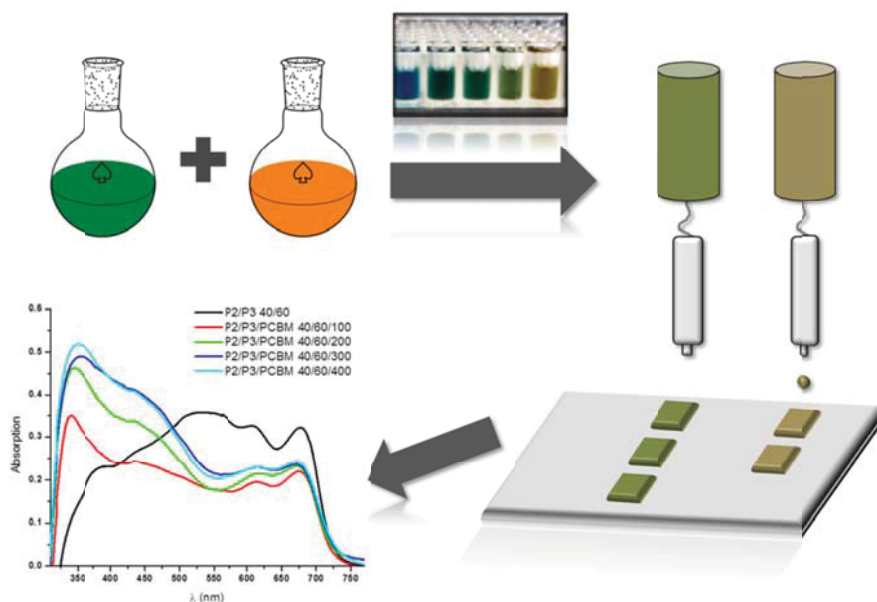
- [15] Rehahn M, Schlueter AD, Feast WJ. A high-yield route to 2,5-di-N-alkyl-1,4-benzenedicarboxylic acids. *Synthesis*–Stuttgart 1988;5: 386–8.
- [16] Wild A, Egbe DAM, Birckner E, Cimrova V, Baumann R, Grummt UW, et al. Anthracene- and thiophene-containing MEH–PPE–PPVs: synthesis and study of the effect of the aromatic ring position on the photophysical and electrochemical properties. *J Polym Sci Part A: Polym Chem* 2009;47(9):2243–61.
- [17] Wild A, Friebe C, Winter A, Hager MD, Grummt UW, Schubert US. Pi-Conjugated 2,2':6',2''-Bis(terpyridines): systematical tuning of the optical properties by variation of the linkage between the terpyridines and the pi-conjugated system. *Eur J Org Chem* 2010; 10:1859–68.
- [18] Egbe DAM, Bader C, Klemm E, Ding LM, Karasz FE, Grummt UW, et al. Influence of the conjugation pattern on the photophysical properties of alkoxy-substituted PE/PV hybrid polymers. *Macromolecules* 2003;36(25):9303–12.
- [19] Roncali J, Frere P, Blanchard P, de Bettignies R, Turbiez M, Roquet S, et al. Molecular and supramolecular engineering of pi-conjugated systems for photovoltaic conversion. *Thin Solid Films* 2006;511: 567–75.
- [20] de Gans B-J, Schubert US. Inkjet printing of well-defined polymer dots and arrays. *Langmuir* 2004;20(18):7789–93.
- [21] Jang D, Kim D, Moon J. Influence of fluid physical properties on inkjet printability. *Langmuir* 2009;25(5):2629–35.
- [22] Perelaer J, Smith PJ, van den Bosch E, van Grootel SSC, Ketelaars PHJM, Schubert US. The spreading of inkjet-printed droplets with varying polymer molar mass on a dry solid substrate. *Macromol Chem Phys* 2009;210(6):495–502.
- [23] Friend RH, Gymer RW, Holmes AB, Burroughes JH, Marks RN, Taliani C, et al. Electroluminescence in conjugated polymers. *Nature* 1999; 397(6715):121–8.
- [24] Nguyen TQ, Doan V, Schwartz BJ. Conjugated polymer aggregates in solution: control of interchain interactions. *J Chem Phys* 1999; 110(8):4068–78.
- [25] Teichler A, Perelaer J, Schubert US. Inkjet printing of organic electronics – comparison of deposition techniques and state-of-the-art developments. *J Mater Chem C* 2013;1(10):1910–25.
- [26] Romero B, Arredondo B, Alvarez AL, Mallavia R, Salinas A, Quintana X, et al. Influence of electrical operating conditions and active layer thickness on electroluminescence degradation in polyfluorene-phenylene based light emitting diodes. *Solid State Electron* 2009; 53(2):211–7.

Publication 5

“Combinatorial Screening of Inkjet Printed Ternary Blends for Organic Electronics – Absorption Behavior and Morphology”

Anke Teichler, Stefan Hölzer, Jürgen Nowotny, Jolke Perelaer, Stephanie Hoepfener, Florian Kretschmer, Cornelia Bader, Martin D. Hager, Ulrich S. Schubert

ACS Comb. Sci. **2013**, *15*, 410-418.



Combinatorial Screening of Inkjet Printed Ternary Blends for Organic Photovoltaics: Absorption Behavior and Morphology

Anke Teichler,^{†,‡,§} Stefan Hölzer,^{†,‡} Jürgen Nowotny,^{†,‡} Florian Kretschmer,^{†,‡} Cornelia Bader,^{†,‡} Jolke Perelaer,^{†,‡,§} Martin D. Hager,^{†,‡,§} Stephanie Hoepfener,^{†,‡} and Ulrich S. Schubert^{*,†,‡,§}

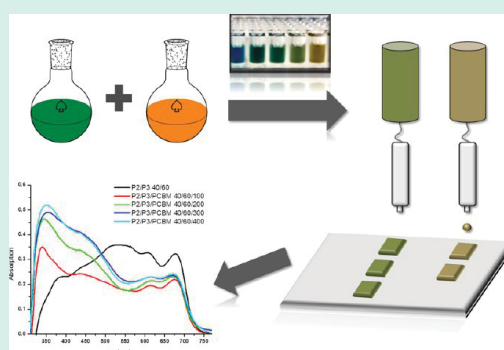
[†]Laboratory of Organic and Macromolecular Chemistry (IOMC), Friedrich Schiller University Jena, Humboldtstraße 10, 07743 Jena, Germany

[‡]Jena Center for Soft Matter (JCSM), Philosophenweg 7, 07743 Jena, Germany

[§]Dutch Polymer Institute (DPI), P.O. Box 513, 5600 MB Eindhoven, The Netherlands

ABSTRACT: Inkjet printing was used for the preparation of ternary polymer/polymer/fullerene layers for organic solar cell application, as part of a combinatorial setup for the preparation and characterization of thin-film libraries. Poly(phenylene-ethynylene)-*alt*-poly(phenylene-vinylene) (PPE-*alt*-PPV) and poly(diketopyrrolopyrrole-*alt*-fluorene) (P(DPP-*alt*-F)) were systematically blended with poly(3-octylthiophene) (P3OT) and investigated by UV-vis spectroscopy to improve the photon harvesting by extending the absorption range. The blends with the broadest absorption range (20 and 40 wt % of PPE-*alt*-PPV and P(DPP-*alt*-F), respectively) were mixed with mono(1-[3-(methoxycarbonyl)propyl]-1-phenyl)-[6,6]C₆₁ (PCBM). The blend with the low band gap polymer P(DPP-*alt*-F) revealed the most extended absorption, which ranges over the whole visible spectrum (350 to 750 nm). The mixing with PCBM (ratio 1/3) led to an optimal emission quenching and revealed a smooth film formation. In this contribution, we show that the combinatorial screening using inkjet printing represents an effective, time- and material-saving workflow for the investigation of polymer blend libraries, which is of high interest for the development of new materials for active layers in organic photovoltaics.

KEYWORDS: combinatorial screening, inkjet printing, ternary blends, absorption, morphology



INTRODUCTION

The development of smaller, more flexible and cheaper optoelectronic devices, for example, organic light emitting diodes (OLEDs)¹ and organic photovoltaics (OPVs),² benefits from the tunable characteristics of conjugated polymers, in particular variable optical properties. Conjugated polymer structures in the field of OPVs include poly(phenylene-vinylene) (PPV),^{3,4} poly(phenylene-ethynylene)-*alt*-poly(phenylene-vinylene) (PPE-*alt*-PPV),^{5,6} poly(thiophene) (PT),^{7,8} poly(fluorene) (PF),^{9,10} and poly(diketopyrrolopyrrole) (PDPP).^{11,12}

Thereby, a low polymer band gap² as well as a broad absorption range are required to improve quantum efficiencies of the final organic solar cell devices.¹³ For instance, low band gap donor-acceptor copolymers were found to reveal improved photon harvesting properties.^{14,15} In the past years, DPP moieties have gained an increased interest as a building unit for polymers used for organic solar cells because of their strong absorption in the visible region and their electron-withdrawing behavior.¹⁶ For this reason, DPP represents a suitable building moiety for donor-acceptor polymers. Fluorene (F) moieties are rigid and planar building units that in contrast to DPP, act as an electron-donating unit.¹⁷ As a

result, P(DPP-*alt*-F) is a donor-acceptor copolymer, which represents a low-band gap polymer.¹⁸ Although fine-tuning of the optical properties can be enabled by attaching side chains to the polymer backbone, the polymer shows absorption only in a specific wavelength-range.

A straightforward approach to increase the absorption range is blending of two polymers with different absorption characteristics. Improved performances of organic solar cell devices have been reported in literature by using a ternary mixture of polymer/polymer/fullerene^{19,20} or polymer/small molecule/fullerene.²¹ Thereby, the fullerene derivatives act as electron acceptor in the active layer.

For the preparation of the active layer of an organic solar cell, inkjet printing as well as spin-coating can be used as solution deposition method.^{22,23} In contrast to spin-coating, where more than 90% of the material is wasted, inkjet printing represents a highly material-efficient deposition method that requires only small amounts of functional materials and produces a minimal

Received: January 11, 2013

Revised: March 20, 2013

Published: April 26, 2013

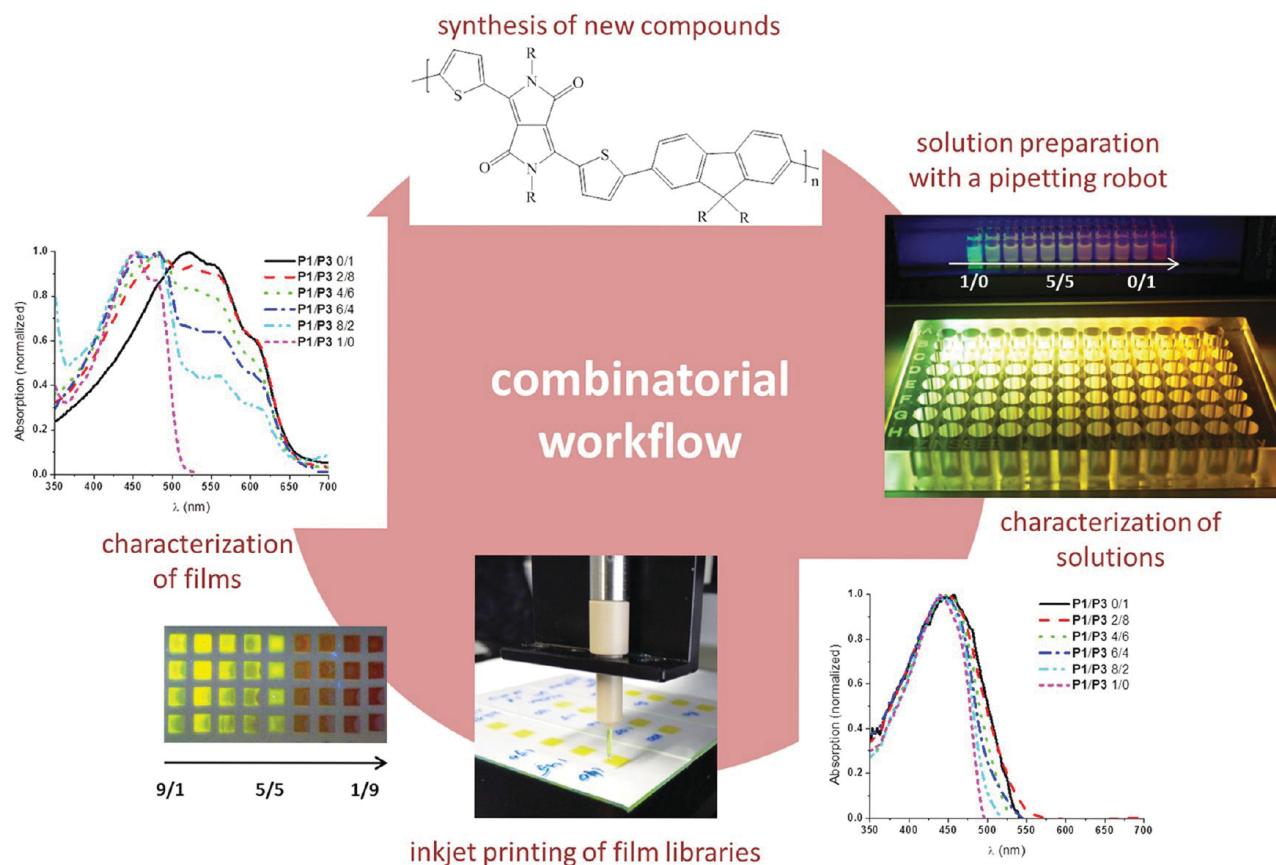


Figure 1. Experimental workflow for the combinatorial screening of binary polymer/polymer and ternary polymer/polymer/fullerene blends for the use in organic solar cells.

amount of waste, since the material is placed on-demand and where required.^{24,25}

Many processing parameters influence the fabrication of the active layer and, as a consequence, the final device properties. Ink formulations, like the solvent, the concentration, and the polymer/fullerene ratio, as well as the process parameters, including film thickness, temperature, and, obviously, the processing technique itself, have a significant influence on the properties of the active layer. Furthermore, with the addition of more components to the mixture the number of combinations is exponentially increasing.

Therefore, a combinatorial screening approach is necessary to elucidate important structure–property relationships as well as to identify the most promising blends and blend ratios for the use as active bulk heterojunction solar cell layers. To reveal correlations between printing conditions and solar cell activities the investigation of the performance of the inkjet printed active layers in solar cells is the scope of future publications.

Inkjet printing is a precise and noncontact patterning technique, which can be used as a combinatorial screening tool to discover quantitative structure–property relationships, as described recently for the optimization of donor/acceptor materials for solar cells.^{26,27} By using inkjet printing, synergies between ink properties and film characteristics can be found,²⁸ which significantly accelerates research and, subsequently, leads to a fast and simple handling of promising compounds for OPVs. Because of the continuous development of new polymers, many blend combinations might be promising as active layers. By using the presented workflow high perform-

ance materials and mixtures can be identified in a time- and material-efficient procedure.

In this contribution, we report the screening of two polymer/polymer blends, using a combinatorial experimental setup. To optimize the absorption of the active layer materials, two blend systems from poly(3-octylthiophene) (P3OT) with (i) PPE-*alt*-PPV and (ii) P(DPP-*alt*-F) were investigated according to their film formation and optical behavior.

RESULTS AND DISCUSSION

Combinatorial screening. The experimental setup for the combinatorial screening of various binary polymer/polymer and ternary polymer/polymer/fullerene mixtures is depicted in Figure 1. The following combinatorial workflow was used:

(i) The mixtures with the desired compound ratios, solvent system, and concentration were prepared in a quartz 96-well microtiter plate. For each polymer a solvent mixture of chlorobenzene/*ortho*-dichlorobenzene (CB/*o*-DCB) in a ratio of 90/10 was used.

(ii) The filled microtiter plate was used for UV–vis absorption and emission measurements of the blend solutions with a UV–vis plate reader.

(iii) Individual wells of the plate were used as small solution reservoirs for the inkjet printing process.

(iv) Thin-film libraries were printed in a microtiter plate pattern according to the positions to the wells of a 96-well plate to screen the optical properties of the films using a high-throughput UV–vis plate reader.

Single Polymers. At first, the individual polymers poly(phenylene-ethynylene)-*alt*-poly(phenylene-vinylene) (PPE-*alt*-PPV) **P1** (Figure 2a), poly(diketopyrrolopyrrole-*alt*-fluoro-

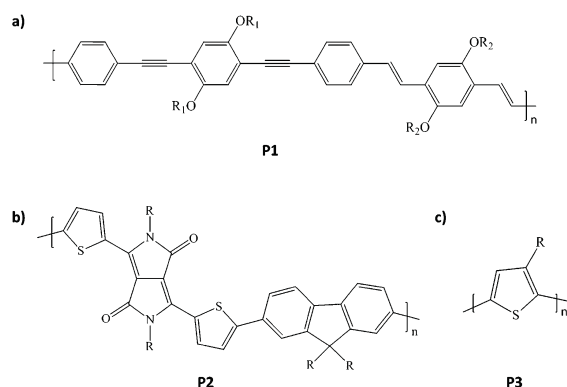


Figure 2. Schematic representation of the chemical structure of the investigated polymers. (a) Poly(phenylene-ethynylene)-*alt*-poly(phenylene-vinylene) **P1** ($R_1 = \text{octyl}$, $R_2 = \text{octadecyl}$), (b) poly(diketopyrrolopyrrole-*alt*-fluorene) **P2** ($R = \text{ethylhexyl}$ on DPP, octyl on F) and (c) poly(3-octylthiophene) **P3** ($R = \text{octyl}$).

rene) P(DPP-*alt*-F) **P2** (Figure 2b), and poly(3-octylthiophene) (**P3OT**) **P3** (Figure 2c) were investigated concerning their printability, film formation, and absorption behavior in solution and film. The results are summarized in Table 1. The surface roughness R_a of **P1**, **P2**, and **P3**, as estimated by optical interferometry, was found to be 8, 15, and 30 nm, respectively (Table 1). Thus, the film formation via inkjet printing seems to be better for the polymers **P2** and **P3** under the given processing conditions.

To investigate the polymers as potential candidates for the use in ternary mixtures, the absorption of the single polymers in solution and as film needs to be measured. **P1** reveals in solution an absorption maximum at 443 nm (Figure 3a), whereas two absorption peaks are observed in the inkjet printed film at 451 and 480 nm (Figure 3c). A red-shift of the absorption peak in the solid state occurs because of an improved planarization of the polymer backbone.²⁹ According to literature, the revealed band-splitting in the film absorption spectra is correlated to the formation of aggregates.³⁰

The absorption spectrum of the **P2** solution shows four peaks, which can be assigned to moieties of PDPP (417 nm, 609 nm, 661 nm) and PF (370 nm, Figure 3b). The absorption of **P2** of a printed film reveals only a small red-shift in comparison to the solution (Figure 3d). In contrast, polymer **P3** shows a more significant bathochromic shift between the solution (454 nm, Figure 3a) and the inkjet printed film ((522 nm, Figure 3c). Thereby, the three absorption peaks of

the inkjet printed film can be assigned to the $\pi-\pi^*$ transition (522 nm) and interchain interactions (550 nm, 610 nm). This behavior can be explained by an improved planarization and aggregation of the polymer in the solid state.²⁹

The optical band gap of all three polymers was determined from the UV-vis spectra of the polymers in solution (Table 1).³¹ The different optical properties of **P1**, **P2**, and **P3** can be explained by their chemical structures taking structural criteria for the design of conjugated polymers with reduced bandgaps into consideration.² **P1** has a relative high optical band gap of 2.4 eV, which is not favorable for their use in OPV as a single photon harvesting species. The high bandgap originates from a single bond rotation and therefore, from the hindered formation of the quinoid structure and delocalization of π -electrons. **P3** has a lower bandgap of 1.9 eV because of the high density of bulky side-chains, which cause a steric hindrance of the single bond rotation. Therefore, **P3** has a higher planarity of the aromatic backbone, which results in a higher degree of delocalization of π -electrons. Furthermore, the absorption spectrum of **P3** in the solid state is characterized by PT crystals that lead to a more ordered phase of the polymer and, hence, to a lower bandgap.¹⁸ The copolymer of PDPP and PF, **P2**, reveals a band gap of 1.7 eV, which is classified as being a low bandgap polymer and which is favorable for solar cell applications.¹¹ Copolymer **P2** has a very rigid structure that does not undergo further planarization in the solid state and, as a consequence, no strong red-shift of the absorption in the solid state compared to the solution is observed.

Polymer/Polymer Blends. Since all individual polymers **P1**, **P2**, and **P3** show different absorption spectra in the solid state, a combination of the polymers is promising to improve the overall yield of photon harvesting.

The first investigated polymer/polymer blend consists of **P1**/**P3**. The polymers were mixed in different ratios ranging from 8/2 to 2/8 by weight. The absorption spectra of the blends in solution (Figure 3a) showed a single absorption peak at 439 nm for the ratio 8/2, which is compared to **P1** 4 nm blue-shifted. With increasing **P3**-content the maximum peak shifts to 445 nm for the ratio 2/8 and the absorption spectra become broader.

The spectra of the inkjet printed films of the blends **P1**/**P3** (Figure 3c) show a broad absorption from 350 to 650 nm; the observed absorption features can be assigned to **P1** (452 nm, 480 nm) and **P3** (557 nm, 610 nm, Table 1). Thereby, the intensity of the two absorption peaks at 557 and 610 nm increases systematically with the **P3**-content. However, even with a high **P3**-content in the blend, the **P1** absorption peaks show high intensities because of a high absorption coefficient of the **P1** material.³² This implies that only a small addition of **P1** is required to increase the total absorption range of the polymer films significantly. Upon decreasing **P1**-content in the blend,

Table 1. Optical Properties in Solution and as Inkjet Printed Film As Well As Film Formation Characteristics of the Pristine Polymers **P1**, **P2**, and **P3** and the Binary Blends **P1**/**P3** 2/8 and **P2**/**P3** 4/6

	solution		inkjet printed film			
	$\lambda_{\text{max, abs}}$ [nm]	E_g^{opt} [eV]	$\lambda_{\text{max, abs}}$ [nm]	film thickness [nm]	surface roughness R_a [nm]	dot spacing [μm]
P1	443	2.43	451	160	30	120
P2	661	1.70	660	190	8	100
P3	454	1.89	522	150	15	160
P1 / P3 (2/8)	445		482	140	30	100
P2 / P3 (4/6)	660		666	170	20	110

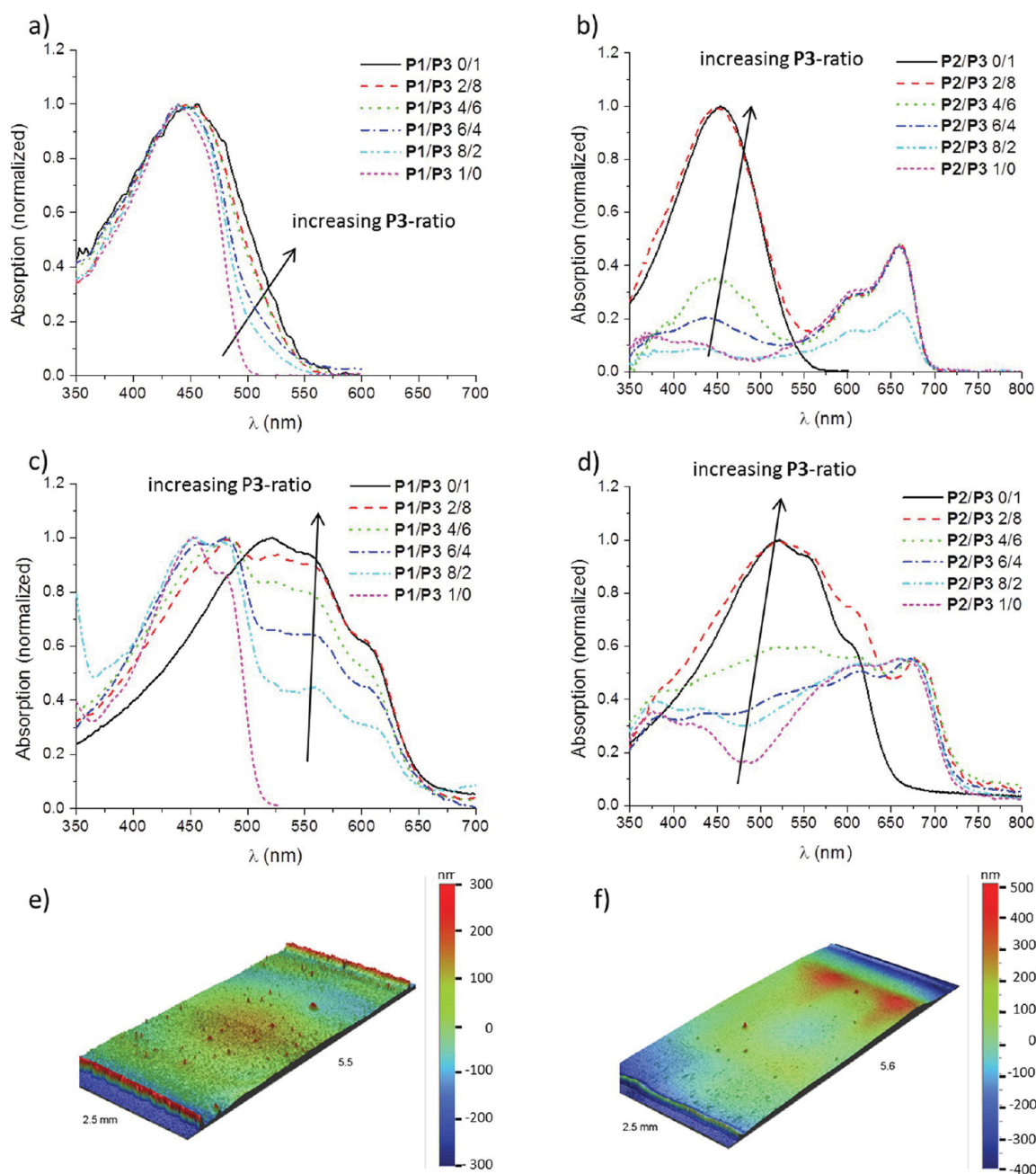


Figure 3. Absorption spectra of P1, P3, and P1/P3 blends (a) and P2, P3, and P2/P3 blends (b) in solution and inkjet printed films (c, d). Optical profiler images of the inkjet printed blend films P1/P3 2/8 (e) and P2/P3 4/6 (f).

the absorption peak of P1 (452 nm) shifts to 462 nm. Further decreasing of the P1-content leads to lower intensities. It can be assumed that the polymer P1 shows with increased P3-content a preferred formation of aggregates (as observed by the absorption at 480 nm) when inkjet printed from a P1/P3 mixture.³⁰ From Figure 3c it can be concluded that the blend ratio P1/P3 2/8 shows the best absorption performance, since the absorption range is the broadest when compared to the other ratios.

Figure 3e shows an optical profilometer image of the blend ratio P1/P3 2/8. Although inkjet printing of the films was performed directly after mixing the polymers and the mixtures are continuously stirred during printing, rough films with a

surface roughness R_a of 30 to 40 nm were formed. In contrast, a smooth surface with R_a of 15 nm was obtained when printing the single polymer P3 using the same solvent. The binary blends containing P1 and P3 reveal a similar roughness as the single polymer P1 (Table 1).

In summary, blending P3 with a small amount of P1 copolymer leads to an increased absorption range in the region from 350 to 630 nm. However, to improve the solar emission match, an absorption at higher wavelengths is required.¹³

Figure 3b shows the absorption spectra for the mixtures of P2 and P3 in solution. The peak at around 450 nm is assigned to P3 and the peaks at 376 nm, 430 nm, 608 nm, and 660 nm to P2. In the region between 430 and 450 nm, an overlay of

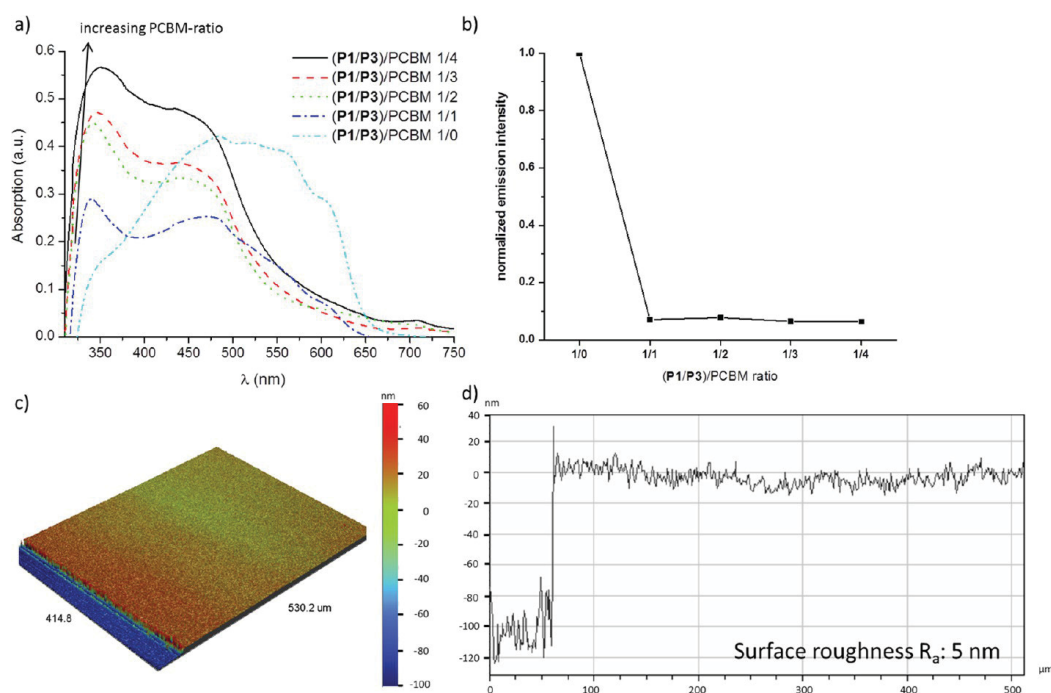


Figure 4. Absorption spectra (a) and normalized photoluminescence spectra (b) of inkjet printed films of **P1/P3** 2/8 in the mixture with PCBM with varied polymer/PCBM ratios. Optical profiler image (c) and corresponding cross-section (d) of an inkjet printed film of the polymer/PCBM ratio 1/1.

absorption from both polymers is observed. After printing, the UV–vis spectra show a significant broadening in the region of 650 to 750 nm, by adding a small fraction of **P2**, leading to an overall absorption range between 350 and 750 nm (Figure 3d). The absorption peaks of the printed samples are in comparison to the absorption in solution more structured as well as red-shifted; **P3** (520 nm, 550 nm, 610 nm) and **P2** (383 nm, 435 nm, 610 nm, 673 nm). From the absorption spectra in Figure 3d it was concluded that the blend ratio **P2/P3** 4/6 shows the broadest and most intense absorption of the investigated blends. Hence, this ratio was used for further investigations. In Figure 3f an optical profilometer image of an inkjet printed film of the blend ratio 4/6 is depicted. The image represents a 170 nm thick film with a surface roughness R_a of 20 nm (Table 1).

It is worth noting that the specific P3OT interchain interactions in the solid state (**P3**, 550 nm, 610 nm) is still observed when mixed with **P1** or **P2**, even at low **P3** contents. Thus, it can be assumed that the addition of **P1** or **P2** does not suppress the formation of highly ordered thiophene crystals.

Polymer/Polymer/Fullerene Blends. Optical Properties. As described in the previous sections the blend mixtures **P1/P3** 2/8 and **P2/P3** 4/6 were chosen from the combinatorial study of the binary blends for further investigations. Ternary blends were prepared from these mixtures by adding mono(1-[3-(methoxycarbonyl)propyl]-1-phenyl)-[6,6] C_{60} (PCBM) as electron-accepting unit, which is commonly used in active layers of organic solar cells. The chosen polymer blend/PCBM ratios of 1/1, 1/2, 1/3, and 1/4 were inkjet printed and investigated according to their film formation behavior and optical properties.

Figure 4a shows the absorption spectra of inkjet printed films of the ternary blends that consist of **P1/P3** 2/8 and PCBM in the prescribed ratios. The absorption peak at 320 nm originates

from the fullerene derivative and increases in intensity with the PCBM content in the blend. The wavelength, at which the polymer **P3** absorbs in the ternary blend, differs from the binary polymer/polymer mixture. Whereas in the spectrum of the polymer/PCBM ratio 1/1 the absorption bands of **P3** (520 nm, 550 nm, 610 nm) are still visible, this band structure is not observed at higher PCBM contents. For the films with a higher fullerene content only a blue-shifted main absorption peak of the π - π^* transition is present. This is an indication for reduced interchain interactions of **P3** in the presence of PCBM in the blend. The polymer emission is quenched by a factor of 10 when PCBM was added in a ratio of polymer/PCBM 1/1, as can be seen in Figure 4b. Increasing the amount of PCBM did not lead to a further decrease of the polymer emission. The significant quenching is an indication for a good mixing of the components in the ternary blends, which lead to an efficient charge transfer from the electron-donor to the electron-acceptor.

The absorption spectra of the polymer blend **P2/P3** 4/6 in a mixture with different amounts of PCBM are shown in Figure 5a. Similar to the (**P1/P3**)/PCBM blend, the intensity of the absorption peak at 320 nm is increasing with higher PCBM contents. Figure 5b shows the emission measurements of the (**P2/P3**)/PCBM blends. A high quenching of the emission was observed for all investigated (**P2/P3**)/PCBM blends. The maximum quenching was found for a ratio of ((4/6)/30) (Figure 5b), indicating an appropriate charge transfer in the blend. A quick indication of effective mixing and charge separation could be obtained by measuring the photoluminescence quenching of the ternary blends. Combinatorial screening of different blend compositions yields the most promising mixtures, based on the optical and film formation behavior, being (**P1/P3**)/PCBM ((2/8)/10) and (**P2/P3**)/PCBM ((4/6)/30), respectively.

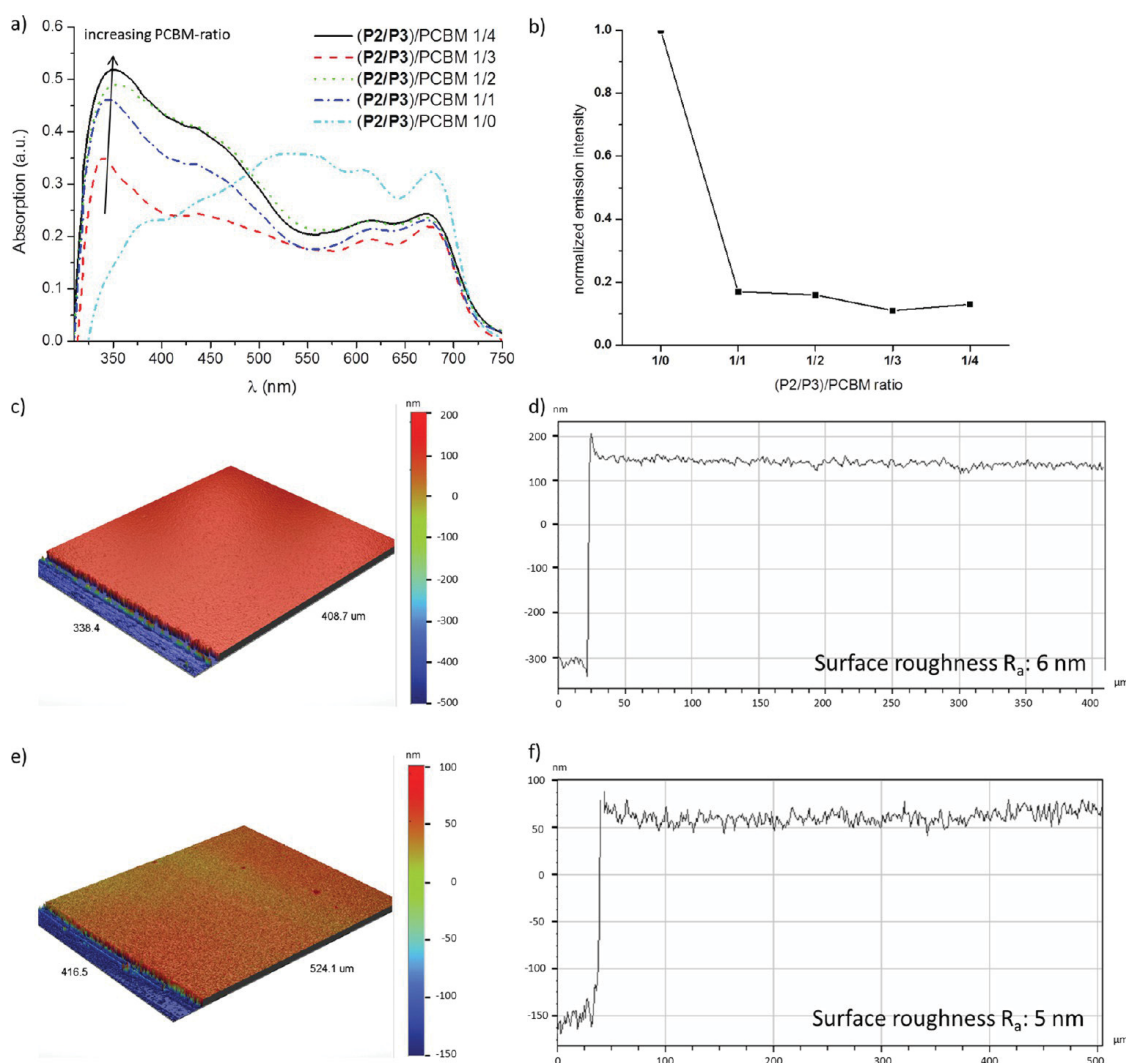


Figure 5. Absorption spectra (a) and normalized photoluminescence spectra at maximum (b) of inkjet printed films of P2/P3 4/6 in the mixture with PCBM with varied polymer/PCBM ratios. Optical profiler images (c, e) and corresponding cross sections (d, f) of inkjet printed films of the polymer/PCBM ratio 1/3 with a concentration of 0.8 wt % (c, d) and 0.5 wt % (e, f).

Morphological Characterization. The optical profilometer image of the inkjet printed film of the blend (P1/P3)/PCBM (2/8)/10 is depicted in Figure 4c, which shows a smooth film with a thickness of approximately 100 nm and a surface roughness R_a of 5 nm (Figure 4d). In Figure 5c an optical profiler image of an inkjet printed film of the blend (P2/P3)/PCBM (4/6)/30 is depicted, which demonstrates a smooth film formation ($R_a = 6$ nm) with a thickness of approximately 450 nm (Figure 5d). To reveal the required optimal thickness for an active layer of solar cells, which is between 100 and 200 nm,¹³ the concentration was reduced to 0.5 wt %, leading to a film thickness of approximately 200 nm with a low roughness ($R_a = 5$ nm), as depicted in Figure 5e,f.

The active layer morphology affects the charge transport through the active layer and is crucial for an evaluation of applicable polymer/fullerene blends or active layer preparation conditions for OPVs.³³ Therefore, atomic force microscopy (AFM) measurements were performed on selected blends, although the required time for these measurements is far too long for a combinatorial screening method.

AFM images of the P1/PCBM 1/1 blend reveals a rough film with R_a of 17 nm (Figure 6a), which is also reflected in the results from the interferometric profiler. Inkjet printing of the PPE-*alt*-PPV polymer in the mixture with PCBM reveals an unfavorable morphology by the formation of PCBM clusters and a strong phase separation of the individual compounds. This observation is in good agreement with literature.⁶

For the binary polymer/fullerene blends P2/PCBM 1/3 (Figure 6b) and P3/PCBM 1/1 (Figure 6c) smooth film surfaces with R_a of 1 nm are obtained. The inkjet printed film of P2/PCBM reveals different phases in the range of 10 nm, which is reported to be suitable for active layer morphologies.³⁴

P3/PCBM films prepared by inkjet printing from CB/*o*-DCB revealed fibrillar domains of P3OT that represent a highly ordered self-organization of the chains (Figure 6f). Note that the differences between the domain spacing in Figure 6f (being approximately 10 nm in the image) and the real distances between the thiophene crystals (of approximately 1 nm)³⁵ are screened by the convolution with dimensions of the AFM tip. The morphology observed for the as-printed film is comparable to the spin-coated films after annealing or additive addition.^{34,36}

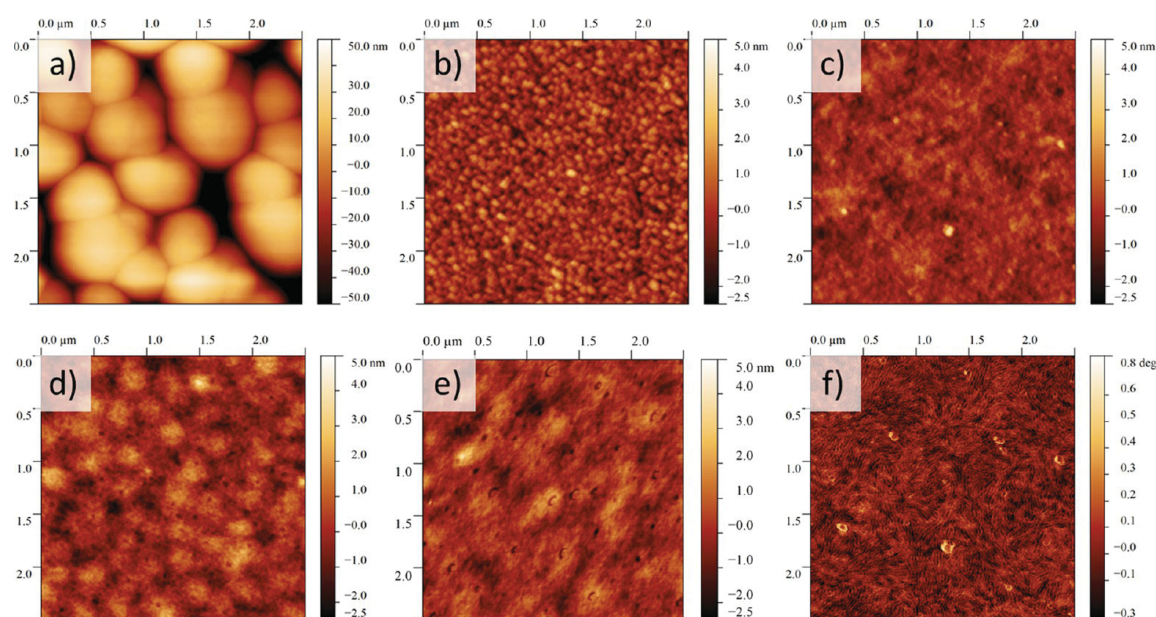


Figure 6. Atomic force microscopy height images of inkjet printed films of P1/PCBM 1/1 (a), P2/PCBM 1/3 (b), P3/PCBM 1/1 (c), (P1/P3)/PCBM (2/8)/10 (d), and (P2/P3)/PCBM 4/6/30 (e). Phase image of inkjet printed P3/PCBM 1/1 blend (f).

In the presence of PCBM, polythiophenes typically lose their chain alignment. As a result, postprocessing annealing methods, like thermal or solvent annealing, were developed to reorganize the polythiophene chains into the preferred fibrillar structure, which result in improved charge transport properties. As shown here, P3OT reveals self-organized domains in the blend with PCBM already in the as-inkjet printed films (Figure 6f). The reasons for the differences in film formation characteristics are explained by the use of the different film preparation techniques as well as processing solvents. When using conditions that cause a slow film drying, for example, by inkjet printing or by using the high boiling solvent chlorobenzene, the polythiophene chains may form highly ordered structures already during drying of the film. In contrast, when the drying proceeds too fast, for example, by using spin-coating or the low boiling solvent chloroform, the formation of the thermodynamically preferred crystalline polythiophene phases cannot take place.

AFM measurements of the ternary blends (P1/P3)/PCBM (2/8)/10 (Figure 6d) and (P2/P3)/PCBM (4/6)/30 (Figure 6e) revealed smooth (surface roughness $R_a = 1$ nm) and well mixed layer morphologies. The typical main chain crystals of the P3OT, which are observed in the binary P3/PCBM blend, were not observed in the ternary blend films. This is in agreement with the findings of the absorption spectra of the (P2/P3)/PCBM blend, where only weak signals were found, which correspond to the P3OT interchain interactions. The band structure of P3 was observed in the absorption spectra of both binary blends, P1/P3 2/8 and P2/P3 4/6. Hence interchain interactions of P3 should also occur in polymer/P3 blends. As a result, the interruption of the self-organization of P3OT is only observed in the ternary blend film. Although improved absorption characteristics of the ternary blend films are observed, morphological investigations reveal an unpreferred P3OT morphology in comparison to the binary P3OT/PCBM mixture. To answer the question whether the successful mixing of two polymers with PCBM in a ternary blend reveals

an enhanced photon harvesting, solar cell characteristics need to be measured, which will be executed in the future.

Since not only optical film characteristics but also morphological properties are important for an evaluation of promising donor/acceptor blends for solar cells, the combinatorial screening workflow presented here can only reduce the amount of samples to be tested, but cannot provide a selection of one best donor/acceptor combination. Since morphological investigations represent a serious bottleneck for a fast and efficient screening procedure, the combinatorial screening workflow, which allows to identify promising formulations and reveals a reduction of the amount of samples, is of high importance.³⁷

CONCLUSIONS

We have demonstrated that the mixing of conjugated polymers represents a straightforward strategy for improving the absorption of the active layers for organic solar cells. An experimental setup for a combinatorial screening was presented here to investigate the absorption behavior of polymer/polymer blends in solution and films. The used polymers include poly(phenylene-ethynylene)-*alt*-poly(phenylene-vinylene) (PPE-*alt*-PPV), poly(diketopyrrolopyrrole-*alt*-fluorene) (P(DPP-*alt*-F)), and poly(3-octylthiophene) (P3OT). An optimum absorption spectrum was found when mixing the compounds P(DPP-*alt*-F) and P3OT in a ratio of 4/6, while a quenching optimum was revealed when using a polymer/PCBM ratio of 1/3.

This ternary blend was found to cover a large absorption spectrum from 350 to 750 nm. Inkjet printing enabled a homogeneous film formation as well as a successful combinatorial screening of thin film properties of various compounds and blends for possible solar cell applications that lead to important structure–property-relationships. The next steps include the investigations of the inkjet printed active layers for their solar cell activity and the measurements of the resulting power conversion efficiencies.

EXPERIMENTAL PROCEDURES

Materials. The polymers poly(phenylene-ethynylene)-*alt*-poly(phenylene-vinylene) (PPE-*alt*-PPV) **P1** ($M_n = 10,200 \text{ g}\cdot\text{mol}^{-1}$, $M_w = 39,400 \text{ g}\cdot\text{mol}^{-1}$, PDI = 3.86) and poly(diketopyrrolopyrrole-*alt*-fluorene) (P(DPP-*alt*-F)) **P2** ($M_n = 26,000 \text{ g}\cdot\text{mol}^{-1}$, $M_w = 56,000 \text{ g}\cdot\text{mol}^{-1}$, PDI = 2.15) were synthesized as described elsewhere.^{11,32} Poly(3-octylthiophene) (P3OT) **P3** ($M_n = 34,500 \text{ g}\cdot\text{mol}^{-1}$), mono(1-[3-(methoxycarbonyl)propyl]-1-phenyl)-[6,6]C₆₁ (PCBM), the used solvents chlorobenzene (CB) and *ortho*-dichlorobenzene (*o*-DCB) were purchased from Sigma-Aldrich (Steinheim, Germany) and were used without further purification. The polymers were dissolved in the required ratios in a solvent mixture of CB and *o*-DCB with a concentration of 0.8 wt % and 0.5 wt %, respectively, which is known to show a stable droplet formation and enables a homogeneous thin-film formation of such polymers.^{26,28} For the ternary blends, the fullerene derivative was added to the polymer mixtures by using a constant polymer concentration. The solutions were filtered before printing (pore size 1 μm) to prevent nozzle clogging. Glass slides (3 \times 1 in.) were used as substrates and cleaned before printing by first rinsing with *iso*-propanol and subsequent drying with an air flow.

Instrumentation. UV-vis absorption and emission measurements of the blend solutions and films were carried out with a FLASHScan 530 (Analytik Jena, Jena, Germany) UV-vis plate reader. Inkjet printing was carried out with an Autodrop system from microdrop Technologies (Norderstedt, Germany). The printer was equipped with a piezo-based micropipette printhead with an inner diameter of 70 μm . A voltage of 70 V and a pulse length of 35 μs revealed a stable droplet formation for all inks in the solvent CB/*o*-DCB. The printing speed was set to 20 $\text{mm}\cdot\text{s}^{-1}$ for all experiments.

Surface topography and film thicknesses were measured with an optical interferometric profiler Wyko NT9100 (Veeco, Mannheim, Germany). Atomic force microscopy (AFM) measurements were performed in tapping mode with a NTegra Aura (NT-MDT, Moscow, Russia) on selected polymer/polymer/fullerene blends.

AUTHOR INFORMATION

Corresponding Author

*E-mail: ulrich.schubert@uni-jena.de.

Notes

The authors declare no competing financial interest.

ACKNOWLEDGMENTS

For financial support the authors thank the Dutch Polymer Institute (DPI, technology area HTE, project #620) as well as the European Community's Seventh Framework Programme (FP7/2007-2013) under grant agreement no. 248816.

REFERENCES

- (1) Grimsdale, A. C.; Chan, K. L.; Martin, R. E.; Jokisz, P. G.; Holmes, A. B. Synthesis of light-emitting conjugated polymers for applications in electroluminescent devices. *Chem. Rev.* **2009**, *109*, 897–1091.
- (2) Winder, C.; Sariciftci, N. S. Low bandgap polymers for photon harvesting in bulk heterojunction solar cells. *J. Mater. Chem.* **2004**, *14*, 1077–1086.
- (3) Shaheen, S. E.; Brabec, C. J.; Sariciftci, N. S.; Padinger, F.; Fromherz, T.; Hummelen, J. C. 2.5% efficient organic plastic solar cells. *Appl. Phys. Lett.* **2001**, *78*, 841–843.
- (4) van Duren, J. K. J.; Yang, X. N.; Loos, J.; Bulle-Lieuwma, C. W. T.; Sieval, A. B.; Hummelen, J. C.; Janssen, R. A. J. Relating the morphology of poly(*p*-phenylene vinylene)/methanofullerene blends to solar-cell performance. *Adv. Funct. Mater.* **2004**, *14*, 425–434.
- (5) Jadhav, R.; Türk, S.; Kühnlenz, F.; Cimrova, V.; Rathgeber, S.; Egbe, D. A. M.; Hoppe, H. Anthracene-containing PPE-PPV copolymers: Effect of side-chain nature and length on photophysical and photovoltaic properties. *Phys. Status Solidi A* **2009**, *206*, 2695–2699.
- (6) Hoppe, H.; Egbe, D. A. M.; Mühlbacher, D.; Sariciftci, N. S. Photovoltaic action of conjugated polymer/fullerene bulk heterojunction solar cells using novel PPE-PPV copolymers. *J. Mater. Chem.* **2004**, *14*, 3462–3467.
- (7) Li, G.; Shrotriya, V.; Yao, Y.; Huang, J. S.; Yang, Y. Manipulating regioregular poly(3-hexylthiophene): [6,6]-phenyl-C-61-butyric acid methyl ester blends - route towards high efficiency polymer solar cells. *J. Mater. Chem.* **2007**, *17*, 3126–3140.
- (8) Schilinsky, P.; Asawapirom, U.; Scherf, U.; Biele, M.; Brabec, C. J. Influence of the molecular weight of poly(3-hexylthiophene) on the performance of bulk heterojunction solar cells. *Chem. Mater.* **2005**, *17*, 2175–2180.
- (9) Pacios, R.; Bradley, D. D. C.; Nelson, J.; Brabec, C. J. Efficient polyfluorene based solar cells. *Synth. Met.* **2003**, *137*, 1469–1470.
- (10) Mammo, W.; Admassie, S.; Gadisa, A.; Zhang, F. L.; Inganäs, O.; Andersson, M. R. New low band gap alternating polyfluorene copolymer-based photovoltaic cells. *Sol. Energy Mater. Sol. Cells* **2007**, *91*, 1010–1018.
- (11) Zoombelt, A. P.; Mathijssen, S. G. J.; Turbiez, M. G. R.; Wienk, M. M.; Janssen, R. A. J. Small band gap polymers based on diketopyrrolopyrrole. *J. Mater. Chem.* **2010**, *20*, 2240–2246.
- (12) Sonar, P.; Ng, G. M.; Lin, T. T.; Dodabalapur, A.; Chen, Z. K. Solution processable low bandgap diketopyrrolopyrrole (DPP) based derivatives: novel acceptors for organic solar cells. *J. Mater. Chem.* **2010**, *20*, 3626–3636.
- (13) Günes, S.; Neugebauer, H.; Sariciftci, N. S. Conjugated polymer-based organic solar cells. *Chem. Rev.* **2007**, *107*, 1324–1338.
- (14) Janietz, S.; Krueger, H.; Schleiermacher, H. F.; Würfel, U.; Niggemann, M. Tailoring of low bandgap polymer and its performance analysis in organic solar cells. *Macromol. Chem. Phys.* **2009**, *210*, 1493–1503.
- (15) Roncali, J. Molecular engineering of the band gap of π -conjugated systems: Facing technological applications. *Macromol. Rapid Commun.* **2007**, *28*, 1761–1775.
- (16) Huo, L. J.; Hou, J. H.; Chen, H. Y.; Zhang, S. Q.; Jiang, Y.; Chen, T. L.; Yang, Y. Bandgap and molecular level control of the low-bandgap polymers based on 3,6-dithiophen-2-yl-2,5-dihydropyrrolo-[3,4-*c*]pyrrole-1,4-dione toward highly efficient polymer solar cells. *Macromolecules* **2009**, *42*, 6564–6571.
- (17) Cheng, Y. J.; Yang, S. H.; Hsu, C. S. Synthesis of conjugated polymers for organic solar cell applications. *Chem. Rev.* **2009**, *109*, 5868–5923.
- (18) Bundgaard, E.; Krebs, F. C. Low band gap polymers for organic photovoltaics. *Sol. Energy Mater. Sol. Cells* **2007**, *91*, 954–985.
- (19) Kim, H.; Shin, M.; Kim, Y. Distinct annealing temperature in polymer:fullerene:polymer ternary blend solar cells. *J. Phys. Chem. C* **2009**, *113*, 1620–1623.
- (20) Kim, Y.; Shin, M.; Kim, H.; Ha, Y.; Ha, C. S. Influence of electron-donating polymer addition on the performance of polymer solar cells. *J. Phys. D: Appl. Phys.* **2008**, *41*, 225101.
- (21) Huang, J. H.; Velusamy, M.; Ho, K. C.; Lin, J. T.; Chu, C. W. A ternary cascade structure enhances the efficiency of polymer solar cells. *J. Mater. Chem.* **2010**, *20*, 2820–2825.
- (22) Hoth, C. N.; Choulis, S. A.; Schilinsky, P.; Brabec, C. J. On the effect of poly(3-hexylthiophene) regioregularity on inkjet printed organic solar cells. *J. Mater. Chem.* **2009**, *19*, 5398–5404.
- (23) Hoth, C. N.; Schilinsky, P.; Choulis, S. A.; Brabec, C. J. Printing highly efficient organic solar cells. *Nano Lett.* **2008**, *8*, 2806–2813.

(24) Tekin, E.; Smith, P. J.; Schubert, U. S. Inkjet printing as a deposition and patterning tool for polymers and inorganic particles. *Soft Matter* **2008**, *4*, 703–713.

(25) Singh, M.; Haverinen, H. M.; Dhagat, P.; Jabbour, G. E. Inkjet Printing-Process and Its Applications. *Adv. Mater.* **2010**, *22*, 673–685.

(26) Teichler, A.; Eckardt, R.; Hoepfener, S.; Friebe, C.; Perelaer, J.; Senes, A.; Morana, M.; Brabec, C. J.; Schubert, U. S. Combinatorial screening of polymer:fullerene blends for organic solar cells by inkjet printing. *Adv. Energy Mater.* **2011**, *1*, 105–114.

(27) Marin, V.; Holder, E.; Wienk, M. M.; Tekin, E.; Kozodaev, D.; Schubert, U. S. Inkjet printing of electron donor/acceptor blends: Towards bulk heterojunction solar cells. *Macromol. Rapid Commun.* **2005**, *26*, 319–324.

(28) Teichler, A.; Eckardt, R.; Friebe, C.; Perelaer, J.; Schubert, U. S. Film formation properties of inkjet printed poly(phenylene-ethynylene)-poly(phenylene-vinylene)s. *Thin Solid Films* **2011**, *519*, 3695–3702.

(29) Miteva, T.; Palmer, L.; Kloppenburg, L.; Neher, D.; Bunz, U. H. F. Interplay of thermochromicity and liquid crystalline behavior in poly(p-phenyleneethynylene)s: π - π interactions or planarization of the conjugated backbone? *Macromolecules* **2000**, *33*, 652–654.

(30) Tekin, E.; Wijlaars, H.; Holder, E.; Egbe, D. A. M.; Schubert, U. S. Film thickness dependency of the emission colors of PPE-PPVs in inkjet printed libraries. *J. Mater. Chem.* **2006**, *16*, 4294–4298.

(31) Hellstrom, S.; Lindgren, L. J.; Zhou, Y.; Zhang, F. L.; Inganäs, O.; Andersson, M. R. Synthesis and characterization of three small band gap conjugated polymers for solar cell applications. *Polym. Chem.* **2010**, *1*, 1272–1280.

(32) Egbe, D. A. M.; Tillmann, H.; Birckner, E.; Klemm, E. Synthesis and properties of novel well-defined alternating PPE/PPV copolymers. *Macromol. Chem. Phys.* **2001**, *202*, 2712–2726.

(33) Kästner, C.; Susarova, D. K.; Jadhav, R.; Ulbricht, C.; Egbe, D. A. M.; Rathgeber, S.; Troshin, P. A.; Hoppe, H. Morphology evaluation of a polymer-fullerene bulk heterojunction ensemble generated by the fullerene derivatization. *J. Mater. Chem.* **2012**, *22*, 15987–15997.

(34) Nguyen, L. H.; Hoppe, H.; Erb, T.; Gunes, S.; Gobsch, G.; Sariciftci, N. S. Effects of annealing on the nanomorphology and performance of poly(alkylthiophene): fullerene bulk-heterojunction solar cells. *Adv. Funct. Mater.* **2007**, *17*, 1071–1078.

(35) Beiner, M.; Huth, H. Nanophase separation and hindered glass transition in side-chain polymers. *Nat. Mater.* **2003**, *2*, 595–599.

(36) Yao, Y.; Hou, J.; Xu, Z.; Li, G.; Yang, Y. Effects of solvent mixtures on the nanoscale phase separation in polymer solar cells. *Adv. Funct. Mater.* **2008**, *18*, 1783–1789.

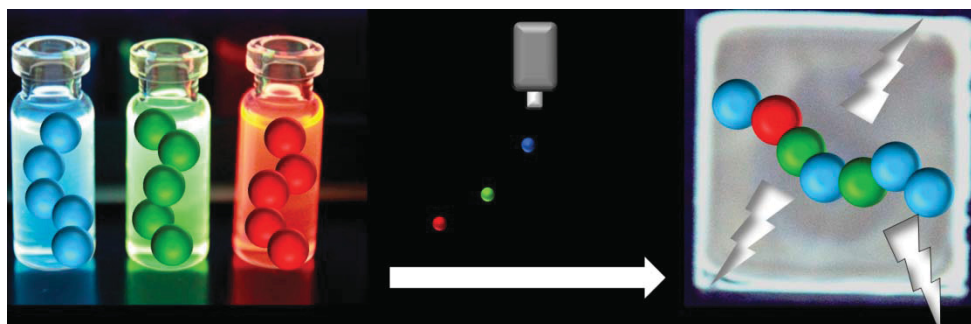
(37) Neffati, R.; Alexeev, A.; Saunin, S.; Brokken-Zijp, J. C. M.; Wouters, D.; Schmatloch, S.; Schubert, U. S.; Loos, J. Automated scanning probe microscopy as a new tool for combinatorial polymer research: Conductive carbon black/poly(dimethylsiloxane) composites. *Macromol. Rapid Commun.* **2003**, *24*, 113–117.

Publication 6

“Formation of Dynamic Metallo-Polymers by Inkjet Printing: Towards White-Emitting Materials”

Andreas Wild, Anke Teichler, Cheuk-Lam Ho, Xing-Zhu Wang, Hongmei Zhan, Florian Schlütter, Andreas Winter, Martin D. Hager, Wai-Yeung Wong, Ulrich S. Schubert

J. Mater. Chem. C **2013**, *1*, 1812-1822.



Formation of dynamic metallo-copolymers by inkjet printing: towards white-emitting materials†

Cite this: *J. Mater. Chem. C*, 2013, **1**, 1812Andreas Wild,^{ab} Anke Teichler,^{abc} Cheuk-Lam Ho,^d Xing-Zhu Wang,^d Hongmei Zhan,^d Florian Schlütter,^e Andreas Winter,^{ab} Martin D. Hager,^{ab} Wai-Yeung Wong^{*d} and Ulrich S. Schubert^{*abc}

The variation of the central chromophore in bisterpyridine Zn^{II} coordination polymers allowed the assembly of blue-, green- and red-emitting materials. The dynamic nature of the Zn^{II} complex enabled the systematic assembly of a library of statistical copolymers in an efficient way by simply mixing the respective homopolymer solutions. Depending on the ratios used and the consequent energy transfer processes, the resulting emission colors can be tailored. The kinetic lability of the Zn^{II} bisterpyridine polymers was, moreover, utilized to assemble thin films of statistical copolymers in a simple and material-saving manner by inkjet printing. For this purpose, the pure color inks were printed separately on top of each other, followed by one solvent layer to enable the assembly of statistical copolymers. The emission spectra of the resulting films are bathochromically shifted, due to aggregation of the chromophores. The obtained data allowed an estimation of CIE coordinates of the emission color for most ratios of the three polymers used and, thereby, to produce tailor-made emission colors.

Received 2nd November 2012
Accepted 12th December 2012

DOI: 10.1039/c2tc00552b

www.rsc.org/MaterialsC

Introduction

White organic light emitting materials are of interest both in the scientific and in the industrial communities, due to their great potential in lighting applications and as back-lights in liquid-crystal displays. Usually, the white light results from a simultaneous emission of red, green and blue chromophores or of two complementary colors (*e.g.*, orange and blue).¹ According to the literature, white emitting materials can be classified into two main categories: in the first approach several individual emitters are either arranged in different layers in a multilayer device (a) or combined in one single layer (b).^{1–4} In the second category the emission arises from one single material, that is either a short-wavelength-emitting substance that exhibits bathochromically shifted emission of aggregated excited states (c) or a more complex system bearing different chromophores (d).^{1,4–8}

When polymeric materials are used and an easy device architecture is desired, approaches (b) and (d) are mainly the methods of choice. Mixing of different polymers will potentially result in phase separated regions in (b). Approach (d) requires additional synthetic work for every single mixing ratio of the different chromophores in the material. The usage of a dynamic polymer could combine the advantages of both approaches and diminish the disadvantages. In such a dynamic supramolecular polymer, mixing of two homopolymers in a suitable solvent will result in a statistical copolymer.^{9–13}

Supramolecular polymers are obtained when the covalent bonds that connect the monomeric units in a classical macromolecule are replaced by reversible, highly directional, non-covalent interactions.^{9,12,13} Caused by the reversible nature of the binding, these supramolecular polymers benefit from their thermodynamic equilibrium and, thus, their properties can be adjusted by external stimuli in a way that is not possible for traditional macromolecules.^{10,13} Among the variety of non-covalent bonds applied for the assembly of supramolecular systems, metal ion complexation by various types of N-heterocyclic ligands has attracted much interest in research and application.^{14,15} The prevention of Δ/Λ -chirality or facial isomers in comparison to related metal complexes with 2,2'-bipyridine or 2,6-di(quinolin-8-yl)pyridine ligands and the easy access to 4'-substituted derivatives make 2,2':6',2''-terpyridine ideally suited for the construction of coordination polymers by $d\pi-p\pi^*$ bonding of different metal ions.^{16–21}

The photophysical behavior of such materials can easily be tuned by coordination to suitable metal ions and choosing an

^aLaboratory of Organic and Macromolecular Chemistry (IOMC), Friedrich-Schiller-University Jena, Humboldtstr. 10, 07743 Jena, Germany. E-mail: ulrich.schubert@uni-jena.de; Fax: +49 3641 948202

^bJena Center for Soft Matter (JCSM), Friedrich-Schiller-University Jena, Philosophenweg 7, 07743 Jena, Germany

^cDutch Polymer Institute (DPI), P.O. Box 902, 5600 AX Eindhoven, The Netherlands

^dInstitute of Molecular Functional Materials, Department of Chemistry and Institute of Advanced Materials, Hong Kong Baptist University, Waterloo Road, Hong Kong, P.R. China. E-mail: rwywong@hkbu.edu.hk

^eMax Planck Institute for Polymer Research (MPI-P), Ackermannweg 10, 55128 Mainz, Germany

† Electronic supplementary information (ESI) available: See DOI: 10.1039/c2tc00552b

appropriate spacer unit.^{19,22} Besides the heavy transition metal ions, such as Ru^{II}, Os^{II}, Ir^{III}, and Pt^{II}, metal ions with filled electron shells, in particular Zn^{II}, have recently gained much interest as templates for the development of new photoluminescent and electroluminescent materials as well as sensor systems.^{20,23–26}

An enormous number of donor-based π -conjugated bisterpyridines have been published so far, however, the absorption and emission maxima are most often in the region of $\lambda_{\text{abs}} = 400$ nm and $\lambda_{\text{PL}} = 450$ to 470 nm, respectively.¹⁹ In contrast to metal-free conjugated polymers, there are only a few examples of donor-acceptor-based bisterpyridines reaching emission maxima of $\lambda_{\text{PL}} > 550$ nm.^{27,28} For potential applications of these materials in photovoltaic devices, the absorption has to cover the red and near-infrared range of the terrestrial solar spectrum, and thereby exhibit band gaps clearly below 2.0 eV.²⁹ In addition, conjugated systems with band gaps of 2.2 eV or higher usually feature blue or green emission.²⁷ For OLED devices, however, materials emitting in the red region (λ_{EL} around 650 nm) are also required.²⁷

Due to this fact, systems with a broader absorption and consequently lower band gaps had to be synthesized. Based on this concept, we assembled a library of Zn^{II} bisterpyridine coordination polymers with a central dye moiety, surrounded by thiophene donors. Systematic modification of the dye and the conjugation length enabled the tuning of the absorption and emission maxima.

In contrast to classical π -conjugated covalent polymers, these coordination polymers allow the assembly of different independent chromophores in one polymeric backbone and in every desired ratio. Moreover, an auxiliary monomer to decouple the electronic properties is not necessary and the dynamic nature ensures a statistical assembly. The different monomers of the resulting coordination polymers are consequently able to emit simultaneously at different wavelengths and to produce thereby mixed colors, for example, white light.

On the way to dynamic white light emitting materials, this contribution demonstrates a simple and efficient way to tailor the emission of one single polymeric system avoiding the use of expensive heavy metal ions. To enable an efficient screening and to reduce the materials consumption the solution experiments were performed using a quartz microtiter plate. Thin films of functional organic materials were inkjet-printed, allowing an efficient material usage, a flexible change of processing the conditions, and a mask-less, digital processing. The dynamic nature of the Zn^{II} bisterpyridine polymers combined with the possibility of tailoring the amount of deposited material by the inkjet printing technique enables thereby the separate printing of every single color and the subsequent assembly to statistical copolymers.

Experimental

Materials

Solvents were dried and distilled according to standard procedures. Except for the synthesis of **1**, all solvents or solutions were degassed by bubbling with argon one hour prior to use. **3**, **5** to **9** as well as **P2**, **P4**, **P10** and **P11** were synthesized according to literature procedures.^{28,30–35}

Instrumentation

¹H and ¹³C NMR spectra were recorded on a Bruker Cryomagnat BZH 400 (400 MHz) or Bruker AC 300 (300 MHz) instrument (for all NMR spectra: 298 K). Chemical shifts are reported in parts per million (ppm, δ scale) relative to the residual signal of the solvent; coupling constants are given in Hz. MALDI-TOF mass spectra were recorded on a Voyager-DE PRO biospectrometry workstation (Applied Biosystems) time-of-flight mass spectrometer with dithranol as a matrix. UV-Vis absorption, emission and excitation spectra were recorded on an Infinite 200 PRO plate reader (Tecan) using 5×10^{-6} M DMF solutions or films. Elemental analysis was carried out on a CHN-932 Automat Leco instrument. Inkjet printing was performed using an Autodrop professional system from microdrop technologies (Norderstedt, Germany). The inkjet printer was equipped with piezo-based micropipettes with an inner nozzle diameter of 70 μm . A voltage of 75 V and a pulse length of 30 μs led to a stable and reproducible droplet formation. The films with a size of 6×6 mm² were printed onto microscope slides (Marienfeld). The substrate temperature was set to 50 °C. A drop count of 1 and a printing speed of 20 mm s⁻¹ were used as standard settings.

Synthesis

4'-(4-Ethynylphenyl)-2,2':6',2''-terpyridine (1). This protocol represents an optimized procedure based on the solvent-free procedures of Raston and Cave.³⁶

2-Acetylpyridine (3.63 g, 30 mmol), 4-ethynylbenzaldehyde (1.95 g, 15 mmol) and NaOH (1.2 g, 30 mmol) were placed in a mortar and ground until a yellow powder was obtained. Subsequently, the powder was transferred into a solution of ethanol (200 mL) and concentrated aqueous NH₃ solution (100 mL). The suspension was stirred at room temperature for 1 day. The formed precipitate was isolated by vacuum filtration and washed with water and ethanol. After recrystallization from ethanol, **1** was obtained as white needles (2.44 g, 7.32 mmol, 49%).

¹H NMR (400 MHz, CDCl₃, δ): 8.71 (s, 2H; H^{3',5'}), 8.66 (d, $J = 4.9$ Hz, 2H; H^{6,6''}), 8.62 (d, $J = 8.2$ Hz, 2H; H^{3,3''}), 7.90 (m, 6H, H^{4,4''}, H^{a,b}), 7.63 (m, 2H, H^{a,b}), 7.31 (d, $J = 5.4$ Hz, 2H, H^{5,5''}), 3.19 (s, 1H). Anal. calcd for C₂₃H₁₅N₃: C 82.86, H 4.54, N 12.60; found: C 82.77, H 4.59, N 12.55%.

General synthetic procedure for the Sonogashira cross-coupling reaction for the synthesis of T3 and T5 to T9

The dibromo compound (0.2 mmol) and **1** (140 mg, 0.42 mmol) were dissolved in THF (10 mL) and NEt₃ (4 mL). Subsequently, Pd(PPh₃)₄ (23 mg, 0.02 mmol) and CuI (4 mg, 0.05 mmol) were added and the solution was stirred for 24 h at 40 °C. The solvent was evaporated and the residue was dissolved in chloroform and washed with NH₄Cl (aq.) and water. The crude product was purified by passing through an AlO_x column and precipitation into methanol.

4,7-Bis(5-((4-([2,2':6',2''-terpyridin]-4'-yl)phenyl)ethynyl)thiophen-2-yl)benzo[c][1,2,5]thiadiazole (T3). According to the general synthetic procedure **T3** (135 mg, 0.14 mmol, 70%) was

obtained as an orange powder. ^1H NMR (400 MHz, CDCl_3 , δ): 8.80–8.65 (m, 12H, $\text{H}^{3',5'}$, $\text{H}^{6,6''}$, $\text{H}^{3,3''}$), 7.96 (m, 6H, $\text{H}^{4,4''}$, $\text{H}^{\text{a,b}}$), 7.70 (m, 2H, $\text{H}^{\text{a,b}}$), 7.68 (d, 2H, H^{thio}), 7.41 (m, 4H, $\text{H}^{5,5''}$), 7.36 (d, 2H, H^{thio}). Anal. calcd for $\text{C}_{60}\text{H}_{34}\text{N}_8\text{S}_3$: C 74.82, H 3.56, N 11.63; found: C 75.20, H 3.81, N 11.33%.

5,5'-Bis((4-([2,2':6',2''-terpyridin]-4'-yl)phenyl)ethynyl)-4,4'-dibutyl-2,2'-bithiazole (T5). According to the general synthetic procedure, T5 (160 mg, 0.17 mmol, 86%) was obtained as a yellow powder. ^1H NMR (400 MHz, CDCl_3 , δ): 8.81 (s, 4H, $\text{H}^{3',5'}$), 8.77 (d, $J = 4.8$ Hz, 4H, $\text{H}^{6,6''}$), 8.71 (d, $J = 8.00$ Hz, 4H, $\text{H}^{3,3''}$), 7.96 (m, 6H, $\text{H}^{4,4''}$, $\text{H}^{\text{a,b}}$), 7.69 (m, 2H, $\text{H}^{\text{a,b}}$), 7.40 (t, $J = 6.10$ Hz, 4H, $\text{H}^{5,5''}$), 2.98 (t, $J = 7.5$ Hz, 4H), 1.82 (m, 4H), 1.32 (m, 4H), 0.88 (t, $J = 6.6$ Hz, 6H). Anal. calcd for $\text{C}_{60}\text{H}_{46}\text{N}_8\text{S}_2$: C 76.40, H 4.92, N 11.88; found: C 76.73, H 5.14, N 11.67%.

5,5'-Bis(5-((4-([2,2':6',2''-terpyridin]-4'-yl)phenyl)ethynyl)-thiophen-2-yl)-4,4'-dibutyl-2,2'-bithiazole (T6). According to the general synthetic procedure, T6 (179 mg, 0.16 mmol, 81%) was obtained as a yellow powder. ^1H NMR (400 MHz, CDCl_3 , δ): 8.80 (s, 4H, $\text{H}^{3',5'}$), 8.76 (d, $J = 4.9$ Hz, 4H, $\text{H}^{6,6''}$), 8.71 (d, $J = 8.10$ Hz, 4H, $\text{H}^{3,3''}$), 7.94 (m, 6H, $\text{H}^{4,4''}$, $\text{H}^{\text{a,b}}$), 7.69 (m, 2H, $\text{H}^{\text{a,b}}$), 7.40 (t, $J = 6.10$ Hz, 4H, $\text{H}^{5,5''}$), 7.30 (d, $J = 3.90$ Hz, 2H, H^{thio}), 7.12 (d, $J = 3.90$ Hz, 2H, H^{thio}), 3.00 (t, $J = 7.5$ Hz, 4H), 1.85 (m, 4H), 1.49 (m, 4H), 1.00 (t, $J = 7.1$ Hz, 6H). Anal. calcd for $\text{C}_{68}\text{H}_{50}\text{N}_8\text{S}_4$: C 73.75, H 4.55, N 10.12; found: C 74.02, H 4.63, N 10.07%.

5,5'-Bis(5'-((4-([2,2':6',2''-terpyridin]-4'-yl)phenyl)ethynyl)-[2,2'-bithiophen]-5-yl)-4,4'-dibutyl-2,2'-bithiazole (T7). According to the general synthetic procedure, T7 (188 mg, 0.15 mmol, 74%) was obtained as an orange powder. ^1H NMR (400 MHz, CDCl_3 , δ): 8.79 (s, 4H, $\text{H}^{3',5'}$), 8.76 (d, $J = 4.9$ Hz, 4H, $\text{H}^{6,6''}$), 8.70 (d, $J = 8.10$ Hz, 4H, $\text{H}^{3,3''}$), 7.93 (m, 6H, $\text{H}^{4,4''}$, $\text{H}^{\text{a,b}}$), 7.69 (m, 2H, $\text{H}^{\text{a,b}}$), 7.62 (m, 4H, H^{thio}), 7.40 (t, $J = 6.10$ Hz, 4H, $\text{H}^{5,5''}$), 7.30 (d, $J = 3.90$ Hz, 2H, H^{thio}), 7.12 (d, $J = 3.90$ Hz, 2H, H^{thio}), 3.00 (t, $J = 7.5$ Hz, 4H), 1.85 (m, 4H), 1.49 (m, 4H), 1.00 (t, $J = 7.1$ Hz, 6H). Anal. calcd for $\text{C}_{76}\text{H}_{54}\text{N}_8\text{S}_6$: C 71.78, H 4.28, N 8.81; found: C 72.05, H 4.43, N 8.74%.

3,7-Bis(5-((4-([2,2':6',2''-terpyridin]-4'-yl)phenyl)ethynyl)-thiophen-2-yl)-10-hexadecyl-10H-phenothiazine (T8). According to the general synthetic procedure, T8 (173 mg, 0.14 mmol, 69%) was obtained as a yellow powder. ^1H NMR (400 MHz, CDCl_3 , δ): 8.75 (s, 4H, $\text{H}^{3',5'}$), 8.73 (d, $J = 4.9$ Hz, 4H, $\text{H}^{6,6''}$), 8.67 (d, $J = 8.10$ Hz, 4H, $\text{H}^{3,3''}$), 7.90 (m, 6H, $\text{H}^{4,4''}$, $\text{H}^{\text{a,b}}$), 7.65 (m, 2H, $\text{H}^{\text{a,b}}$), 7.40 (m, 6H, $\text{H}^{5,5''}$, H^{thio}), 7.27 (s, 2H), 7.24 (m, 4H), 7.30 (m, 4H), 6.89 (d, $J = 3.90$ Hz, 2H, H^{thio}), 3.81 (t, $J = 7.2$ Hz, 2H), 1.85 (m, 2H), 1.46–1.25 (m, 26H), 0.89 (t, $J = 7.1$ Hz, 3H). Anal. calcd for $\text{C}_{82}\text{H}_{71}\text{N}_7\text{S}_3$: C 78.75, H 5.72, N 7.84; found: C 79.13, H 5.92, N 7.64%.

3,7-Bis(5'-((4-([2,2':6',2''-terpyridin]-4'-yl)phenyl)ethynyl)-[2,2'-bithiophen]-5-yl)-10-hexadecyl-10H-phenothiazine (T9). According to the general synthetic procedure, T9 (181 mg, 0.13 mmol, 64%) was obtained as a yellow powder. ^1H NMR (400 MHz, CDCl_3 , δ): 8.76 (s, 4H, $\text{H}^{3',5'}$), 8.73 (d, $J = 4.9$ Hz, 4H, $\text{H}^{6,6''}$), 8.67 (d, $J = 8.10$ Hz, 4H, $\text{H}^{3,3''}$), 7.89 (m, 6H, $\text{H}^{4,4''}$, $\text{H}^{\text{a,b}}$), 7.64 (m, 2H, $\text{H}^{\text{a,b}}$), 7.40 (m, 8H, $\text{H}^{5,5''}$, H^{thio}), 7.27 (s, 2H), 7.24 (m, 6H), 7.30 (m, 4H), 6.89 (d, $J = 3.90$ Hz, 2H, H^{thio}), 3.81 (t, $J = 7.2$ Hz, 2H), 1.85 (m, 2H), 1.46–1.25 (m, 26H), 0.89 (t, $J = 7.1$ Hz, 3H). Anal. calcd for $\text{C}_{90}\text{H}_{75}\text{N}_7\text{S}_5$: C 76.40, H 5.34, N 6.93; found: C 76.67, H 5.60, N 7.04%.

General synthetic procedure for the synthesis of P3 and P5 to P9

To the bisterpyridine monomers T3 and T5 to T9 (0.1 mmol) in *N*-methylpyrrolidone (NMP, 5 mL), zinc(II) acetate (22 mg, 0.1 mmol) in NMP (2 mL) was added. The resulting solution was stirred at 100 °C for 12 h. Subsequently, NH_4PF_6 (163 mg, 1 mmol) was added and after 1 h the solution was poured into diethyl ether (50 mL), and the resulting metallopolymer was collected by filtration and washed with diethyl ether (20 mL), methanol (20 mL) and toluene (5 mL).

{[Zn(T3)](PF₆)₂]_n (P3). According to the general synthetic procedure, P3 (82 mg, 0.07 mmol, 72%) was obtained as a red powder. ^1H NMR (400 MHz, DMSO-d_6 , δ): 9.46 (m, $\text{H}^{3',5'}$), 9.18 (m, $\text{H}^{3,3''}$), 8.78 (m, H^{aryl}), 8.571 (m, H^{aryl}), 8.30 (m, $\text{H}^{4,4''}$), 8.10–7.90 (m), 7.71 (m, $\text{H}^{5,5''}$), 7.52 (m, H^{aryl}). Anal. calcd for $\text{C}_{64}\text{H}_{40}\text{N}_8\text{O}_4\text{S}_5\text{Zn}$: C 67.04, H 3.52, N 9.77; found: C 67.62, H 3.71, N 9.54%.

{[Zn(T5)](PF₆)₂]_n (P5). According to the general synthetic procedure, P5 (86 mg, 0.08 mmol, 75%) was obtained as a yellow powder. ^1H NMR (400 MHz, DMSO-d_6 , δ): 9.44 (m, $\text{H}^{3',5'}$), 9.19 (m, $\text{H}^{3,3''}$), 8.78–8.22 (m), 7.97 (m), 7.51 (m, H^{aryl}), 1.39 (m), 0.83 (m). Anal. calcd for $\text{C}_{64}\text{H}_{52}\text{N}_8\text{O}_4\text{S}_4\text{Zn}$: C 68.23, H 4.65, N 9.95; found: C 68.70, H 4.92, N 9.61%.

{[Zn(T6)](PF₆)₂]_n (P6). According to the general synthetic procedure, P6 (104 mg, 0.08 mmol, 81%) was obtained as an orange powder. ^1H NMR (400 MHz, DMSO-d_6 , δ): 9.44 (m, $\text{H}^{3',5'}$), 9.16 (m, $\text{H}^{3,3''}$), 8.75–8.19 (m), 7.97 (m), 7.59 (m, H^{aryl}), 7.50 (m, H^{aryl}), 1.39 (m), 0.83 (m). Anal. calcd for $\text{C}_{72}\text{H}_{56}\text{N}_8\text{O}_4\text{S}_4\text{Zn}$: C 66.99, H 4.37, N 8.68; found: C 67.31, H 4.72, N 8.60%.

{[Zn(T7)](PF₆)₂]_n (P7). According to the general synthetic procedure, P7 (90 mg, 0.06 mmol, 62%) was obtained as a yellow powder. ^1H NMR (400 MHz, DMSO-d_6 , δ): 9.45 (m, $\text{H}^{3',5'}$), 9.18 (m, $\text{H}^{3,3''}$), 8.70–8.12 (m), 7.89–7.61 (m), 7.59 (m, H^{aryl}), 7.48 (m, H^{aryl}), 1.41 (m), 0.89 (m). Anal. calcd for $\text{C}_{80}\text{H}_{60}\text{N}_8\text{O}_4\text{S}_6\text{Zn}$: C 66.03, H 4.16, N 7.70; found: C 66.62, H 4.52, N 7.56%.

{[Zn(T8)](PF₆)₂]_n (P8). According to the general synthetic procedure, P8 (113 mg, 0.08 mmol, 79%) was obtained as an orange powder. ^1H NMR (400 MHz, DMSO-d_6 , δ): 9.44 (m, $\text{H}^{3',5'}$), 9.17 (m, $\text{H}^{3,3''}$), 8.83–8.63 (m), 8.55 (m), 8.30 (m), 7.96 (m), 7.52 (m), 7.09 (m), 1.41 (m), 0.83 (m). Anal. calcd for $\text{C}_{86}\text{H}_{77}\text{N}_7\text{O}_4\text{S}_3\text{Zn}$: C 72.02, H 5.41, N 6.84; found: C 72.53, H 5.62, N 6.59%.

{[Zn(T9)](PF₆)₂]_n (P9). According to the general synthetic procedure, P9 (113 mg, 0.07 mmol, 71%) was obtained as an orange powder. ^1H NMR (400 MHz, DMSO-d_6 , δ): 9.46 (m, $\text{H}^{3',5'}$), 9.16 (m, $\text{H}^{3,3''}$), 8.84–8.61 (m), 8.58 (m), 8.35 (m), 7.96–7.62 (m), 7.50 (m), 7.05 (m), 1.39 (m), 0.88 (m). Anal. calcd for $\text{C}_{94}\text{H}_{81}\text{N}_7\text{O}_4\text{S}_5\text{Zn}$: C 70.63, H 5.11, N 6.13; found: C 71.07, H 5.48, N 5.87%.

Results and discussion

Synthesis and characterization of monomers and homopolymers

The π -conjugated bisterpyridines T2–T11 were synthesized applying the well-known Sonogashira-coupling of an

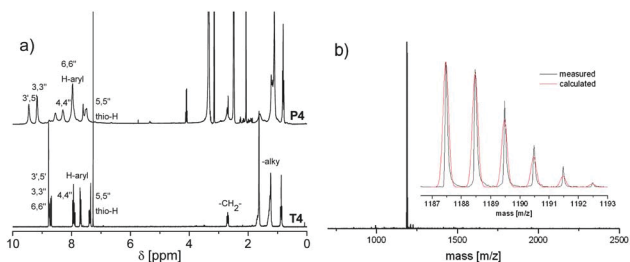


Fig. 1 (a) ^1H NMR spectrum of **T4** (CDCl_3 , 300 MHz) and **P4** (DMSO-d_6 , 300 MHz); (b) MALDI-TOF MS spectrum of **T4** (matrix: dithranol).

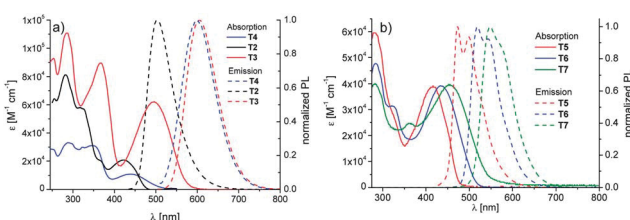


Fig. 2 Absorption and emission spectra of (a) **T2–T4**; (b) **T5–T7** (CHCl_3 , 10^{-6} M).

ethynyl-functionalized terpyridine (**1**) with the bromine-functionalized spacer units **2–11** (Scheme 1).^{19,22} The bisterpyridines **T3**, **T4** and **T6–T10** feature a comparable chromophore structure, consisting of a central dye unit surrounded by thiophene-donor moieties. The systems **T2**, **T5** and **T11** where the central chromophore is a pure acceptor were synthesized for comparison purposes.²⁸

The chemical structure of all synthesized bisterpyridines was confirmed by ^1H NMR, MALDI-TOF MS and elemental analysis (EA). The substances **T3–T11** showed good solubility in common organic solvents like dichloromethane or toluene. The absence of any alkyl chains in **T2**, however, resulted in π -stacking and consequently poor solubility of this substance. Fig. 1 shows a typical ^1H NMR spectrum and MALDI-TOF MS spectrum of bisterpyridine **T4** and the ^1H NMR spectrum of the corresponding Zn^{II} coordination polymer (**P4**).

The molar mass of the resulting polymers could not be determined by standard methods because both size exclusion chromatography (SEC) and MALDI-TOF mass spectrometry

were not applicable to the characterization of Zn^{II} -based metallopolymers. In both techniques, the labile Zn^{II} -terpyridine bond is not stable under the measurement conditions, and, consequently, only the monomers can be detected. A first hint for the polymeric nature of the material was given by the broadening of the ^1H NMR signals (Fig. 1a). Moreover, the typical downfield shift of the (3,3')- and (3',5')- as well as the highfield shift of the (6,6')-terpyridine signals was observed upon coordination to the Zn^{II} ions. The absence of any end group signal indicates a high conversion and, consequently, the molar masses were estimated from NMR to be at least $20\,000\text{ g mol}^{-1}$.

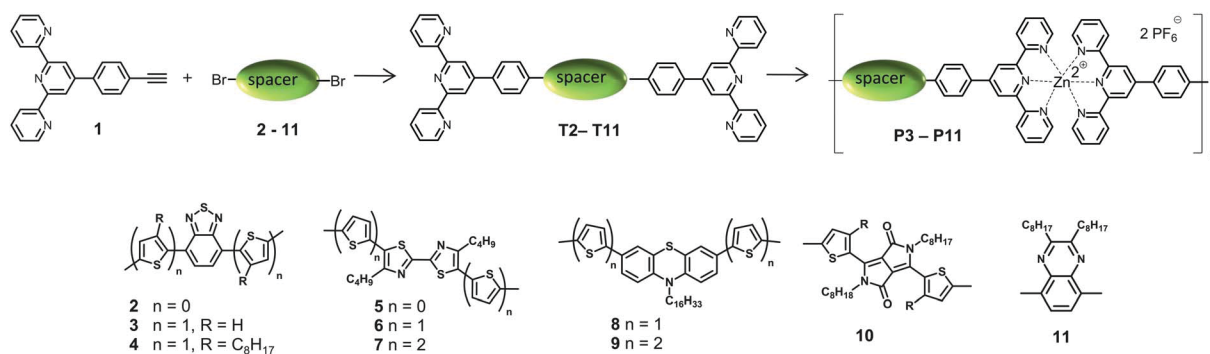
Referring to the binding constant of the bisterpyridine Zn^{II} complex ($\beta > 10^8$), the real molar mass is probably much higher.¹¹ The relative composition of the final polymers was additionally proven by elemental analysis. The obtained values are close to a stoichiometric 1 : 1 ratio of the Zn^{II} ions and bisterpyridine ligands and support thereby the polymeric nature of the materials.

The metallopolymers were realized in *N*-methylpyrrolidone (NMP) solution at $100\text{ }^\circ\text{C}$ for 12 h using an equimolar amount of $\text{Zn}(\text{OAc})_2$, followed by anion exchange with ammonium hexafluorophosphate. After precipitation into diethyl ether, the crude polymer was washed with methanol and toluene, to remove the possibly remaining salt or monomer. Subsequently, the polymers were isolated in 62 to 81% yield.

Photophysical properties

The photophysical investigation of the synthesized bisterpyridines and the corresponding metallopolymers was performed in chloroform or DMF solution and the obtained data are summarized in Table 1.

Apparently, the π -extended systems **T3**, **T4**, **T6**, **T7** and **T9** exhibit a bathochromic shift corresponding to a lowered energy band gap in comparison to their analogues with smaller π -conjugated units **T2**, **T5** and **T8**. A comparison of **T2**, **T3** and **T4** reveals that the influence of the π extension is partially compensated by a steric hindrance of the alkyl chains. The introduction of octyl chains in the 3-position of the thiophene induces a sterical repulsion and, consequently, a torsion of the conjugated system out of plane, resulting in a higher band gap ($E_g = 2.39$) (**T4**, Table 1, Fig. 2a).^{29,37,38} Owing to the pronounced



Scheme 1 Schematic representation of the synthesis of the bisterpyridines **T2** to **T11**.

Table 1 Selected photophysical properties of bisterpyridines **T2** to **T11** (CHCl_3 , 10^{-6} M) and the corresponding Zn^{II} coordination polymers **P2** to **P11** (DMF, 5×10^{-6} M)

Code	λ_{abs} [nm]	ϵ [$\text{M}^{-1} \text{cm}^{-1}$]	E_g^a [eV]	λ_{PL}^b [nm]
T2	423	20 700	2.62	503
T3	496	62 300	2.17	606
T4	441	45 500	2.39	598
T5	416	112 500	2.64	475
T6	435	131 700	2.44	525
T7	452	106 700	2.24	554
T8	407	59 000	2.58	533
T9	420	82 400	2.52	549
T10	619	67 900	1.90	643
T11	395	30 100	2.83	443
P2	415	25 700	2.59	513
P3	483	32 600	2.18	614
P4	426	35 900	2.36	605
P5	416	38 700	2.62	476
P6	433	39 100	2.43	525
P7	449	65 200	2.26	561
P8	409	46 700	2.53	480
P9	421	62 800	2.48	518
P10	586	22 400	1.60	641
P11	392	69 000	2.78	443

^a Calculated from 0.1 λ_{abs} . ^b Excited at λ_{abs} .

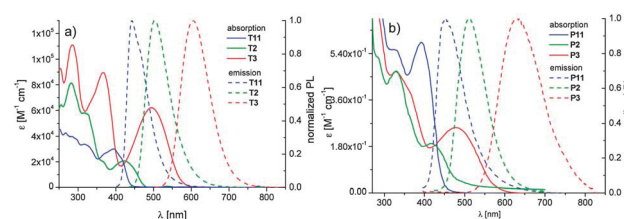


Fig. 3 Absorption and normalized emission spectra of (a) **T2**, **T3** and **T11** (CHCl_3 , $\lambda_{\text{ex}} = 365$ nm, 10^{-6} M); (b) **P2**, **P3** and **P11** (DMF, $\lambda_{\text{ex}} = 365$ nm, 5×10^{-6} M).

quinoid character and consequent planarization of the conjugated system in the excited state, the emission maxima are only slightly influenced by the attached substituents, which disturb the coplanarity of the π -conjugated segment (Fig. 2a).

In contrast to this, the bithiazole derivatives bear a short alkyl chain in the central chromophore (**T5**). The attachment of additional thiophene rings (**T6** and **T7**) results in an increased conjugation length and therefore bathochromically shifted absorption and emission maxima (Fig. 2b).

Upon polymerization, the polarity of the materials increases significantly. The photophysical investigation of the metal-polymers was, for that reason, performed in DMF solution. Depending on the electronic nature of the spacer unit, the absorption maximum shifted upon polymerization. When electron-rich spacer units were used, the π - π^* transition shows a bathochromic shift of about 400 to 1000 cm^{-1} .^{19,28,39} In this case, the HOMO is prevalently located in the electron-rich chromophore and the LUMO at the terpyridine. Upon complexation, the LUMO is stabilized, resulting in a bathochromic shift. In contrast, when electron-poor bisterpyridines (e.g., **T2**) were polymerized, no or a small hypsochromic shift of

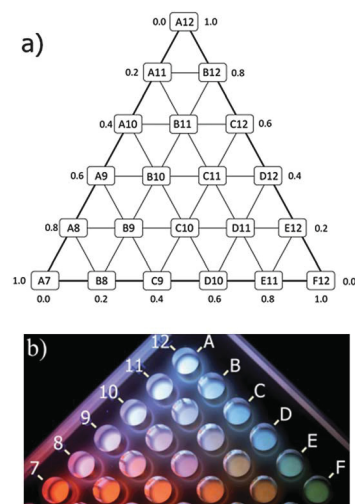


Fig. 4 (a) Mixing triangle I of polymers **P2**, **P3** and **P11** with the corresponding well positions; (b) picture of the corresponding solutions in a quartz microtiter plate ($\lambda_{\text{ex}} = 365$ nm).

the absorption maximum occurs. In this case, the LUMO is predominantly located in the central chromophore, and is thereby not influenced that much.

Synthesis and characterization of copolymers

One of the innovative features of the kinetically labile Zn^{II} bisterpyridine polymers ($t_{1/2} < 0.1$ min)¹¹ is the modular approach to synthesize statistical copolymers. Different monomers with various emission colors can easily be combined within one

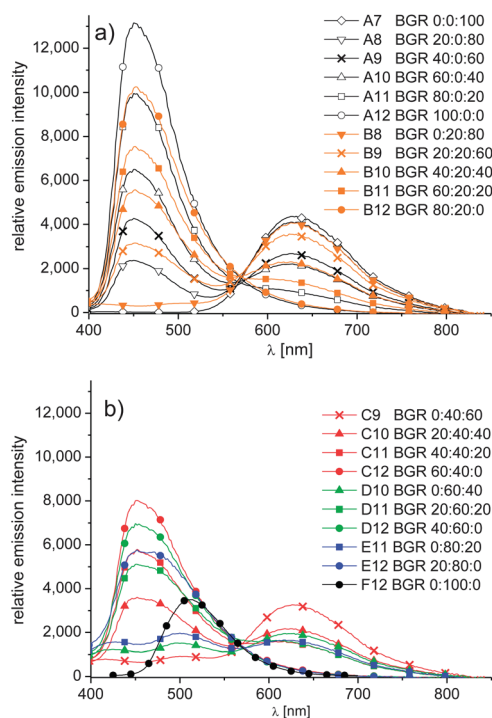


Fig. 5 Emission spectra of the mixtures (a) A7–A12 and B8–B12; (b) C9–C12, D10–D12, E11–E12 and F12 (DMF, $c = 5 \times 10^{-6}$ M, $\lambda_{\text{ex}} = 365$ nm).

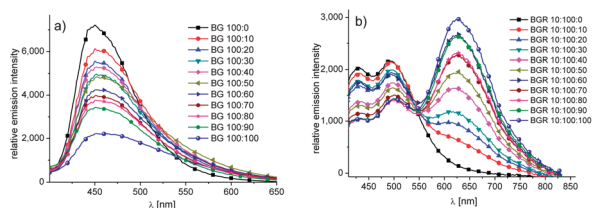


Fig. 6 Emission spectra of (a) **P11** upon addition of **P2** and (b) **P11** and **P2** (10 : 100) upon addition of **P3** (DMF, $c = 5 \times 10^{-6}$ M, $\lambda_{\text{ex}} = 365$ nm).

coordination polymer in every desired ratio. The relevance of the Zn^{II} metal to mediate potential energy transfer processes in the resulting copolymers has already been proven.²⁸ Out of the described monomers, we chose the red-emitting **T3** ($\lambda_{\text{PL}} = 606$ nm) and the green-emitting **T2** ($\lambda_{\text{PL}} = 503$ nm), both based on the 2,1,3-benzothiadiazole system. Additionally, the blue-emitting quinoxaline-containing bisterpyridine **T11** ($\lambda_{\text{PL}} = 424$ nm) was utilized.²⁸

Fig. 3a depicts the absorption and emission spectra of **T2**, **T3** and **T11** in chloroform solution. The corresponding Zn^{II} coordination polymers show blue ($\lambda_{\text{PL}} = 443$ nm, **P11**), green ($\lambda_{\text{PL}} = 513$ nm, **P2**) and red ($\lambda_{\text{PL}} = 614$ nm **P3**) emission (Fig. 3b).

Initially, the emission colors ($\lambda_{\text{ex}} = 365$ nm) of copolymers of these three polymers were screened in a systematical manner in solution (Fig. 4a). To enable a fast and efficient workflow, mixtures of the polymers (150 μL , $c = 5 \times 10^{-6}$ M) were prepared in a quartz microtiter plate (Fig. 4b). The corners of this triangle represent the pure polymers **P2** (G, F12), **P3** (R, A7) and **P11** (B, A12), whereas the edges are mixtures of two polymers. The six wells in the middle are composed of all three polymers. The polymer ratio was varied in 20% steps (Fig. 4a).

Fig. 4b shows a picture of the polymer solutions, excited at $\lambda_{\text{ex}} = 365$ nm. Along the rows of the microtiter plate (constant letters) and columns (constant numbers) one component stays the same and only the ratio of the other two changes. This fact is reflected in the isosbestic points in the absorption (Fig. S1, ESI†) and emission spectra (Fig. 5).

Even though all three polymers were used with the same concentrations and the quantum yields are comparable (**P2** $\Phi = 0.38$; **P3** $\Phi = 0.36$; **P11** $\Phi = 0.56$), the emission of **P3** ($\lambda_{\text{PL}} \sim 620$ nm) and **P11** ($\lambda_{\text{PL}} \sim 450$ nm) is clearly dominating most emission spectra. Only the wells with a large excess of **P2** (E11, D10) display a balanced emission over the whole visible spectrum (Fig. 5b). To verify the occurrence of energy transfer processes, fluorescence titration spectra were recorded (Fig. 6).

Initially, the energy transfer from **P11** to **P2** was investigated. The titration revealed that even in a 1 : 1 mixture, the blue **P11** emission is clearly dominating, even though it is partially quenched by the addition of **P2**. Apparently, most transferred energy is released by non-radiative decay. Since the emission intensity of **P2** is enhanced in the presence of **P11**, and for the final white-emitting polymer a blue component is required, the second titration was performed with a 10 : 100 mixture of **P11** : **P2** and **P3** was added in 0.1 equivalent steps (Fig. 6b). Already after addition of 0.2 equivalents of **P3**, the short-wavelength emission intensity decreases, indicating energy transfer.

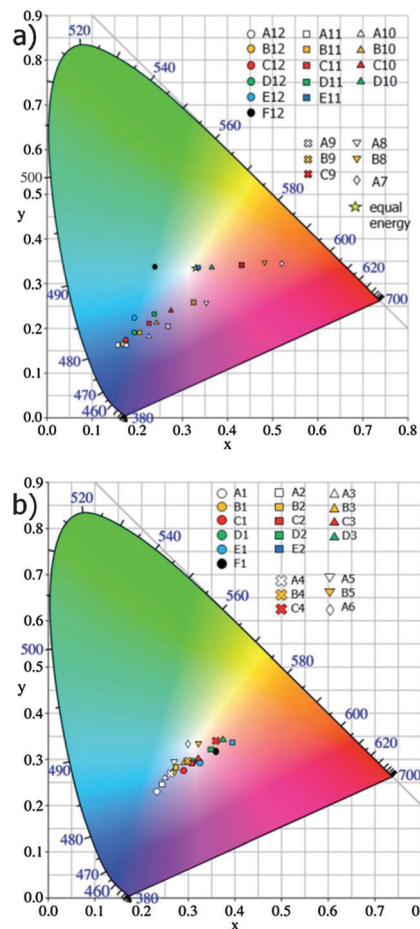


Fig. 7 Position of the PL obtained from wells (a) A7–A12, B8–B12, C9–C12, D10–D12, E11–E12 and F12 and (b) A1–A6, B1–B5, C1–C4, D1–D3, E1–E2 and F1 (DMF, $c = 5 \times 10^{-6}$ M, $\lambda_{\text{ex}} = 365$ nm) in the CIE color space.

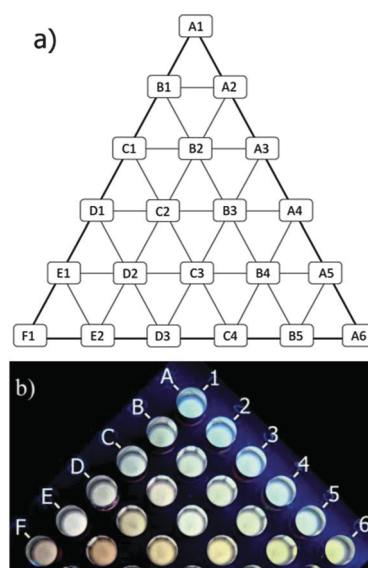


Fig. 8 (a) Mixing triangle II of polymers **P2**, **P3** and **P11** with the corresponding well positions. (b) Picture of the corresponding solutions in a quartz microtiter plate ($\lambda_{\text{ex}} = 365$ nm).

Table 2 CIE coordinates and absolute quantum yields obtained from wells A7–A12, B8–B12, C9–C12, D10–D12, E11–E12 and F12 (left) and A1–A6, B1–B5, C1–C4, D1–D3, E1–E2 and F1 (right) (DMF, $c = 5 \times 10^{-6}$ M, $\lambda_{\text{ex}} = 365$ nm)

Well	Composition P11/P2/P3	CIE coordinates (x, y)	Φ_{PL}	Well	Composition P11/P2/P3	CIE coordinates (x, y)	Φ_{PL}
A7	0/0/100	0.518, 0.343	0.36	A1	25/65/10	0.235, 0.235	0.32
A8	20/0/80	0.353, 0.253	0.38	A2	20/70/10	0.245, 0.245	0.32
A9	40/0/60	0.266, 0.204	0.40	A3	15/75/10	0.250, 0.257	0.30
A10	60/0/40	0.223, 0.182	0.46	A4	10/80/10	0.262, 0.266	0.29
A11	80/0/20	0.180, 0.157	0.51	A5	5/85/10	0.269, 0.285	0.29
A12	100/0/0	0.152, 0.158	0.56	A6	0/90/10	0.302, 0.331	0.26
B8	0/20/80	0.482, 0.348	0.35	B1	20/65/15	0.272, 0.267	0.32
B9	20/20/60	0.325, 0.257	0.37	B2	15/70/15	0.278, 0.273	0.29
B10	40/20/40	0.244, 0.211	0.40	B3	10/75/15	0.288, 0.289	0.29
B11	60/20/20	0.203, 0.185	0.46	B4	5/80/15	0.293, 0.297	0.26
B12	80/20/0	0.167, 0.161	0.50	B5	0/85/15	0.322, 0.335	0.25
C9	0/40/60	0.438, 0.342	0.32	C1	15/65/20	0.285, 0.269	0.28
C10	20/40/40	0.275, 0.241	0.36	C2	10/70/20	0.317, 0.291	0.28
C11	40/40/20	0.225, 0.213	0.41	C3	5/75/20	0.323, 0.301	0.26
C12	60/40/0	0.172, 0.175	0.47	C4	0/80/20	0.357, 0.343	0.27
D10	0/60/40	0.361, 0.334	0.27	D1	10/65/25	0.318, 0.294	0.27
D11	20/60/20	0.237, 0.230	0.39	D2	5/70/25	0.349, 0.320	0.30
D12	40/60/0	0.192, 0.191	0.40	D3	0/75/25	0.374, 0.346	0.28
E11	0/80/20	0.337, 0.333	0.29	E1	5/65/30	0.325, 0.294	0.29
E12	20/80/0	0.192, 0.225	0.39	E2	0/70/30	0.392, 0.336	0.28
F12	0/100/0	0.239, 0.330	0.38	F1	0/65/35	0.357, 0.313	0.26

The final 10 : 100 : 100 mixture of **P11** : **P2** : **P3** reveals a dominating red emission (**P3**). To overcome the subjective color perception, also a comparable value, the CIE coordinates of all metalpolymers were measured with an Ulbricht globe. Table 2 (left part) summarizes the obtained data and Fig. 7a shows the position of the PL emission in the CIE color space.

As expected from the emission spectra, most of the tested wells display emission in the blue region (Fig. 7a). Only E11 shows emission next to the equal energy point (marked with a star) where the coordinates are $x = y = 0.33$. Since the human eye is more sensitive to red and green than to blue light, the small shift of E11 into the red region makes this emission already appearing orange. To gain a deeper insight into the emission characteristics, mixing triangle II with a higher share of **P2** was prepared (Fig. 8a).

The corners of this second triangle represent 25 : 65 : 10 (A1), 0 : 90 : 10 (A6) and 0 : 65 : 35 (F1) mixtures of the polymers **P11** : **P3** : **P2** (Table 2, right). The absorption spectra are depicted in Fig. S2 (ESI[†]) and the emission spectra are shown in Fig. 9. Fig. 8 depicts the mixing scheme and an image of the solutions excited at 365 nm.

With increasing well number, the ratio of **P11** decreases, whereas that of **P2** increases. In alphabetical order, the ratio of **P11** to **P3** is reduced. These changes of the composition are reflected by the emission spectra (Fig. 9). As shown already in the titration spectra (Fig. 6), even though there is a larger share of **P2** in the copolymers of A1–A3, B1 and C1, the blue emission of **P11** is dominant. In contrast, the emission of rows D, E and F is dominated by the red emission of **P3**. All the other wells show balanced emission spectra and thereby white emission (Fig. 8b). This color perception is also reflected by the coordinates of the CIE color spectrum (Fig. 7b). In contrast to Fig. 7a, most of the spots are located in the center of the spectrum, representing

white emission color. Moreover, all data points with the same letters follow a line in the CIE spectrum. This feature reveals the reliability of these measurements and enables thereby a tailoring of the emission color.

Inkjet printing of the coordination polymers

To enable, besides a fast and efficient tailoring of the PL in solution, also a systematic and material-saving screening of the emission properties in thin films, the polymers were inkjet-printed according to mixing triangle I and the optical properties of these films were investigated. In order to avoid the preparation of 21 different inks, the single colors were printed separately on top of each other. This printing procedure represents a material-efficient as well as variable approach.⁴⁰ The assembly of statistical copolymers and thereby a homogeneous film formation was ensured by printing a solvent layer after the last layer. The kinetic lability of the Zn^{II} bisterpyridine complex ($t_{1/2} < 0.1$ min) in the solution state allows thereby the reorganization and formation of statistical copolymers within the printed films. We recently showed the printability of similar bisterpyridine coordination polymers.³¹ The combinatorial, two-dimensional variation of multiple parameters revealed a solvent DMF/acetophenone (9/1) mixture at a concentration of 5 mg mL⁻¹ and a substrate temperature of 50 °C to be suitable to print bisterpyridine Zn^{II} coordination polymers.³¹ Using these parameters, homogeneous films of the pure blue (A12), green (F12) and red (A7) polymers could be printed (Fig. S3, ESI[†]).

The amount of deposited material in the inkjet printing process can easily be varied by the dot spacing which is the center-to-center spacing between two adjacent droplets. The films of pure polymers were printed with a dot spacing of 90 μm ,

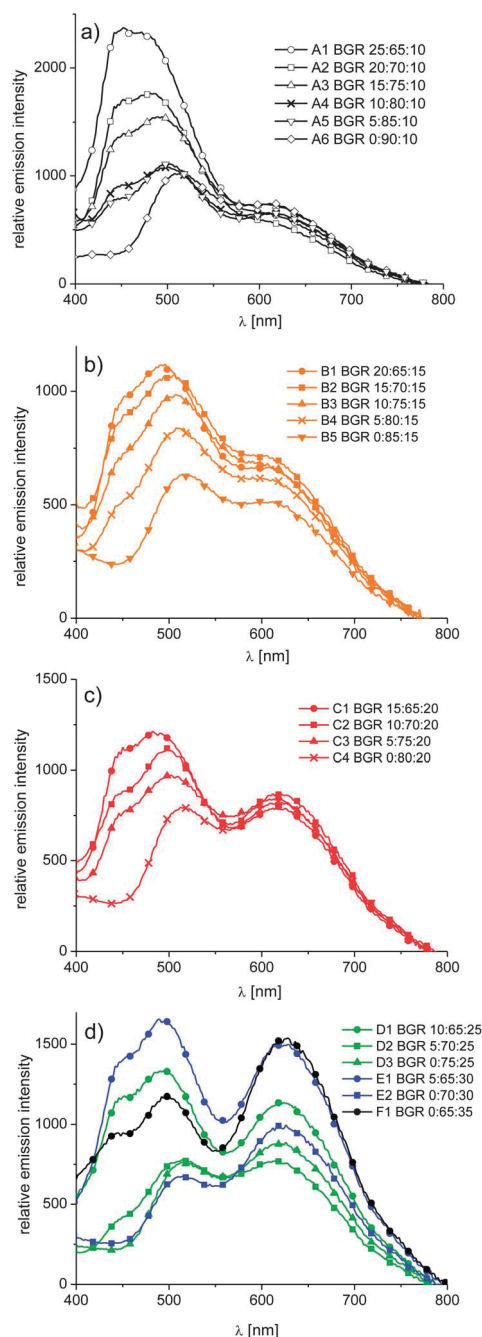


Fig. 9 Emission spectra of the wells (a) A1–A6; (b) B1–B5; (c) C1–C4; (d) D1–D3, E1–E2 and F1 (DMF, $c = 5 \times 10^{-6}$ M, $\lambda_{\text{ex}} = 365$ nm).

resulting in film thicknesses of approximately 300 nm. All other ratios could be realized by adjusting the dot spacing accordingly. To enable an efficient process, the printing sequence was

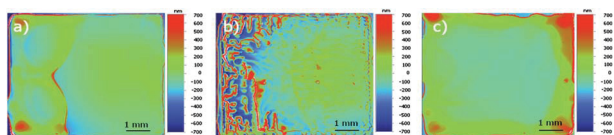


Fig. 10 Optical profiler images after printing of (a) P11 (dot spacing 100 μm); P3 (dot spacing 200 μm) and (c) solvent (dot spacing 90 μm).

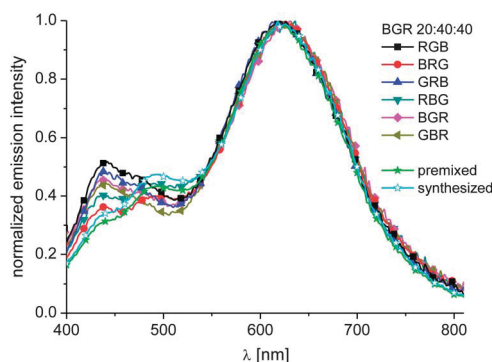


Fig. 11 Emission spectra of the film C10 printed in different order in comparison to the premixed polymer (film, $\lambda_{\text{ex}} = 365$ nm).

maintained, starting from blue followed by green, red, and a subsequent layer of pure solvent. Fig. 10 depicts typical optical profiler images of the workflow for the printing of A11. After printing the bottom layer (blue, dot spacing 100 μm), the red layer was printed with a dot spacing of 200 μm . Due to this high spacing between two droplets, the achieved film quality is very low (Fig. 10b). However, after a final layer of pure solvent (dot spacing 90 μm), a homogeneous film was obtained (Fig. 10c).

To prove, besides the optical quality of the films, also the formation of homogeneous copolymers, the film C10 (BGR 20 : 40 : 40) was prepared applying different printing order. The emission spectra of these films were compared with metallo-copolymer ones of the same composition, which were prepared beforehand and printed at once (Fig. 11). For that reason, both the inks of the homopolymers P11, P2 and P3 (20 : 40 : 40) were mixed in a closed vial (green line, Fig. 11) and a copolymer with the respective monomer ratio was prepared analogous to the homopolymers and printed (cyan line, Fig. 11).

The emission spectra are only slightly influenced by the printing order and also the films of the premixed homo- and the copolymer display similar emission behavior (Fig. 11). Thereby, the concept of metallo-copolymerization by inkjet printing could be proven.

For comparison, films of different compositions were printed without the additional solvent layer. Fig. S4 (ESI[†]) depicts the optical profiler images and Fig. S5 (ESI[†]) depicts their emission spectra. The emission wavelength of the polymer with the highest share in these inhomogeneous films is always overrepresented in comparison to the homogeneous ones (Fig. S5, ESI[†]). Taking the poor morphology of these films into account, this behavior is reasonable. The deposited material with the lowest ratio is, in most cases, not smoothly distributed over the whole film (Fig. S4, ESI[†]). Therefore, its emission wavelength is underrepresented in the emission spectrum (Fig. 5, ESI[†]). After printing a solvent layer, the metallo-copolymers are formed and the emission spectra are comprehensible (Fig. S4 and S5, ESI[†]).

After proving the applicability of this concept, copolymer films in analogy to mixing triangle I were printed (Fig. 12).

Fig. 12a displays a picture of the printed films excited at $\lambda_{\text{ex}} = 365$ nm. As visible also in the emission spectra (Fig. 13) the PL

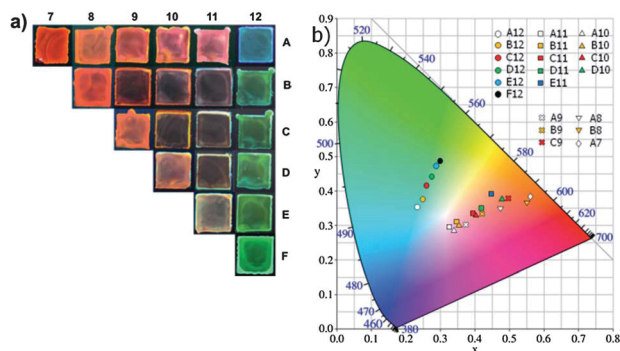


Fig. 12 (a) Picture of the inkjet-printed films (6×6 mm each, $\lambda_{\text{ex}} = 365$ nm) and (b) position of the PL in the CIE color space.

color differs clearly from the respective solutions (Fig. 4b and 5). However, the coordinates in each column of the mixing triangle follow a line, enabling the estimation of the color of unknown mixtures (Table S1, ESI†).

As expected, the PL maxima of all three homopolymers are bathochromically shifted upon printing, due to strong π - π interaction. In particular, blue emitting polymer **P11** reveals a shift of 2200 cm^{-1} comparing the solution and thin-film spectra. The high local concentrations in the inkjet-printed copolymer films enable moreover efficient energy transfer processes (Fig. 13). Fig. 13a depicts the emission spectra of A12–F12. In contrast to the solution spectra (Fig. 5), the green emission of **P2** is dominant already at a **P11** : **P2** (B : G) ratio of 4 : 1 (B12). This could also be confirmed by the color impression given in Fig. 12a as well as the CIE coordinates depicted in Fig. 12b. Further increase of the share of **P2** leads to a continuous decrease of the shoulder at $\lambda_{\text{PL}} \sim 450$ nm and, thereby, to a pure green color (Fig. 12).

Energy transfer processes, in general, require a reasonable spectral overlap of the PL of the donor with the absorption of the acceptor. The absorption spectra of the films are given in Fig. S6†. The emission maxima of **P2** and **P11** at $\lambda_{\text{PL}} \sim 500$ nm match well the absorption maximum of **P3** ($\lambda_{\text{abs}} \sim 500$ nm) (Fig. 13, Fig. S6†). For that reason, the emission colors of all copolymers containing **P3** appear red (Fig. 12). This effect is clearly apparent in the emission spectra of the binary copolymers of **P11** and **P3** (Fig. 13b) as well as **P2** and **P3** (Fig. 13c). Both the blue (**P11**) and green (**P2**) emission are quenched and the energy partially transferred to the excited state of **P3** (red). To prove the origin of the emission, excitation spectra were recorded. Fig. 14a shows a comparison of the excitation spectra of the pure polymer films (A7, A12, F12) with the respective absorption spectra. As expected for pure substances without any energy transfer processes, they match (Fig. 14a).

The origin of the red emission of the binary copolymers of **P11** and **P3** was investigated by measuring excitation spectra at $\lambda_{\text{PL}} = 650$ nm (Fig. 14b). The blue emitting polymer **P11** (A12) displays only very weak emission at $\lambda_{\text{PL}} = 650$ nm. Therefore, the intensity of the excitation response with a maximum at around $\lambda = 410$ nm is weak compared to the signal of the red emitting polymer **P3** (A7) (Fig. 14b). The spectra of the binary

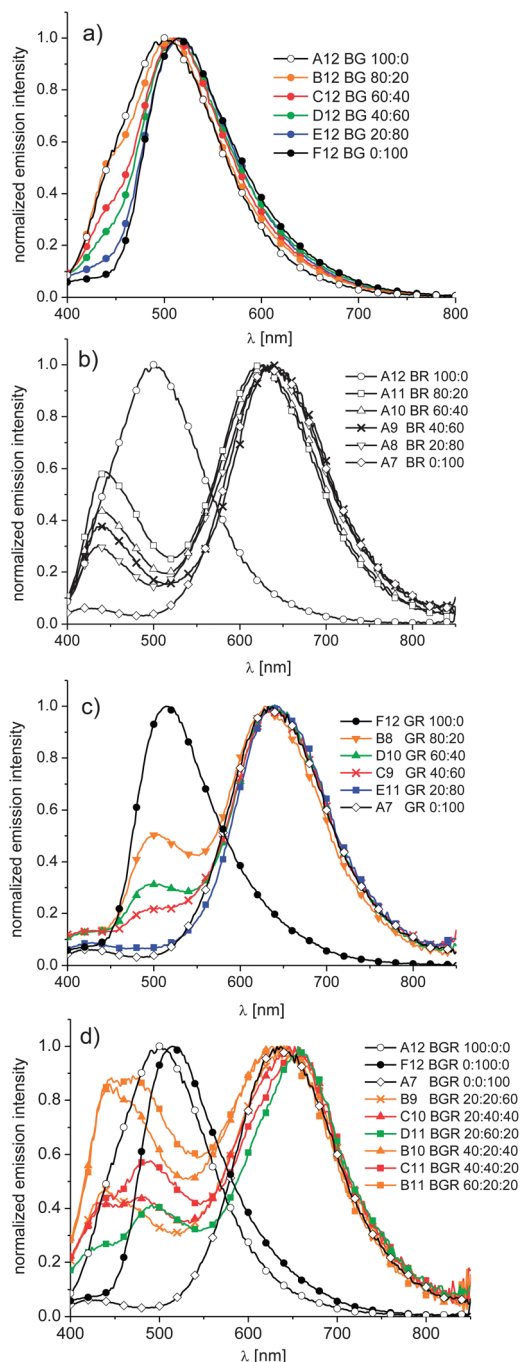


Fig. 13 Emission spectra of A7–A12, B8–B12, C9–C12, D10–D12, E11–E12, and F12 (film, $\lambda_{\text{ex}} = 365$ nm).

mixtures (A8–A11) distinctly prove the energy transfer from **P11** to **P3** by the intense signal at $\lambda = 410$ nm (Fig. 14b).

Since the absorption maximum of green emitting polymer **P2** ($\lambda_{\text{abs}} \sim 450$ nm) correlates with a local minimum of the absorption of **P3** (Fig. S6†), the energy transfer is not that obvious as in the case of **P11** (Fig. 14b). However, the excitation spectra of the binary mixtures of **P2** and **P3** display a distinct share of **P2** at the emission at $\lambda_{\text{PL}} = 650$ nm (Fig. S7, ESI†).

Finally, the possibility to assemble a white emitting film was proven. According to the CIE graph depicted in Fig. 12b, the

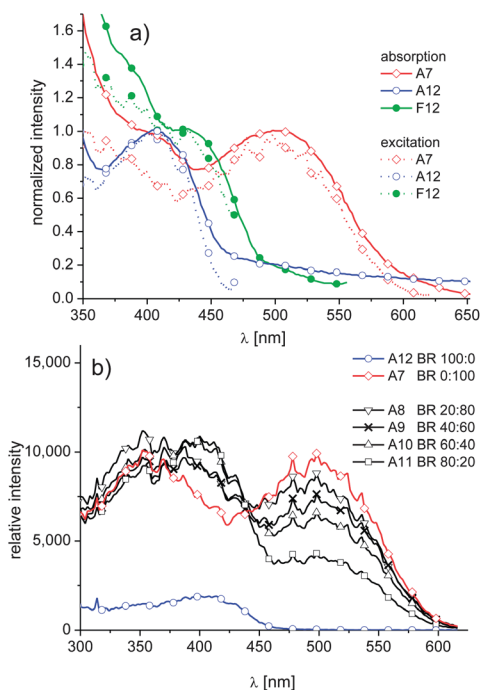


Fig. 14 Excitation spectra of (a) A7, A12 and F12 (film, $\lambda_{\text{ex}} = \lambda_{\text{PL}}$); (b) A7–A12 (film, $\lambda_{\text{ex}} = 650$ nm).

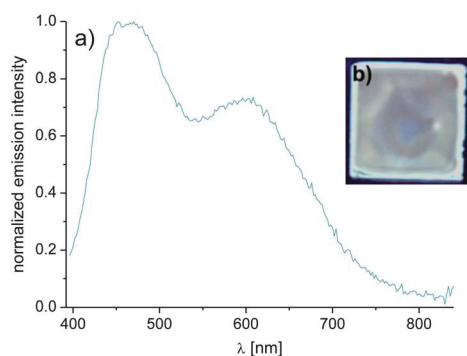


Fig. 15 (a) Emission spectrum of an inkjet-printed film with a ratio of **P11** : **P2** : **P3** of 80 : 10 : 10 (film, $\lambda_{\text{ex}} = 365$ nm) and (b) picture of the respective inkjet-printed film ($\lambda_{\text{ex}} = 365$ nm).

aimed white color is located between films A12 (100 : 0 : 0) and B11 (60 : 20 : 20). Therefore, the new film was printed using a polymer ratio of 80 : 10 : 10. The respective emission spectrum ($\lambda_{\text{ex}} = 365$ nm) shows a broad emission over the visible region with a maximum in the blue ($\lambda_{\text{PL}} = 452$ nm) and the orange/red ($\lambda_{\text{PL}} = 608$ nm) region (Fig. 15). The resulting CIE coordinates of $x = 0.311$ and $y = 0.307$ confirm the white color perception.

Conclusions

The variation of the central chromophore in bisterpyridine Zn^{II} coordination polymers allowed the assembly of materials exhibiting optical band gaps from 2.78 to 1.60 eV and emission colors from $\lambda_{\text{PL}} = 443$ –641 nm in solution. The dynamic nature

of the Zn^{II} complex enabled the systematic assembly of a library of statistical copolymers in an efficient way by simply mixing the respective homopolymer solutions. Using a blue- (**P11**), a green- (**P2**) and a red-emitting polymer (**P3**) a great number of emission colors, including white, can be generated by selecting respective mixtures. To screen the thin-film photophysical properties in a reproducible and material-saving manner, inkjet printing was used. This technique enables, in combination with the dynamic nature of the Zn^{II} bisterpyridine polymers, the separate printing of every single color and the assembly of statistical copolymers by subsequent printing of one solvent layer. As in solution the photophysical data were obtained by automated measurements of 21 samples in a row, enabling an efficient screening. The obtained data allowed the estimation of the CIE coordinates of the emission color for most ratios of the three polymers used, thereby producing tailor-made emission color.

Acknowledgements

Financial support by the Dutch Polymer Institute (DPI, technology area HTE) and the DAAD (#54368503, Phosphorescent Metallopolymers) is kindly acknowledged. The authors thank A. Baumgärtel for the MALDI-TOF MS measurements. W.-Y. Wong thanks the Hong Kong Baptist University (FRG2/11-12/156), Hong Kong Research Grants Council (G_HK020/11, HKBU202709 and HKUST2/CRF/10) and Areas of Excellence Scheme, University Grants Committee of HKSAR (Project no. [AoE/P-03/08]) for financial support. W.-Y. Wong also thanks the Institute of Creativity at Hong Kong Baptist University for research support. X.-Z. Wang thanks the National Natural Science Foundation of China (No. 20974091), Natural Science Foundation of Hunan Province of China (No. 10JJ1002) and the Foundation of the Hunan Provincial Education Department (10B107).

References

- 1 G. M. Farinola and R. Ragni, *Chem. Soc. Rev.*, 2011, **40**, 3467–3482.
- 2 X. F. Qi, M. Sliotsky and S. Forrest, *Appl. Phys. Lett.*, 2008, **93**, 193306.
- 3 Q. Wang, J. Q. Ding, D. G. Ma, Y. X. Cheng, L. X. Wang and F. S. Wang, *Adv. Mater.*, 2009, **21**, 2397–2401.
- 4 M. M. Alam and S. A. Jenekhe, *Macromol. Rapid Commun.*, 2006, **27**, 2053–2059.
- 5 A. H. Shelton, I. V. Sazanovich, J. A. Weinstein and M. D. Ward, *Chem. Commun.*, 2012, **48**, 2749–2751.
- 6 U. Giovanella, P. Betti, A. Bolognesi, S. Destri, M. Melucci, M. Pasini, W. Porzio and C. Botta, *Org. Electron.*, 2010, **11**, 2012–2018.
- 7 T. H. Kim, H. K. Lee, O. O. Park, B. D. Chin, S. H. Lee and J. K. Kim, *Adv. Funct. Mater.*, 2006, **16**, 611–617.
- 8 V. Vohra, G. Calzaferri, S. Destri, M. Pasini, W. Porzio and C. Botta, *ACS Nano*, 2010, **4**, 1409–1416.
- 9 L. Brunsveld, B. J. B. Folmer, E. W. Meijer and R. P. Sijbesma, *Chem. Rev.*, 2001, **101**, 4071–4097.

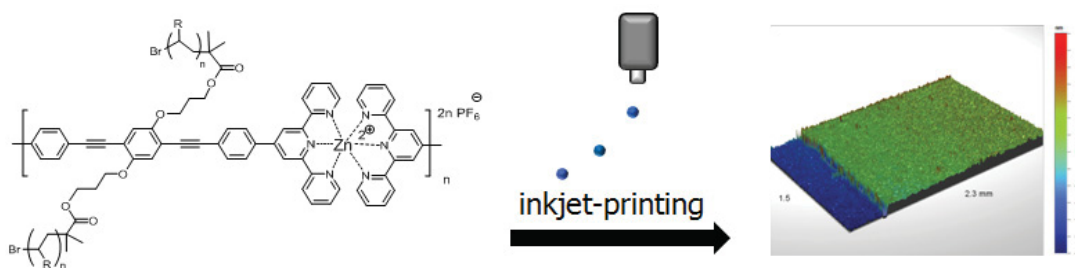
- 10 G. M. Whitesides and B. Grzybowski, *Science*, 2002, **295**, 2418–2421.
- 11 R. Dobrawa and F. Würthner, *J. Polym. Sci., Part A: Polym. Chem.*, 2005, **43**, 4981–4995.
- 12 T. F. A. De Greef, M. M. J. Smulders, M. Wolffs, A. P. H. J. Schenning, R. P. Sijbesma and E. W. Meijer, *Chem. Rev.*, 2009, **109**, 5687–5754.
- 13 T. Aida, E. W. Meijer and S. I. Stupp, *Science*, 2012, **335**, 813–817.
- 14 J. P. Sauvage, J. P. Collin, J. C. Chambron, S. Guillerez, C. Coudret, V. Balzani, F. Barigelletti, L. Decola and L. Flamigni, *Chem. Rev.*, 1994, **94**, 993–1019.
- 15 C. Ulbricht, B. Beyer, C. Friebe, A. Winter and U. S. Schubert, *Adv. Mater.*, 2009, **21**, 4418–4441.
- 16 R. Shunmugam and G. N. Tew, *Polym. Adv. Technol.*, 2008, **19**, 596–601.
- 17 U. S. Schubert, A. Winter and G. R. Newkome, *Terpyridine-Based Materials: For Catalytic, Optoelectronic and Life Science Applications*, Wiley-VCH, Weinheim, 2011.
- 18 S. Bonnet, J. P. Collin, M. Koizumi, P. Mobian and J. P. Sauvage, *Adv. Mater.*, 2006, **18**, 1239–1250.
- 19 A. Wild, A. Winter, F. Schlütter and U. S. Schubert, *Chem. Soc. Rev.*, 2011, **40**, 1459–1511.
- 20 Y. Y. Chen, Y. T. Tao and H. C. Lin, *Macromolecules*, 2006, **39**, 8559–8566.
- 21 F. S. Han, M. Higuchi and D. G. Kurth, *J. Am. Chem. Soc.*, 2008, **130**, 2073–2081.
- 22 A. Wild, C. Friebe, A. Winter, M. D. Hager, U. W. Grummt and U. S. Schubert, *Eur. J. Org. Chem.*, 2010, 1859–1868.
- 23 S. M. Brombosz, A. J. Zuccherro, R. L. Phillips, D. Vazquez, A. Wilson and U. H. F. Bunz, *Org. Lett.*, 2007, **9**, 4519–4522.
- 24 A. Wild, A. Winter, M. D. Hager and U. S. Schubert, *Analyst*, 2012, **137**, 2333–2337.
- 25 A. Wild, A. Winter, M. D. Hager and U. S. Schubert, *Chem. Commun.*, 2012, **48**, 964–966.
- 26 H. Padhy, D. Sahu, I. H. Chiang, D. Patra, D. Kekuda, C. W. Chu and H. C. Lin, *J. Mater. Chem.*, 2011, **21**, 1196–1205.
- 27 A. C. Grimsdale, K. L. Chan, R. E. Martin, P. G. Jokisz and A. B. Holmes, *Chem. Rev.*, 2009, **109**, 897–1091.
- 28 F. Schlütter, A. Wild, A. Winter, M. D. Hager, A. Baumgärtel, C. Friebe and U. S. Schubert, *Macromolecules*, 2010, **43**, 2759–2771.
- 29 Y. J. Cheng, S. H. Yang and C. S. Hsu, *Chem. Rev.*, 2009, **109**, 5868–5923.
- 30 S. C. Yu, C. C. Kwok, W. K. Chan and C. M. Che, *Adv. Mater.*, 2003, **15**, 1643–1647.
- 31 C. Friebe, A. Wild, J. Perelaer and U. S. Schubert, *Macromol. Rapid Commun.*, 2012, **33**, 503–509.
- 32 W. Y. Wong, G. J. Zhou, Z. He, K. Y. Cheung, A. M. C. Ng, A. B. Djuricic and W. K. Chan, *Macromol. Chem. Phys.*, 2008, **209**, 1320–1332.
- 33 W. Y. Wong, X. Z. Wang, Z. He, A. B. Djuricic, C. T. Yip, K. Y. Cheung, H. Wang, C. S. K. Mak and W. K. Chan, *Nat. Mater.*, 2007, **6**, 521–527.
- 34 W. Y. Wong, X. Z. Wang, Z. He, K. K. Chan, A. B. Djuricic, K. Y. Cheung, C. T. Yip, A. M. C. Ng, Y. Y. Xi, C. S. K. Mak and W. K. Chan, *J. Am. Chem. Soc.*, 2007, **129**, 14372–14380.
- 35 W. Y. Wong, W. C. Chow, K. Y. Cheung, M. K. Fung, A. B. Djuricic and W. K. Chan, *J. Organomet. Chem.*, 2009, **694**, 2717–2726.
- 36 G. W. V. Cave and C. L. Raston, *Chem. Commun.*, 2000, 2199–2200.
- 37 W. Barford, I. Boczarow and T. Wharram, *J. Phys. Chem. A*, 2011, **115**, 9111–9119.
- 38 J. Casado, M. Z. Zgierski, P. C. Ewbank, M. W. Burand, D. E. Janzen, K. R. Mann, T. M. Pappenfus, A. Berlin, E. Perez-Inestrosa, R. P. Ortiz and J. T. L. Navarrete, *J. Am. Chem. Soc.*, 2006, **128**, 10134–10144.
- 39 Y. N. Hong, S. J. Chen, C. W. T. Leung, J. W. Y. Lam, J. Z. Liu, N. W. Tseng, R. T. K. Kwok, Y. Yu, Z. K. Wang and B. Z. Tang, *ACS Appl. Mater. Interfaces*, 2011, **3**, 3411–3418.
- 40 E. Tekin, P. J. Smith and U. S. Schubert, *Soft Matter*, 2008, **4**, 703–713.

Publication 7

“Zn^{II} Bisterpyridine Metallopolymers: Improved Processability by the Introduction of Polymeric Side Chains”

Andreas Wild, Anke Teichler, Christian von der Ehe, Andreas Winter, Martin D. Hager, Bing Yao, Baohua Zhang, Zhiyuan Xie, Wai-Yeung Wong, Ulrich S. Schubert

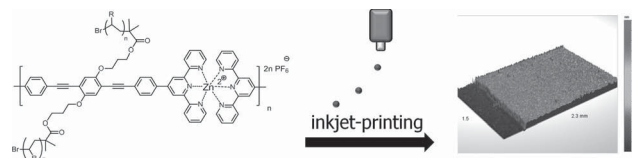
Macromol. Chem. Phys. **2013**, *214*, 1072-1080.



Zn^{II} Bisterpyridine Metallopolymers: Improved Processability by the Introduction of Polymeric Side Chains

Andreas Wild, Anke Teichler, Christian von der Ehe, Andreas Winter, Martin D. Hager, Bing Yao, Baohua Zhang, Zhiyuan Xie, Wai-Yeung Wong,* Ulrich S. Schubert*

Introducing well-defined polymeric side chains to *bisterpyridine* coordination polymers enables the synthesis of materials with tailor-made optical and mechanical properties. The polymers are introduced either by a copper-catalyzed azide–alkyne cycloaddition (grafting-onto) or an atom transfer radical polymerization (polymerization-from) method. The resulting metallopolymers exhibit improved solubility in common organic solvents and can, therefore, be inkjet-printed from chlorinated benzene solutions. The photophysical properties of the so-produced homogeneous films are investigated and a proof-of-principle polymer light-emitting device can be constructed.



1. Introduction

Metallopolymers represent, due to the combination of both organic polymers and metal ions, via reversible metal ion complexation, a fruitful approach to new functional materials.^[1–9] As a coordinative system, various types of *N*-heterocyclic ligands (e.g., 2,2'-bipyridine (bpy), 1,10-phenanthroline and 2,2':6',2''-terpyridine (tpy)) are used, since they form stable coordination complexes with various transition metal ions by $d\pi-p\pi^*$ bonding.^[10] In

particular, tpy is ideally suited for the construction of coordination polymers.^[1] The prevention of Δ/Λ chirality or facial isomers in comparison with related metal complexes with bpy or 2,6-di(quinolin-8-yl)pyridine ligands and the easy access to 4'-substituted terpyridines enables the efficient coupling to stiff conjugated spacer molecules and, therefore, offers the possibility to synthesize linear main-chain metallopolymers.^[1,11–14] Besides the heavy transition metal ions, such as Ru^{II}, Os^{II}, Ir^{III}, and Pt^{II}, metal ions with filled electron shells, in particular Zn^{II}, are also used as

Dr. A. Wild, A. Teichler, C. von der Ehe, Dr. A. Winter,
Dr. M. D. Hager, Prof. U. S. Schubert
Laboratory of Organic and Macromolecular Chemistry (IOMC),
Friedrich-Schiller-University Jena,
Humboldtstr.10, 07743 Jena, Germany
E-Mail: ulrich.schubert@uni-jena.de
Dr. A. Wild, A. Teichler, C. von der Ehe, Dr. A. Winter,
Dr. M. D. Hager, Prof. U. S. Schubert
Jena Center for Soft Matter (JCSM), Friedrich-Schiller-
University Jena, Philosophenweg 7, 07743 Jena, Germany
A. Teichler, C. von der Ehe, Prof. U. S. Schubert
Dutch Polymer Institute (DPI), P.O. Box 902, 5600 AX
Eindhoven, The Netherlands

Prof. W.-Y. Wong
Institute of Molecular Functional Materials, Department of
Chemistry and Institute of Advanced Materials, Hong Kong
Baptist University, Waterloo Road, Hong Kong, P.R. China
E-Mail: rwywong@hkbu.edu.hk
B. Yao, Dr. B. Zhang, Prof. Z. Xie
State Key Laboratory of Polymer Physics and Chemistry,
Changchun Institute of Applied Chemistry, Chinese Academy
of Sciences, Changchun 130022, P. R. China

templates for the development of new photoluminescent and electroluminescent materials as well as sensor systems.^[10,13,15–25] The photophysical behavior of such materials can easily be tuned by coordination to suitable metal ions and choosing an appropriate spacer unit.^[1,26]

However, a broad application of bisterpyridine coordination polymers is still hindered by their low solubility and, consequently, poor processability and film morphology of the final devices. A promising pathway to improve the solubility of these materials is the introduction of polymeric side chains to the π -conjugated element.^[27] Depending on the aimed application, tailor-made polymeric side chains can be used to develop materials with defined optical and mechanical properties. To reveal specific advantages and disadvantages, poly(styrene) (PS) and poly(methacrylate) chains were attached to the metallopolymers using two different methods. The resulting highly soluble quasi-comb-polymers could easily be processed via inkjet printing, resulting in homogeneous films.

2. Experimental Section

2.1. Materials

Solvents were dried and distilled according to standard procedures. All of the solvents or solutions were degassed by purging with argon 1 h prior to use. Compounds **9**, **11a**, and **11b** were purchased from Sigma–Aldrich. The synthesis of 1,4-bis(3-bromopropoxy)-2,5-diiodobenzene (**1**),^[28] 4'-(4-ethynylphenyl)-2,2':6',2''-terpyridine (**2**),^[26] ethynyl-functionalized PS₂₅₀₀ (**5**),^[29] and 3,3'-[(2,5-diiodo-1,4-phenylene)bis(oxy)]bis(propan-1-ol) (**7**)^[28] has been published elsewhere.

2.2. Instrumentation

¹H and ¹³C NMR spectra were recorded on a Bruker Cryomagnēt BZH 400 (400 MHz) or Bruker AC 300 (300 MHz) instrument (at 298 K for all of the NMR spectra). Chemical shifts are reported in parts per million (ppm, δ scale) relative to the residual signal of the solvent; coupling constants are given in Hertz. Preparative size-exclusion chromatography (SEC) was carried out on Bio-Rad S-X1 beads (size exclusion 600–14 000 g mol⁻¹), swollen in toluene. Size-exclusion chromatograms were recorded with a Shimadzu system equipped with an SCL-A10 system controller, an LC-10AD pump, a RID-10A refractive-index detector, an SPD-10A UV detector at 254 nm, and a PL gel 5 mm Mixed-D column at 50 °C utilizing a chloroform/NEt₃/2-propanol (94:4:2 ratio) mixture as eluent at a flow rate of 1 mL min⁻¹. The molar masses were calculated against linear PS and poly(methyl methacrylate) (PMMA) standards, respectively. Matrix-assisted laser desorption–ionization time-of-flight (MALDI-TOF) mass spectra were measured using a Voyager-DE PRO biospectrometry workstation (Applied Biosystems) time-of-flight mass spectrometer with dithranol as matrix. UV–vis absorption, emission, and excitation spectra of thin films were recorded

using a Infinite 200 PRO plate reader (Tecan). UV–vis absorption and emission spectra of the solutions were recorded at 298 K using Perkin–Elmer Lambda 45 and Jasco FP6500 instruments, respectively. Measurements were carried out using CH₂Cl₂ (spectroscopy grade) in 1 cm cuvettes. Elemental analysis was carried out using a CHN-932 Automat Leco instrument. Inkjet printing was performed using an Autodrop professional system from microdrop Technologies (Norderstedt, Germany). The inkjet printer was equipped with piezo-based micropipettes with an inner nozzle diameter of 70 μ m. The polymers were dissolved in the solvent system chlorobenzene/*ortho*-dichlorobenzene (CB/*o*DCB) in a ratio of 90/10 using a concentration of 5 mg mL⁻¹. In order to prevent nozzle clogging, the inks were filtered using a polytetrafluoroethylene (PTFE) syringe filter with a pore size of 0.45 μ m. A voltage of 75 V and a pulse length of 30 μ s led to a stable and reproducible droplet formation. The films with a size of 6 mm \times 6 mm were printed onto microscope slides (Marienfeld). A drop count (i.e., the number of drops that are dispensed at the set position) of 1 and a printing speed of 20 mm s⁻¹ were used as standard settings. Polymer light-emitting devices were fabricated on indium tin oxide (ITO)-coated glass substrates. The substrates were cleaned sequentially with detergent, deionized water, and then dried at 130 °C for 0.5 h to remove the water before use. For device fabrication, the emissive layer ([[Zn(**13**)](OAc)₂]_n (10 w%): polyvinyl carbazole (PVK) (60 nm), chlorobenzene as solvent) was spin-coated onto a UV–ozone-treated ITO substrate in a glovebox. Subsequently, the substrate was transferred into a vacuum chamber and the layers of 2-(4-biphenyl)-5-(4-*tert*-butylphenyl)-1,3,4-oxadiazole (PBD) (30 nm), LiF (1 nm) and aluminum (150 nm) were thermally evaporated in sequence under a vacuum of 5 \times 10⁻⁷ Torr. The device characteristics were measured with a Keithley 2400 source meter and a coupled PR650 spectroscan photometer. All of the measurements were carried out at room temperature under ambient conditions.

2.3. Synthesis

2.3.1. 4',4''''-(((2,5-Bis(3-bromopropoxy)-1,4-phenylene)bis(ethyne-2,1-diyl))bis(4,1-phenylene)) di-2,2':6',2''-terpyridine (**3**)

A solution of 1,4-bis(3-bromopropoxy)-2,5-diiodobenzene (**1**) (151 mg, 0.25 mmol) and **2** (171 mg, 0.51 mmol) in tetrahydrofuran (THF) (12 mL) and NEt₃ (6 mL) was degassed by bubbling with argon for one h. Subsequently, Pd(PPh₃)₄ (29 mg, 0.025 mmol) and CuI (0.012 mmol, 2 mg) were added and the solution was stirred overnight at room temperature. The suspension was filtered, washed with acetone (20 mL) and water (10 mL) to yield almost pure **3**. Further purification was achieved by gel filtration over aluminum oxide (dichloromethane) and subsequent precipitation into methanol. **3** was obtained as a yellow solid (213 mg, 0.21 mmol, 84%). ¹H NMR (CDCl₃, 300 MHz, δ): 8.78 (s, 4H, H^{3',5'}), 8.75 (d, *J* = 4.8 Hz, 4H, H^{6,6'}), 8.70 (d, *J* = 8.00 Hz, 4H, H^{3,3''}), 7.96–7.86 (m, 6H, H^{4,4''}, H^{a,b}), 7.69 (m, 2H, H^{a,b}), 7.38 (m, 4H, H^{5,5''}), 7.12 (s, 2H, H^{ar}), 4.24 (t, *J* = 5.6 Hz, 4H), 3.76 (t, *J* = 6.3 Hz, 4H), 2.44 (q, *J* = 6.2 Hz, 4H). MALDI-TOF (MS) (dithranol): *m/z* = 1013.18 ([*M* + H]⁺). Anal. Calcd. for C₅₈H₄₂N₆O₂Br₂: C 68.65, H 4.17, N 8.28; found: C 68.92, H 4.47, N 7.93.

2.3.2. 4',4''''-(((2,5-Bis(3-azidopropoxy)-1,4-phenylene)bis(ethyne-2,1-diyl))bis(4,1-phenylene) di-2,2':6',2''-terpyridine (**4**))

3 (101.5 mg, 0.1 mmol) and NaN_3 (26 mg, 0.4 mmol) were dissolved in *N,N*-dimethylformamide (DMF) (15 mL) and stirred at 50 °C for 20 h. Subsequently, the suspension was precipitated into water (150 mL). Further purification was carried out by gel filtration over neutral aluminum oxide (dichloromethane) and subsequent precipitation into methanol. **4** was obtained as a yellow solid (66 mg, 0.07 mmol, 70%). $^1\text{H NMR}$ (CDCl_3 , 300 MHz, δ): 8.69 (s, 4H, $\text{H}^{3',5'}$), 8.67 (d, $J = 5.1$ Hz, 4H, $\text{H}^{6,6''}$), 8.61 (d, $J = 8.10$ Hz, 4H, $\text{H}^{3,3'}$), 7.68–7.82 (m, 6H, $\text{H}^{4,4''}$, $\text{H}^{\text{a,b}}$), 7.61 (m, 2H, $\text{H}^{\text{a,b}}$), 7.30 (m, 4H, $\text{H}^{5,5''}$), 7.02 (s, 2H, H^{aryl}), 4.12 (t, $J = 5.8$ Hz, 4H), 3.59 (t, $J = 6.5$ Hz, 4H), 2.08 (q, $J = 6.1$ Hz, 4H). MALDI-TOF MS (dithranol): $m/z = 939.36$ ($[\text{M} + \text{H}]^+$). Anal. Calcd. for $\text{C}_{58}\text{H}_{42}\text{N}_{12}\text{O}_2$: C 74.18, H 4.51, N 17.90; found: C 74.41, H 4.83, N 17.59.

2.3.3. Poly(styrene)-Functionalized Bisterpyridine **6**

Compounds **4** (18.8 mg, 0.02 mmol) and **5** (150 mg, 0.06 mmol) were dissolved in THF (5 mL). Subsequently, CuI (2 mg, 0.01 mmol) and 1,8-diazabicycloundec-7-ene (DBU) (3 mg, 0.02 mmol) were added and the reaction mixture stirred at 50 °C. The reaction progress was followed by SEC measurements and the reaction was quenched by precipitating into methanol, when no further conversion was observable (12 h). Subsequently, the polymer was dissolved in chloroform, filtered over aluminium oxide, and precipitated into methanol. The polymer was obtained as a pale yellow powder (130 mg, 0.016 mmol, 79%). The excess of **5** could not be efficiently removed by preparative SEC (Biobeads) or precipitation. The exact terpyridine content was determined by UV-vis titration with Fe^{II} ($\bar{M}_n = 5650$ g mol^{-1}). $^1\text{H NMR}$ (CDCl_3 , 300 MHz, δ): 8.80 (s, 4H, $\text{H}^{3',5'}$), 8.75 (d, $J = 5.3$ Hz, 4H, $\text{H}^{6,6''}$), 8.76 (d, $J = 8.00$ Hz, 4H, $\text{H}^{3,3'}$), 7.96–7.86 (m, 6H, $\text{H}^{4,4''}$, $\text{H}^{\text{a,b}}$), 7.71 (m, 2H, $\text{H}^{\text{a,b}}$), 7.37–6.40 (PS backbone), 4.05 (m, 4H), 3.15 (m, 4H), 2.10–1.20 (backbone), SEC (PS calibration): $\bar{M}_n = 5500$ g mol^{-1} , polydispersity index (PDI) = 1.13.

2.3.4. Metallopolymer $\{[\text{Zn}(\mathbf{6})](\text{PF}_6)_2\}_n$

Zinc(II) acetate (2.2 mg, 0.01 mmol) in NMP (0.5 mL) was added to the PS-functionalized bisterpyridine monomer **6** (81 mg, 0.01 mmol) in *N*-methylpyrrolidone (NMP) (3 mL). The resulting solution was stirred at 100 °C for 12 h. To perform anion exchange, NH_4PF_6 (33 mg, 0.2 mmol) was added and stirring continued for 1 h. Subsequently, the solution was poured into methanol (30 mL). The resulting metallopolymer was collected by filtration and washed with toluene (10 mL). Finally, the polymer was dried under vacuum to obtain $\{[\text{Zn}(\mathbf{6})](\text{PF}_6)_2\}_n$ as a yellow solid (48 mg, 0.0076 mmol, 76%). $^1\text{H NMR}$ (300 MHz, CD_2Cl_2 , δ): 9.11–8.92 (broad m), 8.83–8.78 (broad m), 8.75–8.65 (broad m), 7.95–7.80 (broad m), 7.77–7.60 (broad m), 7.30–6.27 (PS backbone), 3.99 (m, 4H), 3.35 (m, 4H), 2.05–1.16 (backbone). Anal. Calcd: C 80.43, H 7.26, N 2.65; found: C 81.27, H 7.65, N 2.26.

2.3.5. 3,3'-((2,5-Bis(4-([2,2':6',2''-terpyridin]-4'-yl)phenyl)ethynyl)-1,4-phenylene)bis(oxy))bis-(propan-1-ol) (**8**)

A solution of 3,3'-((2,5-diiodo-1,4-phenylene)bis(oxy))bis(propan-1-ol) (**7**) (478 mg, 1 mmol), 4'-([2,2':6',2''-terpyridin]-4'-yl)phenyl

terpyridine (**2**) (683 mg, 2.05 mmol) in THF (20 mL) and NEt_3 (15 mL) was degassed by purging with argon for 1 h. Subsequently, $\text{Pd}(\text{PPh}_3)_4$ (116 mg, 0.1 mmol) and CuI (0.05 mmol, 10 mg) were added and the solution stirred overnight at room temperature. The suspension was filtered and washed with acetone (20 mL) and water (10 mL). Further purification was carried out by gel filtration over neutral aluminium oxide (dichloromethane) and subsequent precipitation into methanol. **8** was obtained as a yellow solid (693 mg, 0.78 mmol, 78%). Due to its low solubility, no NMR spectrum was measurable. MALDI-TOF MS (dithranol): $m/z = 889.34$ ($[\text{M} + \text{H}]^+$). Anal. Calcd. for $\text{C}_{58}\text{H}_{44}\text{N}_6\text{O}_4$: C 78.36, H 4.99, N 9.45; found: C 78.58, H 5.32, N 9.23.

2.3.6. ((2,5-Bis(4-([2,2':6',2''-terpyridin]-4'-yl)phenyl)ethynyl)-1,4-phenylene)bis(oxy))bis(propane-3,1-diyl)bis(2-bromo-2-methylpropanoate) (**10**)

NEt_3 (0.5 mL) and 2-bromo-2-methylpropanoyl bromide **9** (74 μL , 138 mg, 0.6 mmol) were added dropwise to a suspension of **8** (178 mg, 0.2 mmol) in dichloromethane (15 mL), and the mixture was stirred overnight at 30 °C. Subsequently, aqueous NaHCO_3 and dichloromethane were added, the phases were separated and the organic phase was washed with water and dried over MgSO_4 . The MgSO_4 was removed by filtration and the solvent was evaporated. After gel filtration over neutral aluminium oxide (dichloromethane) and precipitation into methanol, **10** was obtained as a yellow solid (188 mg, 0.16 mmol, 79%). $^1\text{H NMR}$ (CDCl_3 , 300 MHz, δ): 8.78 (s, 4H, $\text{H}^{3',5'}$), 8.75 (d, $J = 4.4$ Hz, 4H, $\text{H}^{6,6''}$), 8.70 (d, $J = 8.00$ Hz, 4H, $\text{H}^{3,3'}$), 7.97–7.86 (m, 6H, $\text{H}^{4,4''}$, $\text{H}^{\text{a,b}}$), 7.71 (m, 2H, $\text{H}^{\text{a,b}}$), 7.38 (m, 4H, $\text{H}^{5,5''}$), 7.11 (s, 2H, H^{aryl}), 4.53 (t, $J = 5.8$ Hz, 4H), 4.24 (t, $J = 6.5$ Hz, 4H), 2.30 (q, $J = 6.1$ Hz, 4H), 1.96 (s, 12H). MALDI-TOF MS (dithranol): $m/z = 1185.25$ ($[\text{M} + \text{H}]^+$), 1106.33 ($[\text{M} - \text{Br} + \text{H}]^+$), 771.25 ($[\text{M} - \text{sidechains} + \text{H}]^+$). Anal. Calcd. for $\text{C}_{66}\text{H}_{54}\text{N}_6\text{O}_2\text{Br}_2$: C 66.78, H 4.59, N 7.08, Br 13.46; found: C 67.05, H 4.87, N 6.78, Br 13.12.

2.3.7. Macroligand **12**

CuBr (29 mg, 0.2 mmol) and **10** (0.119 g, 0.1 mmol) were added to a 10-mL round-bottomed flask. The flask was sealed with a rubber septum and purged with argon. Methyl acrylate **11a** (1.72 g, 0.02 mol) and *N,N,N',N''*-pentamethyldiethylenetriamine (PMDETA) (0.084 mL, 0.4 mmol) were dissolved in anisole (2 mL) and the solution was purged with argon. The solution was transferred to the reaction flask via a syringe. The flask was placed in an oil bath for 2 h at 90 °C. Subsequently, the flask was taken from the oil bath and the reaction mixture was precipitated in ice-cold methanol. The crude product was separated by filtration, dissolved in dichloromethane, passed through a basic aluminium oxide column, and reprecipitated into ice-cold methanol to obtain **12** as a yellowish solid. $^1\text{H NMR}$ (CDCl_3 , 300 MHz, δ): 8.75–8.66 (m, 12H, $\text{H}^{3',5'}$, $\text{H}^{6,6''}$, $\text{H}^{3,3'}$), 7.88 (m, 8H, $\text{H}^{4,4''}$, $\text{H}^{\text{a,b}}$), 7.68 (m, 4H, $\text{H}^{\text{a,b}}$), 7.36 (m, 4H, $\text{H}^{5,5''}$), 3.61 (m, PMA backbone), 1.98–1.05 (PMA backbone), SEC (PMMA calibration): $\bar{M}_n = 7600$ g mol^{-1} (Degree of polymerization (DP) = 37 per arm), PDI = 1.18.

2.3.8. Macroligand **13**.

Styrene **11b** (3.51 g, 33.7 mmol) and PMDETA (57 μL , 0.27 mmol) were dissolved in 5.0 mL anisole and the solution was degassed

with argon for 2 h. CuBr (19.6 mg, 0.137 mmol) and hydroquinone dimethyl ether (318 mg, 2.3 mmol), as internal standard, were placed in a second flask, sealed with a rubber septum and purged with argon for 1 h. The degassed monomer solution was added to the second flask with a degassed syringe. A solution of **10** (80.0 mg, 0.067 mmol) in 5.2 mL anisole was purged with argon for 2 h and subsequently added to the monomer/catalyst solution. After taking a sample for kinetic analysis (100 μ L), the solution was placed in an oil bath and stirred at 110 $^{\circ}$ C for 4 to 5 h. Samples were taken periodically with a degassed syringe for a kinetic study. After 171 min, 12 mL of the reaction mixture was withdrawn with a degassed syringe, exposed to air to terminate the polymerization and diluted with 20 mL chloroform. The solution was eluted over a short aluminum oxide column to remove the copper catalyst and the solvent was removed under reduced pressure. The residue was precipitated from chloroform into cold methanol and the precipitate was collected by filtration and dried under vacuum to yield **13** as a yellowish solid (246 mg, 0.032 mmol). $^1\text{H NMR}$ (CDCl_3 , 300 MHz, δ): 8.91–8.68 (broad m), 8.03–7.87 (broad m), 7.77–7.67 (broad m), 7.48–7.37 (broad m), 7.33–6.37 (PS backbone), 4.02 (m, 4H), 3.90 (m, 4H), 2.05–1.25 (backbone), SEC (PS calibration): $\bar{M}_n = 7700 \text{ g mol}^{-1}$ (DP = 31 per arm), PDI = 1.11.

2.3.9. Metallopolymer $\{[\text{Zn}(\mathbf{12})](\text{PF}_6)_2\}_n$

Zinc(II) acetate (2.2 mg, 0.01 mmol) in NMP (0.5 mL) was added to the PMA-functionalized bisterpyridine monomer **12** (61 mg, 0.01 mmol) in NMP (3 mL). The resulting solution was stirred at 100 $^{\circ}$ C for 12 h. To perform anion exchange, NH_4PF_6 (33 mg, 0.2 mmol) was added and stirring continued for 1 h. Subsequently, the solution was poured into diethyl ether (30 mL). The resulting metallopolymer was collected by filtration and washed with toluene (10 mL). Finally, the polymer was dried under

vacuum to obtain $\{[\text{Zn}(\mathbf{12})](\text{PF}_6)_2\}_n$ as yellow solid (43 mg, 0.0064 mmol, 64%). $^1\text{H NMR}$ (300 MHz, $\text{DMF-}d_7$, δ): 9.41–9.16 (broad m), 8.75–8.61 (broad m), 8.30 (m), 7.90–7.81 (broad m), 3.92 (m), 3.57 (m, PMA backbone), 2.06–0.95 (PMA backbone). Anal. Calcd: C 53.97, H 6.61, N 2.52; found: C 54.51, H 6.91, N 2.29.

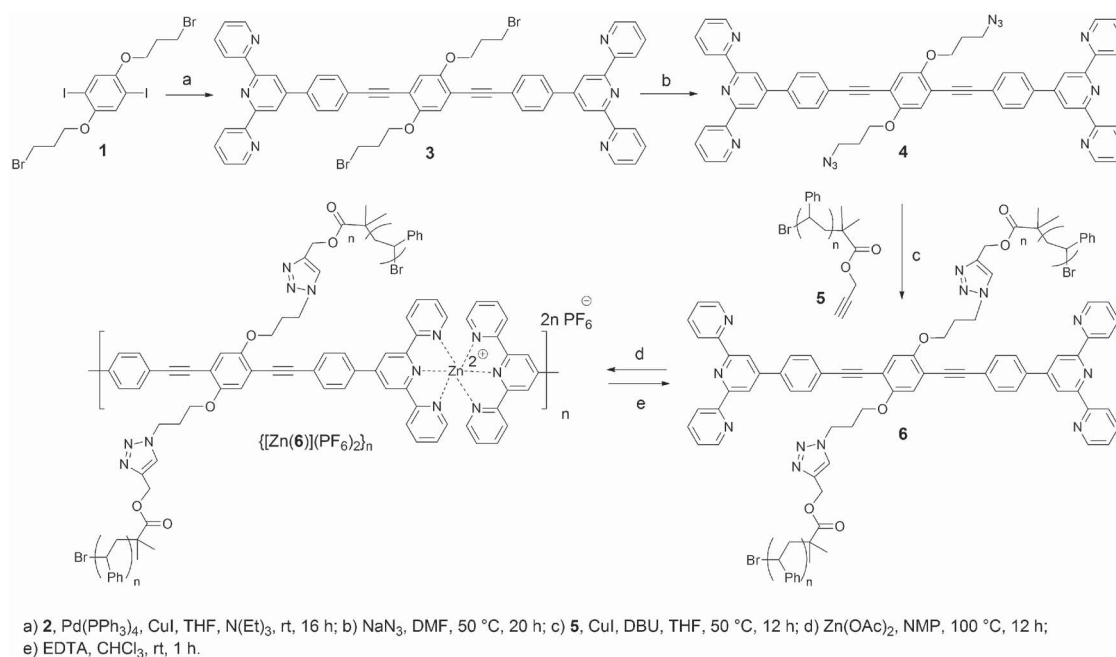
2.3.10. Metallopolymer $\{[\text{Zn}(\mathbf{13})](\text{PF}_6)_2\}_n$

To the PS-functionalized bisterpyridine monomer **13** (77 mg, 0.01 mmol) in NMP (3 mL), zinc(II) acetate (2.2 mg, 0.01 mmol) in NMP (0.5 mL) was added. The resulting solution was stirred at 100 $^{\circ}$ C for 12 h. To perform anion exchange, NH_4PF_6 (33 mg, 0.2 mmol) was added and stirring continued for 1 h. Subsequently, the solution was poured into methanol (30 mL). The resulting metallopolymer was collected by filtration and washed with toluene (10 mL). Finally, the polymer was dried under vacuum to obtain $\{[\text{Zn}(\mathbf{13})](\text{PF}_6)_2\}_n$ as a yellow solid (64 mg, 0.0081 mmol, 81%). $^1\text{H NMR}$ (300 MHz, $\text{DMF-}d_7$, δ): 9.43–9.12 (broad m), 8.81–8.63 (broad m), 7.93–7.60 (broad m), 7.31–6.27 (PS backbone), 4.03 (m), 2.15–1.26 (PS backbone). Anal. Calcd: C 80.43, H 7.26, N 2.65; found: C 80.90, H 7.61, N 2.28.

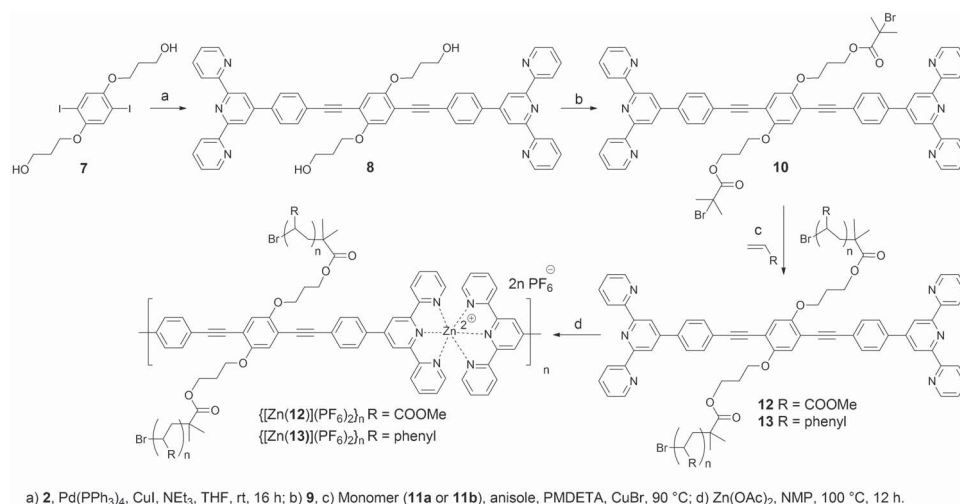
3. Results and Discussion

3.1. Synthesis (Polymerization)

Two strategies were applied to introduce polymeric side chains, as shown in Scheme 1 and 2. Either a preformed polymer is attached to a bisterpyridine via an efficient coupling reaction (“grafting-onto”, Scheme 1) or a bisterpyridine is used as polymerization initiator (“polymerization-from”, Scheme 2).



■ Scheme 1. Schematic representation of the synthesis of metallopolymer $\{[\text{Zn}(\mathbf{6})](\text{PF}_6)_2\}_n$.



■ Scheme 2. Schematic representation of the synthesis of metallopolymers {[Zn(12)](PF₆)₂]_n and {[Zn(13)](PF₆)₂]_n.

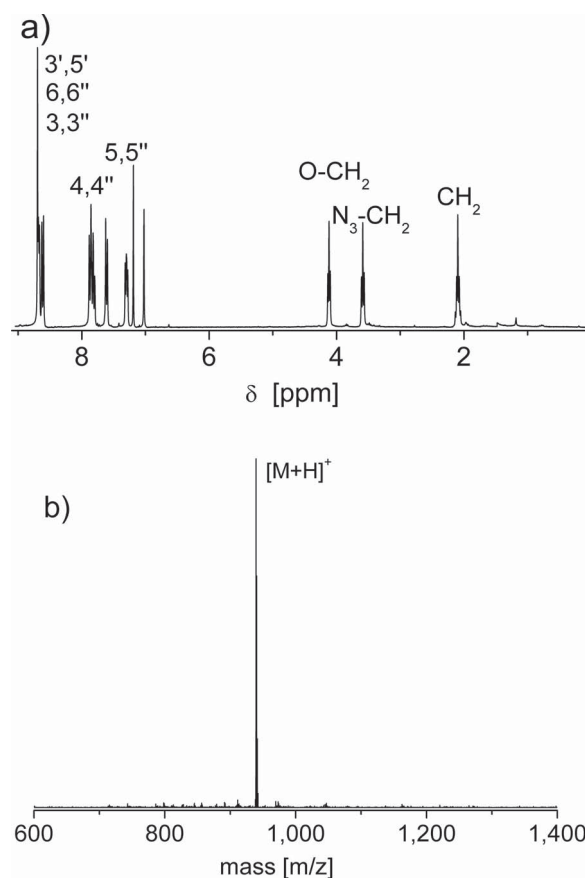
3.2. Grafting Onto Bisterpyridines

The synthesis of endgroup-functionalized polymers, in particular those synthesized via controlled techniques (anionic, controlled radical, Grignard metathesis), is well known and enables the introduction of a variety of different polymers with defined properties.^[30–32]

Since the copper-catalyzed azide–alkyne cycloaddition (CuAAC) is a very efficient reaction that tolerates a variety of conditions and functionalities, it is suitable to be used for the coupling of the polymer to the terpyridine unit.^[33] For that reason, an azide-functionalized bisterpyridine **4** was synthesized starting from 1,4-bis(3-bromopropoxy)-2,5-diiodobenzene (**1**). The terpyridine moieties were subsequently introduced via Sonogashira coupling with 4'-(4-ethynylphenyl)-2,2':6',2''-terpyridine (**2**). The conversion of the alkyl bromide to an azide was performed in DMF with an excess of NaN₃ and resulted in the azide-functionalized bisterpyridine **4** in 70% yield.

Figure 1 depicts the ¹H NMR and MALDI-TOF MS spectra of **4**. The ethynyl-functionalized PS **5** ($\bar{M}_n = 2500 \text{ g mol}^{-1}$, DP = 23) was synthesized in an atom transfer radical polymerization (ATRP), using a functionalized initiator.^[29] Due to the controlled character of the polymerization, a narrow PDI (1.08) could be achieved (Figure 2a). The CuAAC coupling of **4** and **5** was performed in THF solution with DBU as a base. SEC monitoring proved a fast reaction progress (Figure 2a): after 12 h at 50 °C, the SEC chromatogram revealed the end of the reaction by a second signal at $V_e = 9.2 \text{ mL}$ (refractive-index (RI) detection), which did not shift or increase further for longer reaction times. The drawback of this reaction is the purification process. To obtain full conversion, an excess of the polymer is always required. The subsequent separation of bisterpyridine **6** and the excess of **5**, clearly visible in SEC

($V_e = 10.1 \text{ mL}$, filled dots, Figure 2a), via preparative SEC was not successful. For that reason, the crude product of **6** was polymerized using Zn(OAc)₂ and the low solubility of the Zn^{II} coordination polymer in cold toluene was utilized



■ Figure 1. a) ¹H NMR spectrum of **4** (300 MHz, CDCl₃). b) MALDI-TOF MS of **4** (matrix: dithranol).

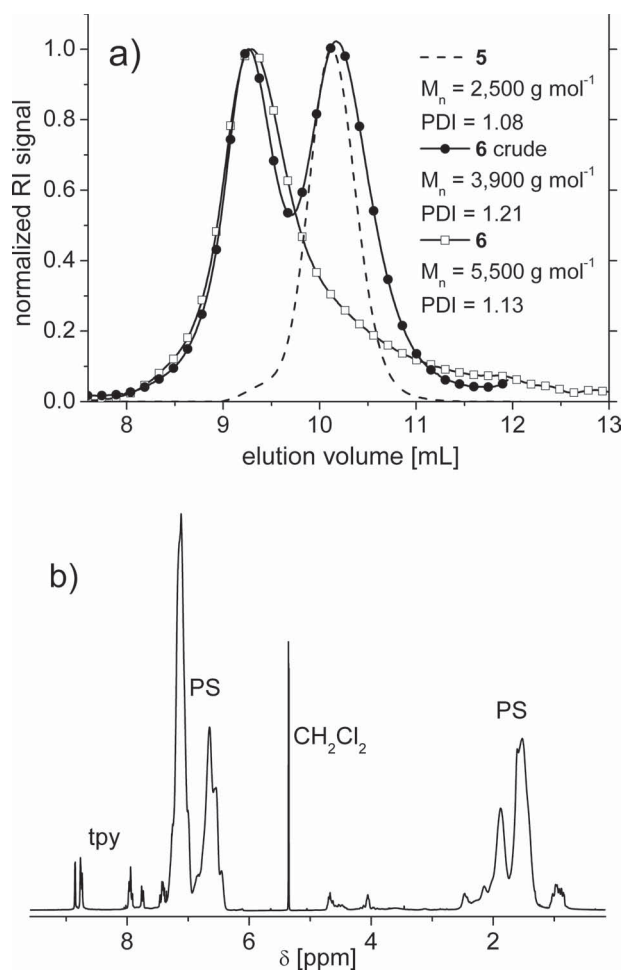


Figure 2. a) SEC traces of **5** and **6** (chloroform:NEt₃:2-propanol 94:4:2 ratio, RI detection). b) ¹H NMR spectrum of **6** (300 MHz, CD₂Cl₂).

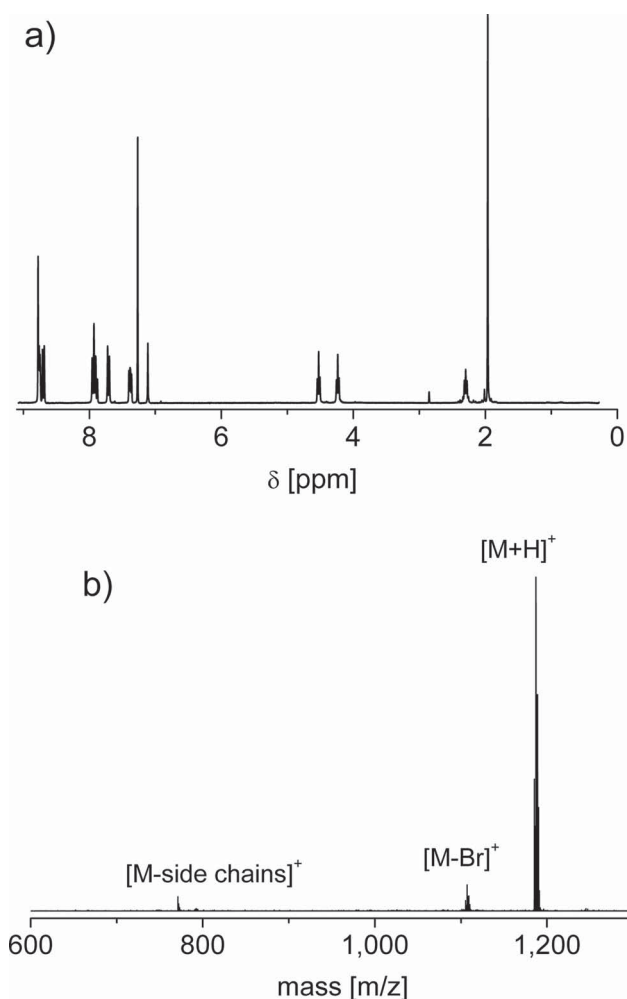


Figure 3. a) ¹H NMR spectrum of **10** (300 MHz, CDCl₃). b) MALDI-TOF MS of **10** (matrix: dithranol).

for separation (Scheme 1). After an anion exchange to PF₆⁻, washing with toluene and subsequent metallo depolymerization using ethylenediaminetetraacetic acid, the pure PS-functionalized bisterpyridine was obtained (Figure 2a, open squares).

A comparison of the SEC before (Figure 2a, filled dots) and after (empty squares) the purification revealed the disappearance of the pure PS signal. The achieved molar mass of 5500 g mol⁻¹, according to PS standard, corresponds well to the expected mass. Besides SEC, also ¹H NMR and MALDI-TOF MS spectra were used to estimate the molar mass of the material. The ¹H NMR spectrum of **6** is depicted in Figure 2b. Integration of the terpyridine signal at 8.7 to 8.8 ppm (3,3'', 6,6'' and 3',5') and the whole aromatic region reveal a similar molar mass as SEC. The MALDI-TOF MS spectrum of **6** (Figure S1a, Supporting Information) shows two main distributions. The second distribution with the higher *m/z* value also indicates a molar mass of about 5500 g mol⁻¹. The one

with a maximum at *m/z* = 2500 g mol⁻¹ corresponds to a fragment due to the triazole cleavage. To ensure a high degree of polymerization for the subsequent metallo polymerization, the exact molar mass of **6** was determined by UV-vis titration to be $\bar{M}_n = 5650$ g mol⁻¹ (Figure S2, Supporting Information). The metallo polymerization of **6** was performed in NMP as solvent using Zn(OAc)₂ to give the coordination polymer {[Zn(**6**)](OAc)₂}_n and, after anion exchange with NH₄PF₆, {[Zn(**6**)](PF₆)₂}_n. Due to the dynamic nature of the Zn^{II} bisterpyridine complex, the degree of polymerization of the resulting Zn^{II} bisterpyridine metallo polymers could not be determined by standard characterization methods like SEC or MALDI-TOF MS. In both techniques, the labile Zn^{II}-terpyridine bond is not stable under the measurement conditions. However, ¹H NMR spectroscopy can be used to estimate the molar masses (\bar{M}_n) and the absence of any end-group signal indicate a high conversion.

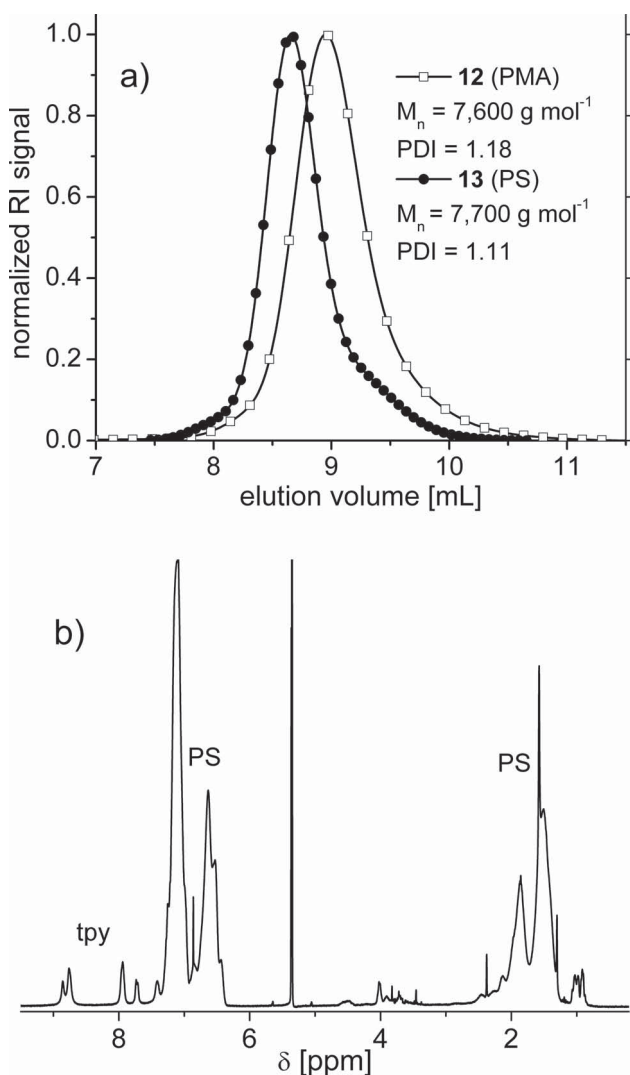


Figure 4. a) SEC traces of the bisterpyridines **12** and **13** (chloroform:NEt₃:2-propanol (94:4:2 ratio), RI detection). b) ¹H NMR spectrum of **13** (300 MHz, CD₂Cl₂).

3.3. Polymerization with Bisterpyridine Initiators

The bisterpyridine **10**, possessing two ATRP initiator groups, was synthesized starting from 3,3'-(2,5-diiodo-1,4-phenylene)bis(oxy))bis(propan-1-ol) (**7**) (Scheme 2).

After reaction with 4'-(4-ethynylphenyl)-2,2':6',2''-terpyridine (**2**), the ATRP initiator groups were introduced by esterification reaction with 2-bromo-2-methylpropanoyl bromide **9**.

Figure 3 shows the ¹H NMR and MALDI-TOF MS spectra of **10**. The subsequent ATRPs of styrene and methyl acrylate, respectively, resulted in materials with molar masses around

7700 g mol⁻¹ and PDI values below 1.2 (Figure 4a). Owing to the “polymerization-from” procedure, both polymers (**12**, **13**) could easily be purified by precipitation and passing through a short aluminum oxide column, to remove the remaining monomer and the copper catalyst. The ¹H NMR spectrum of **13** is shown in Figure 4b. The molar mass estimated by integration of the characteristic terpyridine signal at 8.7 to 8.8 ppm confirmed the values as determined via SEC. The absence of a labile triazole connecting unit, in comparison to **6**, resulted in a more simple MALDI-TOF MS spectrum (Figure S1b, Supporting Information). The main signal corresponds to the target structure **13**, whereas the fragments are caused by ester cleavage. Subsequent self-assembly with Zn(OAc)₂ and anion exchange resulted in the formation of the metallopolymers {[Zn(**12**)](PF₆)₂]_n as well as {[Zn(**13**)](PF₆)₂]_n, respectively (Scheme 2). The introduced polymeric side chains increased the solubility of the materials in common organic solvents, such as chloroform, THF and chlorinated benzenes (i.e., typical solvents for the processing of π-conjugated polymers).

3.4. Inkjet Printing of the Metallopolymers

To confirm the improved solubility and film-forming behavior, the bottle-brush metallopolymers were inkjet-printed and the optical properties of these films were investigated. The inkjet printing technique enables thereby an efficient material usage, a flexible change of the processing conditions, and a maskless digital processing.^[34] Recently, we proved the printability of Zn^{II} bisterpyridine coordination polymers without polymeric side chains.^[26] However, only the solvent system DMF/acetophenone (90/10) at a substrate temperature of 50 °C ensured a good film formation. In contrast, the polymer-functionalized materials {[Zn(**6**)](PF₆)₂], {[Zn(**12**)](PF₆)₂]_n and {[Zn(**13**)](PF₆)₂]_n could be printed using a CB/oDCB (90/10) solvent system, at room temperature. All three polymers were printed from 5 mg mL⁻¹ solutions revealing a stable droplet formation without satellites. A uniform film formation over a range of dot spacings (140 to 200 μm) enabled the preparation of a variation of film thicknesses (50 to 100 nm). Figure 5

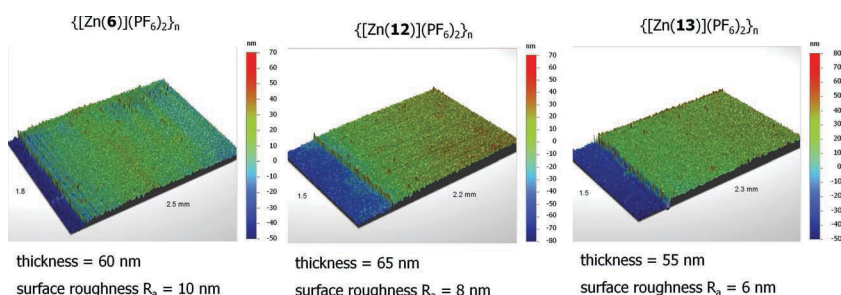


Figure 5. Optical profiler images and film properties of the polymer-functionalized {[Zn(**6**)](PF₆)₂], {[Zn(**12**)](PF₆)₂]_n and {[Zn(**13**)](PF₆)₂]_n.

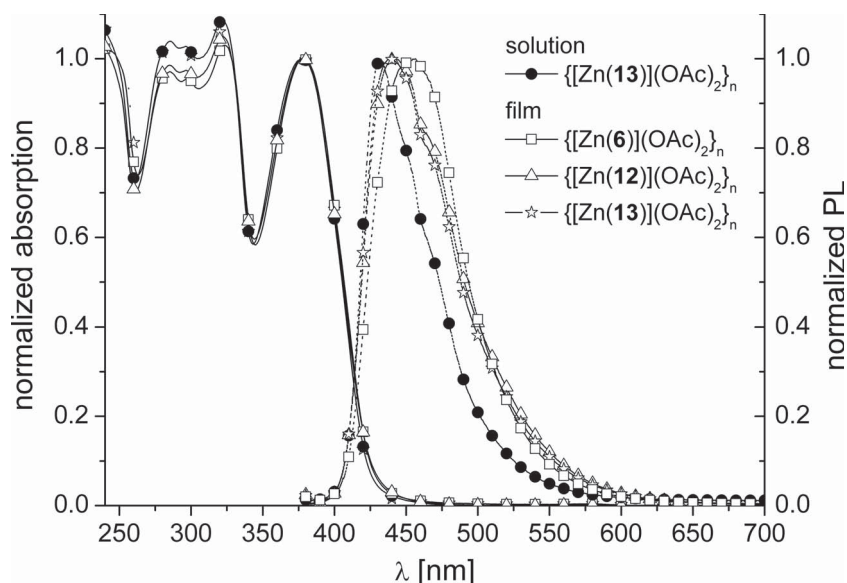


Figure 6. Normalized absorption and photoluminescence spectra (dotted lines) of the metallopolymers, (film or CH₂Cl₂, 10⁻⁶ M, λ_{ex} = λ_{abs}).

a better mixing of PS and PMA side chain, respectively, and main chain metallopolymer.^[27] Thereby, only a small bathochromic shift occurs in the thin films due to a “shielding” of the polymeric aliphatic side chains.

3.5. Device Architecture

As a proof-of-principle demonstration, a polymer light-emitting device with the architecture ITO/{[Zn(13)](PF₆)₂}_n (10 wt%):PVK (60 nm)/PBD (30 nm)/LiF (1 nm)/Al (150 nm) was fabricated. Owing to the polymeric side chains, the processability was markedly improved. The turn-on voltage of the device is around 10 V and it exhibits the highest brightness (λ_{EL} = 424 nm) of 4 cd m⁻² at 14 V. At a voltage of 12 V, the highest

depicts the profilometer images of the most-homogeneous inkjet-printed films with surface roughnesses below 10 nm using a dot spacing of 180 μm.

A comparison of both PS-functionalized polymers displayed thereby a slightly higher roughness for the polymer {[Zn(6)](PF₆)₂}_n, which was synthesized by the grafting-onto method. As both polymers showed a good solubility in the applied solvent system, the higher surface roughness may originate from the lower molar mass and the higher polydispersity of 6.

The photophysical investigation of all polymers was done both in solution and in thin film. Due to an identical chromophoric system, the solution spectra of all three polymers are equivalent and the one of {[Zn(13)](PF₆)₂} is shown representatively in Figure 6. The polymer solutions show absorption and emission maxima at λ_{abs} = 379 nm and λ_{PL} = 432 nm, respectively. The spectra of the inkjet-printed films were measured in an automated fashion, using a plate reader. Owing to the polymeric side chains, the usually observed π-stacking and the consequent bathochromic shift in thin film was hardly visible (Figure 6). The absorption spectra of the printed films are very similar to the solution spectra. Also the photoluminescence spectra differ only slightly. Polymer {[Zn(6)](PF₆)₂}_n, possessing the shortest side chains and the highest surface roughness, reveals also the strongest stacking and, thereby, a redshift in emission (λ_{PL} = 456 nm), that is only visible as a shoulder in {[Zn(12)](PF₆)₂}_n (λ_{PL} = 441 nm) and {[Zn(13)](PF₆)₂}_n (λ_{PL} = 439 nm).

Comparing these data to the ones obtained previously from a similar bisterpyridine Zn^{II} coordination polymer, where poly(caprolactone) side chains were used, indicate

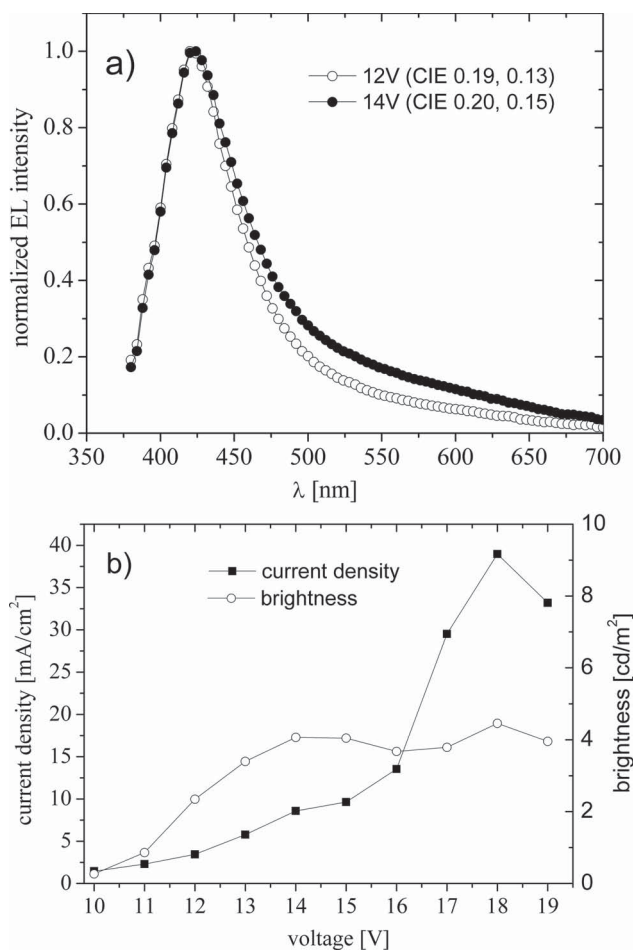


Figure 7. a) Electroluminescent spectrum of the device with architecture ITO/{[Zn(13)](OAc)₂}_n (10 wt%):PVK (60 nm)/PBD (30 nm)/LiF (1 nm)/Al (150 nm) at 14 V. b) Luminance–voltage–current density diagram of the respective device.

current efficiency (0.07 cd A^{-1}) and the peak external quantum efficiency (0.07%) were obtained (Figure 7, and Supporting Information, Figure S3). Expectedly, the PS side chains act as an insulator, and, thereby, hamper charge transport in the photoactive layer. To overcome this problem, the introduction of well-defined, semi-conductive side chains, like poly(thiophenes), could represent an alternative. Work is still underway to improve the device performance.

4. Conclusion

The introduction of polymeric side chains to π -conjugated bisterpyridine monomers enables the assembly of materials with tailor-made optical and mechanical properties. The well-defined polymers were introduced to the bisterpyridine either by a grafting-onto or a polymerization-from method. The use of a bisterpyridine initiator for ATRP proved to be the best choice for functionalization, even though only selected monomers can be polymerized. The metallopolymerizations using Zn^{II} ions resulted in bottle-brush metallopolymer, which revealed improved solubility in common organic solvents. For that reason, homogeneous films of the metallopolymer could be produced via inkjet printing technique and a proof-of-principle polymer light-emitting device was assembled.

Supporting Information

Supporting Information is available from the Wiley Online Library or from the author.

Acknowledgements: Financial support by the Dutch Polymer Institute (DPI, technology area HTE) and the DAAD (#54368503, Phosphorescent Metallopolymer) is kindly acknowledged. The authors thank S. Crotty for the MALDI-TOF MS measurements. W.-Y.W. thanks the Hong Kong Baptist University (FRG2/11-12/156), Hong Kong Research Grants Council (G_HK020/11, HKBU202508 and HKUST2/CRF/10) and Areas of Excellence Scheme, University Grants Committee of HKSAR (Project No. [AoE/P-03/08]) for financial support. W.-Y.W. also thanks the Institute of Creativity at Hong Kong Baptist University for research support.

Received: January 2, 2013; Revised: February 23, 2013; Published online: April 2, 2013; DOI: 10.1002/macp.201300003

Keywords: atom-transfer radical polymerization (ATRP); conducting polymers; inkjet printing; metal-polymer complexes; self-assembly

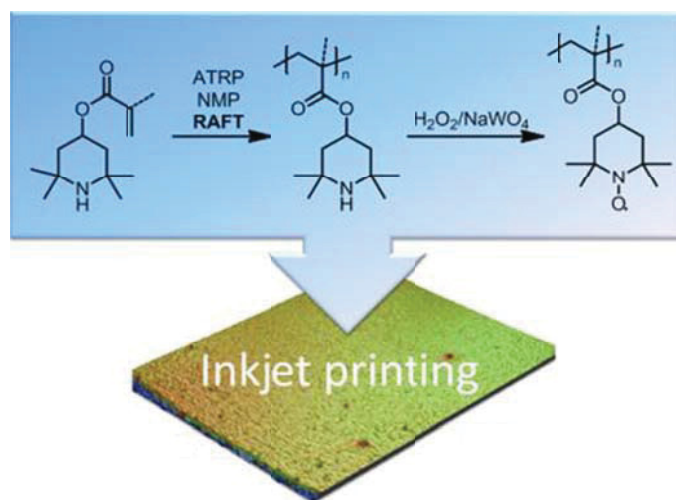
- [1] A. Wild, A. Winter, F. Schlütter, U. S. Schubert, *Chem. Soc. Rev.* **2011**, *40*, 1459.
- [2] G. R. Whittell, M. D. Hager, U. S. Schubert, I. Manners, *Nat. Mater.* **2011**, *10*, 176.
- [3] M. Burnworth, L. M. Tang, J. R. Kumpfer, A. J. Duncan, F. L. Beyer, G. L. Fiore, S. J. Rowan, C. Weder, *Nature* **2011**, *472*, 334.
- [4] W. Y. Wong, X. Z. Wang, Z. He, A. B. Djuricic, C. T. Yip, K. Y. Cheung, H. Wang, C. S. K. Mak, W. K. Chan, *Nat. Mater.* **2007**, *6*, 521.
- [5] J. C. Eloi, L. Chabanne, G. R. Whittell, I. Manners, *Mater. Today* **2008**, *11*, 28.
- [6] S.-L. Li, T. Xiao, C. Lin, L. Wang, *Chem. Soc. Rev.* **2012**, *41*, 5950.
- [7] F. S. Han, M. Higuchi, D. G. Kurth, *J. Am. Chem. Soc.* **2008**, *130*, 2073.
- [8] A. Harriman, R. Ziessel, *Chem. Commun.* **1996**, 1707.
- [9] F. C. Grozema, C. Houarner-Rassin, P. Prins, L. D. A. Siebbeles, H. L. Anderson, *J. Am. Chem. Soc.* **2007**, *129*, 13370.
- [10] J. P. Sauvage, J. P. Collin, J. C. Chambron, S. Guillerez, C. Coudret, V. Balzani, F. Barigelletti, L. Decola, L. Flamigni, *Chem. Rev.* **1994**, *94*, 993.
- [11] H. Padhy, D. Sahu, I. H. Chiang, D. Patra, D. Kekuda, C. W. Chu, H. C. Lin, *J. Mater. Chem.* **2011**, *21*, 1196.
- [12] R. Dobrawa, F. Würthner, *J. Polym. Sci., Part A: Polym. Chem.* **2005**, *43*, 4981.
- [13] S. C. Yu, C. C. Kwok, W. K. Chan, C. M. Che, *Adv. Mater.* **2003**, *15*, 1643.
- [14] E. C. Constable, A. M. W. C. Thompson, *J. Chem. Soc., Dalton Trans.* **1992**, 3467.
- [15] A. Wild, A. Winter, M. D. Hager, U. S. Schubert, *Analyst* **2012**, *137*, 2333.
- [16] A. Wild, A. Winter, M. D. Hager, U. S. Schubert, *Chem. Commun.* **2012**, 48, 964.
- [17] Y. Y. Chen, Y. T. Tao, H. C. Lin, *Macromolecules* **2006**, *39*, 8559.
- [18] D. Knapton, M. Burnworth, C. Weder, S. J. Rowan, *Angew. Chem. Int. Ed.* **2006**, *45*, 5825.
- [19] W. Goodall, J. A. G. Williams, *Chem. Commun.* **2001**, 2514.
- [20] I. Eryazici, C. N. Moorefield, G. R. Newkome, *Chem. Rev.* **2008**, *108*, 1834.
- [21] G. N. Tew, R. Shunmugam, *Chem. Eur. J.* **2008**, *14*, 5409.
- [22] S. M. Brombosz, A. J. Zuccherro, R. L. Phillips, D. Vazquez, A. Wilson, U. H. F. Bunz, *Org. Lett.* **2007**, *9*, 4519.
- [23] R. Siebert, Y. Tian, R. Camacho, A. Winter, A. Wild, A. Krieg, U. S. Schubert, J. Popp, I. G. Scheblykin, B. Dietzek, *J. Mater. Chem.* **2012**, *22*, 16041.
- [24] Y. Y. Chen, H. C. Lin, *J. Polym. Sci., Part A: Polym. Chem.* **2007**, *45*, 3243.
- [25] Y. Y. Chen, H. C. Lin, *Polymer* **2007**, *48*, 5268.
- [26] A. Wild, A. Teichler, C.-L. Ho, X.-Z. Wang, H. Zhan, F. Schlütter, A. Winter, M. D. Hager, W.-Y. Wong, U. S. Schubert, *J. Mater. Chem. C* **2013**, *1*, 1812.
- [27] A. Winter, C. Friebe, M. D. Hager, U. S. Schubert, *Macromol. Rapid Commun.* **2008**, *29*, 1679.
- [28] E. Ji, D. G. Whitten, K. S. Schanze, *Langmuir* **2011**, *27*, 1565.
- [29] R. Thorwirth, A. Stolle, B. Ondruschka, A. Wild, U. S. Schubert, *Chem. Commun.* **2011**, 47, 4370.
- [30] M. Jeffries-El, G. Sauve, R. D. McCullough, *Adv. Mater.* **2004**, *16*, 1017.
- [31] H. Hsieh, R. P. Quirk, *Anionic Polymerization: Principles and Practical Applications*, Marcel Dekker Inc, New York **1996**.
- [32] U. Mansfeld, C. Pietsch, R. Hoogenboom, C. R. Becer, U. S. Schubert, *Polym. Chem.* **2010**, *1*, 1560.
- [33] V. V. Rostovtsev, L. G. Green, V. V. Fokin, K. B. Sharpless, *Angew. Chem. Int. Ed.* **2002**, *41*, 2596.
- [34] E. Tekin, B. J. de Gans, U. S. Schubert, *J. Mater. Chem.* **2004**, *14*, 2627.

Publication 8

“Polymerization of Free Secondary Amine Bearing Monomers by RAFT Polymerization and Other Controlled Radical Techniques”

Tobias Janoschka, Anke Teichler, Andreas Krieg, Martin D. Hager, Ulrich S. Schubert

J. Polym. Sci., Part A: Polym. Chem. **2012**, *50*, 1395-1407.



Polymerization of Free Secondary Amine Bearing Monomers by RAFT Polymerization and Other Controlled Radical Techniques

Tobias Janoschka,^{1,2} Anke Teichler,^{1,2,3} Andreas Krieg,^{1,2,3}
Martin D. Hager,^{1,2} Ulrich S. Schubert^{1,2,3}

¹Laboratory of Organic and Macromolecular Chemistry (IOMC), Friedrich-Schiller-University Jena, Humboldtstr. 10, D-07743 Jena, Germany

²Jena Center for Soft Matter (JCSM), Friedrich-Schiller-University Jena, Humboldtstr. 10, D-07743 Jena, Germany

³Dutch Polymer Institute (DPI), P.O. Box 902, 5600 AX Eindhoven, The Netherlands

Correspondence to: U. S. Schubert (E-mail: ulrich.schubert@uni-jena.de)

Received 20 September 2011; accepted 5 December 2011; published online 24 January 2012

DOI: 10.1002/pola.25907

ABSTRACT: This work describes the polymerization of the free secondary amine bearing monomer 2,2,6,6-tetramethylpiperidin-4-yl methacrylate (TMPMA) by means of different controlled radical polymerization techniques (ATRP, RAFT, NMP). In particular, reversible addition-fragmentation chain transfer (RAFT) polymerization enabled a good control at high conversions and a polydispersity index below 1.3, thereby enabling the preparation of well-defined polymers. Remarkably, the polymerization of the secondary amine bearing methacrylate monomer was not hindered by the presence of the free amine that commonly induces degradation of the RAFT reagent. Subsequent oxidation of the polymer yielded the polyradical poly(2,2,6,6-tetramethylpiperidinyloxy-4-yl

methacrylate), which represents a valuable material used in catalysis as well as for modern batteries. The obtained polymers having a molar mass (M_n) of 10,000–20,000 g/mol were used to fabricate well-defined, radical-bearing polymer films by inkjet-printing. © 2012 Wiley Periodicals, Inc. *J Polym Sci Part A: Polym Chem* 50: 1394–1407, 2012

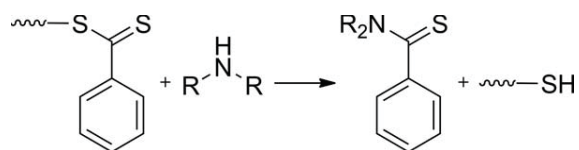
KEYWORDS: atom transfer radical polymerization (ATRP); battery material; nitroxide mediated polymerization (NMP); organic radical battery; radical polymerization; reversible addition fragmentation chain transfer polymerization (RAFT); secondary amine; TEMPO polymer

INTRODUCTION Controlled radical polymerization (CRP) of free amine bearing monomers is a demanding task. Although reversible addition-fragmentation chain transfer (RAFT) polymerization excels in versatility with respect to the choice of monomer, functional group tolerance as well as the required experimental conditions, the RAFT polymerization of amines has usually to be carried out with protected amine functionalities. This is necessary to omit the aminolysis of the thiocarbonylthio chain transfer agents (Scheme 1) that commonly occurs with free primary and secondary amines. Aminolysis not only renders the polymerization of free amines impossible, it is even used to intentionally cleave thiocarbonylthio end groups. While the polymerization of tertiary amines such as 2-(dimethylamino)ethyl methacrylate is possible, monomers with primary and secondary amine functionalities may only be polymerized in a controlled manner with the amine being protected as an ammonium salt. Common examples include 2-aminoethyl methacrylate hydrochloride and *N*-(2-aminoethyl)-methacrylamide hydrochloride.^{1–3}

Additional obstacles hinder the successful polymerization of amine bearing monomers by atom transfer radical polymer-

ization (ATRP). The growing polymer chain may displace the ligand of the copper catalyst complex bringing the reaction to a premature halt. Monomers that were successfully polymerized by ATRP, for example, supported by the use of polydentate ligands, include the tertiary amine 2-(dimethylamino)ethyl methacrylate as well as the hydrochloride of the primary amine 2-aminoethyl methacrylate.^{4,5}

The polymerization of the secondary amine bearing monomer 2,2,6,6-tetramethylpiperidin-4-yl methacrylate (TMPMA) is of special interest as its polymers can be further processed to obtain polyradical bearing polymers.⁶ Up to now, such polymers have been prepared in several different ways: (i) polymer-analogous reactions, for example, transesterification of poly(methyl methacrylate) (PMMA) with 2,2,6,6-tetramethyl-4-aminopiperidinyloxy⁷ or poly(pentafluorophenyl acrylate) with 4-amino-2,2,6,6-tetramethyl-1-oxyl-piperidine,⁸ (ii) free radical polymerization (FRP) with a subsequent oxidation of the formed amine bearing precursor polymer⁹ as well as (iii) direct anionic polymerization of a free radical bearing monomer.¹⁰ While the transesterification route (i) is marked by only a low degree of functionalization (<25%)



SCHEME 1 Schematic representation of the aminolysis of thio-carbonylthio chain transfer agents by secondary amines.

that can be achieved, anionic polymerization (iii) permits good functionalization but requests stringent reaction conditions. As radical polymerizations are uncomplicated in their general handling they are to be preferred over ionic procedures. Nevertheless, an intrinsic drawback of free radical polymerization is the lack of control over the molar mass and the broad polydispersity index (PDI) value of the polymers formed.

Our goal was to use the polyradical bearing polymers for inkjet printing. For this advanced processing technique it is essential to have well-defined polymers at hand. As the solubility of the polymer and its solution's viscosity have a significant influence on the printability of an ink-formulation the molar mass needs to be adjusted accordingly. For this reason, the preparation of the PTMA-NO precursor polymer from TMPMA by CRP techniques such as ATRP, RAFT, and nitroxide mediated polymerization (NMP) was evaluated. When the limitations of the polymers prepared by free radical polymerization—like high viscosity and undefined molar mass distribution—are overcome, inkjet printing can be used to process the polymers. Inkjet printing is a noncontact and drop-on-demand film preparation technique, which requires only small amounts of solutions and serves over a high reproducibility.^{11–13} Furthermore, inkjet printing is a noncontact patterning technique that does not need expensive masks, showing clear advantages in comparison to other solution deposition or film formation methods like doctor blading, spin-coating or gravure printing. This advanced processing technique is able to bridge the gap between polymer synthesis and solid-state property characterization, since this particular technique opens the way for an automated preparation of thin-film libraries, with a systematic variation of parameters, such as the chemical composition or the film thickness.¹⁴

To our best knowledge, there have only been two previous reports using CRP techniques for the preparation of TEMPO radical bearing polymers.¹⁵ Surface-initiated ATRP was used to fabricate patterned thin-film electrodes, whereas RAFT was used in the preparation of the second block of an amphiphilic copolymer subsequently used as ESR probe in bioimaging. Even though the latter polymerization is the first example of a polymerization of a free amine bearing monomer by the RAFT process, no explanation for this noteworthy exception is given. As the authors of the previously published reports on CRP of piperidine bearing monomers peruse an application-focused approach we herein investigate the preparation by the most versatile CRP techniques in detail from a synthetic point of view as to create a valid

foundation for future applications of this resourceful material. Special emphasis is focused on the optimization of the reaction conditions to obtain polymers that exhibit good printability as to permit a flexible and fast processing of radical bearing polymers by means of inkjet printing.

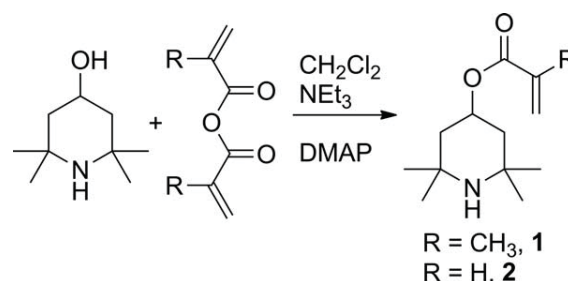
RESULTS AND DISCUSSION

Monomer Synthesis

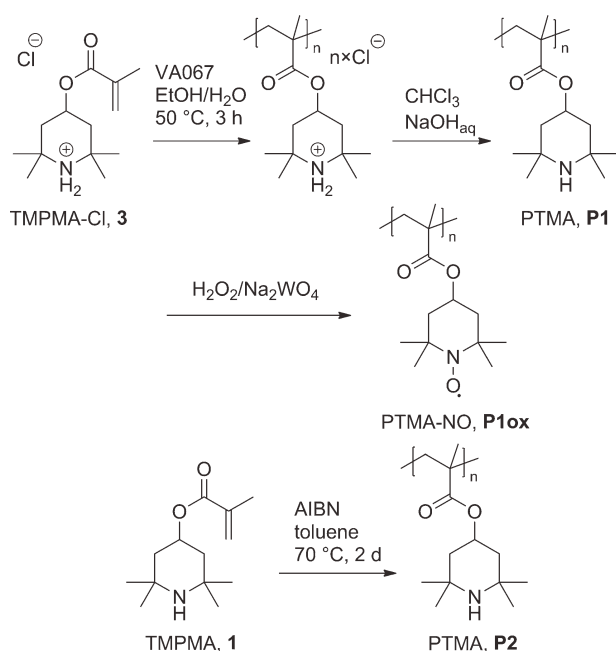
Numerous industrial polymers are prepared by a radical polymerization process. Because this technique is robust and cost effective its use in the synthesis of radical-bearing polymers is desirable. Although the radical polymerization technique is compatible with many monomers and versatile with respect to the reaction conditions, the polymerization of free radical (TEMPO) bearing monomers is not possible. For this reason, a precursor polymer has to be prepared. Based on the inexpensive and commercially available 2,2,6,6-tetramethylpiperidin-4-ol the synthesis of a poly(methacrylate) represents an useful approach.

The preparation of the required methacrylate monomer TMPMA, **1** by esterification is complicated by the simultaneous presence of, both, a hydroxyl and an amino group, since both functionalities show similar reactivity towards carboxylic acid derivatives. Previous publications have used methacryloyl chloride without providing detailed information of the synthetic protocol or the obtained yields.^{16,17} Our experiments indicate that methacryloyl chloride is not a suitable reagent because it shows no significant OH-selectivity. The desired TMPMA is only obtained in low yields (<15%) with the *bis*-substituted 2,2,6,6-tetramethylpiperidin-4-ol **1a** being the main product, as could be proven by mass spectrometry (MS) and nuclear magnetic resonance (NMR) spectroscopy.

Using the less reactive methacrylic anhydride in combination with 1 mol-% of a nucleophilic catalyst, 4-dimethylaminopyridine (DMAP), results in improved yields up to 60% (Scheme 2); the formation of **1a** was minimized. By using the anhydride and catalytic amounts of DMAP the concentration of the active electrophilic reagent was constantly kept at a low level, self-controlled by the reaction rate of the esterification. Since no excess of the active electrophilic reagent was present and the reaction with the sterically less hindered hydroxyl group was kinetically favored, the formation of a *bis*-substituted product is suppressed.



SCHEME 2 Schematic representation of the synthesis of the free secondary amine bearing monomers **1** (TMPMA) and **2** (TMPA) by DMAP catalyzed esterification.



SCHEME 3 Schematic representation of the preparation of PTMA (**P1** and **P2**) via the polymerization of TMPMA hydrochloride (top) and of the free amine (bottom) as well as of the oxidation of PTMA to **P1ox** (middle).

The corresponding acrylate monomer 2,2,6,6-tetramethylpiperidin-4-yl acrylate (TMPA, **2**) was prepared in a similar manner in moderate yield. Therefore acrylic anhydride was prepared by the reaction of acrylic acid with sodium hydride and acryloyl chloride before use.¹⁸

Free radical Polymerization

Methacrylates can be polymerized by conventional free radical polymerization using standard initiators. TMPMA was polymerized in toluene at 70 °C initiated by 2,2'-azobis(2-methylpropionitrile) (AIBN) to obtain poly(2,2,6,6-tetramethylpiperidin-4-yl methacrylate), PTMA (Scheme 3, bottom). The polymer obtained can easily be isolated and purified by precipitation making this a robust and reliable method. Nevertheless, the technique has to be marked rather inefficient, since the polymerization proceeds slowly resulting in only 40% conversion after 48 hours of reaction time. The reason for this slow reaction lies in the nature of the monomer: As known from literature reports amines can function as retarders in free radical polymerizations.^{19,20}

When TMPMA is reacted with hydrochloric acid, the retarding amine-functionality is protonated and rendered innocuous. Polymerization of the ionic TMPMA-Cl **3** can be carried out in a mixture of water and ethanol (1:1) using the water-soluble 2,2'-azobis(2-methyl-propionamidine) dihydrochloride (VA067) as initiator at 50 °C (Scheme 3, top). The use of this system reduces the reaction time to 3 hours while doubling the yield of the polymer. The slow addition of a solution of the protonated polymer in water/ethanol to a vigorously stirred mixture of aqueous sodium hydroxide and

chloroform was established as the most suitable procedure for conducting the deprotonation of the prepolymer in homogeneous phases. PTMA **P1** is finally isolated from the chloroform layer in good yields. Its molar mass exceeds $M_n > 300,000$ g/mol as determined by size exclusion chromatography (SEC) using dimethylacetamide (DMAc) as mobile phase and poly(styrene) as standard. An absolute molar mass of $M_n = 60,000$ g/mol was obtained by universal calibration using tetrahydrofuran/triethylamine (96:4) as mobile phase. This result indicates an overestimation of the molar mass with respect to a poly(styrene) standard on the dimethylacetamide based SEC system, which one needs to keep in mind upon interpreting further results on this class of polymers.

The precursor polymer obtained by free radical polymerization was subsequently oxidized with hydrogen peroxide and sodium tungstate as catalyst to form the nitroxide radical bearing polymer.²¹ The orange colored, oxidized polymer precipitates from the aqueous methanol solution, permitting a simple separation of the oxidized polymer from the reaction mixture and excellent yields.

The formation of the free nitroxide radical is indicated by the typical orange color with absorption maxima at 251 nm (π - π^*) and 451 nm (n - π^*). Further prove is provided by infrared (IR) and electron spin resonance (ESR) spectroscopy (Fig. 1). The IR spectrum exhibits a dominant signal at 1364 cm^{-1} attributed to N—O stretching vibrations. This signal superimposes the much weaker symmetric C—H deformation vibrations of the CH₃ groups at $1366/1377\text{ cm}^{-1}$. These observations contrast with the precursor polymer's IR spectrum, where the $\delta_s(\text{CH}_3)$ at $1366/1377\text{ cm}^{-1}$ is the only signal present in this region.

Quantitative ESR spectroscopy (internal standard: copper sulfate), elemental analysis, and determination of the spin concentration using a superconducting quantum interference device (SQUID) indicate complete functionalization of the polymer. The ESR spectrum (Fig. 1) of the polymer is dominated by a broad signal at $g = 2.0064$, which is

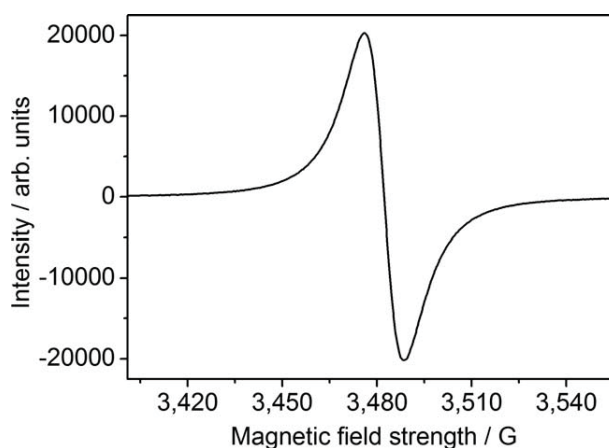


FIGURE 1 ESR spectrum (X-Band) of PTMA-NO (**P1**) with $g = 2.0064$.

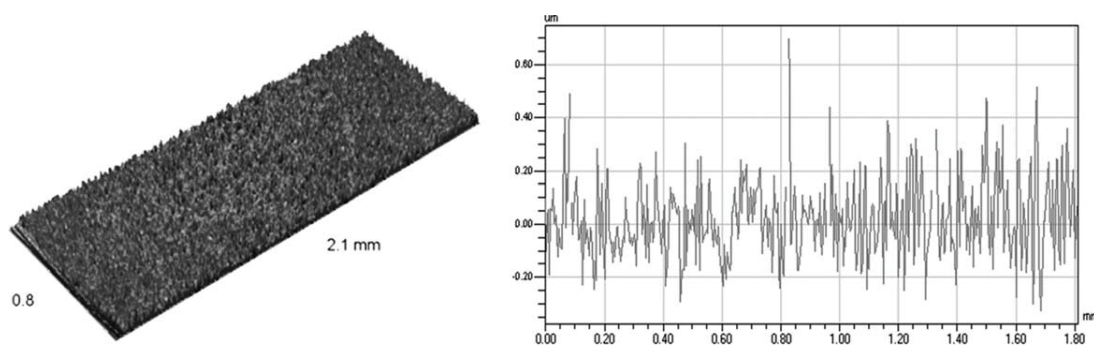


FIGURE 2 Optical profiler image (left) and 2D profile (right) of an inkjet printed film of the radical bearing polymer **P1ox** prepared by free radical polymerization and subsequent oxidation. The film was inkjet-printed on glass from *N*-methylpyrrolidone at a polymer concentration of 4 mg/mL.

characteristic for organic radical polymers. Radical-radical interaction, due to close spatial proximity of the TEMPO moieties, broadens the signal. Therefore, no hyperfine structure is visible.

As a consequence of the oxidation process the high molar mass polymer is partially cross-linked, decreasing its solubility in common organic solvents. For inkjet printing the only suitable solvent was 1-methyl-2-pyrrolidone (NMP). However, even in NMP the polymer is only partially soluble (<4 mg/mL). This makes the processing of **P1ox** via inkjet printing difficult, but is inevitable when using high molar mass PTMA as produced by free radical polymerization. The topography of the printed films was studied with an optical interferometric profiler and the results are summarized in Figure 2. As a consequence of the polymer's low solubility, **P1ox** exhibits poor film formation properties and a very rough film surface as can be seen from the 2D profile of the film. The use of the high boiling solvent NMP (b.p. = 202 °C) resulted in a long drying time of the processed films, that is, characteristic for the formation of rough surfaces. In addition, agglomeration occurs upon drying at elevated temperatures. An optimization of the film formation by varying either the concentration or the solvent could not be performed due to the low solubility of the polymer. For these reasons inkjet printing is no suitable technique to process this kind of polymer prepared by free radical polymerization and subsequent oxidation.

As the polymers prepared by FRP cannot be inkjet printed properly, CRP techniques were used subsequently to obtain more defined PTMA of a lower molar mass. To acquire a complete picture the three most versatile techniques were evaluated.

Nitroxide Mediated Polymerization

The high amount of propagating radicals, that is, caused by a high activation–deactivation equilibrium constant complicates the controlled homopolymerization of methacrylates since it leads to irreversible termination reactions. This can, theoretically, be overcome by (co)polymerization with styrene that exhibits a low activation–deactivation equilibrium

constant leading to a strong reduction of the overall equilibrium constant and, thereby, improving the control.²²

The (co)polymerization of TMPMA was studied, using SG1-based alkoxyamine BlocBuilder™. In addition, the homopolymerization of the corresponding acrylate monomer TMPA, that was expected to show better compatibility with the NMP technique, was examined under similar conditions.

At a reaction temperature of 120 °C reference values for the homopolymerization of TMPMA (conversion, molar mass, PDI) were obtained. The polymer revealed a molar mass of $M_n = 5,800$ g/mol after 6 hours reaction time (21% conversion) with a PDI value of 1.8, indicating loss of the control over the polymerization kinetics. Decreasing the temperature to 90 °C did not improve the control but raised the molar mass due to a lowered initial radical concentration at this temperature (**P3**). In comparison to the reference homopolymerization the addition of 10 mol % styrene enabled an improved PDI value of 1.4 suggesting a better control of the polymerization. In accordance with the previous observations a lowered temperature caused no significant improvement. All results are summarized in Table 1 showing that the values do not meet the requirements.

In comparison with TMPMA the homopolymerization rate of the corresponding acrylate monomer TMPA is much higher, reaching 91% of monomer conversion after 6 hours (Table 2). Expectedly, the reaction control is improved as indicated by a significant decrease of the PDI to 1.51.

Another parameter that was changed to decrease the overall reaction rate is the dynamic equilibrium between the dormant and the active species. By adding an excess of the free nitroxide radical SG-1 or by releasing free SG-1 radicals *in situ* by means of preheating BlocBuilder™ the equilibrium is pushed towards the dormant species.²³ Before the addition of TMPA a BlocBuilder™ solution was heated at 60 °C for 40 minutes. The free nitroxide radical formed has a strong influence on the reaction kinetics, slowing down the reaction by factor 10 with respect to a procedure without additional SG-1. After 16 hours of reaction the monomer conversion amounted to merely 28%. On the other hand, adding 0.1 mol-% of free SG-1 to the standard reaction

TABLE 1 Selected Polymerization Conditions and Characterization Data of PTMA and PTMA-co-PS Prepared by NMP

[TMPMA]: [styrene]	T (°C)	Conv. (%) ^a	t (h)	M_n (g/mol) ^b	M_w (g/mol) ^b	PDI
1:0	120	21	6	5,800	10,400	1.78
9:1	120	12	6	6,500	17,500	1.45
1:0	90	17	6	9,600	9,500	1.81
9:1	90	13	6	11,100	15,900	1.43

^a Conversions determined by GC.^b Molar mass determined by SEC (CHCl₃, PS calibration).

mixture did not slow down the reaction, concluding that a higher amount of the free nitroxide is formed during the preheating step. To obtain results that can be compared with the preheating procedure, the reaction was not quenched before 16 hours of reaction time. The polymer formed exhibits a molar mass and a monomer conversion similar to the polymer prepared without additional SG-1.

Considering the results of the NMP polymerization of TMPMA and TMPA as a whole, it appears that this radical polymerization technique is not suitable to prepare the precursor polymers in a controlled manner. In view of the general restraints of the NMP of (meth)acrylates the choice of another polymerization technique was required.

Atom Transfer Radical Polymerization

N,N,N',N'',N'''-Pentamethyldiethylenetriamine (PMDETA) was chosen for the polymerization of TMPMA in combination with copper(I) bromide and the initiator ethyl 2-bromoisobutyrate. First experiments were conducted in anisole at 130 °C. The polymer obtained revealed a molar mass of $M_n = 3,500$ g/mol and a PDI value of 1.51 (SEC, DMAc, PS calibration), indicating poor control over the polymerization process. The ideal reaction temperature, which was consequently used for all additional experiments, was found to be

TABLE 2 Selected Polymerization Conditions and Characterization Data of PTMA and PTA Prepared by NMP

Monomer	Conv. (%) ^a	t (h)	M_n (g/mol) ^b	M_w (g/mol) ^b	PDI
TMPMA	22	6	5,900	10,600	1.80
TMPA	91	6	3,900	5,900	1.51
TMPA ^c	5	4	3,700	4,600	1.24
TMPA ^c	28	16	13,900	21,500	1.55
TMPA ^d	92%	16	3,800	6,400	1.69

^a Conversion determined by GC.^b Molar mass determined by SEC (CHCl₃, PS calibration).^c Preheating of the initiator.^d Addition of free SG-1.

90 °C. The resulting polymer **P4** exhibits a molar mass of $M_n = 33,900$ g/mol while having a PDI value of 1.14 (20% yield).

For further investigations of the living character kinetic studies were conducted (Figs. 3 and 4). When using PMDETA as ligand, the reaction stopped after about 3 hours of reaction time and a monomer conversion of 15% (GC). All samples taken after this point of time revealed no significant change of the molar mass of polymers and the monomer conversion, respectively. To ensure that no contamination occurred when sampling the reaction mixture the polymerization of a monomer stock-solution was carried out in five separate microwave vials and each vial was only probed once. As a consequence, any disturbance of the reaction can be ruled out as origin of the early termination.

From literature it is known that the use of highly active ligands, such as Me₆TREN, entail equilibrium constants too high to achieve a controlled ATRP polymerization of methacrylates.²⁴ With the intention to rule out the catalyst system as possible source of the polymerization's termination two less reactive ligands, *N*-(pyridin-2-ylmethylene)ethanamine (PMEA) and 2,2'-bipyridine (bpy), were tested. Using bpy resulted in similar values as the use of PMDETA does. When

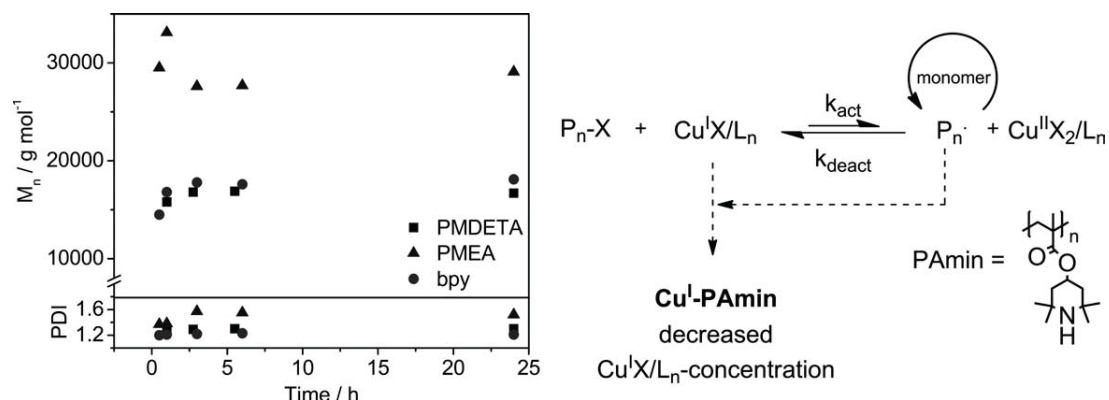


FIGURE 3 Molar masses and PDI values (SEC in DMAc, PS calibration) of the amine bearing precursor polymer PTMA, which was prepared by ATRP using three different ligands, as a function of reaction time (left). Schematic representation of the proposed deactivation mechanism of the polymerization of the amine bearing monomer TMPMA by ATRP (right). The complexation of copper by the growing polymer chain inhibits the activation of the dormant species.

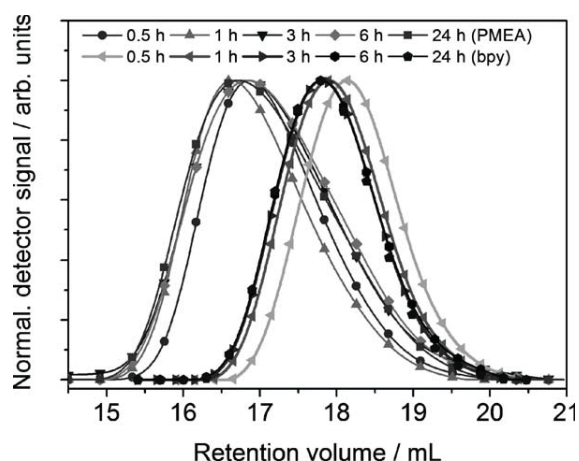


FIGURE 4 SEC traces (DMAc) of the kinetic study of the polymerization of the monomer TMPMA by the ATRP technique using *N*-(pyridin-2-yl-methylene) ethanamine (PMEA) and 2,2'-bipyridine (bpy) as ligand for the catalyst system.

using PMEAs as ligand, the reaction terminated after 3 hours and 18% conversion. Furthermore, the PDI value increased to 1.5 and the molar mass decreased to $M_n = 27,600$ g/mol after it had already reached 31,100 g/mol. These observations indicate poor control over the polymerization kinetics when PMEAs is used since side reactions occur, for example, chain transfer.

Because the use of three different catalysts showed comparable results, the catalyst system can be eliminated as possible reason for the termination of the polymerization after 15 to 20% of monomer conversion. It is more reasonable to assume that the growing polymer chain itself inhibits the reaction as illustrated in Figure 3: The polymer formed exhibits an amine functionality in every single repeating unit and may also act as chelating agent forming a complex with the copper ions of the catalyst system (Cu^{I} -PAMin). Thereby,

the active catalyst is removed from the equilibrium resulting in a decrease of the activation rate of the dormant species and a decrease of the overall reaction rate. When no free catalyst is present anymore, the reaction eventually terminates.

This mechanism may also enhance the persistent radical effect. If the total amount of the activating catalyst is lower than the concentration of the chains that terminate, for example, because it formed a complex with the growing polymer chain, the polymerization will stop at low conversion since all of the catalyst is present as a persistent radical.²⁵

In an additional reaction step polymer **P4** was oxidized with hydrogen peroxide/sodium tungstate according to the procedure explained before. Thereby the molar mass, as determined by SEC measurement (DMAc, PS calibration), decreased from $M_n = 33,900$ g/mol to 26,300 g/mol while the PDI value increased from 1.14 to 1.31 for the oxidized polymer **P4ox** (Fig. 5, left). This change is an indicator for degradation reactions taking place during oxidation of PTMA. Nevertheless, the polymer obtained was soluble in toluene, dichloromethane, tetrahydrofuran, *N*-methylpyrrolidone, and chlorobenzene, making it processable by inkjet printing. Cross-linking phenomena, which hindered the proper processing of the polymer prepared by free radical polymerization, had no significant influence due to the lower molar mass of the polymers.

The precursor polymer **P4** and the radical bearing **P4ox** revealed a good solubility in printable solvents and readily formed films when printed from toluene/*ortho*-dichlorobenzene 90/10 (5 mg/mL). By using toluene as main solvent that has a lower boiling point (111 °C) than NMP a smoother film could be obtained, even though some agglomeration occurred upon drying (Fig. 5, right). It is known that by using a solvent mixture which contains a few percentages of a higher boiling solvent, the coffee-drop-effect, which describes the phenomenon of material accumulation at the rim of a dried feature, can be reduced.²⁶ For this

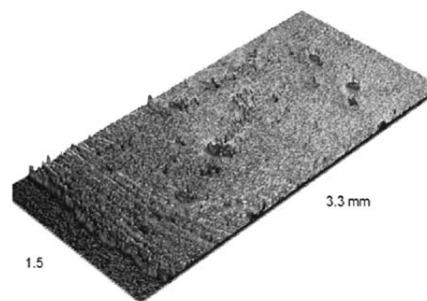
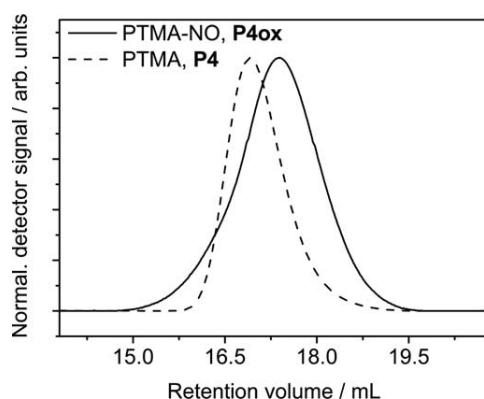


FIGURE 5 SEC trace (DMAc) of the secondary amine bearing precursor polymer **P4** prepared by ATRP and of its oxidized form **P4ox** (left). A shift in the elution volume is clearly visible. Optical profiler image of an inkjet printed film of the stable radical bearing polymer **P4ox** on glass (right). The film was inkjet-printed from toluene/*ortho*-dichlorobenzene (ratio 90/10) at a polymer concentration of 5 mg/mL.

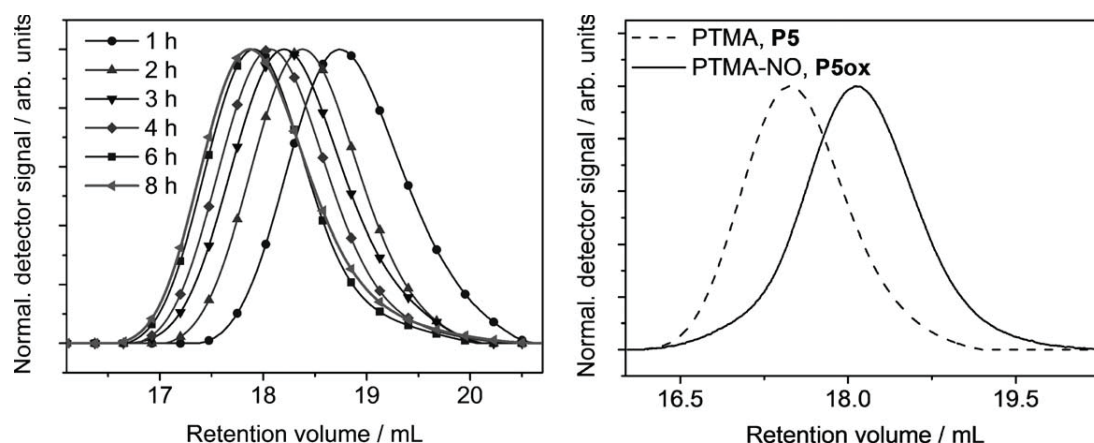


FIGURE 6 SEC traces (DMAc) of the kinetic study of the polymerization of the monomer TMPMA-Cl exhibiting an amine functionality protected by formation of its hydrochloride (left). Comparison of SEC traces (DMAc) of polymer P5 prepared from the protected monomer and of its oxidized polymer P5ox (right).

purpose, *ortho*-dichlorobenzene (179 °C) was used to decrease the coffee-drop-effect and, subsequently, to improve the film formation, but Figure 5 shows that still more material is located at the edge of the film. These results confirm that an enhanced film formation can be obtained from P4 and P4ox in comparison to P1ox, but further investigations need to be done to identify a solvent or solvent system that leads to a film formation without agglomeration and the reduction of a coffee-ring. Although this represents an improvement in comparison to the FRP prepared polymers, a consolidated view of the experimental results indicates that polymerization of TMPMA cannot be the method of choice, since the conversion of the monomer does not exceed 20%.

RAFT Polymerization

Aminolysis of thiocarbonylthio chain transfer agents by primary and secondary amines commonly renders the polymerization of amines impossible. Therefore the polymerization of TMPMA, which bears a secondary amine functionality, appears to be a challenging task. Nevertheless, RAFT polymerization of the hydrochloride TMPMA-Cl 3 and even of the free amine bearing TMPMA 1 is possible.

Polymerization of the Hydrochloride TMPMA-Cl

Hydrolysis of the chain transfer agent represents a known problem of RAFT polymerization in aqueous media. In particular basic conditions facilitate the hydrolysis of thiocarbonylthio compounds, while they are rather stable in an acidic environment.²⁷ To take advantage of the only moderately decreased stability in acidic media a polymerization of TMPMA in water/ethanol (1:3) adjusted to pH = 2 with hydrochloric acid was performed, generating the desired TMPMA-Cl hydrochloride *in situ*. The reaction was carried out at 50 °C using 2-cyano-2-butyl dithiobenzoate (CBDB) as chain transfer agent (CTA 1) and VA067 as initiator. Nevertheless, only 5% monomer conversion were observed after 22 hours of reaction time ($M_n = 13,100$ g/mol, PDI = 1.35). This is an indication of termination reactions, most likely hydrolysis of the chain transfer agent due to the low pH value.

Since a polymerization at a low pH value with *in situ* generation of the hydrochloride resulted in hydrolysis, TMPMA-Cl was prepared in advance and the polymerization was conducted at an increased pH value of 5.5 in phosphate buffer/ethanol (3:1). After 23 hours reaction time a well-defined polymer ($M_n = 5,400$ g/mol, PDI = 1.17) with a yield of 60% was obtained. This proves that polymerization of TMPMA-Cl hydrochloride is possible in slightly acidic environments using CBDB as chain transfer agent.

A mixture of water and ethanol is required to ensure the solubility of all reactants. When using phosphate buffer as aqueous component the ethanol fraction has to be kept low to ensure the stability of the buffer. This is prejudicial to the other reactant's solubility. For this reason polymerization in water/ethanol (1:3) is desirable. When polymerizing TMPMA-Cl in unbuffered water/ethanol the pH ranges between six and three, enabling smooth polymerization of the monomer. The well-defined polymer P5 ($M_n = 24,500$ g/mol, PDI = 1.18) was obtained in 90% yield after deprotonation and oxidized according to the procedure described earlier. As for ATRP the molar mass of the oxidized polymer P5ox decreases upon oxidation to 16,100 g/mol, this may be attributed to degradation reactions or a change in the polymer's hydrodynamic volume (Fig. 6). In contrast to the ATRP polymer P4ox the polymer P5ox did not show an increase of the PDI upon oxidation. The polymer obtained is soluble in dichloromethane, tetrahydrofuran, *N*-methylpyrrolidone, and chlorobenzene making it processable by inkjet printing (*vide infra*).

The polymerization of TMPMA-Cl in water/ethanol (1:3) with CBDB and VA067 as well as subsequent deprotonation can be established as standard procedure for the preparation of PTMA by the RAFT technique. To gain further understanding of the reaction a kinetic study was carried out (Figs. 6 and 7).

Following pseudo first order kinetics the data revealed a linear behavior in the semilogarithmic kinetic plot (Fig. 7, left). This

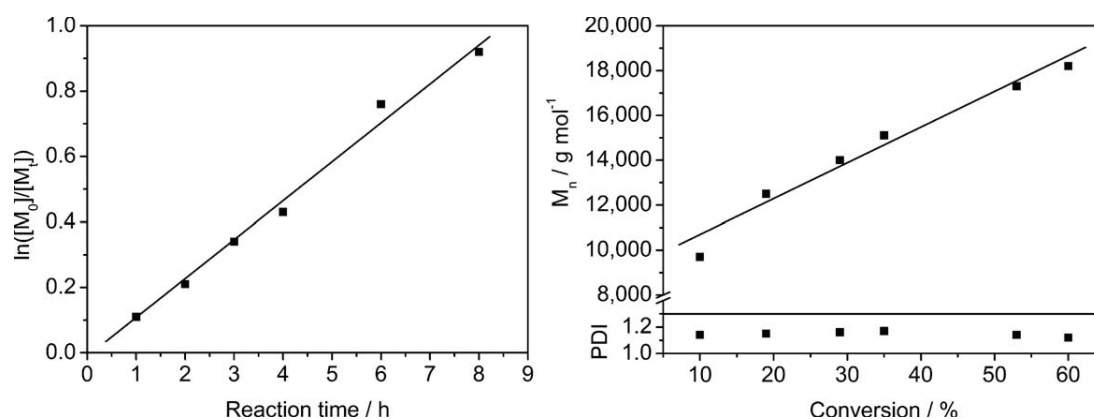


FIGURE 7 Kinetics plots of the RAFT polymerization of the monomer TMPMA-Cl exhibiting an amine functionality protected by formation of its hydrochloride. Monomer concentration determined by ¹H NMR spectroscopy (DMSO-d₆; 300 MHz); M_n and PDI values determined by SEC in DMAc, PS calibration.

indicates a constant radical concentration throughout the reaction due to the absence of termination processes. Moreover, the molar mass of the polymer increases linearly with increasing monomer conversion as illustrated in Figure 7, right. Concluding from the y-intercept being at $M_n = 8,900$ g/mol and not at zero, the initializing radicals add several monomers before the main equilibrium is established. In summary one can state that the RAFT polymerization of TMPMA-Cl can be performed in a controlled manner.

Polymerization of the Free Amine Bearing TMPMA

Aminolysis of the chain transfer agent represents a fundamental problem. Nevertheless, RAFT polymerization of TMPMA, which is bearing a secondary amine functionality, is possible. This exceptional property of TMPMA can be attributed to the steric hindrance of the amine functionality as well as solvent effects: The basicity of a nucleophile is generally raised while its nucleophilicity decreases upon increased steric hindrance, on the one hand. On the other hand, the nucleophile TMPMA is further stabilized by a polar solvent, resulting in decreased reactivity. While the polymerization in

apolar aprotic solvents like toluene is not successful, the use of water/ethanol (1:3) enables the polymerization, because the amine is stabilized through the formation of hydrogen bonds.

Nevertheless, polymerization is only possible if the initiator concentration is raised in comparison to standard RAFT conditions. While the experiments presented before were carried out at a monomer to chain transfer agent to initiator ratio of 80:1:0.33, the polymerization of free amine bearing TMPMA had to be performed at ratios of 80:1:0.5 to even 80:1:1. At lower initiator concentration proper and reproducible initiation of the polymerization is not ensured.

Although the initiator concentration of the latter reaction was twice the concentration of the chain transfer agent, it proceeded in a controlled manner up to conversions of 85%, as proven by a kinetic study (P6; Figs. 8 and 9). At higher conversions termination reactions occurred and the reaction did not follow pseudo first order kinetics anymore. As a consequence, the semilogarithmic kinetic plot exhibited no linear behavior after 2 hours of reaction time (equates 85%

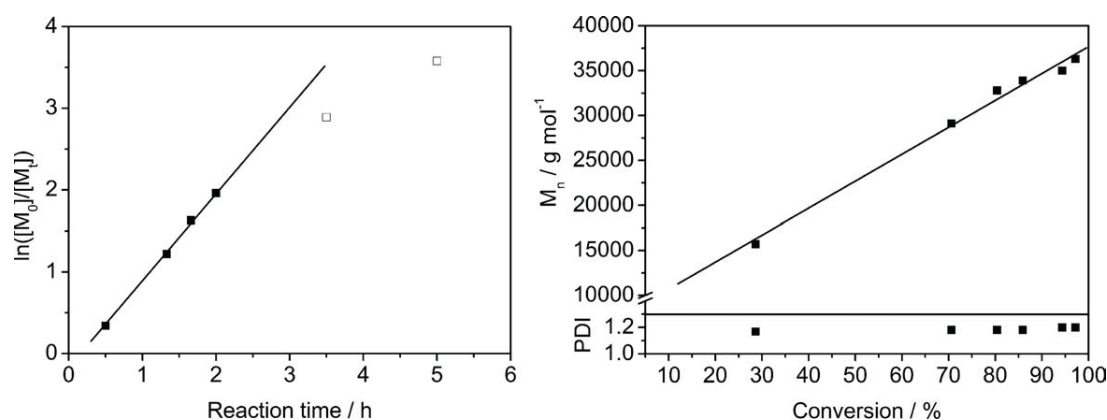


FIGURE 8 Kinetics plots of the polymerization of the free amine bearing monomer TMPMA by the RAFT technique using a dithiobenzoate-type chain transfer agent (CTA 1). Monomer concentration determined by ¹H NMR spectroscopy (DMSO-d₆; 300 MHz); M_n and PDI values determined by SEC in DMAc, PS calibration.

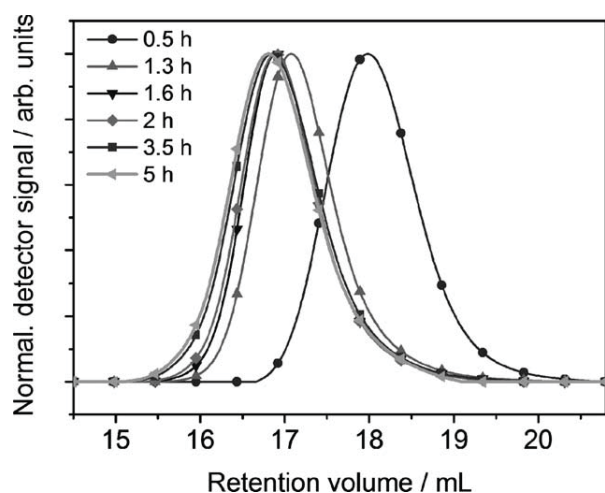


FIGURE 9 SEC traces (DMAc) of the kinetic study of the polymerization of the monomer TMPMA exhibiting an amine functionality via the RAFT technique using a dithiobenzoate-type chain transfer agent (CTA 1).

conversion). Nonetheless, full conversion could be reached in 5 hours yielding a well-defined, low-PDI polymer **P6**.

To reference the results of the SEC measurement, a mere relative method for molar mass determination, the absolute molar mass of the polymer **P6** was determined by vapor pressure osmometry in chloroform revealing a value of $M_n = 5,700$ g/mol. This result indicates an overestimation of the material's molar mass determined by SEC ($M_n = 24,500$ g/mol). The same holds true for the corresponding radical polymer **P6ox** that was obtained by oxidation of **P6** with hydrogen peroxide/ $\text{Na}_2\text{WO}_4 \times 2\text{H}_2\text{O}$. Although SEC indicated a shift in the molar mass from $M_n = 24,500$ to 16,100 g/mol, vapor pressure osmometry measurements prove this to be a only an effect attributed to a change in the materials hydrodynamic volume, as the molar mass is, as expected, slightly increased upon oxidation ($M_n = 5,900$ g/mol). Further verification by absolute SEC techniques, for example, using a multiangle laser light scattering (MALS) detector, were not successful due to the low molar mass of these polymers.

The cyclic voltammogram of the oxidized polymer **P6ox** revealed a distinct and reversible redox reaction at 0.38 V (vs. Fc/Fc^+) that has been absent in the corresponding monomer TMPMA and the precursor polymer **P6**, respectively (Fig. 11). The reaction can be attributed to the oxidation of the free radical units to the related oxammonium cations. This highly reversible and fast redox reaction is of special interest in the development of organic radical batteries.²⁸

Applying the developed technique well-defined polymers with varying molar masses (M_n) covering the area from 3,000 to 25,000 g/mol could be prepared (Table 3). While increased temperatures lead to lower reaction times the disadvantage of obtaining less well-defined polymers becomes obvious.

A MALDI-TOF mass spectrum of the low molar mass polymer revealed the expected variations of the desired distributions (Fig. 10). Cleavage of the dithiobenzoate-type CTA occurs during the measurement which is known in literature for this type of end group. In addition partial cleavage of the side group can be observed.

The precursor polymer **P6** and the radical bearing **P6ox** show a good solubility and form homogeneous films with a thickness of 200 nm when inkjet printed from toluene/*ortho*-dichlorobenzene 90/10 (5 mg/mL). No agglomeration was observed yielding much improved results in comparison to the polymers prepared by the other polymerization techniques (Fig. 11). The polymer films, readily usable in a variety of applications, can be prepared with various film thicknesses and shapes by changing the concentration of the printed solutions or varying the drop-to-drop distance of the deposited droplets.

Besides the described dithiobenzoate CTA a trithiocarbonate RAFT agent was applied for the polymerization of TMPMA. Using 4-cyano-4-(dodecylsulfanylthiocarbonyl)sulfanyl pentanoic acid (CTA 2) increased the control over the polymerization. While preparation of low molar mass polymers ($M_n = 3,800$ g/mol; PDI = 1.13) enabled the analysis via MALDI-TOF mass spectrometry, the synthesis of polymers with higher molar mass ($M_n = 15,400$ g/mol; PDI = 1.17) was possible as well without losing control over the polymerization. A kinetic study indicating the controlled character of the polymerization is depicted in Figures 12 and 13.

The MALDI-TOF mass spectrum of the polymers prepared by RAFT polymerization using the trithiocarbonate type CTA 2 shows several distributions, which, however, can be assigned to the desired structure with an increasing loss of the TMP-side groups (Fig. 14). This is probably caused by the MALDI-TOF MS measurement process itself due to the higher laser energy which is necessary to desorb the polymer.

EXPERIMENTAL

Materials and Preparation

All chemicals and solvents were received from Aldrich, Fluka and Acros. Unless otherwise stated, the chemicals and solvents were used without further purifications.

2,2,6,6-Tetramethylpiperidin-4-yl methacrylate (1)

To 2,2,6,6-Tetramethylpiperidin-4-ol (100 g, 0.64 mol) in dry dichloromethane (500 mL) were added *N,N*-dimethylpyridin-

TABLE 3 Characterizing Data of PTMA Prepared via RAFT Polymerization

[TMPMA]/[CTA]	T (°C)	t (h)	M_n (g/mol) ^a	PDI
25	50	24	3,100	1.18
100	50	13	11,000	1.21
100	70	4	25,200	1.31

^a Molar mass determined by SEC (DMAc, PS calibration).

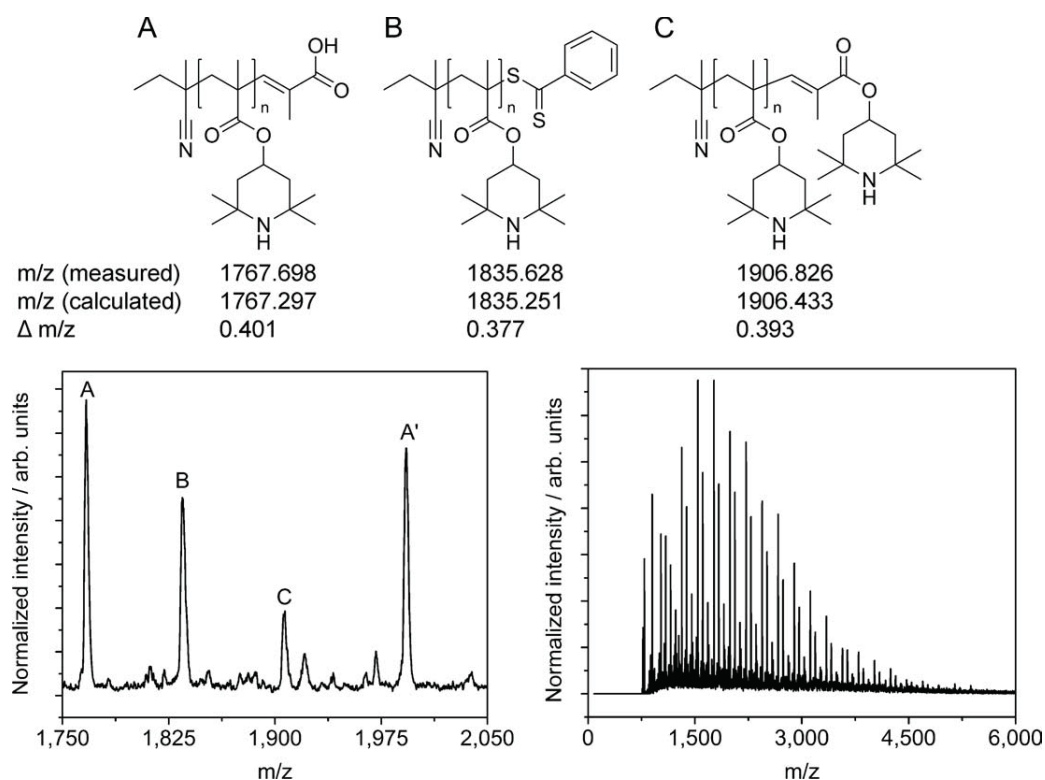


FIGURE 10 MALDI-TOF mass spectrum of the free secondary amine bearing polymer PTMA prepared via RAFT polymerization using a dithiobenzoate type chain transfer agent; matrix: *trans*-3-indoleacrylic acid; reflector mode (bottom) and assigned structures as well as m/z values for the exemplary structure $n = 7 + \text{Na}^+$ (top).

4-amine (7.8 g, 64 mmol) and dry triethylamine (180 mL) under argon atmosphere. Methacrylic anhydride (98 g, 0.64 mol), dissolved in dry dichloromethane (150 mL), was added dropwise under stirring. After stirring the mixture for 40 hours at room temperature the solution was washed twice with saturated aqueous sodium carbonate solution

(250 mL) and brine (250 mL). The organic layer was dried over magnesium sulfate, filtered, and evaporated. Recrystallization from cyclohexane gave **1** (83 g, 58% yield) as a white powder (alternative purification: flash silica gel column chromatography using hexane and ethyl acetate with 3% of methanol as eluent).

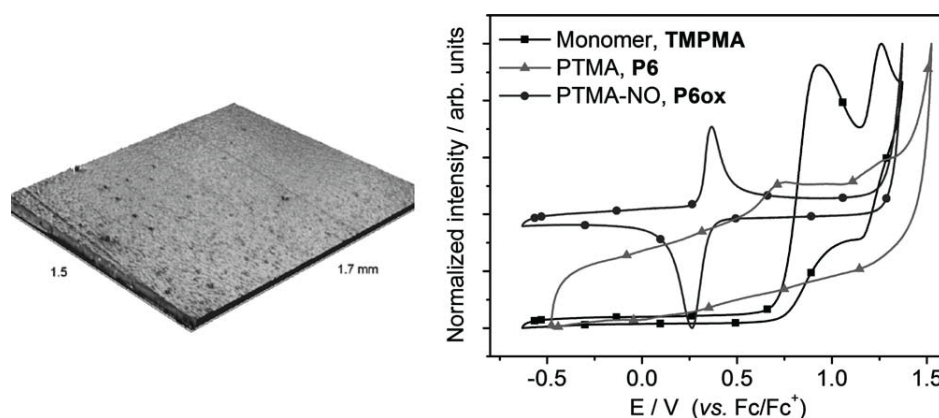


FIGURE 11 Optical profiler image of an inkjet printed film of the radical bearing polymer **P6ox** prepared from an amine precursor polymer **P6** by the RAFT technique and subsequent oxidation (left). The film was inkjet-printed on glass from toluene/*ortho*-dichlorobenzene (ratio 90/10) at a polymer concentration of 5 mg/mL. Cyclic voltammograms of the amine bearing polymer PTMA (**P6**), the stable radical bearing polymer PTMA-NO (**P6ox**), and the corresponding monomer (TMPMA) in CH_2Cl_2 , 200 mV/s, 0.1 mol/L TBAPF₆ (right).

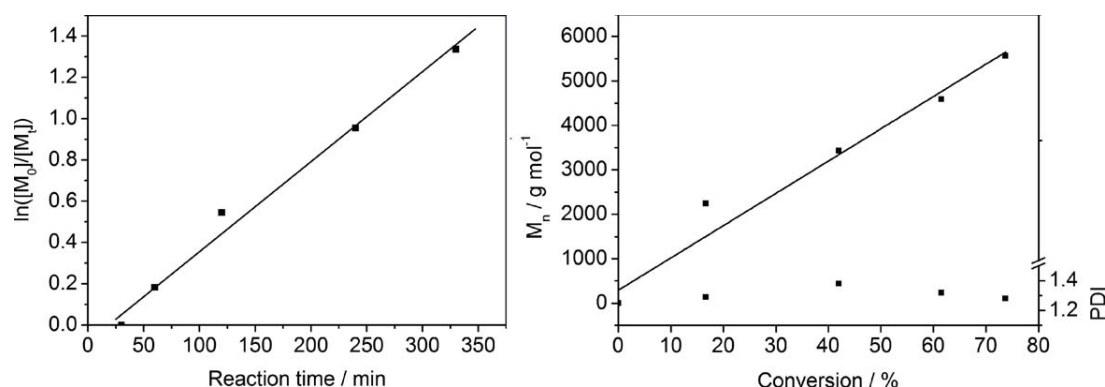


FIGURE 12 Kinetics plots of the polymerization of TMPMA by RAFT using a trithiocarbonate type chain transfer agent (CTA 2). Monomer concentration determined by ^1H NMR spectroscopy (300 MHz); M_n and PDI determined by SEC in DMAc, PS calibration.

^1H NMR (250 MHz, CDCl_3 , δ , ppm): 1.19 (m, 14H; $4\times\text{CH}_3$, CH_2), 1.96 (m, 5H; $\text{CH}_2=\text{C}-\text{CH}_3$, CH_2), 5.24 (m, 1H; $\text{CH}-\text{O}$), 5.53 (s, 1H; $\text{C}=\text{CH}_2$), 6.07 (s, 1H; $\text{C}=\text{CH}_2$). ^{13}C NMR (63 MHz, CDCl_3 , δ , ppm): 18.2 ($\text{CH}_2=\text{C}-\text{CH}_3$), 29.1 ($2\times\text{CH}_3$), 34.7 ($2\times\text{CH}_3$), 43.8 ($2\times\text{C}_q$), 51.4 ($2\times\text{CH}_2$), 69.1 ($\text{CH}-\text{O}$), 124.9 ($\text{C}=\text{CH}_2$), 136.8 ($\text{ROOC}-\text{C}=\text{C}$), 166.9 (COOR). FTIR (ATR, cm^{-1}): 752 (s), 945 (s), 972 (s), 1165 (vs, $\nu_{\text{as}}(\text{O}-\text{CC}=\text{O})$), 1300 (s, $\nu_{\text{as}}(\text{CC}=\text{O})$), 1365 (m, $\delta_s(\text{CH}_3)$), 1456 (w, $\delta(\text{CH}_2)$), 1633 (m, $\nu(\text{C}=\text{CH}_2)$), 1701 (vs, $\nu(\text{C}=\text{O})$), 2970 (m, $\nu(\text{CH})$), 2999 (w, $\nu(\text{CH})$), 3300 (w, $\nu(\text{NH})$). MS (EI, 70 eV) m/z : 107 (9), 124 (100), 410 (3), 210 (6), 225 (0.3, M^+). Anal. calcd. for $\text{C}_{13}\text{H}_{23}\text{NO}_2$: C, 69.29; H, 10.29; N, 6.22; found: C, 69.22; H, 10.53; N, 5.93.

2,2,6,6-Tetramethylpiperidin-4-yl acrylate (2)

Acrylic anhydride was freshly prepared following a literature procedure by the reaction of acrylic acid with sodium hydride and acryloyl chlorid.¹⁸

To 2,2,6,6-tetramethylpiperidin-4-ol (5.0 g, 31.8 mmol) in dry dichloromethane (50 mL) and dry triethylamine (10 mL) *N,N*-dimethylpyridin-4-amine (390 mg, 3.18 mmol) was added. The mixture was stirred at room temperature while acrylic anhydride (4.0 g, 31.8 mmol), dissolved in dry dichloromethane (10 mL), were added dropwise. Subsequently, the reaction was quenched after 20 hours by the addition of saturated aqueous sodium carbonate solution (30 mL). The organic layer was washed twice with aqueous sodium carbonate solution (50 mL) and brine (50 mL), dried over calcium sulfate, and evaporated to dryness. The crude product was purified by flash silica gel column chromatography using hexane and ethyl acetate with 3% of methanol as eluent to give **2** (1.96 g, 30% yield).

^1H NMR (250 MHz, CDCl_3 , δ , ppm): 1.21 (m, 14H; $4\times\text{CH}_3$, CH_2), 1.96 (m, 2H; CH_2), 5.27 (m, 1H; $\text{CH}-\text{O}$), 5.80 (dd, $^2J(\text{H,H}) = 1.6$ Hz, $^3J(\text{H,H}) = 10.3$ Hz, 1H; $\text{CH}=\text{CH}_2$), 6.11 (dd, $^3J(\text{H,H}) = 10.3$ Hz, 17.3 Hz, 1H; $\text{CH}_2=\text{CH}$), 6.39 (dd, $^2J(\text{H,H}) = 1.6$ Hz, $^3J(\text{H,H}) = 10.3$ Hz, 1H; $\text{CH}=\text{CH}_2$). ^{13}C NMR (63 MHz, CDCl_3 , δ , ppm): 29.0 ($2\times\text{CH}_3$), 34.8 ($2\times\text{CH}_3$), 43.9 ($2\times\text{CH}_2$), 51.4 ($2\times\text{C}_q$), 69.0 ($\text{CH}-\text{O}$), 129.0 ($\text{CH}_2=\text{CH}$), 130.3 ($\text{CH}_2=\text{CH}$), 165.7 (COOR). FTIR (ATR, cm^{-1}): 719 (m), 813 (s, $\nu(\text{C}=\text{CH}_2)$), 981 (s), 972 (s), 1055 (vs, $\nu_{\text{as}}(\text{OCC}=\text{O})$), 1190

(m), 1278 (s, $\nu_{\text{as}}(\text{CC}=\text{O})$), 1366 (m, $\delta_s(\text{CH}_3)$), 1452 (w, $\delta(\text{CH}_2)$), 1616 (m, $\nu(\text{C}=\text{CH}_2)$), 1701 (vs, $\nu(\text{C}=\text{O})$), 2972 (m, $\nu(\text{CH})$), 3005 (m, $\nu(\text{CH})$), 3315 (w, $\nu(\text{NH})$). MS (EI, 70 eV) m/z : 107 (10), 124 (100), 196 (6), 211 (0.2, M^+). Anal. calcd. for $\text{C}_{12}\text{H}_{21}\text{NO}_2$: C, 68.21; H, 10.02; N, 6.63; found: C, 68.21; H, 10.16; N, 6.27.

4-(Methacryloyloxy)-2,2,6,6-tetramethylpiperidinium chloride (3)

To TMPMA (50 g, 0.22 mol) dissolved in ethanol (250 mL) hydrochloric acid (4.1 mol/L, 65 mL, 0.27 mol) were slowly added at room temperature. The solution was stirred for 1 hour, evaporated to dryness, and the product was dried at 80 °C (20 mbar) to give **3** (58 g, 99% yield).

^1H NMR (250 MHz, $\text{DMSO}-d_6$, δ , ppm): 1.45 (m, 12H; CH_3), 1.71 (m, 2H; CH_2), 1.86 (s, 3H; $\text{CH}_2=\text{C}-\text{CH}_3$), 2.02 (m, 2H; CH_2), 5.16 (m, 1H; $\text{CH}-\text{O}$), 5.70 (s, 1H; $\text{C}=\text{CH}_2$), 6.01 (s, 1H; $\text{C}=\text{CH}_2$), 8.55 (d, $^2J(\text{H,H}) = 11$ Hz, 1H; NH_2), 9.35 (d, $^2J(\text{H,H}) = 11$ Hz, 1H; NH_2). ^{13}C NMR (63 MHz, $\text{DMSO}-d_6$, δ , ppm): 18.3 ($\text{CH}_2=\text{C}-\text{CH}_3$), 25.7 ($2\times\text{CH}_3$), 29.4 ($2\times\text{CH}_3$), 39.5

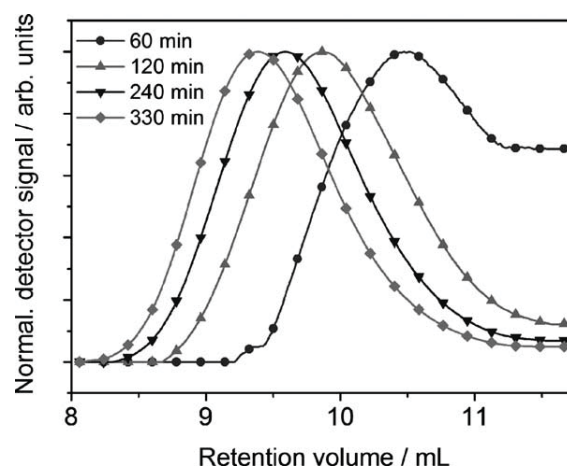


FIGURE 13 SEC traces (DMAc) of the kinetic study of the polymerization of the monomer TMPMA exhibiting an amine functionality via the RAFT technique using a trithiocarbonate type chain transfer agent (CTA 2).

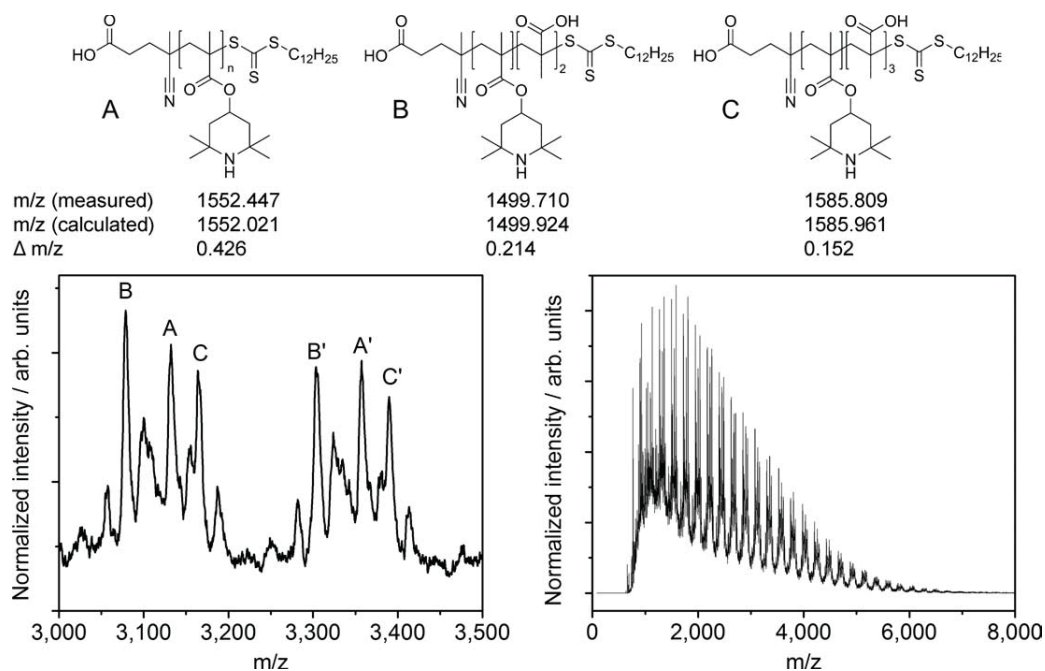


FIGURE 14 MALDI-TOF mass spectrum of the free secondary amine bearing polymer PTMA prepared via RAFT polymerization using a trithiocarbonate type chain transfer agent (CTA2); matrix: *trans*-3-indoleacrylic acid; linear mode (bottom) and assigned structures as well as m/z values for the exemplary structure $n = 5 + \text{Na}^+$ (top).

($2 \times C_q$), 56.9 ($2 \times CH_2$), 66.23 (CH—O), 126.6 (C=CH₂), 136.2 (ROOC—C=C), 166.2 (COOR). FTIR (ATR, cm⁻¹): 661 (s), 929 (m), 1016 (s), 1047 (s, γ (C=CH₂)), 1170 (vs, ν_{as} (O—CC=O)), 1219 (s, ν_{as} (CC=OO)), 1390 (m, δ_s (CH₃)), 1442 (w, δ (CH₂)), 1587 (m, ν (C=CH₂)), 1705 (vs, ν (C=O)), 2465 (m), 2592 (m), 2738 (bs), 2943 (bs, ν (CH)), 3020 (m, ν (CH)), 3171 (m, ν (NH)). Anal. calcd. for C₁₃H₂₄ClNO₂: C, 59.64; H, 9.24; N, 5.35; Cl, 13.54; found: C, 59.33; H, 9.28; N, 5.24; Cl, 13.76.

Polymerization

The polymerizations were carried out in sealed microwave vials under nitrogen atmosphere. Solutions were degassed by bubbling with nitrogen for 30 minutes. Samples for ¹H-NMR spectroscopy, GC, and SEC measurements were taken under inert conditions via a microliter syringe. Oxidation of the precursor polymer PTMA was generally carried out in methanol with hydrogen peroxide catalyzed by Na₂WO₄.

Free Radical Polymerization

4-(Methacryloyloxy)-2,2,6,6-tetramethylpiperidinium chloride (58.0 g, 0.22 mol) were dissolved in a mixture of ethanol (90 mL) and water (90 mL). After degassing the solution with argon 2,2'-azobis(2-methyl-propionamide) dihydrochloride (2.0 g, 7.3 mmol) were added and the mixture was stirred for 3 hours at 50 °C. The viscous solution was diluted with ethanol (300 mL) and added dropwise to a vigorously stirred mixture of chloroform (500 mL) and aqueous sodium hydroxide (500 mL, 1.25 mol/L). The mixture was stirred for 15 hours, the organic layer was subsequently separated and washed with water (500 mL) as well as brine (500 mL).

Precipitation in hexane (2000 mL) yielded 49.7 g PTMA (**P1**) as white powder, which was dried at 40 °C (20 mbar).

Oxidation. PTMA **P1** (25.0 g), disodium ethylenediamine tetraacetate (0.7 g, 1 mmol), and Na₂WO₄·2H₂O (0.4 g, 1.5 mmol) were dissolved in methanol (250 mL). Hydrogen peroxide (150 mL) were added portion wise (40 mL) every 10 hours and the mixture was stirred at room temperature for a total of 48 hours. A red precipitate formed, which was separated and washed thoroughly with water (300 mL) and methanol (300 mL). Upon drying at 40 °C (20 mbar) 24.0 g PTMA-NO (**P1ox**) were obtained.

ATRP. The required amount of copper(I)-bromide, ligand, and half of the required amount of toluene were placed in a microwave vial. In a second vial, (**1**) and the initiator ethyl 2-bromoisobutyrate were dissolved in the other half amount of toluene, required to reach the desired concentration of 1 mol/L. After transferring the degassed monomer/initiator solution to the catalyst solution, the reaction mixture was placed in an oil bath (90 °C).

RAFT. Two stock solutions, one of the chain transfer agent 2-cyano-2-butyl dithiobenzoate (CTA 1) or 4-cyano-4-(dodecylsulfanylthiocarbonyl)sulfanyl pentanoic acid (CTA 2) and the other one of the initiator 2,2'-azobis(2-methyl-propionamide) dihydrochloride, were prepared in 1 mL ethanol/water (3:1). To (**1**) an ethanol/water (3:1) mixture was added in a microwave vial to reach the desired concentration of 1 mol/L. After the addition of the required amount of initiator and CTA solution (monomer/initiator/CTA ratio 80:1:4), the vial was sealed, degassed, and placed in an oil bath (60 °C).

NMP. Procedure I: 0.15 g of **(1)** or **(2)** and BlocBuilder™ (ratio 100:1) were placed in a microwave vial. After the addition of anisole (1 mol/L), the vial was sealed, degassed, and placed in an oil bath (90 or 120 °C). Procedure II: 0.15 g of **(1)** or **(2)**, BlocBuilder™ (ratio 100:1), and SG-1 free radical (0.1% related to BlocBuilder™) were placed in a microwave vial. After the addition of anisole (1 mol/L), the vial was sealed, degassed, and placed in an oil bath preheated at 120 °C. Procedure III: BlocBuilder™ (ratio 100:1) was dissolved in anisole and placed in a sealed microwave vial. In a second microwave vial, 0.15 g of **(2)** was dissolved in anisole (1 mol/L). Subsequently, the degassed BlocBuilder™ solution was placed in an oil bath preheated to 60 °C. After 40 minutes the temperature was raised to 120 °C and the degassed solution of **(2)** was transferred to the preheated BlocBuilder™ solution.

Analytical Data of the Printed Polymers. P1: SEC (DMAc, PS-standard): $M_n > 300,000$ g/mol (exclusion limit of the SEC column). SEC (THF/NEt₃, univ. calibration): $M_n = 60,000$ g/mol. ¹H NMR (300 MHz, CDCl₃, δ , ppm): 0.65–1.55 (17H), 1.60–2.40 (4H), 5.06 (1H). FTIR (ATR, cm⁻¹): 970 (m), 1152 (vs, $\nu_{\text{as}}(\text{OCC}=\text{O})$), 1236 (s, $\nu_{\text{as}}(\text{CC}=\text{OO})$), 1377 (m, $\delta_{\text{s}}(\text{CH}_3)$), 1456 (m, $\delta(\text{CH}_2)$), 1718 (vs, $\nu(\text{C}=\text{O})$), 2960 (m, $\nu(\text{CH})$), 3332 (m), 3427 (m, $\nu(\text{NH})$). Anal. calcd. for repeating unit: C, 69.29; H, 10.29; N, 6.22; found: C, 68.17; H, 10.36; N, 6.33. $T_g = 143$ °C.

P1ox: SEC (DMAc, PS-standard): $M_n > 300,000$ g/mol (exclusion limit of the SEC column; only soluble portion of polymer tested). FTIR (ATR, cm⁻¹): 966 (w), 1141 (vs, $\nu_{\text{as}}(\text{OCC}=\text{O})$), 1238 (m, $\nu_{\text{as}}(\text{CC}=\text{OO})$), 1364 (m, $\nu(\text{N}-\text{O})$), 1463 (m, $\delta(\text{CH}_2)$), 1724 (s, $\nu(\text{C}=\text{O})$), 2974 (m, $\nu(\text{CH})$). Anal. calcd. for repeating unit: C, 64.97; H, 9.23; N, 5.83; found: C, 64.62; H, 9.49; N, 5.51. ESR: $g = 2.0062$, $N_s = 4.02 \times 10^{21}$ g⁻¹. $T_g = 168$ °C.

P4: ¹H NMR (300 MHz, CDCl₃, δ , ppm): 0.65–1.55 (17H), 1.60–2.40 (4H), 5.06 (1H). SEC (DMAc, PS-standard): $M_n = 33,900$ g/mol; $M_w = 38,800$ g/mol; PDI = 1.14. FR-IR (ATR, cm⁻¹): 970 (m), 1148 (vs, $\nu_{\text{as}}(\text{OCC}=\text{O})$), 1238 (s, $\nu_{\text{as}}(\text{CC}=\text{OO})$), 1377 (m, $\delta_{\text{s}}(\text{CH}_3)$), 1460 (m, $\delta(\text{CH}_2)$), 1720 (vs, $\nu(\text{C}=\text{O})$), 2956 (m, $\nu(\text{CH})$). Anal. calcd. for repeating unit and bromine end-group: C, 67.93; H, 10.08; N, 6.09; Br, 1.56; found: C, 67.74; H, 10.08; N, 6.06; Br, 1.51. $T_g = 113$ °C.

P4ox: SEC (DMAc, PS-standard): $M_n = 26,300$ g/mol; $M_w = 34,700$ g/mol; PDI = 1.31. FTIR (ATR, cm⁻¹): 964 (w), 1144 (vs, $\nu_{\text{as}}(\text{OCC}=\text{O})$), 1232 (m, $\nu_{\text{as}}(\text{CC}=\text{OO})$), 1364 (m, $\nu(\text{N}-\text{O})$), 1464 (m, $\delta(\text{CH}_2)$), 1724 (s, $\nu(\text{C}=\text{O})$), 2974 (m, $\nu(\text{CH})$). Anal. calcd. for repeating unit and bromine end-group: C, 57.75; H, 8.20; N, 5.18; found: C, 57.36; H, 8.51; N, 5.10. ESR: $g = 2.0064$, $N_s = 1.09 \times 10^{21}$ g⁻¹. $T_g = 162$ °C.

P6: SEC (DMAc, PS-standard): $M_n = 24,500$ g/mol; $M_w = 29,100$ g/mol; PDI = 1.18. Vapor pressure osmometry (CHCl₃): $M_n = 5720$ g/mol. ¹H NMR (300 MHz, CDCl₃, δ , ppm): 0.65–1.55 (17H), 1.60–2.30 (4H), 5.06 (1H). FTIR (ATR, cm⁻¹): 970 (m), 1147 (vs, $\nu_{\text{as}}(\text{OCC}=\text{O})$), 1238 (s, $\nu_{\text{as}}(\text{CC}=\text{OO})$), 1377 (m, $\delta_{\text{s}}(\text{CH}_3)$), 1460 (m, $\delta(\text{CH}_2)$), 1720 (vs, $\nu(\text{C}=\text{O})$), 2956 (m, $\nu(\text{CH})$). Anal. Calcd. for repeating

unit without endgroups: C, 69.29; H, 10.29; N, 6.22; found: C, 69.06; H, 10.47; N, 6.16. $T_g = 128$ °C.

P6ox: SEC (DMAc, PS-standard): $M_n = 16,100$ g/mol; $M_w = 18,400$ g/mol; PDI = 1.15. Vapor pressure osmometry (CHCl₃): $M_n = 5960$ g/mol. FTIR (ATR, cm⁻¹): 966 (w), 1145 (vs, $\nu_{\text{as}}(\text{OCC}=\text{O})$), 1232 (m, $\nu_{\text{as}}(\text{CC}=\text{OO})$), 1364 (m, $\nu(\text{N}-\text{O})$), 1463 (m, $\delta(\text{CH}_2)$), 1724 (s, $\nu(\text{C}=\text{O})$), 2970 (m, $\nu(\text{CH})$). Anal. Calcd. for repeating unit without endgroups: C, 64.97; H, 9.23; N, 5.83; found: C, 64.03; H, 8.42; N, 5.49. ESR: $g = 2.0064$, $N_s = 1.61 \times 10^{21}$ g⁻¹. $T_g = 160$ °C.

Instrumentation

Size exclusion chromatography (SEC) was used to determine the molar masses and polydispersity indices of the polymer samples with respect to polystyrene standards. Either an Agilent 1200 series system (degasser: Polymer Standard Service Mainz, pump: G1310A, auto sampler: G1329A, oven: Techlab, diode array detector: G1315D, RI detector: G1362A) using a pC/PSS GRAM 1000/30 Å column and dimethylacetamide (+0.21% lithium chloride) as eluent at a flow rate of 1 mL/min (40 °C) or a Shimadzu system (controller: SCL-10A VP, degasser: DGU-14A, pump: LC-10AD VP, auto sampler: SIL-10AD VP, oven: Techlab, UV detector: SPD-10AD VP, RI detector: RID-10A) using a PSS SDV pre/lin S column and chloroform/*iso*-propanol/triethyl-amine [94:2:4] as eluent at a flow rate of 1 mL/min (40 °C). Absolute molar masses were determined on a Shimadzu system (controller: SCL-10A VP, degasser: DGU-14A, pump: LC-10AD VP, auto sampler: SIL-10AD VP, oven: CTO-10A VP, detectors: UVD: SPD-10AD VP, RID: RID-10A, Visco: PSS ETA-2010, MALS: PSS SLD 7000 (BIC) at $\lambda = 635$ nm) using a PSS SDV pre/10⁴/10² Å column and tetrahydrofuran as eluent at a flow rate of 1 mL/min (40 °C). Vapor pressure osmometry was measured on a Knauer vapor pressure osmometer (K 7000) using chloroform solutions (temperature: 30 °C). Conversion was determined by gas chromatography on a Shimadzu GC-2010 (carrier gas helium; flame ionization detector with hydrogen and air as detector gases; Restek Rtx-5 column, 30 m length, 0.25 mm ID, 0.25 μm film thickness, 5% diphenyl polysiloxane 95% dimethyl polysiloxane). NMR spectra were obtained on a Bruker AC 300 spectrometer. The MALDI-TOF MS spectra were measured on an Ultraflex III TOF/TOF (Bruker Daltonics GmbH) equipped with a Nd:YAG laser and a collision cell. All spectra were measured in the positive reflector or linear mode using 2,5-dihydroxy benzoic acid (DHB) or α -cyano-4-hydroxycinnamic acid (CHCA) as matrix. Elementary analysis was performed using a λ EuroVector EuroEA3000 instrument. The inkjet printing experiments were carried out on an Autodrop system (Microdrop Technologies). The printer was equipped with a piezo-based printhead (micropipette system AD-K-501). The inner diameter of the used nozzle was 70 μm . Voltages between 60 and 70 V and pulse lengths between 40 and 50 μs were found as typical print settings to create stable droplets for all tested polymers. Surface topography as well as film thicknesses were measured using an optical interferometric profiler Wyko NT9100 (Veeco, Mannheim, Germany). Electrochemical measurements were performed on an Autolab PGSTAT30 model potentiostat. For

cyclic voltammetry a standard three-electrode configuration, using a platinum-disk working electrode, a platinum-rod auxiliary electrode, and an Ag/AgCl reference electrode. The experiments were carried out in acetonitrile and dichloromethane containing tetra-*n*-butylammonium hexafluorophosphate (0.1 mol/L) and using several scan rates. At the end of each measurement ferrocene was added as an internal standard. Spin concentrations were determined on a X-Band ESR spectrometer (Bruker) using copper bromide as internal standard.

CONCLUSIONS

RAFT polymerization represents the most suitable technique to prepare well-defined, PTMA. Both, the hydrochloride of the monomer TMPMA and even the free secondary amine bearing monomer itself can be polymerized in a controlled manner. Aminolysis of the chain transfer agent, which commonly renders the RAFT polymerization of primary and secondary amines impossible, is no issue in the polymerization of TMPMA. This extraordinary behavior can be attributed to the steric hindrance of the amine functionality as well as stabilizing solvent effects. Opposite to ATRP and NMP, which both show major drawbacks, the RAFT technique enables a practical and fast access to precursor polymers required to produce TEMPO free radical bearing polymers of excellent solubility. This readily allows the preparation of tailor-made polymer-films of defined thickness and shape by means of inkjet printing. Considering the electrochemical and catalytic properties of TEMPO functionalized polymers, the use of these films as printed electrodes for organic radical batteries or as catalytically active layer in a chemical reactor represents promising potential application.

The authors thank Axel Buchholz for SQUID measurements, Christian Friebe for cyclic voltammetry investigations, Bärbel Rambach for ESR measurements, Anja Baumgärtel for MALDI-TOF MS measurements, and the Bundesministerium für Bildung und Forschung (project no. 13N11393), the TAB Thüringen, the TMWAT, as well as the Dutch Polymer Institute (DPI, technology area HTE) for the financial support.

REFERENCES AND NOTES

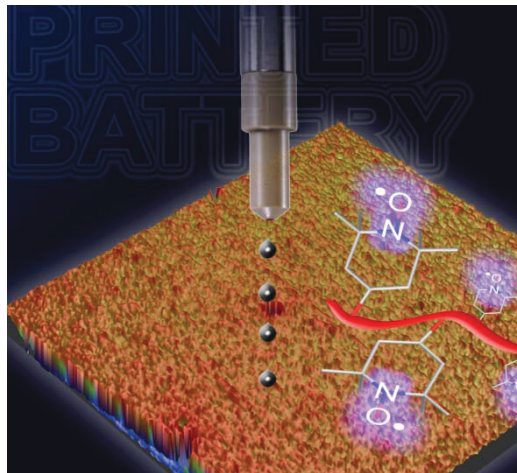
- Moad, G.; Rizzardo, E.; Thang, S. H. *Aust. J. Chem.* **2005**, *58*, 379–410.
- Moad, G.; Rizzardo, E.; Thang, S. H. *Aust. J. Chem.* **2009**, *62*, 1402–1472.
- Barner-Kowollik, C.; Perrier, S. J. *Polym. Sci. Part A: Polym. Chem.* **2008**, *46*, 5715–5723.
- Coessens, V.; Pintauer, T.; Matyjaszewski, K. *Prog. Polym. Sci.* **2001**, *26*, 337–377.
- He, L.; Read, E. S.; Armes, S. P.; Adams, D. J. *Macromolecules* **2007**, *40*, 4429–4438.
- Nakahara, K.; Iriyama, J.; Iwasa, S.; Suguro, M.; Satoh, M.; Cairns, E. J. *Power Sources* **2007**, *165*, 398–402.
- Vekšli, Z.; Miller, W. G. *Macromolecules* **1977**, *10*, 686–692.
- Theato, P.; Schattling, P.; Jochum, F. D. *Chem. Commun.* **2011**, *47*, 8859–8861.
- Kim, J.-K.; Cheruvally, G.; Choi, J.-W.; Ahn, J.-H.; Lee, S. H.; Choi, D. S.; Song, C. E. *Solid State Ionics* **2007**, *178*, 1546–1551.
- Griffith, O. H.; Keana, J. F. W.; Rottschaefer, S.; Warlick, T. A. *J. Am. Chem. Soc.* **1967**, *89*, 5072–5072.
- Tekin, E.; Smith, P. J.; Schubert, U. S. *Soft Matter* **2008**, *4*, 703–713.
- de Gans, B. J.; Duineveld, P. C.; Schubert, U. S. *Adv. Mater.* **2004**, *16*, 203–213.
- Teichler, A.; Eckardt, R.; Hoepfner, S.; Friebe, C.; Perelaer, J.; Senes, A.; Morana, M.; Brabec, C. J.; Schubert, U. S. *Adv. Energ. Mat.* **2011**, *1*, 105–114.
- de Gans, B.-J.; Kazancioglu, E.; Meyer, W.; Schubert, U. S. *Macromol. Rapid Commun.* **2004**, *25*, 292–296.
- Zhuang, X.; Xiao, C.; Oyaizu, K.; Chikushi, N.; Chen, X.; Nishide, H. *J. Polym. Sci. Part A: Polym. Chem.* **2010**, *48*, 5404–5410.
- Nishide, H.; Iwasa, S.; Pu, Y. J.; Suga, T.; Nakahara, K.; Satoh, M. *Electrochim. Acta* **2004**, *50*, 827–831.
- Yonekuta, Y.; Susuki, K.; Oyaizu, K.; Honda, K.; Nishide, H. *J. Am. Chem. Soc.* **2007**, *129*, 14128–14129.
- Cook, G. R.; Beholz, L. G.; Stille, J. R. *J. Org. Chem.* **1994**, *59*, 3575–3584.
- Ihrig, J. L.; Alyea, H. N. *J. Am. Chem. Soc.* **1953**, *75*, 2917–2921.
- Sagawa, S.; Furukawa, J.; Yamashita, S. *Kogyo Kagaku Zasshi* **1969**, *72*, 736–741.
- Volodarsky, L. B.; Reznikov, V. A.; Ovcharenko, V. I. *Synthetic Chemistry of Stable Nitroxides*; CRC Press: Boca Raton, **1994**.
- Nicolas, J.; Dire, C.; Mueller, L.; Belleney, J.; Charleux, B.; Marque, S. R. A.; Bertin, D.; Magnet, S.; Couvreur, L. *Macromolecules* **2006**, *39*, 8274–8282.
- Xia, Q.; Grubbs, R. B. *J. Polym. Sci. Part A: Polym. Chem.* **2006**, *44*, 5128–5136.
- Matyjaszewski, K.; Xia, J. *Chem. Rev.* **2001**, *101*, 2921–2990.
- Braunecker, W. A.; Matyjaszewski, K. *Prog. Polym. Sci.* **2007**, *32*, 93–146.
- Deegan, R. D.; Bakajin, O.; Dupont, T. F.; Huber, G.; Nagel, S. R.; Witten, T. A. *Phys. Rev. E* **2000**, *62*, 756–765.
- Barner-Kowollik, C. *Handbook of RAFT Polymerization*; Wiley-VCH: Weinheim, **2008**.
- Nishide, H.; Koshika, K.; Oyaizu, K. *Pure Appl. Chem.* **2009**, *81*, 1961–1970.

Publication 9

“Reactive Inkjet Printing of Organic Radical Batteries”

Tobias Janoschka, Anke Teichler, Bernhard Häupler, Thomas Jähnert, Martin D. Hager,
Ulrich S. Schubert

Adv. Energy Mater. **2013**, 3, 1025-1028.



Reactive Inkjet Printing of Cathodes for Organic Radical Batteries

Tobias Janoschka, Anke Teichler, Bernhard Häupler, Thomas Jähnert, Martin D. Hager, and Ulrich S. Schubert*

Mobile electrical appliances perpetually require improved batteries. For lightweight and flexible low-cost applications, batteries have to become thin, easy to produce, and also flexible. In this context, printing technology could pave the way for the cost-efficient manufacturing of flexible batteries – comparable to the production of organic solar cells.^[1,2] While printed organic electronics, like organic photovoltaic-powered electrochromic displays^[3] or LED lamps,^[4] receive significant attention, these devices lack flexible organic energy storage and still employ traditional battery concepts.^[5]

Most (printed) batteries rely on metal-based electrode materials, which often show unwanted environmental properties (e.g., release of toxic waste upon mining of metal ores, from landfill disposal sites, and municipal waste combustors); the rapidly evolving class of organic radical batteries (ORB) employs organic polymers as active electrode material.^[6–8] A general problem of printed batteries is the cathode material. In primary cells, the use of manganese dioxide (MnO₂|Zn) is widespread, while secondary cells often employ lithium cobalt oxide (LiCoO₂|Li) or nickel oxyhydroxide (NiOOH|MH). Organic radical batteries, on the other hand, make use of a more environmentally favorable (polymeric) material that carries redoxactive stable radicals, such as 2,2,6,6-tetramethylpiperidine-1-oxyl (TEMPO), **Scheme 1**. The increasing interest in this new class of fast charging, high rate/load capable batteries is reflected in numerous studies with their major focus ranging from polymer design (poly(methacrylate)s,^[9,10] poly(norbornene)s^[11] etc.) and electrolytes (organic carbonates,^[9] water,^[12] ionic liquid)^[11] to the use of suitable conductive additives (vapor grown carbon fibers (VGCF),^[13] graphite,^[9] graphene).^[14] On the other hand, up to now, only little attention was paid to the processing of these materials. Simple, solution-based wet processing techniques like spin-coating^[15] and doctor blading^[16] are generally

employed for the fabrication of ORB electrodes. The disadvantages of such techniques – their tendency to waste much of the employed material and the inflexibility in shape and size of the electrode layout – encouraged us to look for an improved methodology. Advanced processing techniques such as inkjet printing, being contactless and highly flexible, can greatly improve the manufacturing of organic radical battery electrodes. Due to its additive nature, inkjet printing permits easy patterning and layered deposition of materials.

When taking the research from material design to device/electrode design, reconsideration of the polymer composition becomes necessary. On the one hand, the polymer needs to be highly soluble in solvents, which are suitable for the inkjet printing process. Typically, high boiling point solvents (>100 °C) such as chlorobenzene reveal a reliable droplet formation and good rheological properties of the ink.^[17] On the other hand, the polymer has to be insoluble in the electrolyte solution (e.g., organic carbonates, acetonitrile) employed in the assembled device.

As shown earlier, electroactive radical polymers can be inkjet printed.^[17] Nevertheless, the requirement in good solubility, i.e., low and controlled molar mass, renders the printed films useless, as the polymer films are readily soluble in the organic electrolyte solutions commonly used in ORBs. The charge storage capacity is completely lost after only two charging/discharging cycles.

In order to overcome this predicament, defined low molar mass polymers need to be prepared, printed, and subsequently crosslinked in order to provide sufficient stability of the electrode.

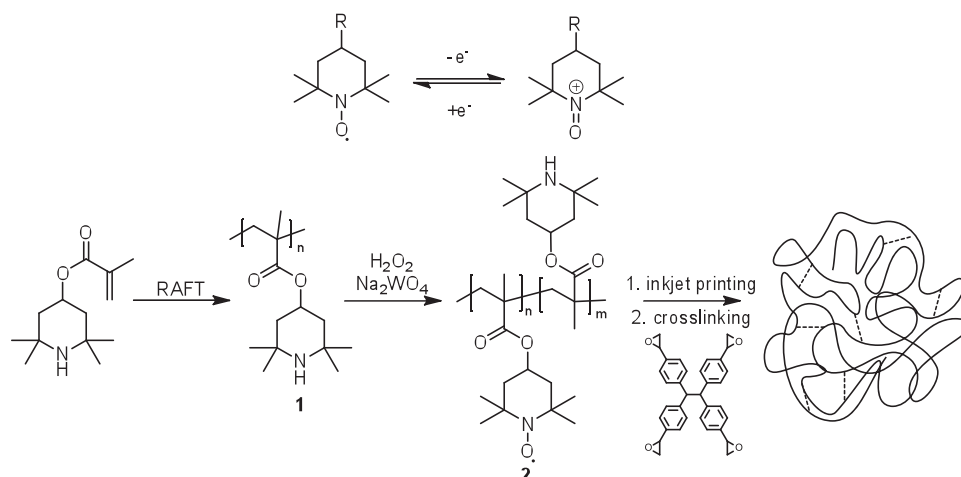
As commonly employed ORB polymers, such as the poly-radical poly(2,2,6,6-tetramethylpiperidinyloxy-4-yl methacrylate) (PTMA), are poor electric conductors, the polymers need to be mixed with conductive additives such as graphite.^[9] The inkjet printing and subsequent crosslinking of such composites is a highly demanding task. Numerous crosslinking techniques, which have been described before, are incompatible with the printing process. In situ crosslinking during the polymerization process, as described for the copolymerization with multifunctional co-monomers,^[18,19] is not an option for inkjet printing due to the insolubility of these materials. In addition, approaches based on photocrosslinking, e.g., of TEMPO-substituted poly(norbornene)s, also work insufficiently with black colored, strongly light absorbing graphite/polymer composites.^[19,20] One possible option to overcome this problem is to introduce a polymerizable co-monomer in the ORB polymer, printing this co-polymer and, subsequently, initiating the crosslinking process by an external stimulus (e.g., heat). The

T. Janoschka,^[†] A. Teichler,^[†] B. Häupler, T. Jähnert, Dr. M. D. Hager, Prof. U. S. Schubert
Laboratory of Organic
and Macromolecular Chemistry (IOMC)
Friedrich Schiller University Jena
Humboldtstr. 10, D-07743 Jena, Germany
Jena Center for Soft Matter (JCSM)
Philosophenweg 7, D-07743 Jena, Germany
E-mail: ulrich.schubert@uni-jena.de

A. Teichler, Prof. U. S. Schubert
Dutch Polymer Institute (DPI)
P.O. Box 902, 5600 AX Eindhoven, Netherlands
[†] A.T. and T.J. contributed equally to this work.



DOI: 10.1002/aenm.201300036



Scheme 1. Schematic representation of the reversible redox reaction of a TEMPO radical (top). Schematic representation of the synthesis of radical polymer poly(2,2,6,6-tetramethyl-piperidinyloxy-4-yl methacrylate) (PTMA) by RAFT polymerization, oxidation, and subsequent thermal crosslinking with a multifunctional epoxide (bottom).

disadvantages of this methodology are numerous: a) The comonomer needs to have two orthogonal polymerizable groups; b) The preparation of co-polymers is more laborious than of simple homo-polymers; c) The initiator needed to start the crosslinking reaction contaminates the electrode composite and may have disadvantageous effects on its electro chemistry; d) Obviously, simple radical-induced methods are not suitable due to the presence of the free TEMPO radical.

For these reasons, we have developed a simple crosslinking approach that is compatible with inkjet printing and does neither require an additional initiator nor the preparation of a co-polymer. This reactive inkjet printing approach is based on the printing of a functional redoxactive polymer and the corresponding crosslinker. For a recent overview on reactive inkjet printing, see a feature article by Smith and Morrin.^[21]

Crosslinking method: The TEMPO radical based polymer PTMA, the most promising of the studied radical polymers in terms of preparation and stability, is commonly prepared from the monomer 2,2,6,6-tetramethylpiperidin-4-yl methacrylate by free radical polymerization and subsequent oxidation of the amine bearing pre-polymer **1** in order to form the redoxactive TEMPO radical bearing polymer **2**.^[9,10,14,22,23] If the oxidation step, affected by *m*-chloroperbenzoic acid^[9] or hydrogen peroxide,^[10] is incomplete a co-polymer is obtained (Scheme 1). The residual amino moieties, which are not oxidized to the nitroxide radicals, can therefore be used for further functionalization or crosslinking.

In order to avoid the use of additional initiators multifunctional epoxides (Scheme 1) were chosen as crosslinking agent. Epoxides readily react with amines and can therefore affect the crosslinking of the radical polymer. Since the polymer shows a good thermal stability (decomposition above 200 °C), the crosslinking could easily be initiated by thermal treatment of the printed patterns.

For inkjet printing the polymer needs to be readily soluble and the solutions require good rheological behavior (viscosity: 0.4 to 20 mPas). For this reason, reversible addition-fragmentation chain transfer (RAFT) polymerization was used as

controlled radical polymerization technique to prepare the polymers.^[17]

Ink formulation: An ink is commonly made of a solvent and the polymer that is to be printed. For ORB-electrodes the ink has to contain a conductive additive as well. Additives, such as VGCF^[13] and graphite,^[9] are commonly used in literature. For inkjet printing these materials proved to be unsuitable, as they cause clogging of the printing nozzle (inner diameter 70 μm). Carbon nanopowder, a material of much lower particle size (<50 nm), was found to be best suited. PTMA is well soluble in many solvents, including dichloromethane, acetonitrile, toluene, *N,N*-dimethylformamide (DMF), *o*-dichlorobenzene, and *N*-methyl-2-pyrrolidone (NMP). Several combinations of these solvents were tested. DMF was found to be most suitable, because it not only dissolves PTMA but also forms excellent dispersions of the carbon nanopowder. Since inkjet printing from a single solvent causes the preferential accumulation of the ink material at the rim of a dried film (coffee-ring-effect),^[24] a co-solvent (NMP) in a content of 10 vol.% was added. As a result, the deposited material is homogeneously distributed all over the film. The dispersions made of other solvents were not sufficiently stable to permit inkjet printing.

Besides the active polymer and the conductive additive the crosslinking agent is the most important component of the ink. To ensure a high degree of crosslinking tetraphenylethane glycidyl ether was chosen, as it can react with up to four amines. As materials inkjet printed from the described ink caused the formation of brittle films, which peel off in the electrolyte solution, a plasticizer (ethylene carbonate (EC)) was used. Upon addition of EC to the prescribed ink formulation in an amount of 5 vol.%, a homogeneous and stable film was formed. Ethylene carbonate, as many other organic carbonates used in battery applications, is electrochemically inert within a broad voltage window. It not only facilitates the formation of stable films but is also miscible with the electrolyte solution used in battery cycling experiments as well, thereby promoting the penetration of the polymer electrode film with the electrolyte.

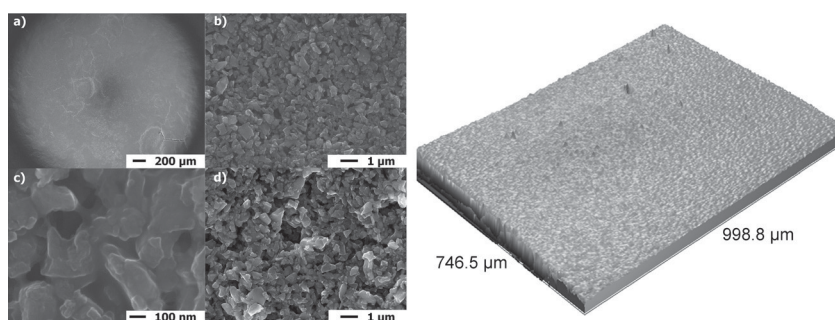


Figure 1. SEM micrographs of inkjet printed PTMA/carbon-nano-powder composite electrodes, (a-c) before charging/discharging, (d) after charging/discharging (left). Optical profiler image of a crosslinked inkjet printed film (right). Ink composition: active polymer PTMA (concentration: 5 mg/mL), crosslinking agent tetraphenylethane glycidyl ether (concentration: 0.7 mg mL⁻¹), and solvent mixture DMF/NMP in a ratio of 9:1.

Electrochemical studies: In order to study the stability of the inkjet printed electrodes half-cells were built and charged/discharged repeatedly. The experiments were carried out in a temperature controlled cell at 30 °C employing a three electrode setup (Ag/AgCl reference electrode, platinum counter electrode, printed working electrode) and a 0.1 M solution of tetrabutylammonium hexafluorophosphate in propylene carbonate as electrolyte.

Inks that did not contain a crosslinking agent revealed a fast decrease in charge storage capacity. After only two cycles no active polymer was left. The stability of the electrode was enhanced by crosslinking the electrode using the optimized procedure described above. About 75% of the initial capacity was retained after 150 charging/discharging cycles. The decline can be attributed to a slow degradation of the electrode due to active polymer being washed out of the polymer composite. Scanning electron microscope (SEM) pictures of the cycled electrodes reveal minor changes in the electrode's surface morphology (Figure 1b/d). Because high molar mass/insoluble PTMA polymer can be considered electrochemically stable^[6–8] and cyclic voltammetry (CV) experiments confirm that even an excess of the epoxy-crosslinker does not influence the redox chemistry of the polymer, the electrode's stability is most likely limited due to the necessity of crosslinking. Even an increase of the amount of the epoxide-crosslinker as well as using PTMA

with up to 40% of free amine groups (60% oxidized to form TEMPO) did not result in a significantly improved stability. About carbon/epoxy resin composites it is known that the interfacial contact between the high surface area of carbon and the crosslinking agents strongly affect the kinetics and the final crosslinking state.^[25–27] As the carbon nanopowder appears to be affecting the crosslinking process, epoxidized carbon nanopowder was prepared by reacting the virgin powder with *m*-chloroperoxybenzoic acid.^[28] The epoxidized carbon can react with the free amine groups of the PTMA polymer and act as crosslinking agent itself, covalently linking the active polymer to the insoluble conductive additive. Thereby an increased cycling

stability was achieved (Figure 2). After a slight increase of the charge storage capacity within the first cycles due to wetting/activation of the electrode the initial capacity was retained even after 150 cycles.

Subsequently, a beaker type battery consisting of a printed polymer composite cathode, a zinc-anode, and a ZnBF₄-electrolyte in propylene carbonate was assembled. The cell exhibits an average discharge voltage of 1.25 V and a capacity of 20.5 μAh (ca. 50 mAh g⁻¹, theor. capacity of the polymer is 66 mAh g⁻¹).

In summary, a reactive inkjet printing strategy for the manufacturing of printed electrodes used in organic radical batteries was developed. Being contactless and highly flexible inkjet printing is superior to conventional solution-based wet processing techniques. The low molar mass, electroactive poly-radical poly(2,2,6,6-tetramethylpiperidinyloxy-4-yl methacrylate) (PTMA), that was used for inkjet printing, was prepared by RAFT-polymerization and a subsequent partial oxidation. The incomplete oxidation is an easy way of obtaining a reactive copolymer, which not only bears electroactive sites but also chemically reactive amine groups; advanced co-polymerization strategies are not necessary. An optimized ink containing the electro active polymer, an epoxy-based crosslinker, carbon nanopowder, and additives/solvents was developed and inkjet printed. Electrodes of good stability, as proven by repeated charging/discharging experiments, were prepared by initiator-free, thermal

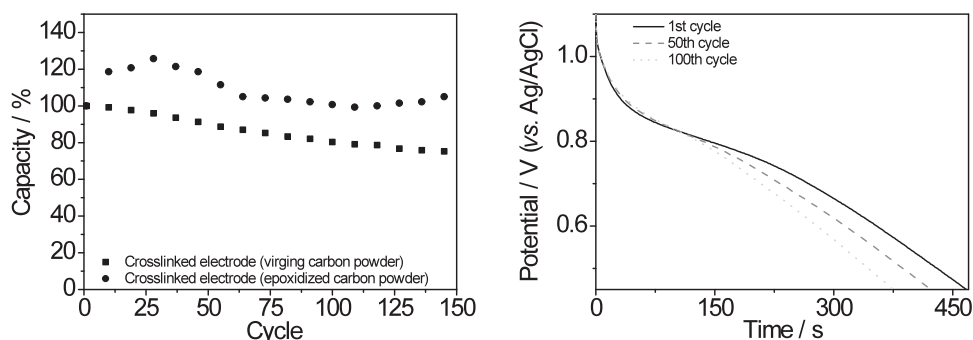


Figure 2. Cycling stability of inkjet printed electrodes at 1.5 A m⁻² over 150 cycles (left). Discharging curves of inkjet printed electrodes at 1.5 A m⁻² using a solution of tetrabutylammonium hexafluorophosphate in propylene carbonate as electrolyte (right).

crosslinking of the free amine-bearing PTMA and the epoxy-based crosslinker. By employing epoxidized carbon nanopowder as chemically reactive conductive additive a further improvement could be observed. The printed electrodes are stable for over one hundred cycles. This technique might be of interest for the manufacturing of patterned, flexible organic radical batteries used in sensor devices, smart packaging, DNA chips, or battery-powered smart cards.

Experimental Section

Synthesis: PTMA was prepared according to literature by means of RAFT polymerization and subsequent oxidation with hydrogen peroxide and a sodium tungstate catalyst.^[17]

Polymer 1: $M_n = 35,600 \text{ g mol}^{-1}$, $M_w = 39,800 \text{ g mol}^{-1}$, $M_w/M_n = 1.12$, amine/nitroxide radical ratio = 2/8.

Polymer 2: $M_n = 51,000 \text{ g mol}^{-1}$, $M_w = 58,200 \text{ g mol}^{-1}$, $M_w/M_n = 1.14$, amine/nitroxide radical ratio = 4/6.

The polymer's degree of nitroxide radical functionalization was determined using UV-vis spectroscopy^[19] (280 nm) on a Perkin-Elmer Lambda-45 UV-vis spectro-photometer at room temperature in tetrahydrofuran (1 cm cuvettes). A fully functionalized PTMA prepared by group transfer polymerization was used as reference standard.

Molar masses were determined by size exclusion chromatography (SEC): Agilent 1200 series system (degasser: Polymer Standard Service Mainz, pump: G1310A, auto sampler: G1329A, oven: Techlab, diode array detector: G1315D, RI detector: G1362A) using a pC/PSS GRAM 1000/30 Å column and dimethylacetamide (+0.21% lithium chloride) as eluent at a flow rate of 1 mL/min (40 °C).

Carbon nanopowder (Aldrich) was epoxidized by refluxing with *m*-chloroperoxybenzoic acid in dichloromethane.^[28]

Electrochemical characterization: A Princeton Applied Research VersaSTAT potentiostat/galvanostat was used for all charging/discharging experiments. The experiments were carried out in a temperature controlled cell (30 °C) using an Ag/AgCl reference electrode and a platinum counter electrode. A 0.1 M solution of tetrabutylammonium hexafluorophosphate in propylene carbonate was used as electrolyte. Before the first charging the printed electrodes were immersed in the electrolyte until a constant open current potential was observed.

Inkjet printing: Inkjet printing was performed using an Autodrop professional system from microdrop technologies (Norderstedt, Germany). The printer was equipped with a micropipette with an inner diameter of 70 μm. The carbon nanopowder (particle size < 50 nm, Aldrich) dispersion was prepared by ultrasonication for 5 h in the solvent system *N,N*-dimethylformamide/*N*-methyl-2-pyrrolidone 90/10. Afterwards the dispersion was filtered by a syringe filter (pore size: 5 μm) to prevent nozzle clogging. The ink was prepared by addition of the dissolved polymer (concentration: 5 mg/mL), the crosslinking agent tetraphenylethane glycidyl ether and the plasticizer ethylenecarbonate (5 vol.%). The ink contained the polymer and the carbon nanopowder in a ratio of 1/1 by weight. The content of crosslinker was varied according to the content of free amine groups of PTMA. Printing was performed by using a drop count of 100 drops, a dot spacing of 100 μm, a printing speed of 20 mm/s and a substrate temperature of 50 °C. As substrate a graphite foil was used. After drying of the film at 50 °C, crosslinking was carried out for 12 h at 130 °C in an oven.

Acknowledgements

The authors acknowledge the Bundesministerium für Bildung und Forschung (project no. 13N11393), the European Social Fund (ESF), the Thüringer Aufbaubank (TAB), the Thuringian Ministry of Economy,

Employment and Technology (TMWAT), the Fonds der Chemischen Industrie (scholarship for TJ) as well as the Dutch Polymer Institute (DPI, technology area HTE) for financial support.

Received: January 10, 2013
Published online: April 19, 2013

- [1] F. C. Krebs, *Sol. Energy Mater. Sol. Cells* **2009**, *93*, 394–412.
- [2] D. Angmo, T. T. Larsen-Olsen, M. Jorgensen, R. R. Sondergaard, F. C. Krebs, *Adv. Energ. Mat.* **2013**, *3*, 172–175.
- [3] J. Jensen, H. F. Dam, J. R. Reynolds, A. L. Dyer, F. C. Krebs, *J. Polym. Sci., Part B: Polym. Phys.* **2012**, *50*, 536–545.
- [4] F. C. Krebs, T. D. Nielsen, J. Fyenbo, M. Wadstrom, M. S. Pedersen, *Energy Environ. Sci.* **2010**, *3*, 512–525.
- [5] F. C. Krebs, J. Fyenbo, D. M. Tanenbaum, S. A. Gevorgyan, R. Andriessen, B. van Remoortere, Y. Galagan, M. Jorgensen, *Energy Environ. Sci.* **2011**, *4*, 4116–4123.
- [6] K. Oyaizu, H. Nishide, *Adv. Mater.* **2009**, *21*, 2339–2344.
- [7] K. Nakahara, K. Oyaizu, H. Nishide, *Chem. Lett.* **2011**, *40*, 222–227.
- [8] T. Janoschka, M. D. Hager, U. S. Schubert, *Adv. Mater.* **2012**, *24*, 6397–6409.
- [9] K. Nakahara, S. Iwasa, M. Satoh, Y. Morioka, J. Iriyama, M. Suguro, E. Hasegawa, *Chem. Phys. Lett.* **2002**, *359*, 351–354.
- [10] Y. Kim, C. Jo, J. Lee, C. W. Lee, S. Yoon, *J. Mater. Chem.* **2012**, *22*, 1453–1458.
- [11] D. Yang, Z. Yixiao, G. Lei, X. Guofeng, X. Jingying, *J. Electrochem. Soc.* **2011**, *158*, A291–A295.
- [12] K. Koshika, N. Sano, K. Oyaizu, H. Nishide, *Chem. Commun.* **2009**, *45*, 836–838.
- [13] K. Nakahara, J. Iriyama, S. Iwasa, M. Suguro, M. Satoh, E. J. Cairns, *J. Power Sources* **2007**, *163*, 1110–1113.
- [14] W. Guo, Y.-X. Yin, S. Xin, Y.-G. Guo, L.-J. Wan, *Energy Environ. Sci.* **2012**, *5*, 5221–5225.
- [15] K. Koshika, N. Sano, K. Oyaizu, H. Nishide, *Macromol. Chem. Phys.* **2009**, *210*, 1989–1995.
- [16] Y.-Y. Cheng, C.-C. Li, J.-T. Lee, *Electrochim. Acta* **2012**, *66*, 332–339.
- [17] T. Janoschka, A. Teichler, A. Krieg, M. D. Hager, U. S. Schubert, *J. Polym. Sci., Part A: Polym. Chem.* **2012**, *50*, 1394–1407.
- [18] T. Ibe, R. B. Frings, A. Lachowicz, S. Kyo, H. Nishide, *Chem. Commun.* **2010**, *46*, 3475–3477.
- [19] L. Bugnon, C. J. H. Morton, P. Novak, J. Vetter, P. Nesvadba, *Chem. Mater.* **2007**, *19*, 2910–2914.
- [20] T. Suga, H. Konishi, H. Nishide, *Chem. Commun.* **2007**, *43*, 1730–1732.
- [21] P. J. Smith, A. Morrin, *J. Mater. Chem.* **2012**, *22*, 10965–10970.
- [22] H. Nishide, S. Iwasa, Y. J. Pu, T. Suga, K. Nakahara, M. Satoh, *Electrochim. Acta* **2004**, *50*, 827–831.
- [23] K. Nakahara, J. Iriyama, S. Iwasa, M. Suguro, M. Satoh, E. J. Cairns, *J. Power Sources* **2007**, *165*, 398–402.
- [24] E. Tekin, B. J. de Gans, U. S. Schubert, *J. Mater. Chem.* **2004**, *14*, 2627–2632.
- [25] A. Garton, W. T. K. Stevenson, S. P. Wang, *J. Polym. Sci., Part A: Polym. Chem.* **1988**, *26*, 1377–1391.
- [26] M. A. Andres, R. Miguez, M. A. Corcuera, I. Mondragon, *Polym. Int.* **1994**, *35*, 345–353.
- [27] D. Puglia, L. Valentini, J. M. Kenny, *J. Appl. Polym. Sci.* **2003**, *88*, 452–458.
- [28] W. Yuan, M. B. Chan-Park, *ACS Appl. Mater. Interfaces* **2012**, *4*, 2065–2073.